

Formation, Accretion and Reworking of Continents

Rixiang Zhu¹, Guochun Zhao², Wenjiao Xiao³, Ling Chen¹, and Yanjie Tang⁴

¹Institute of Geology and Geophysics, Chinese Academy of Sciences

²University of Hong Kong

³Xinjiang Research Center for Mineral Resources, Xinjiang Institute of Ecology and Geography, Chinese Academy of Sciences

⁴Institute of Geology and Geophysics, Chinese Academy of Sciences

November 26, 2022

Abstract

Felsic continental crust is unique to the Earth in the solar system, but it still remains controversial regarding its formation, accretion and reworking. The plate tectonics theory has been significantly challenged in explaining the origin of continents as Archean continents rarely preserve hallmarks of plate tectonics. In contrast, growing evidence emerges to support mantle plume-derived oceanic plateau models as the models can reasonably explain the origin of bimodal volcanic assemblages and nearly coeval emplacement of tonalite-trondjemite-granodiorite (TTG) rocks, presence of ~1600°C komatiites and dominant dome structures, and lack of ultra-high-pressure rocks, paired metamorphic belts and ophiolites in Archean continents. Although plate tectonics seems to fail in explaining the origin of continents, it has been successfully applied to interpret the accretion or outgrowth of continents along subduction zones where new mafic crust is generated at the base of continental crust through partial melting of the mantle wedge with addition of H₂O-dominant fluids from the subducted oceanic slabs, and partial melting of the juvenile mafic crust results in the formation of new felsic continental crust, leading to the outside accretion of continents. Subduction processes also cause the softening, thinning and recycling of continental lithosphere due to the vigorous infiltration of volatile-rich fluids and melts especially along weak layers or weak belts, leading to the widespread reworking and even destruction of continental lithosphere. Reworking of continents also occurs in continental interiors due to plume-lithosphere interactions, which, however, leads to much less degrees of lithospheric modification than subduction-induced craton destruction.

Formation, Accretion and Reworking of Continents

Rixiang Zhu^{1,2}, Guochun Zhao^{3,4}, Wenjiao Xiao^{1,2,5}, Ling Chen^{1,2}, Yanjie Tang^{1,2}

¹State Key Laboratory of Lithospheric Evolution, Institute of Geology and Geophysics, Chinese Academy of Sciences, Innovation Academy of Earth Science, CAS, P.O. Box 9825, Beijing 100029, China, ²College of Earth and Planetary Sciences, University of Chinese Academy of Sciences, Beijing, 100049, China, ³Department of Earth Sciences, The University of Hong Kong, Pokfulam Road, Hong Kong, ⁴State Key Laboratory of Continental Dynamics, Department of Geology, Northwest University, Northern Taibai Street 229, Xi'an 710069, China, ⁵Xinjiang Research Center for Mineral Resources, Xinjiang Institute of Ecology and Geography, Chinese Academy of Sciences, Urumqi 830011, China

Correspondence to: Rixiang Zhu,

rxzhu@mail.igcas.ac.cn

Key Points:

- Archean continental nuclei were likely originated from oceanic plateaus formed by mantle plumes, not from island arcs via oceanic subduction
- Archean continental nuclei underwent accretion/growth at margins by the oceanic subduction, involving juvenile arc formation and accretion
- Continental reworking/destruction occurs mainly at subduction zones by water and volatile infiltration, with minor effects of mantle plumes

Abstract Felsic continental crust is unique to the Earth in the solar system, but it remains controversial regarding its formation, accretion and reworking. The plate tectonics theory has been significantly challenged in explaining the origin of continents as Archean continents rarely preserve hallmarks of plate tectonics. In contrast, growing evidence emerges to support mantle plume-derived oceanic plateau models as the models can reasonably explain the origin of bimodal volcanic assemblages and nearly coeval emplacement of tonalite-trondjemite-granodiorite (TTG) rocks, presence of ~1600°C komatiites and dominant dome structures, and lack of ultra-high-pressure rocks, paired metamorphic belts and ophiolites in Archean continents. Although plate tectonics seems to fail in explaining the origin of continents, it has been successfully applied to interpret the accretion or outgrowth of continents along subduction zones where new mafic crust is generated at the base of continental crust through partial melting of the mantle wedge with addition of H₂O-dominant fluids from the subducted oceanic slabs, and partial melting of the juvenile mafic crust results in the formation of new felsic continental crust, leading to the outside accretion of continents. Subduction processes also cause the softening, thinning and recycling of continental lithosphere due to the vigorous infiltration of volatile-rich fluids and melts especially along weak layers or weak belts, leading to the widespread reworking and even destruction of continental lithosphere. Reworking of continents also occurs in continental interiors due to plume-lithosphere interactions, which, however, leads to much less degrees of lithospheric modification than subduction-induced craton destruction.

Plain language summary All solid planets in the solar system have a core-mantle-crust structure, but the Earth is a unique planet with felsic continental crust and plate tectonics. Controversy has long surrounded the formation, growth (accretion) and reworking of the continents. The plate tectonics theory has been significantly challenged in explaining the origin of continents as Archean (>2.5 billion years) continents rarely preserve hallmarks of plate tectonics. In contrast,

oceanic plateau models can well explain the origin of bimodal volcanic and plutonic assemblages, presence of ~1600°C komatiites and dominant dome structures, and lack of ultra-high-pressure rocks, paired metamorphic belts and ophiolites in Archean continents. The accretion of continents can be successfully interpreted by plate tectonics along subduction zones via partial melting of the juvenile mafic crust which itself is generated at the base of continental crust through partial melting of the mantle wedge. Subduction can also cause softening, thinning and recycling of continental lithosphere due to the vigorous infiltration of volatile-rich fluids and melts especially along weak layers or weak belts, leading to widespread reworking and even destruction of continental lithosphere. Minor continental reworking and destruction also occur in continental interiors due to plume-lithosphere interactions.

1. Introduction

Although all solid planets and the Moon in the solar system have a crust of mostly mafic composition in their outermost shell (Campbell & Taylor, 1983), the Earth is unique in that it has a thick (~40 km on average) felsic continental crust as well as a thin (averagely ~7 km) mafic oceanic crust (Table 1). In many areas, the continental crust is much older than the oceanic crust, with the oldest continental rocks up to ~4.0 Ga and the oldest single zircon crystals up to 4.4 Ga (Harrison, 2009; Hawkesworth et al., 2010; Wilde et al., 2001), whereas the oldest oceanic crust is no more than 250 Ma (Roberts et al., 2015). In this sense, the continental crust preserves much more information about the Earth's geological history than the oceanic crust. Moreover, it is the continental crust that provides suitable places for human beings to live and most of the natural resources for human beings to utilize. Therefore, the issues of when, where and how the continental crust was formed, accreted and reworked or destroyed are very important in earth sciences. However, these issues have not been well resolved though the plate tectonic theory has been established for more than half a century.

Table 1

Comparisons of some physical properties and water content among continental and oceanic lithosphere and asthenosphere

Parameters	Continental lithosphere			~100-200 Ma Oceanic lithosphere	Asthenosphere
	Archean	Proterozoic	Phanerozoic		
Crustal thickness (km) ^{1,2}	~40 (average)			~7	N/A
	~35 - ~50		~15 - ~80		
Lithospheric thickness (km) ^{3,4,5}	~150 - ~250		~50 - ~180	~100	N/A
Crustal density (kg/m ³) ^{1,6,7}	2700 - 2800			2900 - 3000	~3390
^a Root density (kg/m ³) ^{8,9,10}	~3300-3330	~3330-3370	~3340-3390	~3350-3380	
Average heat flow (mW/m ²) ^{4,11}	~41	~48	~58	~48-54	N/A
Mg# ^{8,12,13,14}	92-94	91.5-92.5	90	~90-91 ^b	89.3
Water content (wt ppm) ^{15,16,17}	<24-100 (mostly <30-50) ^c (mostly <10 in olivine)		50-100	50-100	50-200 (50±20 in olivine)

^a at standard temperature and pressure condition. ^b In reference 14, only samples having both Mg# and olivine proportion data are considered. ^c In stable cratonic regions, relatively high-water contents in peridotites (olivine) were associated with localized metasomatism and deformation, and may not represent the overall feature of cratonic mantle root¹⁷. References include 1: Christensen and Mooney (1995); 2: Dick et al. (2003); 3: Artemieva (2009); 4: Jaupart and Mareschal (2015); 5: Priestley et al. (2019); 6: Carlson and Raskin (1984); 7: Frisch et al. (2011); 8: Griffin et al. (1999); 9: Lee et al. (2005); 10: Poudjom Djomani et al. (2001); 11: Stein and Stein (1992); 12: Boyd (1989); 13: Gaul et al. (2000); 14: Warren (2016); 15: Hirschmann (2006); 16: Hirth and Kohlstedt (1996); 17: Peslier et al. (2017).

Established in the middle 1960's and regarded as a revolution in earth sciences, the plate tectonics theory has been used to interpret various geological phenomena, processes and events that happened during Phanerozoic (0.54 Ga to present) time, and has also been successfully applied to the Proterozoic (2.5-0.54 Ga), but it has been significantly challenged in explaining the origin of Archean (>2.5 Ga) felsic continental crust, which consist mainly of orthogneisses and supracrustals

(greenstones) that were metamorphosed from tonalite-trondhjemite-granodiorite (TTG) plutons and mafic-ultramafic volcanic and felsic rocks with minor sedimentary rocks, respectively. For example, plate tectonics can interpret Archean TTG rocks as the products of island arcs in subduction zones, such that the Archean high-pressure-type TTG rocks (adakites) were derived from the partial melting of subducted slabs, whereas the Archean low-pressure-type TTG rocks (equivalent to calc-alkaline granitoids) were derived from the partial melting of juvenile basaltic crust which itself was formed by the partial melting of the mantle wedge with addition of fluids released from the subducted slabs (Arndt, 2013; Condie, 2014; Martin, 1999; Martin et al., 2014; Wyman, 2013). However, such an island arc model is difficult to explain the bimodal volcanic assemblages from the Archean greenstone terranes where basaltic and ultramafic rocks are associated with dacite and rhyolite, without much andesite (Bédard, 2006; Hamilton, 1998, 2007; Van Kranendonk et al., 2007a, 2014; Zhao et al., 1998, 2001). Moreover, island arc models also fail in interpreting domiform structures and anticlockwise P-T paths involving isobaric cooling that characterize the deformation and metamorphism of Archean cratons (craton is an old and long-lived stable continent or continental lithosphere) (Lin & Beakhouse, 2013; Nijman et al., 2017; Van Kranendonk et al., 2007a, 2014; J. Zhang et al., 2014; Zhao et al., 1998, 2001, 2005). For these reasons, more and more researchers are now seeking other tectonic regimes beyond plate tectonics (e.g., mantle plumes, stagnant lid, subduction, etc) to interpret the origin of Archean continents.

Although it is still unclear whether felsic continents were originated from island arcs under the plate tectonics regime or from the non-plate tectonic settings such as oceanic plateaus formed by mantle plumes, it is evident that present-day's large continental blocks developed from the outside accretion of early Archean continental nucleuses or amalgamation of small pieces of early Archean continental nucleuses. However, it remains unknown or controversial regarding the issues of

when and how Archean continental nucleuses were grown up to form present-day's large continents through external accretionary or internal collisional orogenic systems.

Growing data have been emerging to demonstrate that continental cratons have not only experienced outgrowth or accretion along their margins, but also been reworked in their interiors with lithospheric thinning, refertilization or destabilization. The fundamental reworking of a craton that results in the loss of its intrinsic tectonic stability has been termed as craton destruction or decratonization (Wu et al., 2008; Zhu et al., 2011). One of the best examples of cratons that have ever been destroyed is the North China Craton, of which its eastern part underwent intensive thinning and extension in association with extensive volcanic eruption, basin filling, granitic emplacement, and gold mineralization during the late Mesozoic time, indicating that the craton has undergone severe reworking or destruction (Wu et al., 2008, 2014; F. Y. Wu et al., 2019; Xu, 2001; Yang et al., 2018; Zhang, 2005; Zheng et al., 2018; Zhu et al., 2011, 2012a, 2012b, 2017, 2020; Zhu & Xu, 2019). However, what kind of geodynamic mechanism caused the reworking and destruction of a continental craton is still a subject of debate.

To resolve the above controversial issues regarding the formation, accretion and reworking of continental cratons, researchers have carried out extensive and integrative geological and geophysical investigations in the past two decades. In particular, the National Science Foundation of China (NSFC) set up a Major Research Program entitled "Destruction of the North China Craton" (2008-2015) that was aimed to determine what kind of geodynamic mechanisms caused the reworking and destruction of the North China Craton and whether the craton destruction is unique to the North China Craton or a common process for other cratons during Earth's evolution (F. Y. Wu et al., 2019). In the past decade, this NSFC Major Research Program supported 66 key projects on the thinning and destruction of the North China Craton which produced large amounts of new data

and competing interpretations (Wu et al., 2014; F. Y. Wu et al., 2019; Zheng et al., 2018; Zhu et al., 2011, 2012a, 2012b, 2017, 2020; Zhu & Xu, 2019). These new data and those advancements made in other continents forms the justification for us to write this review in which we review current controversies on the origin and reworking of felsic continents, summarize the various lines of evidence for their mechanisms, and finally propose a new model for the formation, accretion and destruction of continents.

2. Formation of Continents

It is well known that in the solar system, Earth is a unique planet that has both plate tectonics and felsic continental crust (Hawkesworth et al., 2010, 2020; Rudnick, 1995; Sleep, 2000; Taylor & McLennan, 2008). This leads some researchers to speculate a cause-and-result relationship between plate tectonics and felsic continental crust (e.g., Hastie et al., 2016; Tang et al., 2016), but controversy has surrounded the issue of whether plate tectonics or continents first appeared on the Earth. Researchers regarding continents as a result of plate tectonics argue that plate tectonics had appeared before the formation of felsic continental crust on Earth, probably starting during Hadean or Eoarchean time, whereas felsic continental crust developed from island arcs under a plate tectonic regime (Arndt, 2013; de Wit, 1998; Furnes et al., 2009; Greber et al., 2017; Grosch & Slama, 2017; Harrison, 2009; Hastie et al., 2016; Jackson & Fyon, 1991; Kerrich & Polat, 2006; Kusky et al., 2013; Langford & Morin, 1976; Leat & Larter, 2003; Martin, 1999; Martin & Moyen, 2002; Martin et al., 2009, 2014; Nutman et al., 2015; Turner et al., 2014; Wyman, 2013). In contrast, another school of thoughts believes that felsic continental crust had formed long before the start of plate tectonics, as a result of non-plate tectonics, such as mantle plumes, sagduction driven by density difference, delamination of thickened crust, etc. (Bédard, 2006, 2018; Brown, 2006; Brown et al., 2020; Campbell et al., 1989; Cawood, 2020; Condie, 1975, 2005, 2014;

[Hamilton, 1998, 2007, 2011, 2019; Hawkesworth et al., 2020; Hill et al., 1992;](#)
[Larson, 1991; Rozel et al., 2017; Van Kranendonk et al., 2004, 2007a, 2007b, 2014;](#)
[Zheng & Zhao, 2020](#)). They also argue that it was just the existence of such
low-density felsic continental crust that induced the subduction of high-density
mafic crust (oceanic crust) beneath felsic continental crust, initializing the operation
of plate tectonics ([Bédard, 2006, 2018; Brown et al., 2020; Lin & Beakhouse, 2013;](#)
[Nair & Chacko, 2008](#)). [Rey et al. \(2014\)](#) demonstrated that because the Archean
oceanic crust was thick and buoyant, early continents may have produced
intra-lithospheric gravitational stresses large enough to drive their gravitational
spreading to initiate subduction at their margins and to trigger episodes of
subduction. Therefore, the existence of felsic continental crust may be a prerequisite
for the initialization of plate tectonics ([Bédard, 2006, 2018; Brown et al., 2020; Lin](#)
[& Beakhouse, 2013; Nair & Chacko, 2008](#)). No matter which model above is valid,
researchers have reached a broad consensus that as the major component of Archean
felsic continental crust, TTG rocks were derived from the partial melting of
thickened mafic crust. The oldest mafic crust on the Earth is also called proto-crust
or primitive crust ([Grenville, 1922](#)), which may have been formed by crystallization
of magma ocean that covered the whole surface of our planet about 4.4 Ga ago
([Elkins-Tanton, 2012](#)). This primitive mafic crust most likely existed as a primitive
oceanic crust after an initial ocean developed with large voluminous H₂O released
out from the magma ocean to form the second atmosphere ([Brown, 1949; Zahnle et](#)
[al., 2010](#)). It is considered that the earliest felsic continental crust was most likely to
have developed from a thickened primitive oceanic crust through its partial melting.
Modern oceanic settings include oceanic basins, mid-oceanic ridges, island arcs and
oceanic plateaus, of which the former two settings have a normal oceanic crust that
is too thin to form felsic continental crust via partial melting. Therefore, the first
continent with felsic composition was most likely to have developed either from an
island arc under a plate tectonic regime or from an oceanic plateau originated from

mantle plumes. This depends on which model (plate tectonics or mantle plumes) can more reasonably explain the magmatic, metamorphic and structural features of Archean cratons.

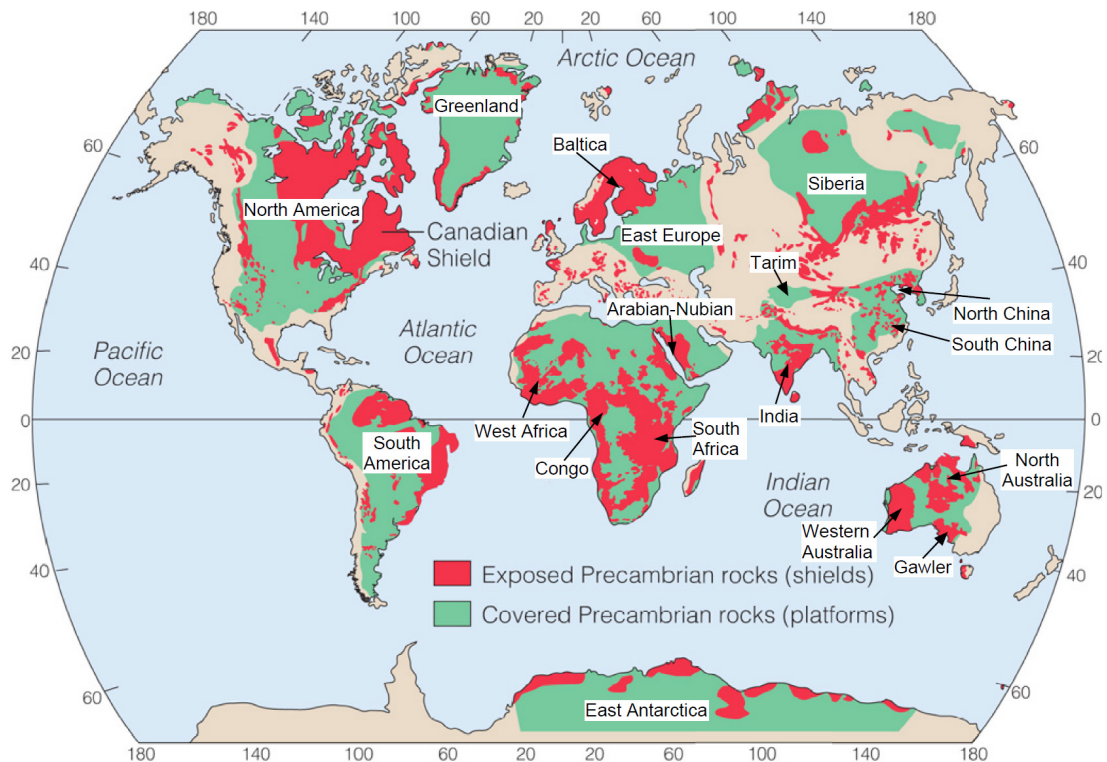


Figure 1. Spatial distribution of major cratons in the world (Wicander & Monroe, 2016).

2.1. Main Features of Archean cratons

Figure 1 shows the spatial distribution of major cratons in the world. Except the ~4.0 Ga Acasta TTG gneisses in North America (Bowring & Williams, 1999), most cratons formed during Archean eon (Arndt, 2013; Hawkesworth et al., 2010). The Eoarchean cratonic crust is represented by the 3.8-3.6 Ga Isua supracrustals and Amitsoq TTG gneisses in Greenland (Nutman et al., 2015), the Paleoarchean cratonic crust is represented by 3.6-3.2 Ga Barberton and Pilbara granite-greenstone terranes in South Africa and Western Australia, respectively, and the Mesoarchean and especially Neoarchean continental crust is widely exposed in all major cratons in the world. The whole-rock Nd and zircon Hf and O isotopic data for Archean

202 felsic rocks from major cratons indicate the existence of Hadean primitive mafic
203 crust ([Arndt, 2013](#); [Guitreau et al., 2014](#); [Harrison, 2009](#); [O'Neil & Carlson, 2017](#);
204 [Reimink et al., 2014](#); [Wilde et al., 2001](#)), but nearly whole of such a primitive crust
205 has been destroyed probably either by the Late Heavy Bombardment Event (LHB)
206 or by plate tectonics that appeared later.

207 Archean TTG rocks are similar to Phanerozoic calc-alkaline granitoids in that they
208 are both high in Si, Ca, Sr, Ba and Na₂O/K₂O and low in heavy REE and depletions
209 in Nb, Ta and Ti, but with temperature decreasing, the former goes to high Na,
210 named the trondhjemitic trend (Tdj), whereas the latter goes to high K, named
211 calc-alkaline trend (CA), indicating that Archean TTG may have been derived from
212 the partial melting of low-K mafic (tholeiitic) rocks under H₂O-saturated conditions
213 with garnet and/or rutile as residual/cumulus phases ([Arth & Barker, 1976](#); [Arth et](#)
214 [al., 1978](#); [Barker & Arth, 1976](#); [Barker, 1979](#); [Jahn et al., 1981](#)). Garnet is assumed
215 to be residual/cumulus phases in order to explain the strong light to heavy REE
216 fractionation (high La/Yb ratios) of Archean TTG rocks, whereas rutile existing as
217 residual/cumulus phases can explain the striking depletions of Nb, Ta and Ti in
218 Archean TTG rocks([Arndt, 2013](#); [Arth et al., 1978](#); [Barker & Arth, 1976](#); [Jahn et al.,](#)
219 [1981](#); [Martin et al., 2014](#); [Moyen & Martin, 2012](#); [Ryerson & Watson, 1987](#)). As
220 shown in Figure 2, most Archean TTG rocks have La/Yb and Sr/Y ratios remarkably
221 higher than those of post-Archean calc-alkaline granitoids, indicating that the former
222 are enriched in light REE (LREE) but depleted in heavy REE (HREE). This led
223 researchers to have proposed that HREE-rich garnet must have existed as the
224 dominant residual phase in the magmas to form TTG, implying that the partial
225 melting of basaltic rocks to form Archean TTG must have occurred under high
226 pressure conditions or in a thickened crust. The metamorphic mafic rocks under
227 such high-pressure conditions are most likely garnet amphibolite and/or eclogite
228 ([Arndt, 2013](#); [Arth & Barker, 1976](#); [Arth et al., 1978](#); [Barker & Arth, 1976](#); [Barker,](#)
229 [1979](#); [Condie, 2014](#); [Martin et al., 2014](#); [Moyen & Laurent, 2018](#)). However, recent

studies suggest that because of relatively high Mg in Archean crust, garnet may have occurred at a normal crustal thickness (~7 kbar), not necessary to require high-pressure conditions (>15 kbar) at a thickened crustal level (Johnson et al., 2017).

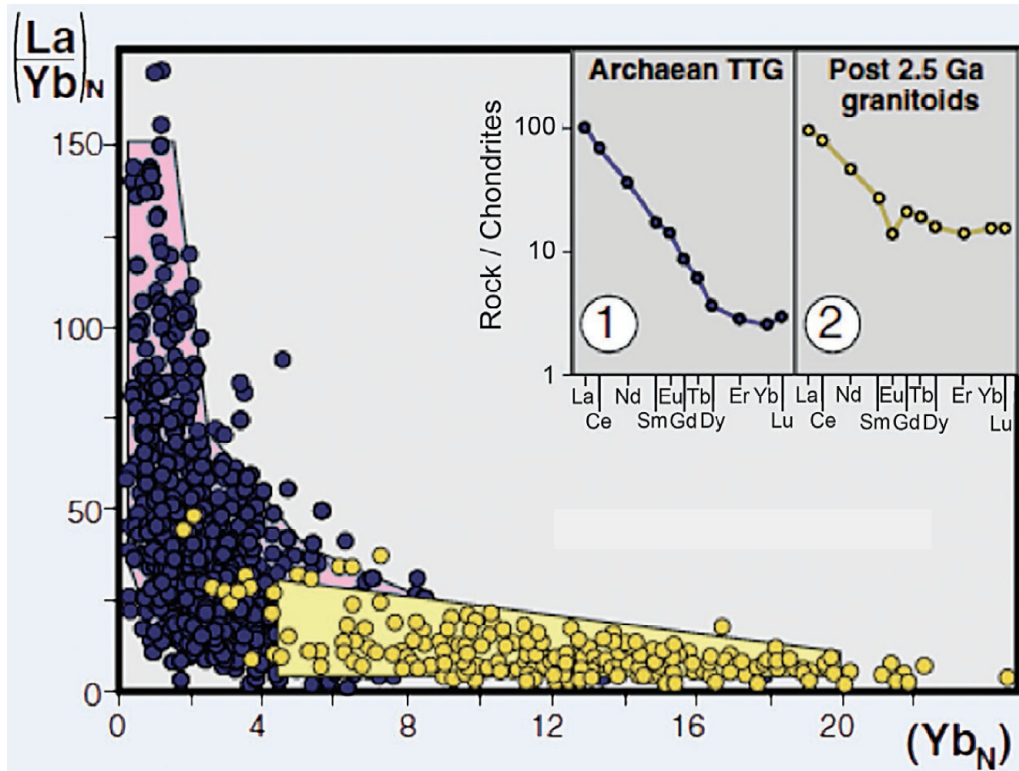


Figure 2. The La/Yb vs Yb diagram to distinguish Archean TTG from post-Archean granitoids (Martin, 1987; Martin & Moyen, 2002; Moyen & Martin, 2012). The subscript N indicates that the ratio or concentration is normalized to primitive mantle. The insets 1 and 2 illustrate the contrasting REE patterns of the two types of granitoid (Moyen & Martin, 2012).

Archean TTG rocks is divisible to low-Al₂O₃ type (Al₂O₃ <15% at SiO₂ = ~70%) and high-Al₂O₃ type (Al₂O₃ >15% at SiO₂ = ~70%). Generally, the low-Al₂O₃ type forms at relatively low-pressure conditions (10-12 kbar), also named low-pressure type, which is characterized by low La/Yb, Sr/Y, Na₂O and Sr and high Y, Yb, Ta and Nd, implying that the dominant residual phases in the magmas to form

low-Al₂O₃ type TTG are plagioclase and pyroxene (Arndt, 2013; Condie, 2014; Martin et al., 2014; Moyen & Laurent, 2018). In contrast, the high-Al₂O₃ type TTG is considered to have formed under relatively high pressure conditions (>20kbar), so called high-pressure type, which is characterized by high La/Yb, Sr/Y, Na₂O and Sr and low Y, Yb, Ta and Nd, implying that the dominant residual phases in the magmas to form high-Al₂O₃ type TTG are garnet and rutile (Arndt, 2013; Condie, 2014; Martin et al., 2014; Moyen & Laurent, 2018). There are also Archean TTG rocks with chemical features between the low- and high-pressure types, called medium-pressure type TTG, which formed at 15-20 kbar, with amphibole, garnet and minor rutile (without plagioclase) as dominant residual phases during the partial melting of mafic crust to form TTG magmas (Moyen, 2011). Except minor adakites, Phanerozoic calc-alkaline granitoids have geochemical characteristics (e.g., La/Yb and Sr/Y values) similar to low-Al₂O₃ (or low-pressure) type Archean TTG rocks (Condie, 2014; Zhang & Zhai, 2012).

In the Archean supracrustals or greenstones, a common protolithic assemblage is bimodal volcanic rock, represented by ultramafic and mafic volcanic rocks (komatiite and tholeiite) at one end, and felsic volcanic rocks such as dacite, rhyolitic dacite and rhyolite at another end, with less or without andesite that is dominant in modern magmatic arcs (Hamilton, 1998, 2019). The komatiite and tholeiite in the Archean supracrustals or greenstones can be derived from the partial melting of mantle. Generally, komatiites in the Archean greenstones contains >18% MgO, which requires the degree of partial melting of mantle as high as 40-60%, indicating that the partial melting must have occurred at high temperatures, which have been estimated at more than 1600°C (Arndt et al., 2008; Campbell et al., 1989; Nisbet et al., 1993). On the other hand, felsic volcanic rocks of Archean greenstones are generally considered to have been derived from the partial melting of mafic lower crust heated by ultramafic to mafic magmas (Arndt, 2013; Campbell et al., 1989; Hamilton, 1998, 2019; Nisbet et al., 1993).

2.1.2. Structural patterns of Archean cratons

There are striking differences in structural styles between Archean cratons and post-Archean orogens, with the former dominated by dome-and-keel structures that mainly resulted from vertical tectonics, whereas the latter are dominated by linear structural belts that resulted from oceanic subduction and continental collision under plate tectonics regime. The dome-and-keel structures in the Archean granite-greenstone terranes consist of circular to elliptical (in plane) domes of granitoid (TTG) gneisses surrounded by trough-shaped keels, containing supracrustal (greenstone) cover rocks (Figure 3), of which the gneiss domes develop from the large-scale diapirism of voluminous TTG magmas and the keels form when the surrounding high-density ultramafic and mafic greenstones sink down, both of which reflect vertical motions as evidenced by vertical lineations in Archean granite-greenstone terranes (Figure 3). Such dome-and-keel structures characterize the major structural patterns of major Archean cratons, including the Barberton and Zimbabwe cratons in South Africa (Figure 3a; [Anhaeusser & Wilson, 1981](#); [Van Hinsbergen et al., 2011](#); [Van Kranendonk et al., 2014](#)), the Yilgarn and Pilbara cratons in Western Australia (Figure 3b; [Collins et al., 1998](#); [Hallberg & Glikson, 1981](#); [Nijman et al., 2017](#); [Van Kranendonk et al., 2004](#)), the Superior craton in North America (e.g., [Lin, 2005](#); [Lin & Beakhouse, 2013](#); [J. Zhang et al., 2014](#)), the Eastern Block in the North China craton ([Zhao et al., 2001](#); [Zhao, 2014](#)), etc. In these old cratons, the structure in the boundaries between the gneiss domes and the supracrustals (greenstones) is characterized by vertical shearing and stretching, as reflected by vertical stretching lineations or L-tectonites, indicating vertical motions, which contrast with the horizontal motions of plate tectonics as reflected by large-scale thrusting, multiple phases of folding, ductile shear zones, sheath folds, horizontal mineral stretching lineations.

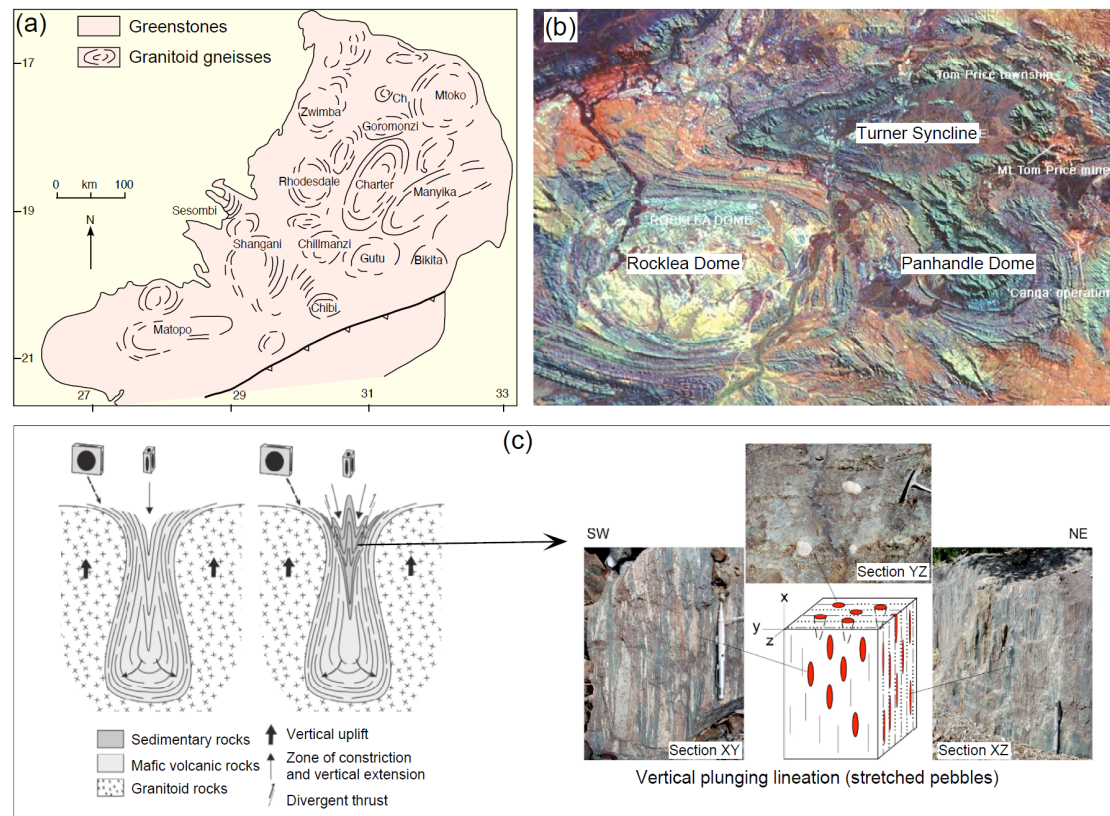


Figure 3. Dome-and-keel structures of Archean cratons. Neoproterozoic domes in the Zimbabwean Craton (Anhaeusser & Wilson, 1981); b) Archean domes (Zhao et al., 2001); c) Vertical stretch lineations or L-tectonites developing at boundaries between gneiss domes and supracrustals (J. Zhang et al., 2014).

2.1.3. Metamorphism of Archean Cratons

The metamorphism of Archean cratons is generally characterized by (1) large-scale regional metamorphism, in contrast with Proterozoic and Phanerozoic metamorphism that is limited to linear structural belts (orogens); 2) low- to medium-pressure greenschist facies, amphibolite facies and granulite facies metamorphism that happened at a normal geothermal gradient range (10-30 °C/km); 3) absence of high-pressure blueschist facies and high-pressure or ultrahigh pressure eclogite facies metamorphism; and (4) metamorphic P-T paths dominated by anticlockwise type involving isobaric cooling (Ge et al., 2003; Halpin & Reid, 2016; Jayananda et al., 2000; Kamber et al., 1996; Kramers et al., 2001; Maas & Henry,

2002; Mvondo et al., 2017; Percival, 1994; Raith et al., 1990, 1999; Rollinson, 1989; Sandiford, 1985; Tsunogae et al., 1992, 1999; Zhao et al., 1998, 2001, 2005; Zulbati & Harley, 2007), though clockwise P-T paths were also reported for some Archean terrains. As shown in Figure 4, for example, the metamorphic evolution of Neoarchean terrains in the Eastern and Western blocks in the North China craton, no matter whether they are low-grade granite-greenstone belts or high-grade gneiss terrains, is characterized by anticlockwise P-T paths mostly involving isobaric cooling (IBC). Similar anticlockwise P-T paths have also reported in other Archean cratons, such as the Kaapvaal craton (Kamber et al., 1996; Kramers et al., 2001; Rollinson, 1989; Tsunogae et al., 1992), Gawler craton (Halpin & Reid, 2016), East Antarctica (Sandiford, 1985; Tsunogae et al., 1999; Zulbati & Harley, 2007), Superior craton (Percival, 1994), Wyoming craton (Maas & Henry, 2002), Slave craton (Mvondo et al., 2017), Southern India craton (Raith et al., 1990, 1999).

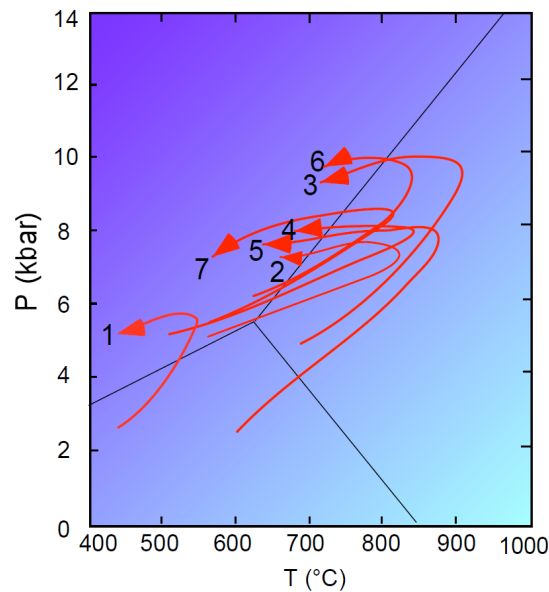


Figure 4. Anticlockwise P-T paths of end-Neoarchean metamorphism in the Eastern Block of the North China Craton (Zhao et al., 2001). 1-Western Shandong; 2-Eastern Hebei; 2, Western Liaoning (Jianping); 4-Northern Liaoning; 5-Eastern Shandong; 6-Miyun; 7-Southern Jilin.

The IBC-type anticlockwise P-T paths is generally considered to reflect metamorphism related to the intrusion and underplating of large voluminous mantle-derived magmas that may occur at the root of an arc or back-arc (Bohlen, 1991; Brown, 2006), intracontinental rifting zones (Sandiford & Powell, 1986), and mantle plumes or hot-spots (Jayananda et al., 2000; Zhao et al., 1998), in which mantle magmas heat continental crust, leading to temperature increasing but meanwhile the mantle magmas may erupt on the surface as continental flood basalts or intrude as sills into the crust, leading to thickening of the metamorphic crust. Therefore, at the early prograde stage, both temperature and pressure increase, but once the mantle magmas cease to rise, the heating stops and the metamorphic crust experiences cooling under a nearly constant pressure condition since there is no much change in the thickness of the crust, leading to an IBC-type anticlockwise P-T path (Zhao et al., 1998, 2001, 2005).

2.2. Island Arc Model for the Formation of Archean Continents

2.2.1. Major Evidence

Whether felsic continental crust originated from island arcs under plate tectonic regime or from some pre-plate tectonics (non-plate tectonics) depends on which model can satisfactorily explain the rocks and their geochemical, structural and metamorphic features as discussed above. Major lines of evidence supporting the island arc model for the formation of Archean felsic continental crust can be summarized as follows:

- (1) The metamorphosed igneous plutons in Archean cratons have rock associations similar to those in the roots of Phanerozoic magmatic arcs, with both consisting of Si-rich and Na-rich felsic granitoid (TTG) suites, though Phanerozoic magmatic arcs have more diorite, quartz diorite and monzogranite.

- (2) Subduction-related adakites in Phanerozoic magmatic arcs are geochemically similar to Archean high-pressure (or high- Al_2O_3) TTG. They are both characterized by relatively high La/Yb, Sr/Y, Al_2O_3 , Na_2O and Sr but relatively low Y, Yb, Ta, Nb and Ti, implying garnet and rutile existing as the residual phases during the partial melting of a mafic crust or as the cumulus phases during the crystallization of TTG magmas. In contrast, the subduction-related calc-alkaline granitoids in Phanerozoic arcs are geochemically similar to Archean low-pressure (or low- Al_2O_3) TTG. They are both characterized by relatively low La/Yb, Sr/Y, Al_2O_3 , Na_2O and Sr but relatively high Y, Yb, Ta, Nb and Ti, suggesting plagioclase and pyroxene existing as the residual phases during the partial melting of a mafic crust or as the cumulus phases during the crystallization of TTG magmas. Generally, subduction-related adakites are considered to have been derived from the partial melting of subducted oceanic slabs, whereas calc-alkaline granitoids were derived from the partial melting of juvenile mafic rocks that themselves were derived from the partial melting of hydrated mantle wedge above the subducted slab. Therefore, the island arc model established on plate tectonics can well explain the origins of Archean high- and low-pressure TTG rocks.
- (3) Geochemical and petrological experimental data have demonstrated that the source rocks to form Archean TTG rocks via partial melting should be garnet-bearing and/or rutile-bearing amphibolites or eclogites, both of which are abundant rocks in subduction zones, though no eclogites have been found in Archean terrains and some previously reported “Archean eclogites” have recently been confirmed to be Paleoproterozoic eclogites (Li et al., 2017).
- (4) Although gneiss domes are the dominant structural patterns of Archean cratons, intervening between gneiss domes are some linear structural belts

(keel structures) that underwent intense compressive deformation, similar to the structural styles of Phanerozoic orogens under a plate tectonic regime.

(5) Despite absence of high-pressure and ultrahigh pressure rocks in Archean craton, medium-high pressure rocks, and especially sillimanite-bearing pelitic gneisses/granulites are ubiquitous in Archean high-grade terrains, with metamorphic pressures as high as 8-10 kbar. The sedimentary protoliths of pelitic gneisses/granulites were shales or mudstones that were deposited in the basins, and thus without subduction under plate tectonic regimes, it's hard to imagine how these sedimentary rocks could be brought down to the lower crust depth where they experienced upper amphibolite- to granulite-facies metamorphism to form pelitic gneisses/granulites (Zhao et al., 2012).

(6) Although most cratons underwent metamorphism characterized by anticlockwise P-T paths involving isobaric cooling (IBC), clockwise P-T paths involving isothermal decompression were reported for a few Archean cratons (e.g., Hölttä & Paavola, 2000; Taylor et al., 2010; Valli et al., 2004). Such clockwise P-T paths involving isothermal decompression are generally considered to reflect metamorphism related to subduction or continent-continent collision (Brown, 1993; Harley, 1988, 1989; Zhao et al., 2000).

(7) The last but most important evidence supporting island arc model for the formation of felsic continental crust is that the partial melting of low-potassium tholeiitic rocks to form Archean TTG magmas needs sufficient water (H₂O), which favors subduction zone settings, not mantle plumes/hot-spots (Arndt, 2013; Martin et al., 2014).

2.2.2. Island Arc Model for the Origin of Continents

Magmatic arcs developing in the subduction zones can be divided into three types.

The first type is island arc, also called the intra-oceanic arc or Mariana-type arc that

415 develops from the subduction of an oceanic lithosphere below another oceanic
416 lithosphere (ocean-ocean subduction). Island arcs have a simpler crustal structure
417 and composition than arcs built on continental crust, because magmas erupted in
418 intra-oceanic arcs are not contaminated by ancient sialic crust and their
419 compositions more accurately record partial melting processes in the mantle wedge.
420 The second type is continental margin arc, also called the Andean-type arc that
421 develops from the subduction of an oceanic lithosphere beneath a continent
422 (ocean-continent subduction). The third type is a transitional one between the first
423 and second types, also called the Japanese-type arc whose early stage was a
424 continental margin arc (Andean-type arc), but with the further development of a
425 back-arc basin into a baby ocean, the magmatic arc was separated from the mainland
426 and thus the arc is getting more and more similar to the Mariana-type arc, like
427 today's Japan island in which most of old continental material has been assimilated.
428 Obviously, the second and third type arcs are not suitable for discussing the origin of
429 felsic continental crust since they developed on the existence of felsic continents.
430 Thus, only island arc that develops from ocean-ocean subduction is a possible site to
431 generate felsic continents ([Zhao & Zhang, 2021](#)).

432 An island arc generally experiences processes from an immature arc to a mature arc
433 ([Stern, 2011](#)). The former represents the initial stage of ocean-ocean subduction,
434 during which the dehydration of subducted oceanic slabs leads to the partial melting
435 of the mantle wedge to form basaltic magmas that rise and penetrate a thin oceanic
436 crust to form basalts on the ocean floor, rather than intermediate to acid volcanic
437 rocks such as andesite, dacite and rhyolite, since the magmas would not change
438 much in composition during their ascent as the magmas and oceanic crust have
439 similar mafic compositions. As a consequence, a large-scale felsic continental crust
440 would not develop from an immature arc, though minor amounts of adakitic rocks
441 may have developed due to the partial melting of the subducted slabs.

With arc magmas on-going, the basaltic arc is getting thicker and thicker so that the root of the arc can experience partial melting to form felsic magmas due to heating from the mantle magmas. The felsic magmas form andesite, dacite and rhyolite when they erupt on the surface and the diorite, quartz diorite, tonalite, trondhjemite, granodiorite suite when they crystallize underground, which are equivalent to low-pressure TTG rocks, whereas the partial melting of the subducted oceanic slabs would lead to the formation of high-pressure TTG rocks. The whole process leads to a transition from an immature arc to a mature arc (Figure 5a). With the further subduction and final closure of the subducted oceanic basins between island arcs, the arcs are growing larger and larger (Figure 5b) and finally collide each other to form a large-scale continent (Figure 5c), which is a generalized island arc model for the formation of felsic continents during Archean eon (Arndt, 2013; Leat & Larter, 2003; Wicander & Monroe, 2016).

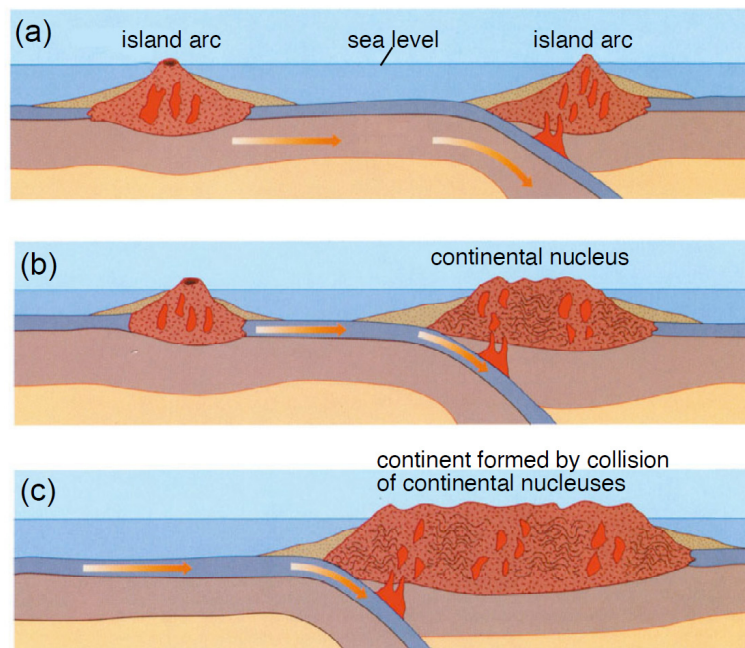


Figure 5. Cartoons showing how continents originated from island arcs under a plate tectonic regime (Wicander & Monroe, 2016). (a) A felsic island arc forms by subduction of oceanic lithosphere and partial melting of basaltic oceanic crust; (b) The island arc with continental composition in (a) collides with a previously formed felsic island arc, thereby

forming a continental core; (c) The process occurs again when the island arc in (b) collides with the evolving continent, thereby forming a craton, the nucleus of a continent.

The above island arc model can reasonably explain the formation of Archean low-pressure (low- Al_2O_3) and high-pressure (high- Al_2O_3) TTG rocks, but typical high-pressure or medium-pressure TTG rocks have not been found in modern island arcs like Mariana island arc in which most igneous plutons are calc-alkaline granitoids and adakitic rocks are mainly volcanic rocks, not plutons (Condie, 2014). In addition, many other geological factors are not supportive for the island arcs model for the origin of felsic continents, which will be discussed in the last section.

2.3. Oceanic Plateau Model for the Formation of Archean Continents

Although the island arc model can well explain the origin of Archean TTG rocks including both the high- and low-pressure types, it cannot satisfactorily explain the bimodal volcanic rocks from the Archean granite-greenstone terranes, which consist predominantly of komatiite-tholeiite at one end and dacite-rhyolite at another end, with less or absence of andesite that is dominant in modern magmatic arcs (Hamilton, 2019). Bimodal volcanic rocks are generally considered to have erupted in an extensional setting, rarely in a compressive tectonic environment.

2.3.1. Mantle Plume Model for the Ultramafic-Mafic Volcanic Rocks from the Archean Greenstones

Extensional tectonic settings allowing large voluminous mantle magmas to rise include intracontinental rifting zones, back-arc basins and mantle plumes/hot-spots. Generally, greenstones in Archean cratons are not limited to some linear structural belts, but irregularly surround granitoids (TTG) gneiss domes (Figure 3a-b), which, together with lack of typical rifting-type sediments in Archean greenstone sequences, precludes the possibility of an intracontinental rifting setting for volcanic protoliths

of the Archean greenstones. The possibility of back-arc basins for volcanic protoliths of the Archean greenstones is also very little because few typical subduction zones that should be associated with back-arc basins have been found in Archean cratons (Bédard, 2006, 2018; Hamilton, 1998, 2007, 2019; Stern, 2007, 2008). Classical lithotectonic elements that characterize a subduction zone include high- and ultrahigh-pressure blueschists/eclogites, ophiolites, paired metamorphic belts, etc., of which paired metamorphic belts are regarded as a hallmark for a subduction zone but have not been identified from Archean cratons (Brown, 2006; Brown et al., 2020). Therefore, the most possible tectonic setting for the volcanic protoliths of the Archean greenstones is related to mantle plumes (Campbell et al., 1989; Hill et al., 1992; Kent et al., 1996; Larson, 1991).

A mantle plume is a cylindrical thermal upwelling of large voluminous low-density material that originates deep in the mantle, either from the D" layer located in the core-mantle boundary at a depth of about 2,900 km or from the 670 km discontinuity at the base of the upper mantle (Campbell, 2005; Condie, 2001; Ernst & Buchan, 2003). The concept was originally proposed by W. Jason Morgan in 1971 on the basis of the Hawaii hot spots (Wilson, 1963) to explain the age-progressive chains of volcanic islands that stretch across the ocean basins (Morgan, 1971). A mantle plume is generally composed of a huge head and a narrow tail that is connected to the deep mantle (Campbell et al., 1989; Campbell & Griffiths, 1990, 1992; Hill et al., 1992; Kent et al., 1996; Larson, 1991; Peters & Day, 2017). During the ascent of a mantle plume, the head would trap large amounts of mantle material to enlarge itself and when it reaches the base of lithosphere, it becomes a flattened mushroom shape and experiences decompressional partial melting to form basaltic magmas. The basaltic magmas erupt on the surface within a very short period (< 1 million years), forming continental flood basalts on continents and oceanic plateaus with diameters ranging from 1000-2000 km on ocean floors (Abbott, 1996). When oceanic plateaus rise to the surface from the floors of the

ocean basins, they are also called oceanic islands. In current oceans under plate tectonic regimes, oceanic islands originated from a single mantle plume can form an age-progressive chain of volcanic islands, like the Hawaiian Emperor seamount chain, which can be utilized to estimate the speed and direction of plate motions.

The oceanic island basalts (OIB) are distinctively different from mid ocean ridge basalts (MORB) and island arc basalts (IAB) in that the former erupt at high temperature in areas far away from the mid ocean ridges and subduction zones, on a scale of several millions km³, geochemically characterized by enrichments in LILE, LREE and high Sr⁸⁷/Sr⁸⁶, Nd¹⁴³/Nd¹⁴⁴, Pb²⁰⁷/Pb²⁰⁴, and He³/H⁴ ratios (Farley et al., 1992; Hart et al., 1992). Owing to these features, more and more researchers favor an oceanic plateau model for the origin of felsic continental crust because the model can well explain the formation of both bimodal volcanic rocks and TTG-dominant granitoids in the Archean granite-greenstone terranes (Campbell et al., 1989; Campbell & Griffiths, 1990, 1992; Hill et al., 1992; Hill, 1993; Kent et al., 1996; Larson, 1991).

The major volcanic rocks of Archean greenstones are mafic tholeiites and ultramafic komatiites. Some researchers once interpreted Archean komatiites as the early cumulates crystallizing from the tholeiitic magmas, and based on high Mg number of komatiites, they estimated that the temperature of Archean mantle was 200-300°C higher than that of today's mantle (McKenzie, 1984; Sleep & Windley, 1982). However, later studies indicated that the mantle temperature did not reduce so much during the past 3.5 billion years, only dropping 97°C (Abbott & Mooney, 1995; Galer, 1991), and Archean komatiites may not have been the early cumulates for the following considerations:

- (1) Nearly all Archean komatiites have MgO contents more than 18%, whereas tholeiites from the Archean greenstones have MgO contents no more than

540 14%, demonstrating a significant compositional gap between komatiites and
541 tholeiites from the Archean greenstones;
542 (2) Komatiites and tholeiites from the Archean greenstones exhibit different
543 isotopic compositions (Abbott, 1996; Tomlinson & Condie, 2001);
544 (3) Experiments have precluded possibility that large amounts of olivine were
545 cumulated from tholeiitic magmas at the early stage (e.g., Drummond, 1988);
546 (4) As mentioned early, the rock-forming temperature of komatiites is as high as
547 1600 °C or above, much higher than the rock-forming temperature
548 (1200-1400°C) of tholeiites.

549 Considering that the rock-forming temperatures and geochemical compositions of
550 komatiites and associated tholeiites from Archean greenstones are similar,
551 respectively, to those of the tail and head of a mantle plume derived from the D”
552 layer of the core-mantle boundary, Campbell et al. (1989) proposed that the Archean
553 komatiites represented the melting products of the tail of a mantle plume, whereas
554 the tholeiites from the Archean greenstones were derived from the decompressive
555 partial melting of the huge head of a mantle plume when it reached the base of
556 lithosphere. In fact, Condie (1975) had proposed a similar model as early as in the
557 1970s, though at that time he did not establish such a cause-and-result link between
558 the tail and head of a mantle plume and komatiites and tholeiites from Archean
559 greenstones, respectively. So far, this model has been accepted by more and more
560 researchers (Abbott, 1996; Bédard, 2006; Brown et al., 2020; Campbell & Hill, 1988;
561 Condie, 1994, 1997; Desrochers et al., 1993; Hill et al., 1992; Hill, 1993; Rey et al.,
562 2003; Tomlinson & Condie, 2001).

563 2.3.2. Oceanic Plateau Model for the Origin of Continents

564 The above successful application of the mantle plume model to the formation of
565 komatiites and tholeiites from Archean greenstones itself is not enough to enable the
566 model to explain the origin of felsic continents because the Archean greenstones

may not be part of continental crust, most likely representing Archean oceanic crust. What represents the Archean felsic continental crust are Archean TTG-dominated granitoid rocks that make up the 60-70% of total exposure of Archean cratons (Abbott, 1996; Arndt, 2013; Zhao & Zhang, 2021). Therefore, whether the mantle plume model is successful in explaining the origin of Archean continents depends on whether the model can reasonably explain the formation of Archean TTG-dominant granitoid rocks or not.

As mentioned early, geochemical data and experiments indicate that like other calc-alkaline granitoids, TTG rocks can also be derived from the partial melting of hydrated basaltic rocks. Thus, the origin of Archean TTG rocks depends on two issues: (1) where and how were the basaltic protoliths of Archean TTG rocks extracted from mantle and (2) how was the basaltic crust extracted from the mantle transformed to Archean TTG? For the first issue, mantle plumes may be the best candidate as discussed above. Considering that TTG rocks make up more than 60-70% of Archean cratons and their geochemical differences from Phanerozoic calc-alkaline granitoids (see Section 2.1.1), we think that the transformation of basaltic crust into Archean TTG-dominant felsic continental crust requires the following three conditions:

- (1) Existence of large igneous provinces (LIP) with basaltic rocks at least three times as much as the amount of Archean TTG. Petrological experiments demonstrate that, to produce Archean TTG, the degree of partial melting of basaltic rocks must be lower than 30% because, when the partial melting degree is higher than 30%, garnet would be melt and enter into the TTG magmas, which would significantly increase HREE and thus reduce La/Yb ratios, making the magmas geochemically different from Archean TTG rocks that are characterized by high LREE and low HREE, as reflected by high La/Yb ratios. This means that, to make the partial melting degree lower than 30%, one portion of TTG at least needs three portions of basaltic protoliths.

- (2) Existence of a very thick basaltic crust to make the partial melting occur in the garnet-stable field (see discussion in Section 2.1.1.).
- (3) The basaltic protoliths must have been hydrated so that aqueous partial melting of basaltic crust to produce TTG magmas occurs under H₂O-saturation conditions. Experiments have shown that partial melting of basaltic crust would be going extremely slowly under H₂O-free (dry) conditions.

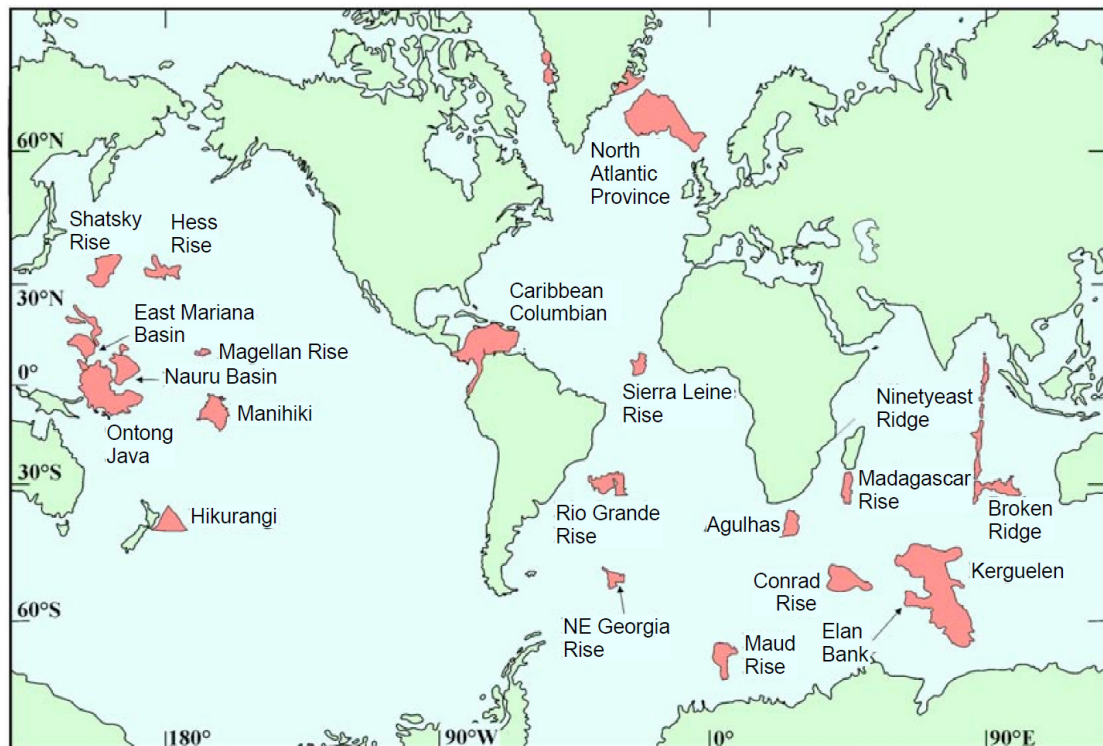


Figure 6. A Map showing all major oceanic plateaus formed within the last 150 Ma (Kerr, 2015).

Oceanic plateaus formed by mantle plumes seem to meet the first and second conditions discussed above. As shown in Figure 6, most of modern oceanic plateaus occur as large igneous provinces (LIP) that make up large areas of over-thickened oceanic crust (Coffin & Eldholm, 1994; Ernst, 2014; Kronenke, 1974). For example, the Ontong-Java oceanic plateau is about 500 km wide and 3000 km long,

occupying an area of $\sim 1,900,000 \text{ km}^2$, and the Ice Island and Kerguelen oceanic plateaus also make up more than $1,500,000 \text{ km}^2$ (Figure 6; [Abbott, 1996](#); [Coffin & Eldholm, 1994](#)). Such huge volumes of basaltic oceanic crust are enough to meet the above first condition that requires the existence of large igneous provinces (LIP) with basaltic rocks at least three times as much as Archean TTG.

The second condition depends on the thickness of an oceanic plateau. Although the thickness of the Ontong-Java oceanic plateau was estimated at 35-42 km based on seismic wave velocity and rock density ([Furumoto et al., 1976](#)), most of other oceanic plateaus have a thickness of 20-30 km ([Abbott & Mooney, 1995](#)), which seems to be insufficient to meet the second condition that requires a very thick oceanic crust so that the partial melting to form high-pressure (high- Al_2O_3) TTG magmas can occur in the garnet-stable field. However, there is a broad consensus that the Archean mantle was hotter than today's mantle, which allowed more oceanic crust to have been produced, and thus the Archean oceanic crust must have been thicker than modern oceanic crust ([Abbott & Mooney, 1995](#)). [Abbot and Mooney \(1995\)](#) utilized thermal modeling to estimate that the temperature of Archean mantle was at least 93°C higher than that of the current mantle. Combining this with seismic wave velocity and rock density, [Abbot and Mooney \(1995\)](#) estimated that the thickness of Archean oceanic plateaus was around 40 km. This was supported by [Kent et al. \(1996\)](#) who, using the adiabatic partial melting model of [McKenzie and Bickle \(1988\)](#) at about 1600°C , estimated the average thickness of Archean oceanic plateaus at about 43 km, which is close to the minimum crustal thickness that allows the partial melting of basaltic rocks to occur in the garnet field in order to produce medium- and high-pressure type TTG magmas with high La/Yb ([Arndt, 2013](#); [Arth et al., 1978](#); [Barker & Arth, 1976](#); [Barker, 1979](#); [Condie, 2014](#); [Martin et al., 2014](#); [Moyen & Laurent, 2018](#)). On the other hand, [Kent et al. \(1996\)](#)'s modeling demonstrated that the Archean crust of basaltic oceanic plateaus are komatiitic with MgO as high as $\sim 19\%$, and in such high MgO rocks, metamorphic

reactions to form garnet may have occurred at 7-8 kbar (Brown et al., 2020; Johnson et al., 2017), which is consistent with the ubiquitous presence of a medium-pressure granulite-facies assemblage (garnet + orthopyroxene + clinopyroxene + plagioclase) in Archean high-grade gneiss terrains (see discussion in Section 1.3), whereas high-pressure granulite-facies assemblage (garnet + clinopyroxene + plagioclase + quartz) or eclogite-facies assemblage (garnet + omphacite) is very rare or absent from Archean terranes. Zellmer et al. (2012) also confirmed that the garnet-stable field can extend to the lower crustal level where mafic crust experiences partial melting to form adakitic or high-pressure type TTG magmas. In addition, based on the results of their partial melting experiment, Qian and Hermann (2013) demonstrated that the most appropriate depth of a mafic lower crust for partial melting to form adakitic and TTG magmas is at 30-40 km, whereas a depth of more than 45-50 km is unfavorable. More recently, Smithies et al. (2019) also argue that there is no direct evidence supporting that the Archean TTG rocks were derived from the partial melting of mafic crust under high-pressure conditions. Taken together, oceanic plateaus can meet the requirement for a thick basaltic crust where the partial melting of basaltic rocks to form Archean TTG rocks occur in the garnet-stable field.

However, oceanic plateaus formed by mantle plumes seem to be difficult to provide enough H₂O for the aqueous partial melting of basaltic rocks to form TTG magmas as the above third condition required. The oxygen isotopic compositions of zircons indicate that most Archean TTG gneisses have $\delta^{18}\text{O}$ values ranging between 5.5-6.5‰, with some reaching to 7-9 ‰ in local areas (e.g., Superior craton), much higher than those $\delta^{18}\text{O}$ value for the mantle (5.3‰), implying that the basaltic source rocks underwent hydration from the surface before the partial melting (Condie, 2014). This means that the partial melting of basaltic crust to form Archean TTG magmas must have occurred in the upper part that was interacted with or hydrothermally altered by the surface water before the partial melting (Condie,

2014). Such an interpretation favors the partial melting of descent subducting slabs, but disfavors the oceanic plateau model in which the partial melting must have occurred at the dried base of the oceanic plateau, which is regarded as the fatal defect of the oceanic plateau model (Arndt, 2013). Even so, compared with the island arc model for the origin of felsic continents, oceanic plateau models have been applied to interpreted the origins of Archean granite-greenstone terranes in major cratonic blocks in the world (e.g., Abbott & Mooney, 1995; Abbott, 1996; Bédard, 2006, 2018; Brown et al., 2020; Campbell & Hill, 1988; Campbell et al., 1989; Campbell & Griffiths, 1990, 1992; Condie, 1975, 1994, 1997, 2014; Johnson et al., 2017; Moyen, 2011; Moyen & Laurent, 2018; Puchtel et al., 1998; Sanislav et al., 2018; Smithies et al., 2009; Tomlinson & Condie, 2001; Van Kranendonk et al., 2004, 2007a, 2007b, 2010, 2011, 2014; Whalen et al., 2002). Further supports for the oceanic plateau model for the origin of felsic continents have come from discoveries of TTG and relevant felsic rocks in modern oceanic plateaus (Hastie et al., 2010; Ponthus et al., 2020; White et al., 1999; Willbold et al., 2009).

As shown in Figure 7, Van Kranendonk et al. (2007a) applied the oceanic plateau model to interpret the formation of Paleoproterozoic (3.6-3.2 Ga) granite-greenstone terranes in East Pilbara, Western Australia. In the model, Van Kranendonk et al. (2007a) proposed that the huge head of a mantle plume underwent decompressional melting when it reached the base of the lithosphere, and the melts rose and erupted on the ocean floor, forming a basaltic oceanic plateau. Some komatiites or komatiitic basalts may have formed in the oceanic plateau when the tail of the mantle plume reached the base of the lithosphere. Meanwhile, the heat from the mantle plume caused multiple phases of partial melting of the pre-existing mafic crust and/or the base of the oceanic plateau to form 3.53-3.24 Ga granitoid rocks, leading to the formation of a felsic continental craton (Figure 7a) and a sub-continental residual mantle core (Figure 7b).

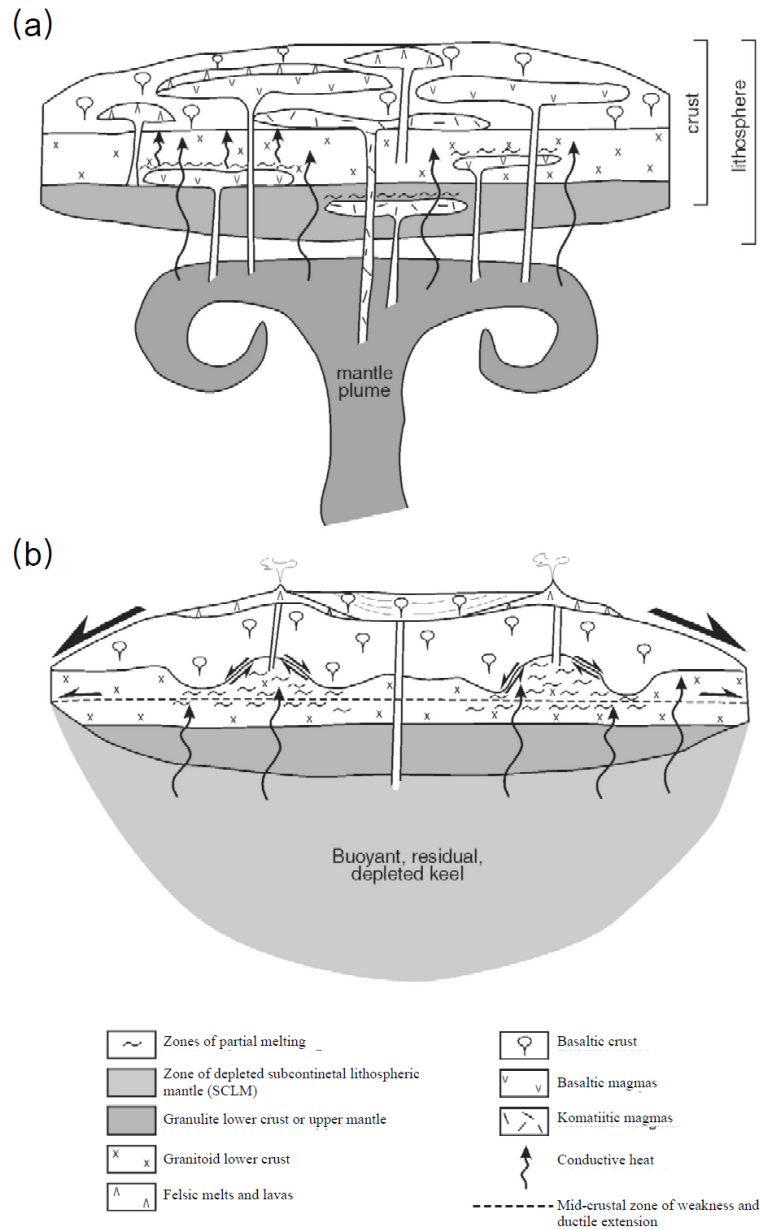


Figure 7. A schematic model showing the development of the East Pilbara granite-greenstone terrane from a thick oceanic plateau that formed by mantle plumes (Van Kranendonk et al., 2007a; Van Kranendonk, 2010).

As one of modified oceanic plateau models for the formation of felsic continents, Bédard (2006) proposed a catalytic delamination-driven model for coupled genesis of Archaean crust and sub-continental lithospheric mantle (Figure 8). In his model, a large mantle plume releases melts that construct a thick volcanic crust (e.g., oceanic

plateau). The underplating magmas of a mantle plume cause melting at the base of the basaltic crust to form the first generation of tonalitic magmas with complementary eclogitic to pyroxenitic restites (Figure 8a). The dense eclogitic to pyroxenitic restites delaminate into the deep mantle, triggering the ascent of mantle diapirs, which reach the base of the mafic crust and causes the partial melting to form tonalitic magmas and eclogitic restites again (Figure 8b-c). Similarly, the newly formed eclogitic restites delaminate into the deep mantle and trigger the ascent of mantle diapirs, leading to the partial melting of basaltic crust to form TTG magmas (Figure 8d). A similar model was also proposed by [Smithies et al. \(2009\)](#).

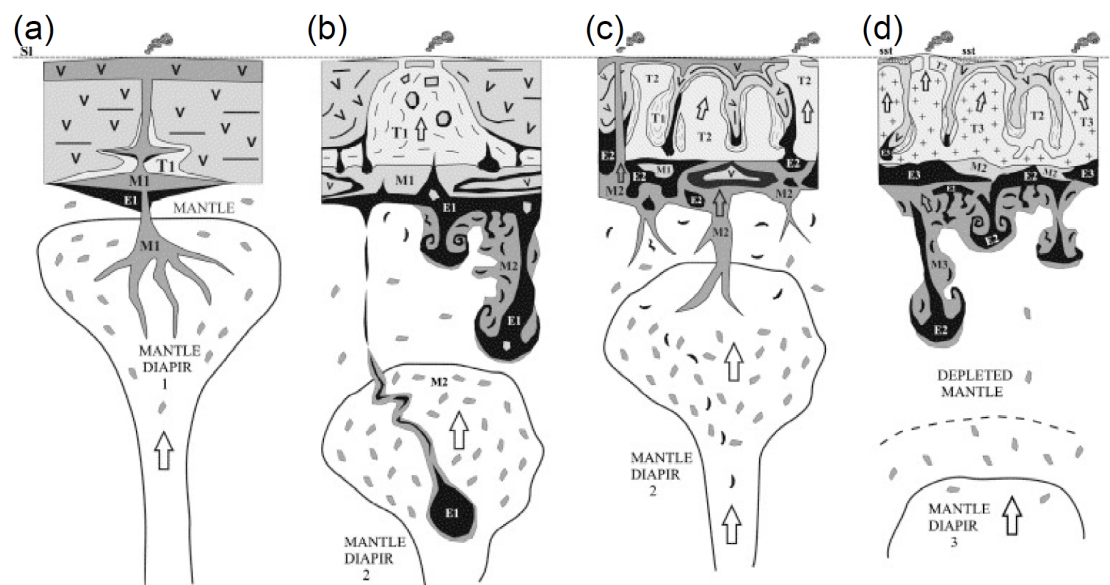


Figure 8. Cartoons illustrating the delamination-driven tectonomagmatic model ([Bédard, 2006](#))

3. Accretion of Continents: A Global Perspective

As discussed above, there is still no broad consensus regarding the origin of felsic continents with one school of thought favoring an island arc model ([Arndt, 2013 and references therein](#)), whereas others advocate an oceanic plateau model ([Van Kranendonk et al., 2007a and references therein](#)). No matter which model is correct,

these two-end-member models only account for the formation of Archean continental nucleuses, whereas present-day's continents must be more complicated and have developed through the accretion (growth) of these Archean continental nucleuses. Available data have demonstrated that the subduction and associated continental accretion under modern-style plate tectonic regimes play an important role in the development from Archean continental nucleuses to present continents (Hoffman, 1988). In this section, we will discuss where, when and how Archean continental nucleuses underwent accretion to form the present-day's continents.

3.1. Accretion of North American continent

Among all the continents, the North America preserves the best and most complete geological records of how small pieces of cratonic blocks gradually grow to the current continent, mainly by oceanic subduction, arc accretion and continental collision processes. The North American continent is mainly composed of the Precambrian North American Craton in the center, the early Paleozoic Appalachia Orogen in the east and the Meso-Cenozoic Cordillera Orogen in the west (Figure 9). The North American Craton (together with Greenland also known as the Laurentia) is one of the oldest and largest cratons in the world. It was amalgamated by several Archean provinces through Proterozoic collisional and accretionary orogenic belts (Canil, 2008; Hoffman, 1988).

3.1.1. Archean Provinces

The Archean provinces, including the Slave, Rae, Hearne, Wyoming, Superior and Nain, are clustered in the northern two thirds of the North America continent and underlie most of the Canadian shield. Each province has an Archean basement comprising a granite-greenstone terrain, overlain by erosional remnants of early Proterozoic sedimentary cover of platformal facies (Hoffman, 1988).

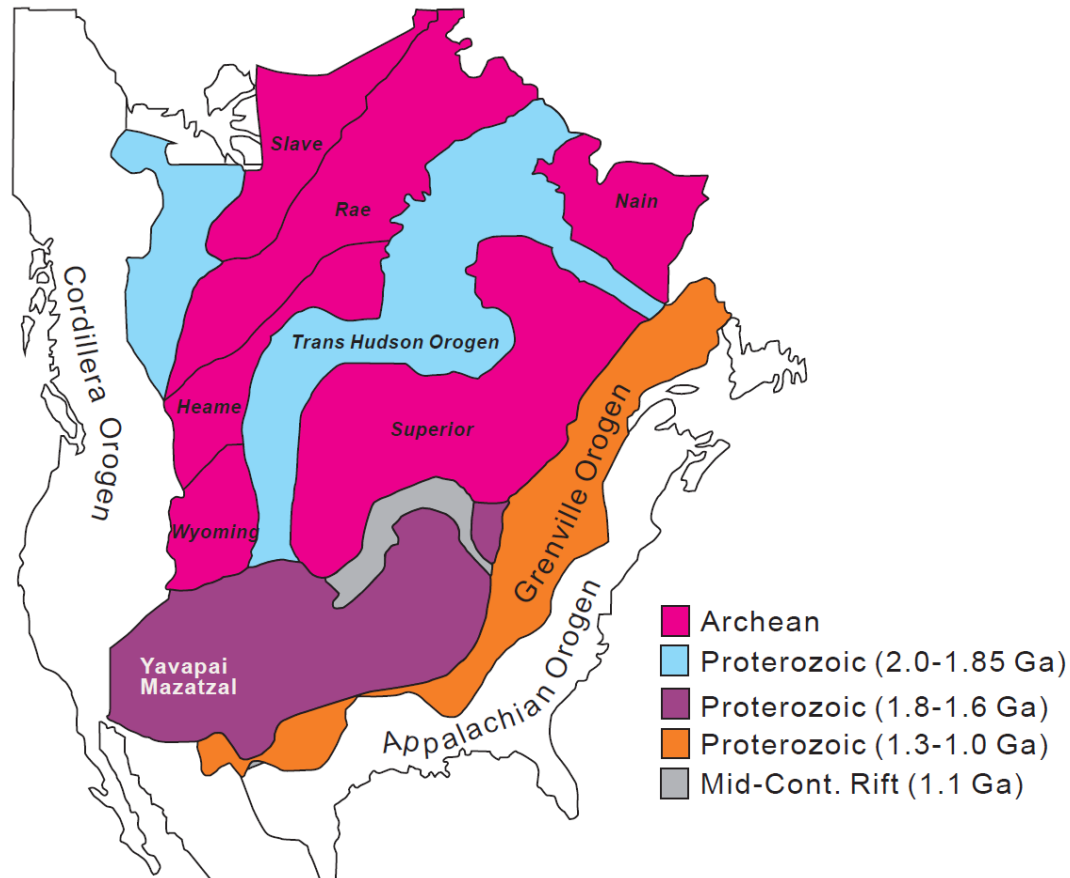


Figure 9. Tectonic sketch map of the North American continent, showing the major Precambrian cratons and Phanerozoic orogens, modified from Hoffmann (1988) and Canil (2008).

The Slave province is an Archean granite-greenstone terrane in the northwestern part of the North America. The main part of the province has an elliptical shape and comprises ca. 172,500 km². Its history spans the interval from 3.48 Ga to 2.6-2.5 Ga, with most of the volcanic and sedimentary rocks formed between 2.7 and 2.65 Ga by oceanic subduction and arc accretion (Kusky, 1989; Kusky et al., 2013). Although initially described as a uniform granite-greenstone terrain, the Slave province is more recently viewed as a tectonic collage consisting of a Mesoproterozoic micro-continental nucleus that was enlarged by the addition of Neoproterozoic juvenile

terrane. The Slave province is subdivided into 5 tectonic domains, at least four of which may be viewed as separate tectonic terranes (Helmstaedt, 2009).

The Rae province can be divided into an ancient (>3.0 Ga) southwestern component and a more juvenile (<3.0 Ga) northeastern component. Evidence for episodic reworking of the evolved southwestern component is recorded in the Sm-Nd and U-Pb signatures of younger Archean and Paleoproterozoic intrusive rocks and sediments (Hartlaub et al., 2005).

To the south of the Rae province, the Hearne province has much in common with the Rae province. It contains gneiss as old as 3.48 Ga and submarine mafic-intermediate-felsic volcanics and associated graywackes of ca. 2.7 Ga.

The Wyoming province was a >100 000 km² Mesoarchean craton that was modified by Neoarchean magmatism and tectonism and Proterozoic extension and rifting. Isotopic evidence for widespread old crust and the local occurrence of early and Mesoarchean rocks suggest that the northern and central portions of the Wyoming province were part of a Mesoarchean craton, a southward-younging series of Neoarchean volcanic arcs were subsequently accreted to the continental core of Paleoproterozoic to Mesoarchean age (Chamberlain et al., 2003). The Beartooth Mountains of the northern Wyoming province contain a suite of ca. 2.8 Ga calc-alkaline and tholeiitic andesite, indicative of a Neoarchean convergent margin process (Mueller & Wooden, 1988). A 2.68-2.67 Ga active margin with accretionary prism, fore-arc basin, magmatic arc and back arc basin was suggested to be developed in the western Wyoming province (Frost et al., 2006). A major episode of Neoarchean crustal growth involved both the lateral accretion of juvenile terranes and the intrusion of arc magmas formed from mantle-derived and (or) juvenile crustal sources occurred within the Wyoming province, and was driven by geologic processes very similar to modern plate tectonics (Frost et al., 2006).

The Superior province is the world's largest Archean craton and provides information on both the nature and scale of ancient process. Five discrete accretionary events assembled fragments of continental and oceanic crust into a coherent Superior craton by 2.6 Ga. They exhibit similar sequences of events at ~10 million-year intervals: cessation of arc magmatism, early deformation, synorogenic sedimentation, sanukitoid magmatism, bulk shortening, regional metamorphism, late transpression, orogenic gold localization, emplacement of crust-derived granites, and postorogenic cooling (Percival et al., 2006). Similarly, many studies suggest that the geological evolution of the southwestern Superior province can be best explained by convergent plate margin processes (Daigneault et al., 2002; Polat et al., 2017). Neoarchean S-type granites were emplaced along some terrane boundary zones in the western Superior province and are interpreted as a marker of Archean collision zones (Yang et al., 2019).

The Nain (or North Atlantic) province lies in the northeastern part of the Laurentia. It is composed of the Saglek block in the north and Hopedale block in the south, which experienced distinct thermotectonic histories until Neoarchean. The Saglek block comprises amphibolite- to granulite-facies orthogneisses and supracrustal rocks ranging from Paleoarchean (>3.7 Ga) to Neoarchean (ca. 2.7 Ga); the Hopedale block comprises crust ranging from 3.3 to 2.8 Ga with mainly greenschist- to amphibolite-facies metamorphism. These two blocks juxtaposed to form a single, stable cratonic mass during the Neoarchean (ca. 2.55 Ga) (Connelly & Ryan, 1996).

3.1.2. Paleoproterozoic orogenic Belts

The above Archean provinces record a long history of Archean tectonism, after which many underwent 2.45-2.1 Ga rifting, as shown by thick miogeoclinal successions on the edges of Archean cratons (Corrigan et al., 2005). The collision between the Archean provinces generated a sequence of Paleoproterozoic orogenic

belts, which led to assembly of a continental core of a scale compatible with modern continents (Whitmeyer & Karlstrom, 2007).

The Thelon orogen resulted from a dextral-oblique collision between the Slave and Rae provinces, followed by the indentation of the Rae hinterland by the Slave foreland province (Hoffman, 1988). The main magmatism related to this collision event took place at 2.02-1.91 Ga.

Between the Rae and Hearne provinces lies the ~2800-km-long Snowbird Tectonic Zone. It is one of the most controversial tectonic features of the North American Craton. It was originally proposed as a Paleoproterozoic continental suture (Gibb & Walcott, 1971), but was later interpreted as an intracontinental shear zone at 2.6 Ga with limited Paleoproterozoic reworking (Hanmer et al., 1994). Field investigations revealed a major granulite facies mylonite belt that records deformation and metamorphism at several intervals in the Archean and early Proterozoic. Early assemblages are dominated by granulite grade gneisses that were deformed in a major left-lateral strike-slip shear zone at ca. 3.2 Ga. The major episode of deformation occurred at ca. 2.6 Ga, again at granulite facies in a dominantly right-lateral strike-slip shear zone (Kopf, 2002). Eclogites occurs in East Athabasca area in association with a variety of high-pressure granulites that record a complex metamorphic history from 2.6 to 1.9 Ga. The timing of peak eclogite facies metamorphism was constrained at 1.9 Ga (Baldwin et al., 2004). Metamorphic and geochronological data revealed that a 1.9 Ga medium- to high-pressure belt extends along most of this tectonic zone, and it was regarded as a collisional belt marking a pre-1.865 Ga phase of the Hudsonian orogeny involving microcontinent accretion that was fundamental to the growth of Laurentia (Baldwin et al., 2003; Berman et al., 2007).

The 500-km-wide Trans-Hudson orogen forms a convex to the northwest, bounded by the Hearne and Superior provinces (Figure 9). The orogen extends southward to

839 the area between the Wyoming and Superior provinces as far as south Dakota, and
840 to the northeast the main part of the orogen passes beneath the Paleozoic Hudson
841 Bay Basin (Hoffman, 1988). The Trans-Hudson orogen is distinguished by the
842 largest exposure of juvenile, arc-derived Proterozoic crust in the Canadian shield.
843 Isotopic and structural data revealed that the Trans-Hudson orogen resulted from an
844 arc-continent collision followed by terminal continent-continent collision at
845 1.83-1.80 Ga (Bickford et al., 1990; Corrigan et al., 2005). It has four principle
846 tectonic domains: (1) a narrow eastern foreland; 2) a broad collage of imbricated
847 magmatic arc, marginal basin and collisional basin rock which structurally overlies
848 Archean basement; 3) an Andean-type continental margin batholith; and (4) a broad,
849 reworked northwestern hinterland (Lewry et al., 1994; Lucas et al., 1993). Eclogite
850 rocks with comparative pressure-temperature conditions to that from the Himalaya
851 orogen have recently been identified within the Trans-Hudson orogen, which imply
852 that modern-day plate tectonic processes featuring deep continental subduction
853 occurred at least 1830 million years ago (Weller & St-Onge, 2017). The
854 Trans-Hudson orogen represents the 1.85-1.78 Ga amalgamation of the Hearne,
855 Wyoming, and Superior provinces into a cratonic core of the North American
856 continent (Weller & St-Onge, 2017), and is regarded as a prototype of modern
857 accretionary processes (Corrigan et al., 2009).

858 In the northeastern part of the North America continent, there are two major
859 Paleoproterozoic orogenic belts, namely the Torngate orogen and New Quebec
860 orogen, respectively. The Torngate orogen is the result of oblique collision between
861 the Nain province in the north and the Rae province in the south (Hoffman, 1988). It
862 is regarded as a narrow doubly divergent collisional orogen (Rivers et al., 1996).
863 Subduction occurred below the Nain province from ca. 1.91-1.87 Ga, and collision
864 between the cratons may have occurred between 1.87 and 1.84 Ga (Scott, 1998).
865 Subduction-related calc-alkaline magmatism of mafic to intermediate composition
866 has been identified along the Torngate orogen (Rawlings-Hinchey et al., 2003). The

867 New Quebec orogen is bounded to the southwest by the flexurally arched Archean
868 foreland of the Superior province and to northeast by the allochthonous Archean
869 hinterland of the Rae province (Hoffman, 1988). It is a Paleoproterozoic fold and
870 thrust belt active from 2.17 to 1.77 Ga and records the collisional history between
871 the Rae and Superior provinces (Machado et al., 1997).

872 3.1.3. Paleoproterozoic Accretion

873 The 2.0-1.8 Ga collision-dominated orogens welded the Archean provinces into the
874 core of the North American continent. At the same time and subsequently, island
875 arcs with mainly juvenile crust developed on the margins of the Archean provinces,
876 which led to outboard growth of the continent.

877 The Wopmay orogen evolved on the active western margin of the Slave province
878 (Hoffman, 1988). Remnants of three compositionally diverse magmatic arcs
879 (1.94-1.90 Ga, 1.89-1.88 Ga, and 1.87-1.84 Ga) are preserved in the Wopmay
880 orogen, and Nd isotopic data reveal the involvement of 2.0-2.4 Ga crust (Bowring &
881 Podosek, 1989; Cook, 2011). There are no exposures of Archean crust west of the
882 Wopmay fault.

883 The Penokean orogen records the Paleoproterozoic growth of the southern margin of
884 the Superior province. It comprises a northern domain of sedimentary and minor
885 tholeiitic volcanic rocks deposited on Archean basement of the Superior province
886 and a southern domain composed mainly of Paleoproterozoic volcanic and plutonic
887 rocks belonging to island-arc suites (Hoffman, 1988). The main orogenic events
888 occurred roughly coeval with the Trans-Hudson deformation, which deformed and
889 metamorphosed Archean basement and Paleoproterozoic superacrustal rocks of the
890 Superior province along the southern margin of Laurentia (Whitmeyer & Karlstrom,
891 2007). The Penokean orogeny began at ca. 1.88 Ga when an oceanic arc
892 (Pembine-Wausau terrane) collided with the southern margin of the Superior
893 province marking the end of a period of south-directed subduction. The docking of

the buoyant craton to the arc at ca. 1.87 Ga resulted in a subduction jump to the south and development of back-arc extension both in the initial arc and adjacent craton margin to the north, which was followed by the accretion of the Marshfield terrane to the Superior province at ca. 1.85 Ga resulting in the development of foreland basin (Schulz & Cannon, 2007). Nd isotopic data for igneous rocks revealed the Penokean events involved major growth of new crust from the mantle, with only limited recycled Archean materials (Barovich et al., 1989).

By ca. 1.80 Ga, the Archean provinces (Slave, Rae, Hearne, Wyoming, Nain and Superior) had amalgamated to form the north-central part of the North American craton by a rapid succession of microcontinent collisions (Hoffman, 1988). The orogens involved are characterized by reworking of Archean crust combined with addition of ca. 2.0-1.8 Ga juvenile crust. Subsequent late Paleoproterozoic (1.80-1.60 Ga) juvenile crust was added mainly to the south of the united Archean provinces. These include the Central Plains, and Yavapai and Mazatzal orogens (Figure 9).

The Central Plains orogen is ca. 1000 km long and ca. 500 km wide which truncates the southern margin of the Superior province and its marginal Paleoproterozoic orogens, the Trans-Hudson (1.95-1.85 Ga) and the Penokean (1.90-1.83 Ga). It is composed of metamorphic and granitoid rocks in the range 1.80-1.63 Ga (Sims & Petermar, 1986).

The Yavapai orogen records the accretion of dominantly juvenile arc crust from 1.80 to 1.70 Ga, including outboard development and collisions of arcs from 1.78 to 1.72 Ga, and an orogenic peak at 1.71-1.68 Ga that resulted in a progressive amalgamation of Yavapai crust to Laurentia (Whitmeyer & Karlstrom, 2007). Accretion and associated deformation took place during several pulses within a long orogenic progression. The oldest rocks include 1.80-1.75 Ga granite-greenstone associations that consist of metabasalt, metaandesite, metarhyolite, and associated

volcanic-sedimentary rocks intruded by calc-alkaline granitoids. A near continuum of deformation between 1.78 and 1.68 Ga are recorded in the Yavapai orogen. Volcanic and granitoid batholith from 1.80 to 1.75 Ga are interpreted to record subduction-related accretion and outboard collision to form the 1.80-1.75 Ga arcs. Southeast migration of granitoid magmatism from 1.80 to 1.75 Ga are explained in terms of subduction flip and from south dipping in the Penokean orogeny to north dipping in the Yavapai orogeny (Holm et al., 2005).

The Mazatzal orogen is marked by exposures of Paleoproterozoic rocks younger than 1.70 Ga in New Mexico, southwestern Arizona, and northern Sonora, Mexico. This orogen mainly consists of juvenile arc-related rocks and associated sedimentary rocks. Nd and Pb isotopic data reveal crust that has a slightly younger mantle derivation model age (1.8-1.7 Ga) than the adjacent Yavapai orogen (Aleinikoff et al., 1993). Geochronological data suggest that the Mazatzal orogeny occurred from 1.68 to 1.64 Ga (Karlstrom & Bowring, 1988), followed by post-orogenic magmatism and extension from 1.63 to 1.62 Ga (Amato et al., 2008).

3.1.4. Mesoproterozoic Accretion-Collision - Grenville Orogen

The Grenville orogen is a globally distributed plate convergent event over a protracted period from ca. 1.3 to 0.9 Ga took place in Laurentia and on many other continents, and culminated in continent-continent collisions that facilitated the final assembly of Rodinia. The Grenville orogen in Laurentia is a NE-trending orogenic system truncating the Archean Superior province and Paleoproterozoic Yavapai, Penokean, and New Quebec orogens. It records an 800 m.y. history of accretionary orogenesis along an east- and southeast-facing, predominantly convergent margin. The exposed segment of the orogen was derived largely from reworked Archean to Paleoproterozoic Laurentian crust, products of a long-lived Mesoproterozoic continental-margin arc and associated back arc, and remnants of one or more

947 accreted mid-Mesoproterozoic island-arc terranes (Hynes & Rivers, 2010; Tollo et
948 al., 2004).

949 The initial stage of the Grenville orogen cycle (Elzevirian orogeny) sutured the
950 Elzevir and Frontenac blocks to the eastern margin of Laurentia ca. 1.3-1.2 Ga,
951 followed by widespread intrusion of the anorthosite-mangerite-charnockite-granite
952 (AMCG) suite from ca. 1.19 to 1.11 Ga likely resulted from orogen collapse of
953 overthickened crust (Whitmeyer & Karlstrom, 2007). The Ottawa orogeny spans
954 the interval ca. 1.09-0.98 Ga and induced renewed northwest thrusting and
955 imbrication of terranes in southeast Canada, involving widespread deformation
956 along the eastern margin of Laurentia, when major collisions appear to have taken
957 place with one or more larger continental masses, probably the Amazonia, at ca.
958 1.09-1.03 Ga (Hynes & Rivers, 2010).

959 **3.1.5. Paleozoic Accretion and Collision - Appalachian Orogen**

960 The Appalachians are a Paleozoic orogen that formed in a complete Wilson cycle
961 along the eastern Laurentia margin following the breakup of Rodinia and the
962 coalescence of all of the continents to form Pangea (Hatcher, 2010). It began by
963 formation of a Neoproterozoic to early Paleozoic rifted margin and platform
964 succession on the eastern margin of Laurentia. Three orogenesis ultimately produced
965 the mountain chain: the Ordovician Taconic orogeny, which involved arc accretion
966 (Karabinos et al., 1998); the Acadian-Neoacadian orogeny, which involved
967 north-to-south, transpressional, zippered, Late Devonian-early Mississippian collision
968 of the Coralina superterrane in the southern-central Appalachians and the
969 Avalon-Gander superterrane in the New England Appalachians, and Silurian
970 collision in the Maritime Appalachians and Newfoundland (Hibbard, 2000; Murphy
971 & Keppie, 2005); and Alleghanian orogeny, which involved late Mississippian to
972 Permian collision of all previously formed Appalachian component with Gondwana
973 to form supercontinent Pangea (Hatcher, 2010).

3.1.6. Meso-Cenozoic Accretion - Cordillera Orogen

In the western portion of the North American continent the Cordillera orogen is a segment of the Circum-Pacific orogenic belt where subduction of oceanic lithosphere has been underway along a great circle of the globe since breakup of the supercontinent Pangea began in Triassic time (Dickinson, 2004). The length of the Cordilleran orogen from the Gulf of Alaska to the mouth of the Gulf of California is ~5000 km.

The Cordilleran orogen has been built by progressive tectonic addition of crustal fragments along the continental edge in Meso-Cenozoic. Such crustal growth is referred to accretionary tectonics (Saleeby, 1983). Accreted tectonic elements include subduction complexes assembled along the Cordilleran margin, intraoceanic island arcs attached to the continental margin by Jurassic arc-continent collision, and subduction complexes associated with the flanks of the exotic island arcs (Dickinson, 2008). The Cordilleran orogen is thought to represent an incomplete Wilson cycle in that it appears to have developed in the absence of a terminal continental collision. Instead, the Cordillera is interpreted as an accretionary orogen, and its evolution is explained as the result of the incremental, thin-skinned addition of terranes to the continental margin above a landward-dipping subduction zone (Monger, 1997). Johnston (Johnston, 2001) demonstrate that a large portion of the continental foreland of the Cordillera orogen is exotic with respect to the autochthon and forms part of a composite ribbon continent, referred to as SAYBIA. The North American Cordilleran orogen is the result of a two-stage process: (a) Triassic-Jurassic accretion within Panthalassa forming SAYBIA, a composite ribbon continent, and (b) Late Cretaceous collision of SAYBIA with North America (Johnston, 2008).

The geological history of North American continent presents a classical example of how continental crust grow gradually from small-sized cratonic nucleus to the current state of the continent. It is demonstrated by the geological records that

accretionary and collisional orogenesis played a key role in enlargement of the continent probably since the first piece of continent was formed from the ocean in Paleoproterozoic. Other continents grow in a similar way as the North American Continent.

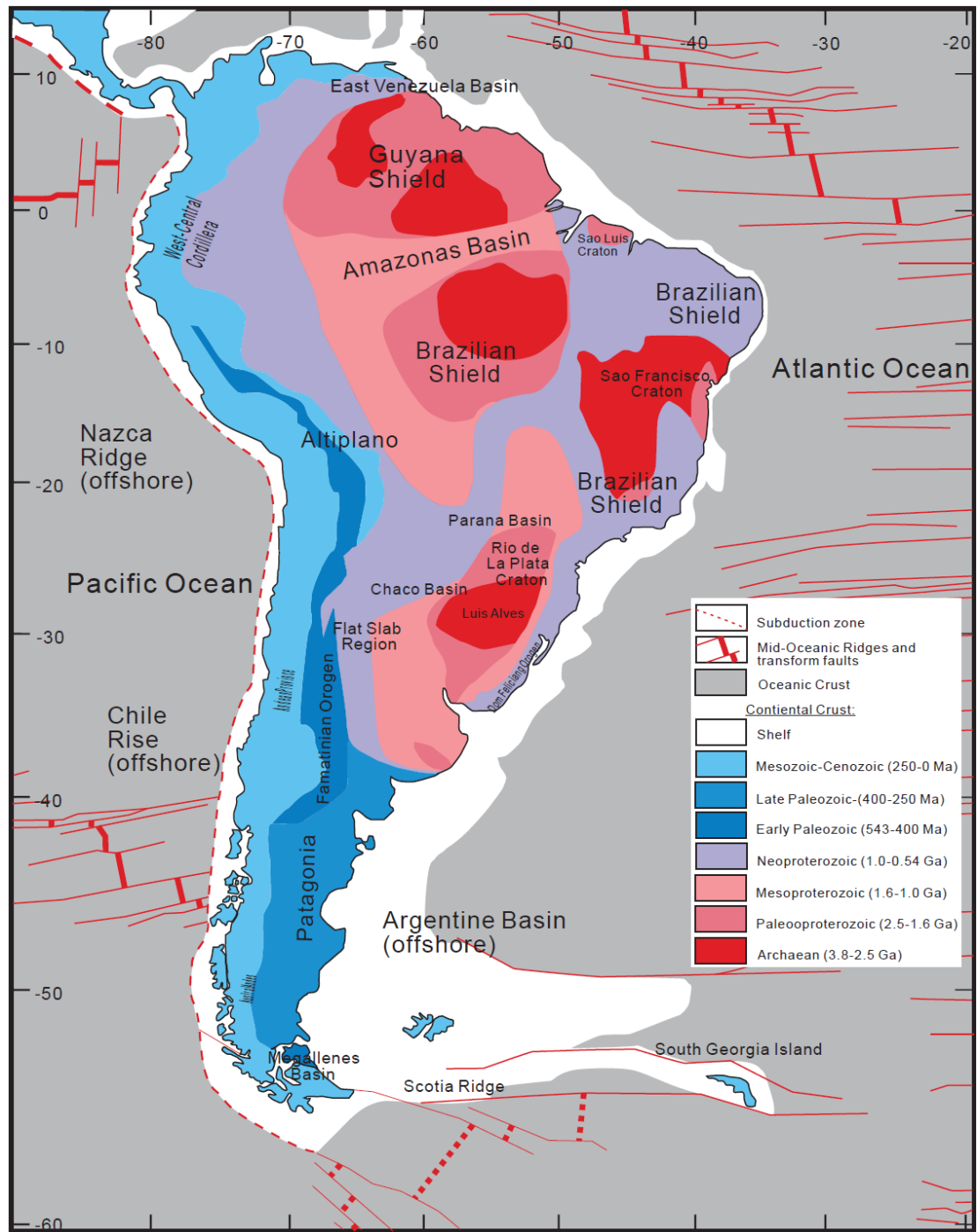


Figure 10. Main geological provinces of the South American continent (after Chulick et al., 2013).

1008

1009 **3.2. Accretion of South American Continent**

1010 The South American continent consists mainly of the Precambrian Brazilian shield
1011 (South American Platform) in the east and late Paleozoic-Cenozoic Andean orogen
1012 in the west, with early Paleozoic Patagonia in the middle (Figure 10). The Brazilian
1013 shield is composed of the large Amazonian (AM) and São Francisco cratons, the
1014 small Rio de La Plata (RP), São Luis (SL) and Luiz Alves (LA) cratonic fragments,
1015 and the mobile belts associated to the Brasiliano-Pan African orogenic Cycle
1016 ([Cordani & Sato, 1999](#)).

1017 The São Francisco craton is represented as a juxtaposition of four Archean
1018 continental blocks brought together during convergent and collisional processes at
1019 approximately 2.1 Ga during the Trans-Amazonian orogeny: the Gavião block, the
1020 granulitic Jequié block, the granulitic Itabuna-Salvador-Curaçá belt, and the
1021 Serrinha block ([Peucat et al., 2002](#)). The Gavião block is mainly composed of
1022 granite-greenstone belts of ca. 2.9-2.8 Ga, as well as an old nucleus with some of the
1023 oldest rocks in South America, with ages ranging from 3.4 to 3.2 Ga. The Jequié
1024 block is mainly formed of enderbite and charnockite with ages of 2.7-2.6 Ga, as well
1025 as migmatite and granulite. The Serrinha block contains 2.9 to 3.5 Ga
1026 amphibolite-facies banded gneisses, amphibolites and granitic orthogneisses
1027 ([Barbosa & Sabaté, 2004](#)).

1028 The Río de la Plata craton is the oldest and southernmost core of South America and
1029 is a key piece in the cratonic assemblage of SW Gondwana. It has long been thought
1030 to comprise a Paleoproterozoic core surrounded by Neoproterozoic-Cambrian
1031 mobile belts ([Gaucher et al., 2011](#)). Sm-Nd T_{DM} model ages between 2.6 and 2.2 Ga
1032 characterize the Piedra Alta Terrane of this craton. Crystallization ages between 2.2
1033 and 2.1 Ga for the metamorphic protoliths and 2.1-2.0 Ga for the post-orogenic
1034 granitoids indicate juvenile crust, followed by a short period of crustal recycling.

1035 Cratonization of this terrane occurred during the late Paleoproterozoic (Oyhantçabal
1036 et al., 2011).

1037 Three major orogenic collages are responsible for the formation of the South
1038 American platform: Middle Paleoproterozoic Trans-Amazonian orogenic cycle, Late
1039 Mesoproterozoic-Early Neoproterozoic, and Late Neoproterozoic-Cambrian
1040 Brasiliano-Pan African orogenic cycle (Brito Neves et al., 1999).

1041 The Andes (Andean orogen) extends along the entire western margin of the South
1042 American continent, formed as a result of the subduction of Nazca plate beneath the
1043 Brazilian Shield, and is the world's second highest orogenic belt. The orogen is
1044 divided into tectonic provinces emblematic of Andean-type convergent margins,
1045 including a forearc region, magmatic arc, retroarc fold-thrust belt, and foreland basin
1046 system that closely follow the western trace of the South American coastline (Jordan
1047 et al., 1983). A protracted history of subduction and arc magmatism along the
1048 western edge of South America commenced in Late Triassic-Jurassic during breakup
1049 of Pangea and westward advance of the South American plate away from Africa
1050 (Pepper et al., 2016). The Andes north of the Golfo de Guayaquil, the Northern
1051 Andes record an important accretion of oceanic crust during Jurassic, late
1052 Cretaceous, and Paleogene times. The Central Andes between the Golfo de
1053 Guayaquil (4°S) and the Golfo de Penas (46°30'S) are a typical Andean-type orogen
1054 where tectonics was driven by subduction. The Southern Andes (46°30'-52°S) are
1055 developed south of the triple junction and are the result of uplift associated with
1056 ridge collision, along different ridge segments (Ramos, 1999).

1057 **3.3. Accretion of Australian Continent**

1058 The North Australian Craton, West Australian Craton and South Australian Craton
1059 underlie the western two-thirds of the Australian continent and are sutured by
1060 orogenic belts of largely Paleoproterozoic to Mesoproterozoic age. They are
1061 bounded on the east by the Phanerozoic Tasmanides, which form the other third of

the continent (Figure 11). The cratons have Archean and/or early Paleoproterozoic cores on which are superimposed later Paleoproterozoic orogenic belts and basins; these, along with younger Proterozoic and Phanerozoic successions, conceal relationships between the older blocks (Withnall et al., 2013). The North, West, and South Australian cratons were independently accreted from older crustal fragments by 1.83 Ga (Myers et al., 1996).

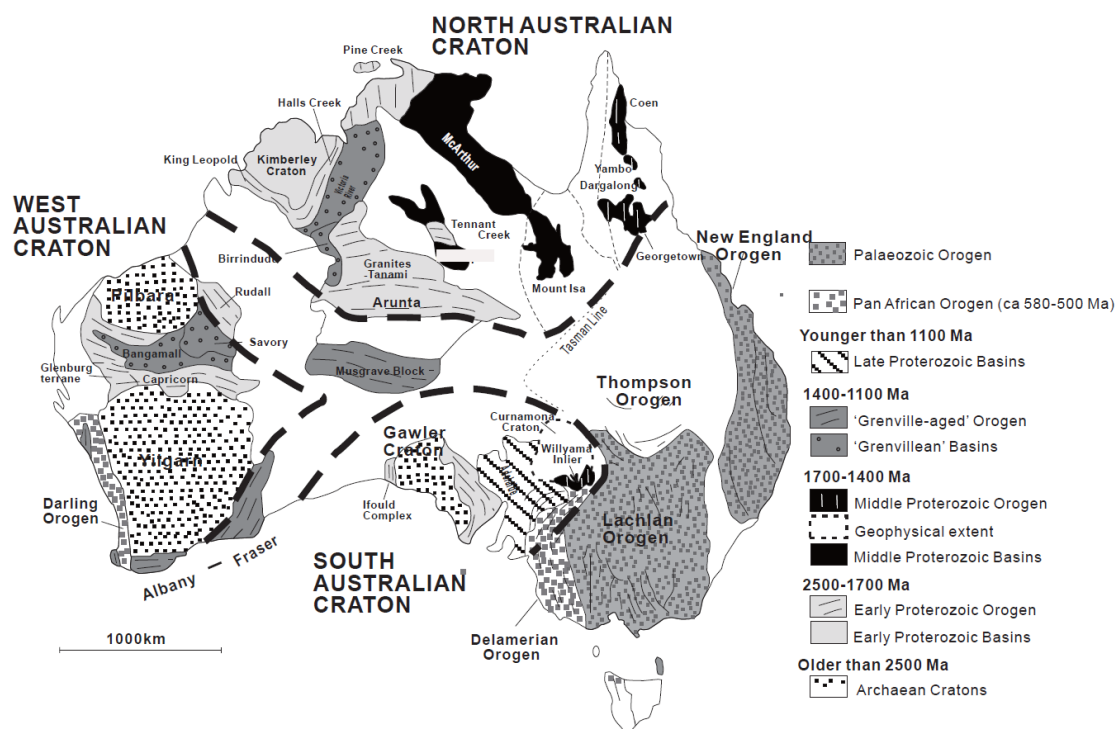


Figure 11. Terrane map of the Australian continent showing major Archean and Proterozoic terranes, as well as the Paleozoic Tasmanides (adapted after Betts et al., 2002).

The North Australian Craton (NAC) includes Paleoproterozoic orogens and basins including the Halls Creek, Pine Creek, McArthur, Mount Isa, Tennant Creek, Tanami, and Aileron geological regions (Myers et al., 1996). Archean basement to the NAC crops out in the Pine Creek and Tanami regions, with ages in the range 2.67 Ga-2.50 Ga. An early phase of basin development at 2.05-2.00 Ga is reflected in the basal units of the Pine Creek Orogen (Scrimgeour, 2006). The Barramundi Orogeny represents a continent-wide accretionary event in which several Archean

1079 cratons amalgamated to form the NAC in a manner that is analogous to the
 1080 Paleoproterozoic amalgamation of Laurentia along the Trans-Hudson Orogen ([Betts
 1081 et al., 2002](#)). A continental strip accreted to the southern margin of the NAC
 1082 between 1.68 and 1.65 Ga. The West Australian Craton formed during the
 1083 Paleoproterozoic (2.0-1.8 Ga) by the collision and combination of the Pilbara and
 1084 Yilgarn cratons which are fragments of formerly more extensive Archean continents.
 1085 The collision zone is marked by the Capricorn Orogen. The West Australian Craton
 1086 was itself fragmented by rifting between 1.6 and 1.3 Ga, and then involved in
 1087 collision and amalgamation with other continental fragments between 1.3 and 1.1
 1088 Ga along the Albany-Fraser and Rudall-Musgrave Orogens ([Myers, 1993](#)). The
 1089 Yilgarn Craton mainly consists of granite-greenstone terranes that formed between
 1090 3.0 and 2.6 Ga. The Pilbara Craton, the largest Archean nucleus in Australia,
 1091 comprises a basement of 3.6 to 2.8 Ga granite-greenstone terrane unconformably
 1092 overlain by a cover sequence between 2.76 and 2.4 Ga. Crustal growth occurred
 1093 throughout the eastern part of the craton between 3.65 and 3.15 Ga. In the western
 1094 parts of the craton, crustal growth is interpreted to have occurred in tectonic
 1095 environments comparable to modern magmatic arc and backarc tectonic settings
 1096 ([Barley et al., 1998](#)) and accretion of outboard island arcs and collisions of
 1097 continental fragments ([Smith et al., 1998](#)). The South Australian Craton formed
 1098 during the Kimban orogeny between ca. 1.84 and 1.70 Ga associated with collision
 1099 and amalgamation of the Gawler and Curnamona cratons ([Myers et al., 1996](#)).

 1100 The North, West and South Australian cratons were combined at ca. 1.3 Ga as an
 1101 early component of the Rodinian supercontinent. The NAC was first joined to the
 1102 northeastern margin of the West Australian Craton. The combined West and North
 1103 Australian cratons were joined to the South Australian Craton along the
 1104 Albany-Fraser orogen ([Myers et al., 1996](#)). The Musgravian Orogen may represent a
 1105 former continuation of the Albany-Fraser Orogen along the northern margin of the

1106 South Australian Craton that was later displaced westward during younger
1107 intracratonic deformation ([Myers et al., 1996](#)).

1108 Eastern Australia is made of Cambrian to Triassic (~550-220 Ma)
1109 subduction-related orogens that are collectively referred to as the Tasmanides
1110 ([Fergusson & Henderson, 2015](#); [Rosenbaum, 2018](#)). This orogenic system is
1111 commonly subdivided into five orogens (Delamerian, Thomson, Lachlan, Mossman,
1112 and New England Orogens) that successively accreted to the Australian continent
1113 ([Glen, 2005](#)). The Tasmanides provide a geological record of the tectonic evolution
1114 of the eastern Gondwanan margin, from the Neoproterozoic breakup of Rodinia to
1115 the fragmentation of Pangea in the Permian-Triassic ([Rosenbaum, 2018](#)). The five
1116 orogens that define the Tasmanides generally become younger from west to east,
1117 with the oldest (Cambrian) components of the Tasmanides dominant in the
1118 Delamerian and Thomson Orogens, and the youngest (Triassic) components found
1119 in the New England Orogen.

1120 The Delamerian Orogen covers the area of the southwestern Tasmanides and
1121 western Tasmania, and separates the Australian Precambrian cratons from the
1122 younger Paleozoic to Mesozoic orogenic belts of eastern Australia. It records the
1123 late Ediacaran (latest Neoproterozoic) to Cambrian evolution of the paleo-Pacific
1124 margin of Gondwana from a passive to a convergent margin ([Turner et al., 2009](#)).
1125 The protoliths of many rocks in the Delamerian Orogen are associated with
1126 rift-related Neoproterozoic sedimentary successions ([Foden et al., 2006](#)), which
1127 were subjected to deformation and metamorphism in the early to middle Cambrian.

1128 The Thomson Orogen is the largest tectonic domain of the eastern Australian
1129 Tasmanides and represents approximately one-eighth of the Australian continent
1130 ([Spampinato et al., 2015](#)). It was a tectonically active area with several episodes of
1131 deposition, deformation and plutonism from Cambrian to Carboniferous time
1132 ([Murray & Kirkegaard, 1978](#)). The Thomson Orogen remains the least-known

1133 component of the Tasmanides because a vast majority of the orogen is covered
1134 under nonmetamorphosed Devonian to Cenozoic sedimentary rocks.

1135 The Lachlan Orogen occupies the central part of the north-south trending
1136 Tasmanides along the eastern margin of Australia. It has long been described as
1137 accretionary orogen that provides an unmodified example of Paleozoic
1138 Circum-Pacific tectonics (Coney, 1992), or as a retreating subduction zone orogen;
1139 it did not suffer a terminal continent-continent collision (Foster & Gray, 2000). The
1140 Lachlan Orogen consists of three separate and distinct subprovinces, each with
1141 differences in rock type, metamorphic grade, structural history, and geological
1142 evolution. The western and central subprovinces are dominated by a turbidite
1143 succession consisting of quartz-rich sandstones and black shales. The eastern
1144 subprovince consists of mafic volcanic, volcanoclastic, and carbonate rocks, as well
1145 as quartz-rich turbidites and extensive black shale in the easternmost part (Foster &
1146 Gray, 2000; Q. Zhang et al., 2019). Shortening and accretion of the Lachlan
1147 occurred through stepwise deformation and metamorphism from Late Ordovician
1148 (~450 Ma) through early Carboniferous times, with dominant events at about
1149 440-430 Ma and 400-380 Ma (Foster & Gray, 2000).

1150 The Mossman Orogen, in the northeastern Tasmanides, mainly comprises deformed
1151 Silurian-Devonian sedimentary and igneous rocks of the Hodgkinson and Broken
1152 River Provinces. Deformation in the Mossman Orogen predominantly took place
1153 from the Late Devonian to earliest Carboniferous; the eastern part of the Mossman
1154 Orogen was subjected to a younger phase of deformation in the Permian and
1155 Triassic (Rosenbaum, 2018).

1156 The New England Orogen is located in the easternmost part of the Tasmanides.
1157 Most of the rocks in the New England Orogen are Devonian to Triassic with a minor
1158 component of Neoproterozoic to Silurian rock units (Harrington & Korsch, 1985).
1159 The Devonian and Carboniferous units likely represent west to east continental arc

1160 and forearc assemblages (forearc basin and accretionary complex). Early Permian
1161 rocks are dominated by voluminous granitic intrusions, bimodal volcanism, and
1162 clastic sedimentary rocks, which were deposited in rift-related basins (Rosenbaum,
1163 2018). A series of sharp bends (oroclines) are recognized in the Paleozoic to early
1164 Mesozoic New England Orogen (Cawood et al., 2011; Rosenbaum et al., 2012).
1165 These oroclines are formed ascribed to an early stage of subduction curvature during
1166 slab rollback at 300-285 Ma, followed by bending associated with dextral
1167 transpression, and final tightening by E-W shortening during the Permian to Triassic
1168 (265-230 Ma) Hunter-Bowen orogeny (Rosenbaum et al., 2012).

1169 **3.4. Accretion of African Continent**

1170 The African continent mainly consists of the Kalachari Craton in the south, the
1171 Congo Craton in the center, the West African Craton in the west, and the East
1172 African Orogen (Figure 12). The Kalahari Craton was spawned from a small
1173 composite Archaean core (Zimbabwe and Kaapvaal) which grew by prolonged
1174 crustal accretion in the Paleoproterozoic along its NW side (Magondi-Okwa-Kheis
1175 Belt, Rehoboth Subprovince) to form the Proto-Kalahari Craton by 1.75 Ga. From
1176 ca. 1.4 to 1.0 Ga, all margins of this crustal entity recorded intense tectonic activity:
1177 the NW margin was a major active continental margin between ca. 1.4 and 1.2 Ga
1178 and along the southern and eastern margins, the Namaqua-Natal-Maud-Mozambique
1179 Belt records a major arc-accretion and continent-collision event between ca. 1.1 and
1180 1.05 Ga. By ca. 1.05 Ga, the Proto-Kalahari nucleus was almost completely rimmed
1181 by voluminous Mesoproterozoic crust and became a larger entity, the Kalahari
1182 Craton (Jacobs et al., 2008). Zircon U-Pb-Hf study clearly indicate that the terranes
1183 of the Kalahari Craton lie on distinct crustal evolution trends, which requires that the
1184 continental crust that constitutes these terranes formed at different times, and
1185 subsequently evolved differently. Furthermore, it requires that the terranes of the
1186 Kalahari Craton were successively accreted (Zeh et al., 2009).

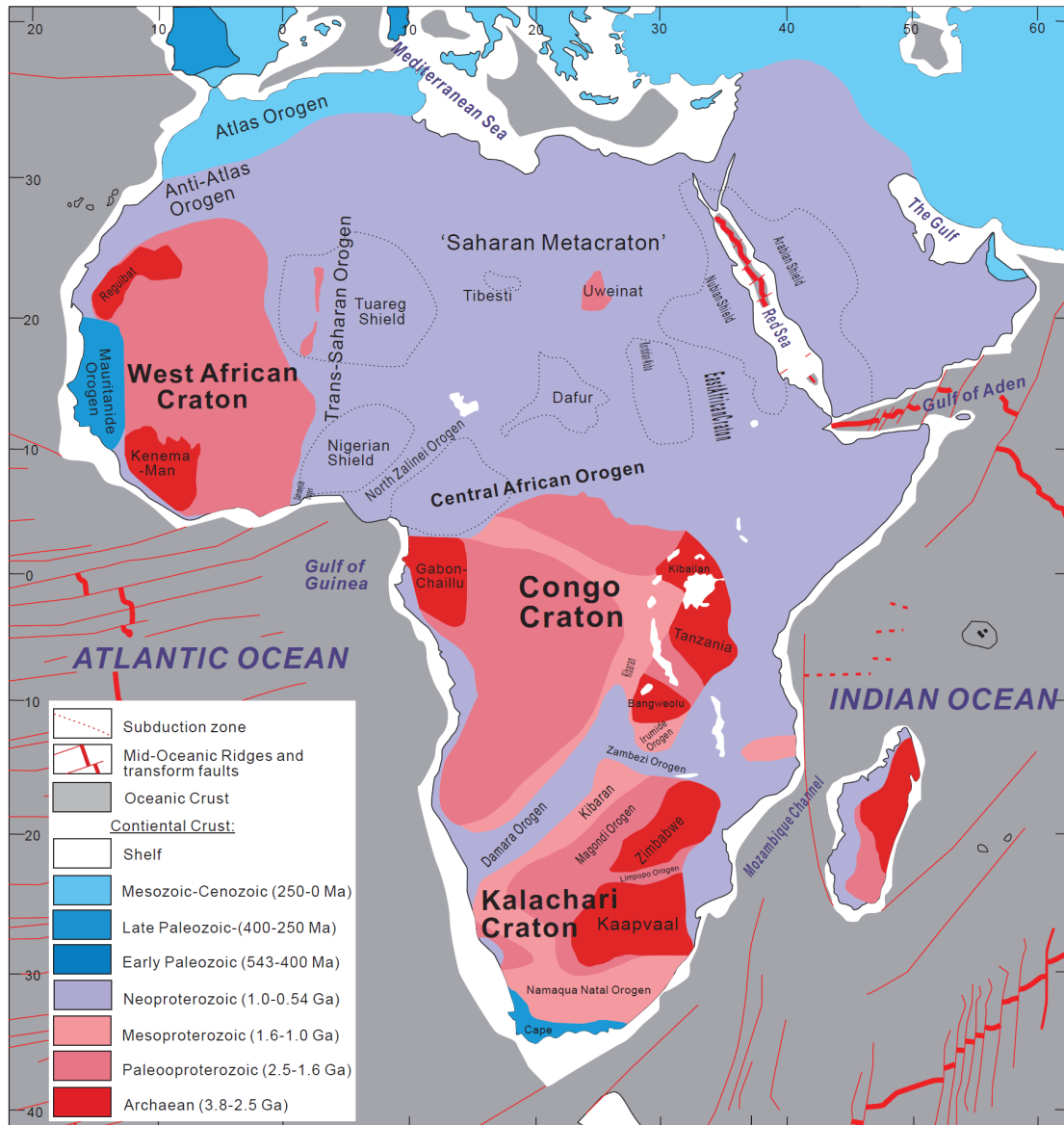


Figure 12. A sketch map showing the major constitutes of the South African continent
(After [Van Hinsbergen et al., 2011](#)).

The Congo Craton is defined as the amalgamated central African landmass at the time of Gondwana assembly. The nucleation of the Congo Craton from its composing cratonic blocks, which include the Angola-Kasai Block, the NE-Congo-Uganda Block and the Cameroon-Gabon-Congo-São Francisco Block to the west and northwest of the Mesoproterozoic Kibaran Belt, and the Bangweulu Block and Tanzania Craton, to the east and southeast, was at the latest completed

1197 after peak compressional tectonism in the Kibaran Belt at 1.38 Ga. Late
1198 Mesoproterozoic tectonism along the southern margin of this proto-Congo Craton,
1199 in a region called the Irumide Belt, marks compressional tectonism at ca. 1.05-1.02
1200 Ga, which produced extensive reworking along this margin, possibly linked to the
1201 participation of the Congo Craton in the Rodinia supercontinent (De Waele et al.,
1202 2008).

1203 The West African Craton is a large slice of Archean to Paleoproterozoic continental
1204 crust divided into two main parts; the Keneman Rise to the south and the Reguibat
1205 Rise to the north, separated by the Neoproterozoic to Devonian Taoudeni Basin. The
1206 Keneman and the Reguibat Rises both consist of a western Archean domain that was
1207 affected by the subsequent Leonian and Liberian tectonothermal events and an
1208 eastern Paleoproterozoic domain accreted during the Birimian cycle around 2.1 Ga
1209 (Thiéblemont et al., 2001). The discovery of blueschist metamorphism in the 2.2-2.0
1210 Gyr old West African metamorphic province suggests that modern-style plate
1211 tectonics existed during the Paleoproterozoic era (Ganne et al., 2012).

1212 The Neoproterozoic orogeny, collectively termed the Pan-African Orogeny, led to
1213 the amalgamation of the Kalachali, Congo, and West African cratons and the final
1214 consolidation of the African continent. The Damara Orogen joins the Kalahari
1215 Craton in the south and the Congo Craton in the north. It contains a Neoproterozoic
1216 succession that was intensely deformed and metamorphosed in the protracted
1217 Neoproterozoic to Cambrian Pan-African Orogeny (Goscombe et al., 2004).

1218 The East African Orogen (EAO), extending from southern Israel, Sinai and Jordan
1219 in the north to Mozambique and Madagascar in the south, is the world's largest
1220 Neoproterozoic to Cambrian orogenic complex. It comprises a collage of individual
1221 oceanic domains and continental fragments between the Archean
1222 Sahara-Congo-Kalahari Cratons in the west and Neoproterozoic India in the east.
1223 Orogen consolidation was achieved during distinct phases of orogeny between ca.

850 and 550 Ma (Fritz et al., 2013; Stern, 1994). The EAO is subdivided into the Arabian-Nubian Shield (ANS) in the north, composed largely of juvenile Neoproterozoic crust, and the Mozambique Belt (MB) in the south comprising mostly pre-Neoproterozoic crust with a Neoproterozoic–early Cambrian tectonothermal overprint (Fritz et al., 2013).

3.5. Accretion of Eurasian Continent

The Eurasian continent is currently the largest continent in the world. It mainly consists of six cratonic blocks: the Russian and Siberian cratons in the north, the Tarim and North China cratons in the middle, and the Afro-Arabian and Indian cratons in the south, and two huge Phanerozoic orogenic systems: the Altaids in the north and the Tethysides in the south (Figure 13).



Figure 13. Tectonic units of Eurasia, showing the locations of major cratonic blocks and orogenic belts, modified after Şengör et al. (2018).

3.5.1. Precambrian Cratonic Blocks

The Russian Craton (also called the East European or Baltica Craton) is the coherent mass of Precambrian continental crust that occupies almost the entire northeastern half of the European continent. It was assembled by the successive collision of three once autonomous crustal segments (Fennoscandia, Sarmatia and Volgo-Uralia) at ca. 1.8-1.7 Ga, roughly concomitantly with the formation of the Paleo- to Mesoproterozoic Columbia/Nuna supercontinent, which appears to have persisted until ca. 1.4 Ga. After its formation, the Russian Craton has never been dismembered completely, but signs of accretion of new crust and, in particular, rifting along its margins as well as truncated tectonic trends indicate that its size and shape have changed repeatedly (Bogdanova et al., 2008). Isotopic data indicate repeated episodes of generation of juvenile continental crust along and outboard of the margin of the dominantly Archean Craton in Sarmatia, which are best explained by accretionary plate tectonics. An Andean-type geodynamic setting between 2.1 and 2.0 Ga ago was succeeded by the formation of several island arcs and accretion of these onto the older continent between 2.0 and 1.8 Ga. Subsequent compression of the newly formed crust lasted until ca. 1.7 Ga (Claesson et al., 2001).

The Siberian Craton was assembled at ca. 2.1-1.8 Ga by Archean blocks through orogenic belts and suture zones. Similarities in ages between the Paleoproterozoic orogenic belts of Siberia and Laurentia cratons suggest that they could have originated from the same proto-craton (Gladkochub et al., 2006). The present-day structure of craton is generally considered as a result of collision, amalgamation and accretion of microcontinents different in age, which turned into heterogeneous tectonic blocks in the course of collision that is consistent with the current concept of accretionary tectonics. The craton comprises the Tungus, Anabar, Olenek, Aldan, and Stanovoi provinces. The latter consist of heterogeneous tectonic blocks with superimposed Paleoproterozoic fold and orogenic belts sometimes. Areas between terranes correspond to Paleoproterozoic island-arc fragments, the largest among

1267 which is the Akitkan orogenic belt. The belt represents a Paleoproterozoic island-arc
1268 system sandwiched between the Anabar and Aldan superterrane (Rosen et al.,
1269 2006). The system development terminated by the collision prism collapse 1.8 Ga
1270 ago.

1271 The Tarim Craton, located in northwestern China, is one of the largest Precambrian
1272 cratonic blocks in East Asia. It is largely covered by Cenozoic desert, and the
1273 Precambrian basement mainly expose along its southwestern and northeastern
1274 margins, i.e. Altyn and Quruqtagh regions. The Tarimian Orogeny resulted in the
1275 final cratonization of the Tarim Craton, and produced an unconformity between the
1276 metamorphosed basement (Archean to early Neoproterozoic) and the sedimentary
1277 cover (middle Neoproterozoic to Phanerozoic) (Lu et al., 2008).

1278 The North China Craton (NCC, or Sino-Korea Craton) is the largest Precambrian
1279 cratonic block in east Asian continent. It contains some fragments of the oldest
1280 continental crust in the world dated back to ca. 3.8 Ga (Liu et al., 1992). Although
1281 different tectonic models exist, it is generally agreed that the NCC was formed
1282 through amalgamation of different small Archean blocks during the
1283 Paleoproterozoic accretionary and collisional orogenesis (Kusky, 2011; Zhai & Liu,
1284 2003; Zhao et al., 2001). The Archean blocks are dominated by
1285 tonalite-trondhjemite-granodiorite (TTG) gneisses and granite-greenstones. Based
1286 on age, lithological assemblage, tectonic evolution and P-T-t paths, Zhao et al. (2000,
1287 2001) divided the NCC into the Western Block, the Eastern Block and the
1288 intervening Trans-North China Orogen. The Western Block forms a stable platform
1289 composed of late Archean to Paleoproterozoic metasedimentary belts that
1290 unconformably overly Archean basement, whereas the Eastern Block consists of
1291 granulite facies TTG gneiss and charnockite with minor mafic granulite and
1292 amphibolite. The Trans-North China Orogen is composed of late Archean
1293 amphibolite and granulite and 2.5 Ga granite-greenstone terrains (Zhao et al., 2000,
1294 2001). The final amalgamation of the Western and Eastern blocks of the craton is

suggested to have occurred at ~1.85 Ga (Zhao et al., 2012), or 2.5 Ga (Kusky & Li, 2003; Kusky, 2011) during an arc/continent collision. The style of tectonic accretion in the NCC changed at circa 2.5 Ga, from an earlier phase of accretion of arcs that are presently preserved in horizontal lengths of several hundred kilometers, to the accretion and preservation of linear arcs several thousand kilometers long with associated oceanic plateaus, microcontinents, and accretionary prisms (Kusky et al., 2016). The style of progressively younger and westward outward accretion of different tectonic components is reminiscent of the style of accretion in the Superior Craton.

3.5.2. Phanerozoic Orogenic Systems

The Altaids (or Altaid Tectonic Collage), also known as the Central Asian Orogenic Belt (CAOB), sandwiched between the Russian Craton, the Siberian Craton and the Tarim-North China Craton, is considered as one of the largest Phanerozoic accretionary orogens in the world (Şengör et al., 1993; Windley et al., 2007). It is proposed that the Asia continent grew by 5.3 million km² during the Paleozoic through the growth of subduction-accretion complexes along a single magmatic arc now found contorted between Siberia and Baltica (Şengör et al., 1993; Şengör & Natal'in, 1996). Isotopic data show that most of the granitoids in the Altaids have depleted Nd-Hf compositions, consistent with the large-scale distribution of juvenile continental crust (Jahn et al., 2000).

The Altaids is formed through complicated amalgamation between subduction-accretion complexes, magmatic arcs, seamounts, forearc and backarc basins, and continental fragments during the progressive subduction and final closure of the Paleo-Asian Ocean (Windley et al., 2007). There are different types of magmatic arcs, including Andean-type arcs, intro-oceanic island arcs and Japan-type island arcs within the Altaids (Song et al., 2015; Xiao et al., 2020). Pre-Altaid basement, although exist, are generally paucity in the Central Asia. In contrast, most

terrane are composed of juvenile crust newly excreted from the mantle, either through ‘syn-subduction lateral accretion of arc complexes’ and ‘post-collisional vertical accretion of underplated mantle material’ (Long et al., 2011). In addition, ridge subduction has also played an important role in the continental growth of Central Asia (Windley & Xiao, 2018).

The timing of accretion of the Altaids generally become younger southwards (present coordinates), and the final closure of the Paleo-Asian Ocean took place along the South Tianshan-Beishan-Solonker suture in the southernmost Altaids. The termination of the Paleo-Asian Ocean was scissor-style eastward from Permian to Middle Triassic (Xiao et al., 2009).

The Tethysides is situated to the south of the North China and Tarim cratons. It contains a record of the progressive closure of the Proto-Tethys, Paleo-Tethys, Meso-Tethys, and Neo-Tethys Oceans resulting from the convergence between the Gondwana and Laurasia continents (Şengör, 1987). In the east the Qinling and Dabie-Sulu orogens formed through closure of the ocean between the North China and South China cratons in the Mesozoic (Ernst & Liou, 1995). In the west there are the Kunlun-Qilian orogen in the north, the Himalayan-Tibetan orogen in the south and southeast, and the Sanjiang orogen in SW China, which formed by progressive closure of oceans caused by Paleozoic to Cenozoic convergence between blocks rifted from the northern margin of the Gondwana and Eurasian continents. The Tethys Ocean was finally terminated by collision between the Indian continent and the southern margin of the Eurasian continent giving rise to the bulk of the Tibetan Plateau (Ding et al., 2005). The India-Asia collision leads to tremendous reworking and transforming of the Asian Continent expressed by high-topography in south-central Asia and large-scale strike-slip deformation in SE Asia.

4. Reworking of Continents

Continents have evolved for several billion years ever since their formation in the Archean time (see section 2). Such long-term evolution of continents involves multiple phases of orogeny and frequent tectono-thermal processes, resulting in not only episodic additions of new continental materials (continental accretion or growth; see section 3), but also repeated modifications of the existing continental lithosphere (continental reworking) (e.g., [Holdsworth et al., 2001](#)). Continents are therefore characterized by both longevity in their evolution and complex modification in the lithosphere.

4.1. Longevity of Continents

The majority of continents consists of long-lived crust and lithosphere, namely cratons that have been isolated from the convecting mantle since the Precambrian, mostly for two or three billion years (e.g., [Lee et al., 2011](#); [Lenardic & Moresi, 1999](#)). There have been numerous lines of evidence suggesting the preservation of Precambrian crustal basement and similarly old deeper mantle roots beneath cratons (e.g., [Pearson, 1999](#); [Richardson et al., 1984](#); [Spetsius et al., 2002](#); [Walker et al., 1989](#)). Compared to the short-lived oceanic lithosphere that is recycled back into the mantle on a timescale of ~100 Ma, continental lithosphere is capable of resisting deformation and avoiding recycling as a whole over a timescale of about one order of magnitude longer ([Lenardic et al., 2003](#); [O'Neill et al., 2008](#)). The longevity and stability of continents, in particular cratons, have been primarily attributed to the structure and intrinsic (physical and chemical) properties of the continental lithosphere, relative to the asthenosphere and oceanic lithosphere (Figure 14 and Table 1).

4.1.1 Intrinsic buoyancy of continental lithosphere

One relevant property to the longevity and stability of continents is thought to be the intrinsic buoyancy of continental lithosphere ([Carlson et al., 2005](#); [Jordan, 1978](#)). This property is closely related to the lithospheric structure and composition of

continents that much differ from their oceanic counterparts. Continental lithosphere is composed of a sialic crust of ~40 km thick on average and a mantle keel of melt depleted residuum composition with highly variable thicknesses (Table 1). The majority of continental lithosphere is thicker than ~120 km, even up to >200 km beneath Archean cratons, with thin lithosphere of a few tens of kilometers in continental margins or active rift zones (Figure 14). In contrast, oceanic lithosphere consists of a ~7-km basaltic crust and a thin mantle keel with a total thickness of mostly no more ~100-110 km (Figure 14, Table 1). These large differences in the crustal and lithospheric thickness and composition are essential for the distinct fates of continents and oceans. With progressive cooling, oceanic lithosphere becomes denser and thicker as ages and eventually downwells to form a subducting slab. In contrast, the continent lithosphere is intrinsically chemically buoyant, which likely offsets its negative buoyancy due to lower temperatures than the underlying asthenosphere (Figure 15a) and makes it in isostatic equilibrium (e.g., [Jordan, 1978, 1988](#)). Continental lithosphere is thus not prone to subduct as oceanic lithosphere does.

The chemical buoyancy of continental lithosphere is contributed from both the melt depleted residuum composition of the mantle root and the sialic composition of the crust. The melt depletion of the mantle root is characterized by less Fe relative to Mg (or high Mg#, Table 1) and a high proportion of olivine to clinopyroxene+garnet, as a result of extensive melt extraction ([Lee et al., 2005; Poudjom Djomani et al., 2001](#)). This chemical depletion generally increases with age of continent and leads to the most refractory nature of Archean mantle root ([Lee et al., 2011; O'Reilly et al., 2001](#)). Accordingly, the densities of subcontinental lithospheric mantle (SCLM) decrease in order and are averaged at standard P-T conditions as ~3310 kg/m³, ~3340 kg/m³ and ~3360 kg/m³ for the Archean, Proterozoic and Phanerozoic periods, respectively (Table 1), corresponding to ~2.5%-1% density reduction compared to asthenospheric mantle at similar depths ([Artemieva, 2009; Deen et al.,](#)

2006; Poudjom Djomani et al., 2001). Compared to the mantle root, the averagely ~40-km sialic continental crust, which is much more buoyant than the ~7 km basaltic oceanic crust and asthenospheric mantle (Table 1), contributes a larger, even dominant part (>70%) to the overall buoyancy of the continental lithosphere. A significant reduction of the crustal contribution by scraping off the most buoyant upper crust would dramatically increase the density of the continental lithosphere and make it readily subductable (e.g., Capitanio et al., 2010). However, recent numeric modeling studies indicate that, although intrinsic buoyancy improves the stability of continental lithosphere, it is insufficient by itself to account for the longevity of cratons (Doin et al., 1997; François et al., 2013; Lenardic & Moresi, 1999; O'Neill et al., 2008).

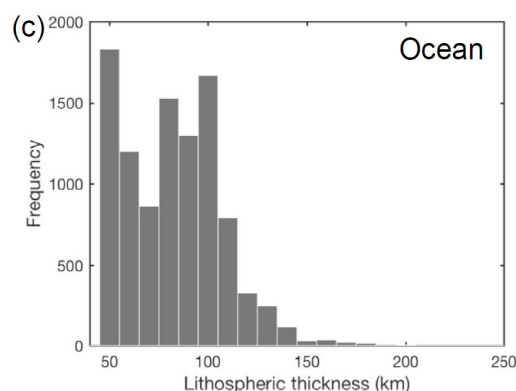
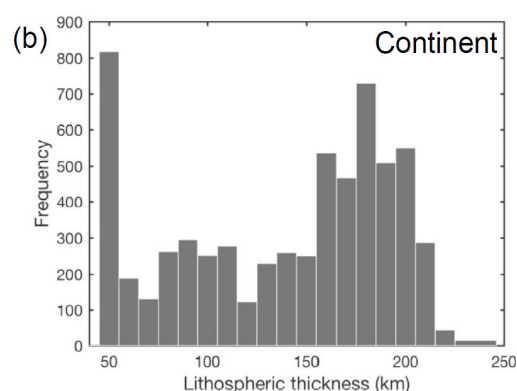
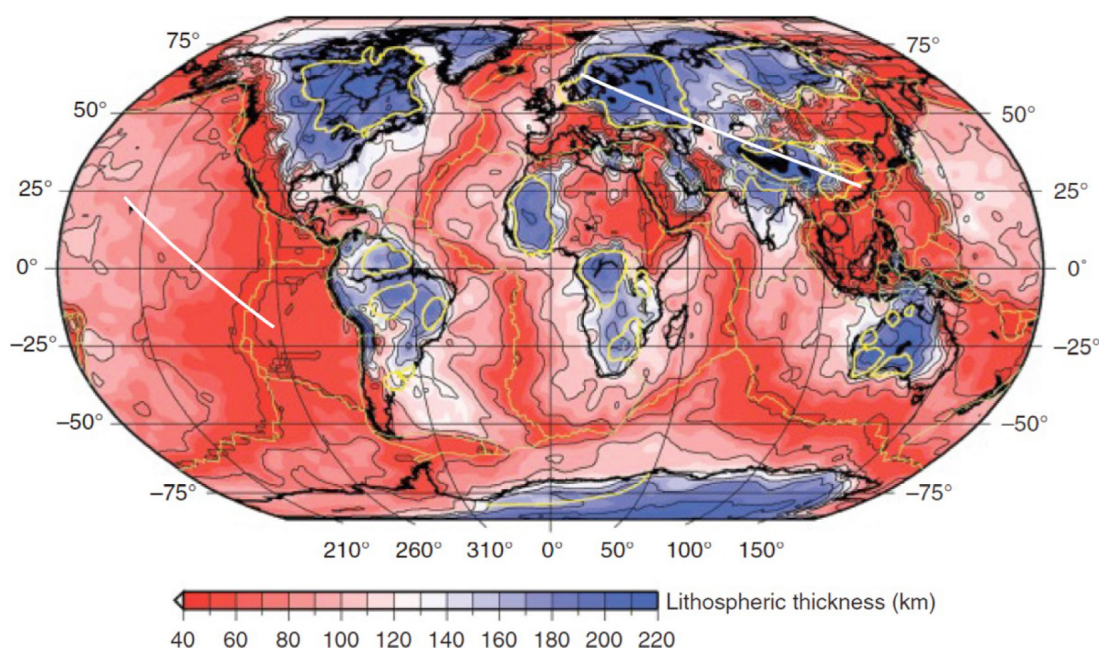
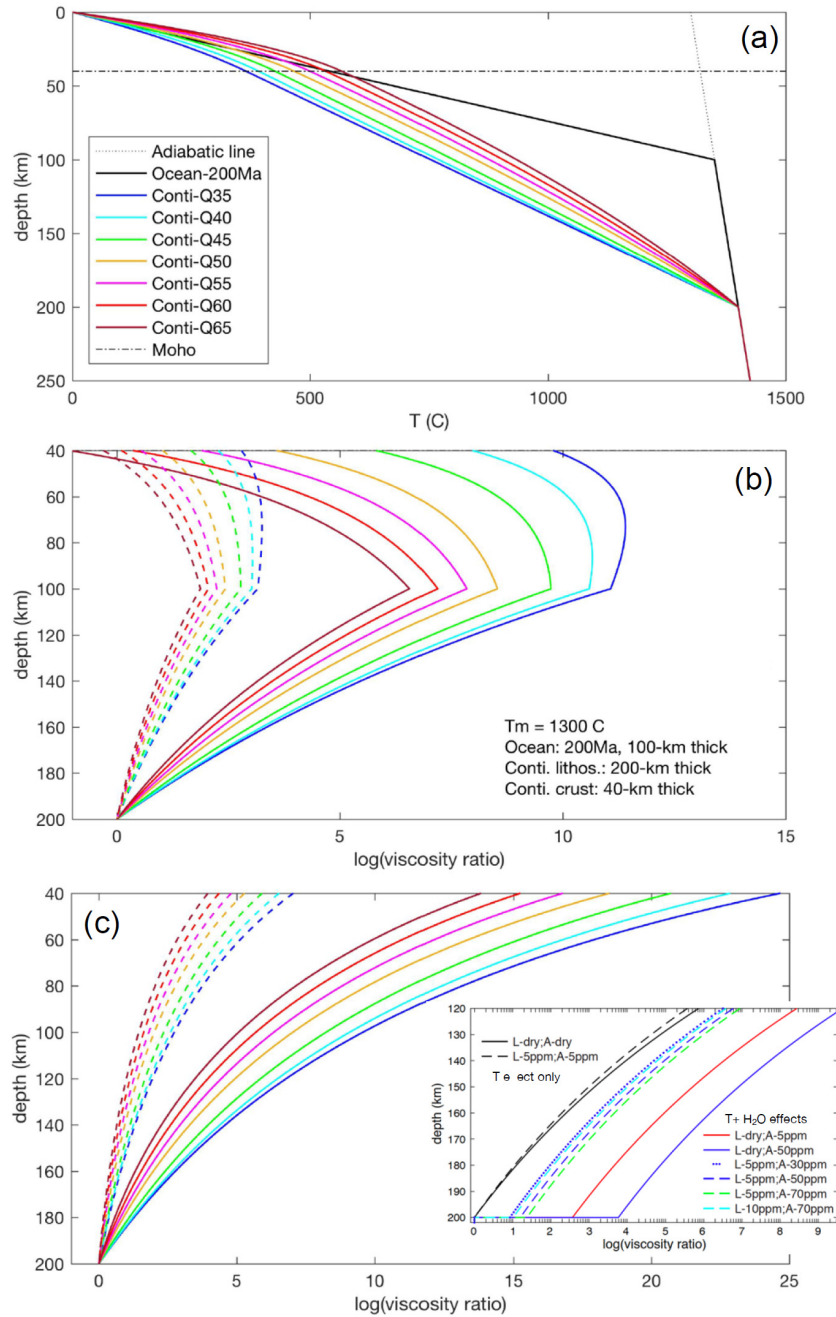


Figure 14. Global lithospheric thickness map (a), and histograms of lithospheric thicknesses beneath continents (b) and oceans (c), respectively. The lithospheric thicknesses were obtained from the upper mantle V_{sv} model CAM2016V_{sv} by surface wave tomography and the V_s(T) relationship given in [Priestley et al. \(2019\)](#), and the thickness data were downloaded from <http://ds.iris.edu/ds/products/emc-cam2016/> provided by Keith Priestley and Tak Ho. (a), modified from [Priestley et al. \(2019\)](#). The yellow contour denotes the geologically mapped boundary of the shields at the surface. The two white lines mark the locations of two cross-sections in Figure 16. (b) and (c) are plotted by separating the lithospheric thickness data for continents and oceans. Note that the lithospheric thicknesses derived by surface wave tomography have uncertainties of a few tens of kilometers ([Fichtner et al., 2010](#)).

4.1.2. High Strength of Continental Lithosphere

It has been suggested that high strength (viscosity) of continental mantle roots is essential for the long-term stability of cratons ([Carlson et al., 2005](#); [Karato, 2010](#); [Pollack, 1986](#)). High root strength compared to both oceanic lithospheric mantle and asthenosphere is primarily due to the low temperatures, but also attributed to the exceptional melt depletion and thus dehydration of cratonic roots (Table 1) (Figure 15b-c). The effect of dehydration is particularly pronounced by a sharply increase in rheological contrast (viscosity ratio) to more than one order of magnitude between the lowermost mantle root and the top of the asthenosphere (inset in Figure 15c) with typically reported water contents in both cratonic lithospheric mantle and asthenosphere (Table 1). This feature differs markedly from the continuously variation of viscosity ratio with depth if only temperature effect is considered (Figure 15c). Geodynamical models argue that a plausible range of rheological contrast between a cratonic root and asthenosphere (2-3 orders of magnitude for a constant stress) could prevent the cratonic root from convecting mantle erosion for



1442

1443 **Figure 15.** (a) Simplified temperature profiles for a 200Ma old and 100-km thick oceanic
 1444 lithosphere and a series of 200-km thick continental lithosphere with various surface heat
 1445 flows (from 35 mW/m² to 65 mW/m² with 5 mW/m² increment); b) Rheological contrasts
 1446 between the continental lithospheric mantle and oceanic lithospheric mantle due to the
 1447 temperature differences shown in (a); c) Rheological contrasts between the continental
 1448 lithospheric mantle and the top of the asthenosphere with only temperature effect (main
 1449 panel) and considering the effects of both temperature and various water contents in olivine

in the cratonic lithosphere (dry to 10 ppm) and asthenosphere (dry to up to 70 ppm) (insert). Solid lines and dash lines in (b) and the main panel of (c) are for constant stress and constant strain rate cases, respectively. The insert in (c) is for surface heat flow of 45 mW/m² and constant stress case. The values of water contents are based on estimates from [Peslier et al. \(2017\)](#) and [Hirth and Kohlstedt \(1996\)](#). See also Table 1. A dislocation creep rheology with the parameters given in [Dixon et al. \(2004\)](#) are used here. The temperature effect is calculated under dry condition.

over billions of years, even without considering the effects of the chemical buoyancy of the root (e.g., [Lenardic & Moresi, 1999](#); [O'Neill et al., 2008](#); [Wang et al., 2014](#)). If the intrinsic buoyancy is further involved in modeling, the value of required viscosity ratios could be further reduced to below two orders of magnitude (~50 for a constant stress, [Wang et al., 2014](#)). It roughly falls into the range both calculated here at around the bottom of the cratonic root (inset in Figure 15c) based on the data of mantle water distribution (e.g., [Peslier et al., 2017](#); [Xia & Hao, 2013](#)) and provided by laboratory experiments (10s up to 10000) for dehydration strengthening for upper mantle minerals, mostly olivine ([Fei et al., 2013](#); [Hirth & Kohlstedt, 1996](#); [Karato, 2010](#)). However, experimental results reported a rather large span of strength drop (> 1-2 order of magnitude) due to similar water abundance in the dislocation creep regime (e.g., [Demouchy & Bolfan-Casanova, 2016](#); [Fei et al., 2013](#)), which indicates that, although the dominant role of high root strength for craton longevity has been a consensus, the effects of volatiles, especially water on mantle rheology is yet not well constrained ([Brodholt, 2013](#)).

In addition to the high strength of the mantle root, the high strength of the crust and strong coupling between crust and lithospheric mantle also contribute to the rigidity and long-term stability of continental lithosphere. This was previously indicated by both numerical simulations on mantle dynamics (e.g., [Lenardic et al., 2003](#)) and

theoretical calculation of rock strength (Burov & Diament, 1995). Isotopic dating (Aulbach et al., 2004; Pearson et al., 1995) and seismic imaging results of continental lithosphere of various ages (Darbyshire et al., 2017; Durrheim & Mooney, 1994; Nguuri et al., 2001) provide further evidence for the crust-mantle coupling during the evolution of continents. In cratonic regions, it is suggested that the crust and lithospheric mantle behave in a coupled manner to keep the lithosphere strong and stable. On the one hand, a strong crust helps to maintain the high strength of the continental lithosphere as a whole and prevents the crust detaching from the subcrustal mantle (Burov & Diament, 1995; Lenardic et al., 2003). On the other hand, the thick and high-viscosity lithospheric mantle separates the crust from the convecting mantle and serves as a stiff root to protect the crust from being heated and thus weakened and being destroyed during mantle processes (e.g., Carlson et al., 2005). Overall, both the strong crust and lithospheric mantle and therefore strong crust-mantle coupling are all of importance for the longevity of continents.

4.1.3. Structural Heterogeneities Within Continental Lithosphere

Beside the intrinsic chemical buoyancy and high strength of cratonic mantle roots, the most distinct feature of continental lithosphere compared to the oceanic counterpart is probably the ubiquitous structural heterogeneities, as revealed increasingly by geophysical observations (e.g., Fichtner et al., 2010; Priestley et al., 2019; Schaeffer & Lebedev, 2014). The heterogeneous structural feature is closely related to the early formation and long-term evolution of continents, which involves complex lithospheric processes of amalgamation and accretion of smaller blocks of various ages and subsequent thermo-tectonic modifications (see sections 2-3). Old cratons are typically surrounded by younger mobile belts of distinctly different evolution histories, resulting in complicated lateral structural variations especially at around the margins of cratons (Figure 16a-d). Ocean basins, on the other hand, have a relatively simple history of evolution, forming at middle ocean ridges, expanding towards both sides and diminishing at subduction zones. Accordingly, the

lithospheric structure of ocean basins mainly monotonously varies with age (Figure 16e), exhibiting relatively more simplified features than the continental lithosphere at similar scales (Figure 16d).

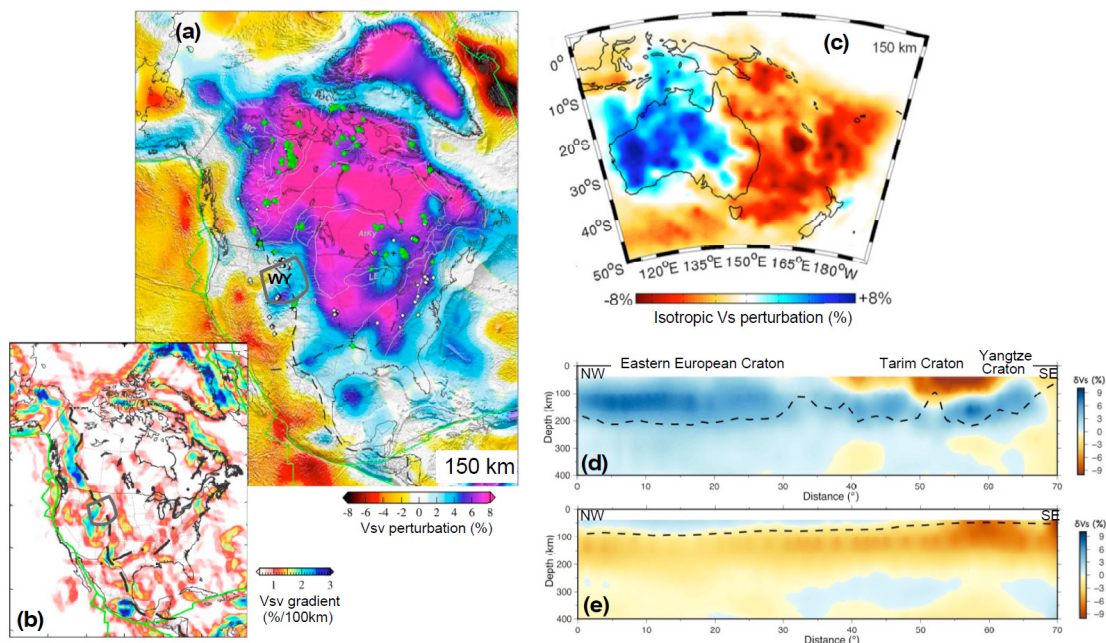


Figure 16. Structural heterogeneities of continental lithosphere and comparison with oceanic lithosphere. (a) Shear wave velocity (Vsv) structure at 150-km depth beneath North America, showing high-velocity cratonic core and lower-velocity younger orogenic belts surrounding the core. Green filled and white diamonds mark the locations of diamondiferous and non-diamondiferous kimberlites and lamproites, respectively. (b) Lateral Vsv gradients shown in (a), plotted in percentage per 100 km. Larger velocity gradients concentrate at around cratonic margins or plate boundary areas. Dashed black line in (a,b) separates the little deformed stable cratonic core from the strongly deformed tectonic region to the west. The Wyoming craton (WY) is outlined in thick gray. (a,b) are modified from [Schaeffer and Lebedev \(2014\)](#). (c) Isotropic shear wave velocity perturbations at 150-km depth beneath Australia ([Fichtner et al., 2010](#)), showing structural variations between cratons and surrounding younger belts similar to (a). (d,e) Shear wave velocity cross-sections within the Eurasian continent (d) and Pacific ocean (e). See Figure 1a for the locations of the cross-sections. Dash line in (d) and (e) marks the base of the

lithosphere from Figure 1a. The velocity model is the global upper mantle tomographic V_{sv} model CAM2016V_{sv} downloaded from <http://ds.iris.edu/ds/products/emc-cam2016/> provided by Keith Priestley and Tak Ho. A-A': (63.562N, 15.204E) -- (27.241N, 115.088E); B-B' : (23.168N, 158.876W) -- (18.460S, 102.600W).

Structural heterogeneities reflect different nature and properties, in particular mechanical strength (rheology) of the lithosphere within continents (e.g., [Hieronymus et al., 2007](#)) and have been invoked to explain the longevity and stability of cratons (e.g., [Lenardic et al., 2003](#); [Yoshida, 2012](#)). Mobile belts surrounding a craton are mechanically weak zones, relative to the craton. Because of their weakness, peripheral mobile belts may themselves become the preferential/favorable loci of intensive heating and strain localization ([Tommasi et al., 2001](#); [Vauchez et al., 1997](#)), and thus could shield the craton from tectonic stressing and thermo-mechanical erosion. Such processes may lead to further sharpening of the already existed variations in lithospheric structure and properties within continents, consistent with plenty of seismic observations that reveal distinct structural changes across cratonic boundary zones (Figure 16a-d), such as Europe ([Shomali et al., 2006](#); [Wilde-Piórko et al., 2010](#)), East Asia ([Chen, 2010](#); [Tao et al., 2018](#)), Australia ([Fichtner et al., 2010](#); [Fishwick et al., 2008](#)), North America ([Schaeffer & Lebedev, 2014](#); [Schmandt & Lin, 2014](#)), and South Africa ([James et al., 2001](#); [Ortiz et al., 2019](#)). The overall effects of structure and property heterogeneities for the longevity and stability of cratons mainly depend on the differences and interactions between a craton and its adjacent mobile zones rather than on the craton itself (thus regarded as external factors, [Wang et al., 2014](#)), which is closely related and probably complementary to the roles played by the high strength and intrinsic chemical buoyancy of cratonic roots (internal factors).

4.2 Evidence for Continental Reworking

Continents, even the most stable cratons are not invariable forever. Despite the long-term stability of continents (cratons) compared to their oceanic counterparts, continental lithosphere is also characterized by episodic tectono-thermal disturbances or reworking throughout its history. Continental reworking typically involves interactions of between lithosphere and asthenosphere, crust and mantle or among tectonic blocks, accompanying mountain building, crustal growth or accretion (e.g., [Griffin et al., 2009](#); [Holdsworth et al., 2001](#); [Peslier et al., 2017](#); [Stern & Scholl, 2010](#)). The styles and processes of reworking are expressed by the way in which the existing lithosphere responds to the tectono-thermal events ([Holdsworth et al., 2001](#)). Significant continental reworking may not only affect the structure and properties of the involved continental lithosphere, but also link to or exert impacts on both the surface processes and mantle dynamics of a broader region, even globally (e.g., [Allen & Armstrong, 2008](#); [Hu et al., 2018](#); [Liu, 2014](#); [Tassara et al., 2017](#)).

Evidence of continental reworking is ubiquitous both in space and time. In the following we provide a number of examples from shallow to deep lithospheric depth, from an integrated geological and geophysical point of view.

4.2.1 Surface Geology and Tectonic Deformation

Reworking of continents is reported to be commonly associated with tectonic processes, i.e., mostly oceanic subduction and continental collision occurring at plate boundaries. Well-known examples come from the circum-Pacific subduction zones and the Tethyan collisional belt (Figure 17, [Müller et al., 2019](#)). In western North America, the Late Mesozoic to Cenozoic subduction of the Farallon plate and associated processes have severely reworked the overlying continental plate. This includes the creation of thick-skinned thrust belts with strong lithospheric deformation over 1000-2000 km inboard by flat Farallon subduction during the 80-40 Ma Laramide Orogeny ([Copeland et al., 2017](#); [Dickinson, 2004](#); [Yonkee &](#)

Weil, 2015), occurrence of mid-Tertiary ignimbrite flare-up following slab rollback and subduction of the Farallon-Pacific mid-ocean ridge (MOR) (e.g., Dickinson & Snyder, 1979), development of the Cordilleran metamorphic core complexes as a result of crustal spreading of an early thickened lithosphere (Coney, 1980; Lister & Davis, 1989; Liu, 2001) and formation of the extremely extensional Basin and Range Province over the slab window due to MOR subduction (e.g., Dickinson & Snyder, 1979). Oceanic subduction with distinct slab morphologies and slab-mantle interactions also took place in other circum-Pacific regions since late Mesozoic. It has resulted in the uplift of the Andes including the Altiplano Plateau (second largest plateau in the world) with overwhelming compressional deformation but episodic extensions in western South America (Chen et al., 2019).

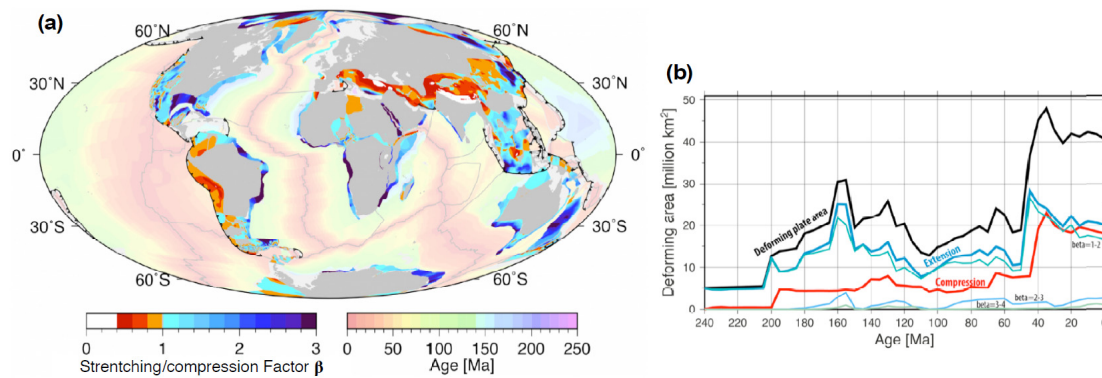


Figure 17. Distributed continental deformation over the last 240 million years (Müller et al., 2019). (a) Spatial distribution accumulated over time, with areas in extension represented by the stretching/compression factor $\beta > 1$ and those in compression by $\beta < 1$; b) Total deforming area (black), that in extension (blue) and that of shortening (red) through time. Extensional areas are further classified into three groups according to the stretching factor β : $\beta = 1-2$ (turquoise), $\beta = 2-3$ (light blue), and $\beta = 3-4$ (light green). Note that continental extension occurred mainly in the Late Jurassic and after 50 Ma, and compressional deformation of continents also increased sharply after ~50 Ma. Continental stretching and shortening since ~50 Ma dominantly reflect lithospheric deformation associated with circum-Pacific subduction and Tethyan collision.

1599

1600 In the western Pacific-eastern Asian region, on the other hand, developed large-scale
1601 extensional basins on land and back-arc basins offshore, eventually giving rise to the
1602 formation of the extension-dominated trench-arc-basin systems with vigorous
1603 volcanism both along arcs and within the continent (Liu et al., 2017). These
1604 circum-Pacific subduction processes are thought to be responsible for the
1605 basement-involved deformation and marked changes in the structure, thermal state
1606 and rheology of not only young tectonic belts but also the presumably strong
1607 cratonic lithosphere, as reported in the western part of the North American craton
1608 including Wyoming craton (e.g., Carlson et al., 2004; Dave & Li, 2016); Figure
1609 16a-b), Brazilian craton in South America (Beck & Zandt, 2002) and North China
1610 Craton (NCC) in eastern China (e.g., Xu, 2001; Zhu et al., 2011). This will be
1611 further described and discussed in 4.2 and 4.3. Along the Tethyan collisional belt,
1612 the subduction and Cenozoic closure of the Neo-Tethys ocean and subsequent
1613 collisions of the Indian, Arabian plates and the micro continental ribbon of Africa
1614 with Eurasia have led to not only the formation of the strongly deformed thrust belts
1615 of the Alps-Zagros-Himalayan orogens at the collisional front, but also severe
1616 reactivation of pre-existing weaknesses and diffuse deformation within the
1617 continental interior in south to central Eurasia (Figure 17), accompanying
1618 widespread syn- and post-collisional igneous activities (Faccenna et al., 2014;
1619 Müller et al., 2019; Yin, 2010). Such processes have given rise to the development
1620 of the giant Tibetan plateau in south Asia featured by the highest topography (~5 km)
1621 and thickest continental crust (~60-80 km) over the world (Figure 18), which has
1622 exerted profound impacts on the tectonic framework, climate and life on Earth (e.g.,
1623 Guo et al., 2002; Jolivet et al., 2018; Molnar et al., 1993).

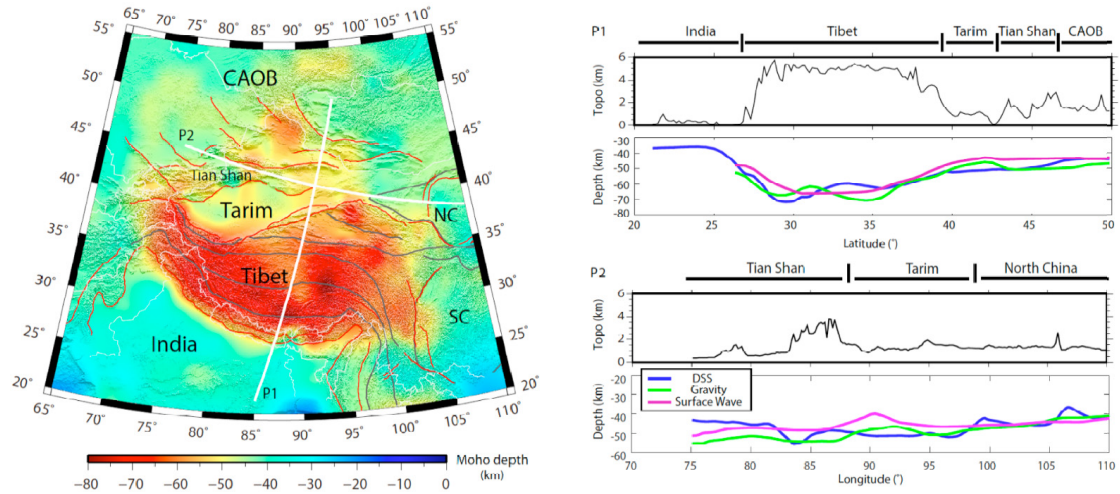


Figure 18. Variations of Moho depth in Tibet and adjacent areas mainly from deep seismic sounding (DSS) data (left) and along two profiles (right). Results from gravity inversion and surface wave tomography are compared with that of DSS along the profiles. The figure is modified from [Teng et al. \(2013\)](#). Note that the Moho is the deepest in Tibet (~60-80 km) and also depressed beneath Tian Shan (>50 km), roughly mirroring the topography. The deepening of the Moho reflects the crustal deformation in both areas induced by the Cenozoic India-Eurasia collision.

As mentioned above, continental reworking happens in broad regions including both active margins and continental interiors, even stable cratons. While reworking of continental margins is always associated with plate boundary processes of subduction or collision, reworking of intracontinental regions may or may not. The latter includes both compressional and extensional types, corresponding to mountain building and rifting, respectively, in regions that are far from plate boundaries. Compression-type intracontinental reworking has been reported worldwide, such in Central Asia, South China, Central Australia, etc., and is characterized by basin inversion, ductile shearing, middle-high temperature metamorphism and widespread magmatism ([Raimondo et al., 2010](#); [Ziegler et al., 1998](#)). This type of reworking is typically related to plate boundary processes. The Cenozoic Tian Shan range, which

is located within the Eurasian plate and originally developed in the Paleozoic as part of the Central Asian Orogenic Belt, experienced intense deformation and exhumation as a result of the India-Eurasia collision (Figure 18, [Avouac et al., 1993](#); [Tapponnier & Molnar, 1977, 1979](#)). In South China, the Early Mesozoic Paleo-pacific subduction reactivated and deformed a large area around the Neoproterozoic suture zone in between the Yangtze craton and the Cathaysian block to form the Xuefengshan orogenic belt ([Chu et al., 2019](#)). Central Australia also contains valuable records of continental reactivation and reworking. The late Neoproterozoic to early Paleozoic Petermann Orogen and the mid-Paleozoic Alice Springs Orogen there were all characterized by strain localization, crustal thickening and subsequent exhumation of mid-lower crust, accompanying spatial and temporal changes in the thermal regime of the lithosphere ([Aitken et al., 2019](#); [Hand & Sandiford, 1999](#); [Sandiford & Hand, 1998](#)), which overprinted the complex Paleoproterozoic and Mesoproterozoic orogenic belts of the region ([Holdsworth et al., 2001](#)).

Continental reworking associated with extensional deformation has also been observed widely within continental interiors, some of which are temporarily correlated with plate boundary processes that are dominated, however, by compressional deformation. For example, during the late Eocene to Oligocene coeval with the Alpine and Pyrenean orogens formed in western Europe was the development of a large rift system in the foreland of the Alps with Variscan basement (European Cenozoic Rift System, ECRIS), extending over 1100 km from the North Sea coast to the Mediterranean ([Dèzes et al., 2004](#)). Similarly, intracontinental rift systems have developed in a large area within Asia as the India-Eurasia collision proceeded in the late Cenozoic, including the N-S trending rifts in southern Tibet ([Armijo et al., 1986](#)), circum-Ordos rift systems in central China ([Zhang et al., 1998](#)), and Baikal rift system at the boundary between the stable Siberian craton and the deforming Baikal-Sayan fold belt ([Logatchev & Florensov, 1978](#)). The relationships between these intracontinental rift systems and the

continental collisional processes have not been well understood, and whether or not a mantle plume regime is required for the formation of the rifts remains debated (e.g., [Lebedev et al., 2006](#); [Merle & Michon, 2001](#); [Molnar & Tapponnier, 1975](#); [Ziegler & Dèzes, 2007](#)).

The continental lithosphere can also be significantly extended, faulted, metasomatized and weakened during either passive or active rifting processes. The present-day Atlantic passive margins are commonly characterized by increasingly high degrees of structural extension seaward, in many cases presenting a zone of marked crustal thinning (with thickness < 15-20 km) of more than 100 km wide in between the oceanic and normal continental crust ([Peron-Pinvidic et al., 2013](#)). Particularly near the ocean-continent transition, the hyperextended continental basement is severely thinned (up to <10 km) and composed of rocks of not only continental crust but also exhumed and variously serpentinized mantle as well as of magmatic intrusions and infiltrations, with faults cutting from the surface to the mantle. These features suggest that the presumably thick and strong pre-rifting intracontinental lithosphere has been modified and thinned or reworked by the rifting process. One typical example is from the Iberian margin of the southern North Atlantic that underwent extreme crustal thinning and mantle exhumation during seafloor spreading in the early Cretaceous, such that the rifting process overprinted the thermal, compositional and structural inheritance of the lithosphere from the earlier Variscan Orogeny ([Sutra & Manatschal, 2012](#)). Similar reworking was also proposed for other passive margins, such as those of the Indian plate and the South China Sea in association with rifting and seafloor spreading processes ([Calvès et al., 2011](#); [Gao et al., 2015](#)). Generally, deep-rooted mantle plumes are considered to have played an important role in many cases of such continental rifting and subsequent reworking and final breakup under extensional regime, based on the spatial and temporary coincidence between LIPs and continental breakup (e.g., [Buiter & Torsvik, 2014](#); [Storey, 1995](#)). There are, however, also

intracontinental rifts that may have not succeed in splitting a continent apart (called aulacogen). Examples of failed rifts include the ~1100 Ma-old Midcontinent Rift System in the center of the North American continent (Green, 1983), Early Cambrian Southern Oklahoma aulacogen in the southern United States (Gilbert, 1983) and Late Devonian Dniepr-Donets aulacogen in the southern part of the East European craton (Stovba et al., 1996). These failed rifts all experienced crustal thinning and extensive volcanism possibly associated with plume impingement in the early stage and crustal thickening and basin inversion with compressional deformation and faulting during later evolution (Keller & Stephenson, 2007; Stein et al., 2015), presenting complex and long-lasting reworking processes. A common tectonic setting of these failed rifts is pericratonic, for they lie within cratons but near the margins of cratons (Keller & Stephenson, 2007). The thick and rigid cratonic lithosphere may have hindered rapid upwelling of plumes and probably contributed to the failure of continental rifting and breakup in these regions.

4.2.2. Crustal Reworking

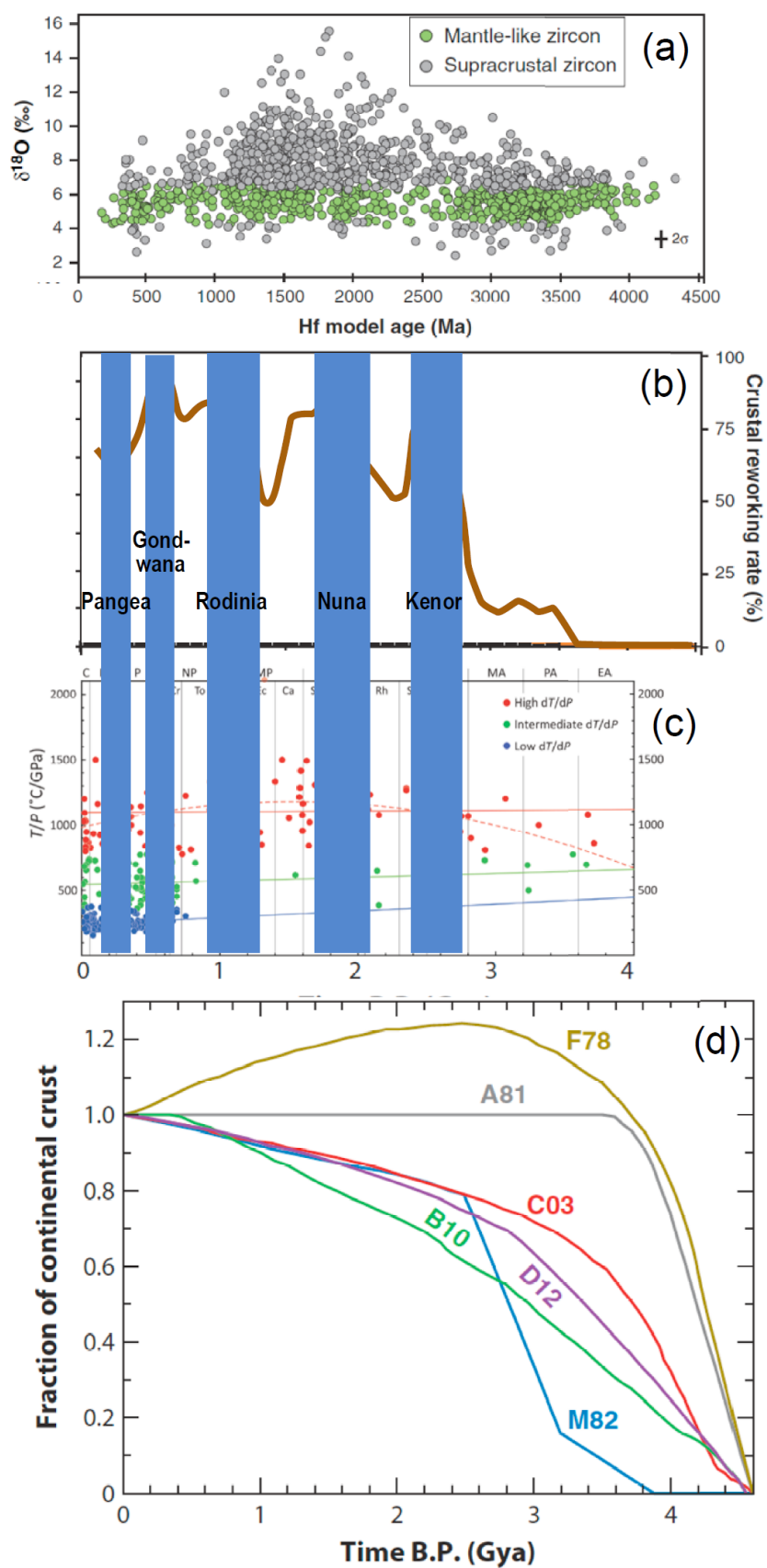
The rock units and structures of continental crust record multiple tectono-thermal events from the early formation through the long-term evolution of continents that led to various degrees of creation, reworking and destruction of continental crust (Hawkesworth et al., 2016; Stern & Scholl, 2010). Felsic granites are widespread on Earth and are the key constituent of continental crust, making the Earth unique among other planets (Campbell & Taylor, 1983; Taylor, 1989; Wu, Li, et al., 2007). It is generally believed that Archean continental crust is stable due at least partially to its lower-density felsic component, including older Na-rich tonalite-trondhjemite-granodiorite (TTG) and younger K-rich granites (Campbell & Taylor, 1983). The K-rich granites, which occupy less than 10% of the surface areas in the Archean but have dominated the exposed upper crust since 2.5 Ga, are essentially the result of intra-crustal melting (Taylor & McLennan, 1981; Wu, Yang, et al., 2007) and thus a representative product of continental crust reworking,

especially since the Archean. New geochemical observations also consistently reveal a marked decrease in the MgO content of the upper continental crust from >11 wt % before the Neoarchean to ~4 wt % at the end of Archean, reflecting a transition from a mafic upper continental crust to a felsic one like the present-day during the Neoarchean (Tang et al., 2016).

A recent combination of oxygen and hafnium isotope ratios in zircons of different ages (Dhuime et al., 2012) further reveal the ubiquitous global crustal reworking through time (Figure 19a), showing higher reworking rates (> 50% proportions of reworked crust versus newly created crust) from around the end of Archean to the present day (Figure 19b). The sharp increase in the degree of crustal reworking in the Neoarchean well coincides with the rapid compositional change of the upper continental crust, as well as the springing-up of UHT metamorphism records (Figure 19c). The significant reworking of continental crust in the Proterozoic and Phanerozoic accompanied the slowdown of continental growth (Figure 19d), probably associated with subduction-driven plate tectonics gaining maturity from the Late Archean to Paleoproterozoic and being dominant since then on the Earth's evolution (e.g., Dhuime et al., 2012; Hawkesworth et al., 2016; Sizova et al., 2010).

Crustal reworking not only affects the rock units and geochemical features, but also exerts significant impacts on the structure and properties of continental crust. For example, reworking typically led to the development of structural and compositional layering in the continental crust. It has been widely accepted that mature continental crust with an intermediate composition evolved from juvenile basaltic crust (as oceanic crust) by refining and differentiation processes, in which the occurrence of fractionation and anatectic melting give rise to the felsic granodioritic upper crust and residual and cumulate mafic gabbroic lower crust accompanied by loss of dense, pyroxene- and garnet-rich mafic to ultramafic material (Hacker et al., 2015; Stern & Scholl, 2010). Although continental crust formation and evolution may follow this general regime, the real processes are more sophisticated and diversified from region

1756 to region, resulting in complex layering and lateral variations in structure,
 1757 composition as well as deformation of continental crust.



1758

Figure 19. (a) $\delta^{18}\text{O}$ versus Hf model ages in 1376 detrital and inherited zircons from Australia, Eurasia, North America, and South America (Dhuime et al., 2012). The Hf model ages of mantle-like zircons record periods of new crust formation, whereas those of supracrustal zircons are referred to as hybrid model ages that record periods dominated by crustal reworking. (b) Variation in the reworking rates of continental crust through time calculated from the preserved proportions of reworked crust and new crust based on U-Pb and Hf analyses of zircons from Phanerozoic sediments (Dhuime et al., 2012); c) Metamorphic thermal gradient (T/P) versus age (Brown & Johnson, 2018). Three types of metamorphism are considered: high dT/dP or UHT (red), intermediate dT/dP (green), and low dT/dP or UHP (blue). Shaded areas mark the ages of supercontinents (from Hawkesworth et al., 2016). (d) Models of continental crust growth from selected literatures (Korenaga, 2013). F78 (Fyfe, 1978), A81 (Armstrong et al., 1981), M82 (McLennan & Taylor, 1982), C03 (Campbell, 2003), B10 (Belousova et al., 2010), and D12 (Dhuime et al., 2012). B.P., before present. Note that slow or even negative crust growth rates (slopes of the growth curves) in Proterozoic and Phanerozoic correspond to higher reworking rates, as exemplified in (b).

For instance, anomalous low-velocity zones (LVZs) have been widely documented in the mid-lower crust of various tectonic settings (Figure 20a-c). In active orogens such as the Himalayan-Tibetan orogen and the central Andes and young tectonic belts or volcanic areas such as the Yellowstone and northeastern China, crustal LVZs are commonly attributed to the presence of partial melts and/or aqueous fluids associated with crustal shortening and thickening (e.g., Beck & Zandt, 2002; Liu et al., 2014; Nelson et al., 1996; Yuan et al., 2000) or induced by intensive heating from mantle (e.g., Fan & Chen, 2019; Huang et al., 2015). Beneath stable cratons or old orogens, on the other hand, partial melts or aqueous fluids are not favored to explain the observed LVZs in the mid-lower crust given the in situ low temperatures and mobility of melts and fluids. Instead, felsic composition resulting from

crystallization of granitic intrusions by crustal remelting associated with ancient tectono-thermal events was thought to be more plausibly responsible for the intra-crustal LVZs in these regions (Chen et al., 2015; Yuan & Bodin, 2018). High-velocity zones (HVZs) have also been observed in continental crust of various ages, especially in the lower crust, often accompanying a transitional Moho character (Figure 20a,c-e). This structural feature is generally attributed to crustal reworking and vertical growth by mafic underplating and intrusion (Thybo & Artemieva, 2013), either during subduction-collision processes for continental assembly (e.g., Darbyshire et al., 2017; Petitjean et al., 2006; Yuan & Bodin, 2018), or associated with rifting to break-up of continents (Bronner et al., 2011; Delph & Porter, 2015; Mjelde et al., 2009; Thybo & Nielsen, 2012) or reactivation of continental interiors (e.g., Cheng et al., 2013; Zheng et al., 2006).

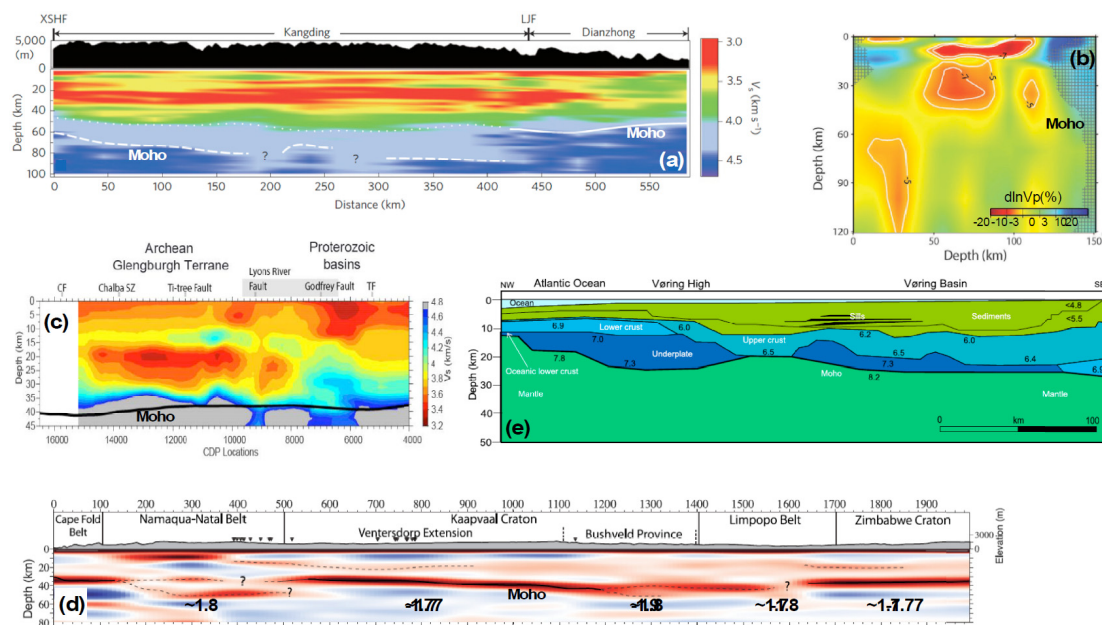


Figure 20. Crustal structures resulted from continental reworking. (a) NNW-SSE S-wave velocity cross section in Eastern Tibet (Liu et al., 2014), showing both a low-velocity zone (LVZ) in the mid crust and high-velocity zone (LVZ) in the lowermost crust (outlined by the white dotted and dashed lines). (b) NE-SW P-wave velocity cross-section traversing Yellowstone (modified from Huang et al., 2015), showing two LVZs in the upper and

mid-lower crust, respectively. These crustal LVZs are interpreted as separate magma reservoirs sourced from mantle. White lines denote the 5% and 7% P-wave velocity reduction contours. (c) S-wave velocity model along a NE-SW transect with annotated surface geological features in the western Australian craton (Yuan & Bodin, 2018). A slow midcrust is imaged beneath the Archean Glengburgh Terrance, whereas a fast lower crust is observed beneath the Paleoproterozoic basin area. SZ: shear zone. (d) NE-SW cross-section of receiver function stack and average crustal V_p/V_s ratios (numbers) in southern Africa (modified from Delph and Porter, 2015). The coincidence of thicker crust, higher V_p/V_s ratios and a gradual Moho discontinuity suggests the presences of HVZs in the lower crust beneath the Bushveld Province and Namaqua-Natal Belt. (e) P-wave velocity structure of the crust along a profile across the Vøring margin at the Norwegian shelf in the North Atlantic (Mjelde et al., 2009; Thybo & Artemieva, 2013). HVZs are observed at around the base of the crust.

Reworking of continental crust often involves significant deformation and metamorphism at depth, accompanying magmatic activities. Geophysical and geological studies suggest marked ductile deformation of the slow and weak mid-lower crust, either induced by channel flow (Bai et al., 2010; Liu et al., 2014; Royden et al., 1997; Searle et al., 2011) or from shearing along a midcrustal detachment (e.g., Gao et al., 2019; Klemperer, 2006), or partial eclogitization of the lowermost crust (e.g., Hetényi et al., 2007; Z. Zhang et al., 2014) at different areas in the Tibetan plateau. Such kind of crustal reworking is attributed to the Cenozoic to present convergence and collision between the Indian and Eurasian plates, which has caused dramatic crustal thickening (Figure 18), strong mantle deformation and crust-mantle decoupling (e.g., Gao et al., 2019; C. Wu et al., 2019). Recent seismic observations also reveal thicker crust (>40 km up to 60-70 km), marked crustal layering in both structure and deformation and a variable Moho character beneath both the Mesoproterozoic Grenville and Paleoproterozoic Trans-Hudson orogens. It

was then proposed that mid-lower crustal flow may also have taken place in these older orogens, similar to that beneath the present-day Tibetan plateau, probably associated with the extensional collapse of the orogenic plateaus during the Proterozoic continental assembly processes (Darbyshire et al., 2017; Pawlak et al., 2012; Petrescu et al., 2016). Seismic and gravity data further suggest that at least parts of the thickened crustal root beneath these and other Proterozoic orogens or tectonic zones and some Paleozoic orogens (such as the Ural Mountains) may have undergone high-grade metamorphism even partial eclogitization (Darbyshire et al., 2017; Delph & Porter, 2015; Fischer, 2002; French et al., 2009; Petrescu et al., 2016), which may have been preserved (e.g., Figure 20d) under fluid-absent conditions and/or possibly with the aid of strong subcontinental lithospheric mantle (Leech, 2001). Such a deformation style of crustal thickening and flow in older orogens is comparable to that inferred beneath the Cenozoic to present Tibetan plateau, but appears distinct from the processes in the Archean time. Lower crustal flow was speculated to also exist in the Archean, but thought to have presumably prevented significant thickening of the hotter and weaker crust and led to a relatively shallow and flat Moho at ~35-40 km depths (Calvert & Doublier, 2018; Rey & Houseman, 2006), as observed today beneath Archean cratons without significant later crustal deformation (Kaapvaal and Zimbabwe cratons in Figure 20d). That is, continental crust may have never been noticeably thickened during its Archean evolution.

Metamorphism and deformation during crustal reworking is probably best represented by UHP or UHT metamorphism and relevant deformation that crustal rocks experienced exclusively at convergent margins associated with subduction to collision orogenesis. UHP metamorphism, which registers low thermal gradients ($\leq 10\text{-}12^{\circ}\text{C}/\text{km}$ or $350\text{-}375^{\circ}\text{C}/\text{GPa}$) and deep subduction of continental crust, was documented mostly in Neoproterozoic to Phanerozoic orogens such as Himalaya-Tibet (Guillot et al., 2008) and references therein), Alps (Chopin, 1984),

Dabie-Sulu (Wang et al., 1989; Xu et al., 1992), Urals (Leech, 2001), etc. On the other hand, UHT metamorphism, the most thermally extreme type of crustal metamorphism (temperatures $\geq 900^{\circ}\text{C}$, thermal gradients $\geq 20\text{-}25^{\circ}\text{C/km}$ or $750\text{-}775^{\circ}\text{C/GPa}$), occurred throughout much of the Earth history, with ages mainly ranging from Neoproterozoic to Cenozoic (Figure 19c, Brown, 2006; Brown & Johnson, 2018; Clark et al., 2011; Kelsey, 2008). Recently, growing geochemical evidence suggests that the deep crust of Precambrian UHT metamorphic terranes could have persisted with the presence of melts under suprasolidus temperatures for $>60\text{-}200$ Ma, accompanying slow cooling and pervasive deformation (Clark et al., 2018; Horton et al., 2016; Jiao et al., 2020; Taylor et al., 2020; Walsh et al., 2015). This is distinctly different from the Phanerozoic UHP metamorphism that sustained only about $10\text{-}20$ Ma with rapid exhumation (e.g., Ernst et al., 1997). The fact that UHT and UHP metamorphism teemed in the Neoproterozoic and Neoproterozoic, respectively (Figure 19c) and the contrasting features between the two may mark significant transitions of tectonic regime at around the end of the Archean and Proterozoic, respectively (e.g., Brown, 2006; Dhuime et al., 2012; Zheng & Zhao, 2020), consistent with the secular variations in the rates of continental crust reworking and growth (Figure 19b and 19d).

4.2.3 Reworking of subcontinental lithospheric mantle

Continental reworking not only affects the structure and properties of the crust, but also changes the characteristics and even nature of subcontinental lithospheric mantle. Reworking of the continental lithospheric mantle is dominantly reflected with ubiquitous modifications in its composition through melt or fluid-induced metasomatism. This is exemplified by the widely varying major element compositions of mantle peridotites in both old cratons (kimberlite-borne xenoliths) and orogenic belts (basalt-borne xenoliths) (Figure 21, Tang, Zhang, Ying, & Su, 2013 and references therein).

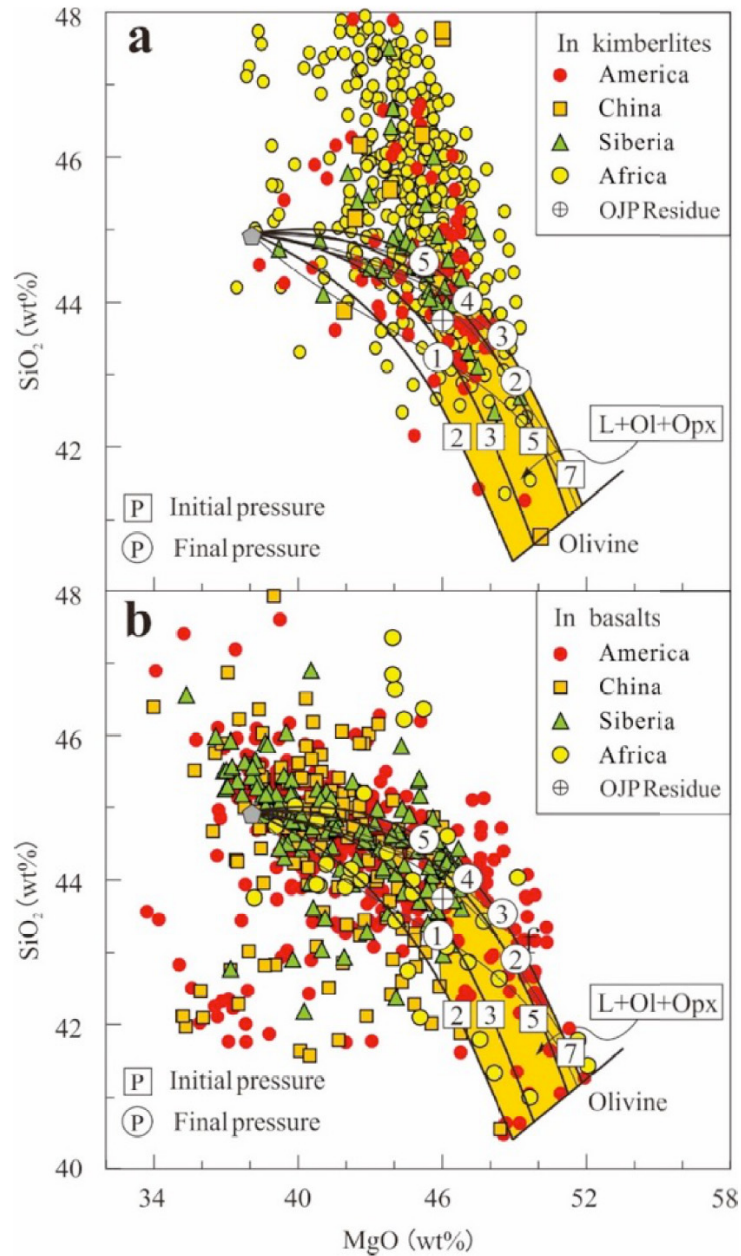


Figure 21. SiO₂ and MgO contents of peridotites in global continental lithospheric mantle. Data sources: Peridotite xenoliths in kimberlites and basalts (Doucet et al., 2012; Gornova et al., 2013; Tang, Zhang, Ying, & Su, 2013 and references therein; Howarth et al., 2014; Lin et al., 2019; Xiao et al., 2013; Yang et al., 2018; Zou et al., 2016). Bold lines labeled with squares, initial melting pressures; light lines labeled with circles, final melting pressures; brown shaded area, compositions of residual harzburgite designated as [L+Ol+Opx] after melting of lherzolite (Herzberg, 2004). The curves are individual melting curves of normal mantle peridotite, and the area covered by the melting curves gives the composition range of

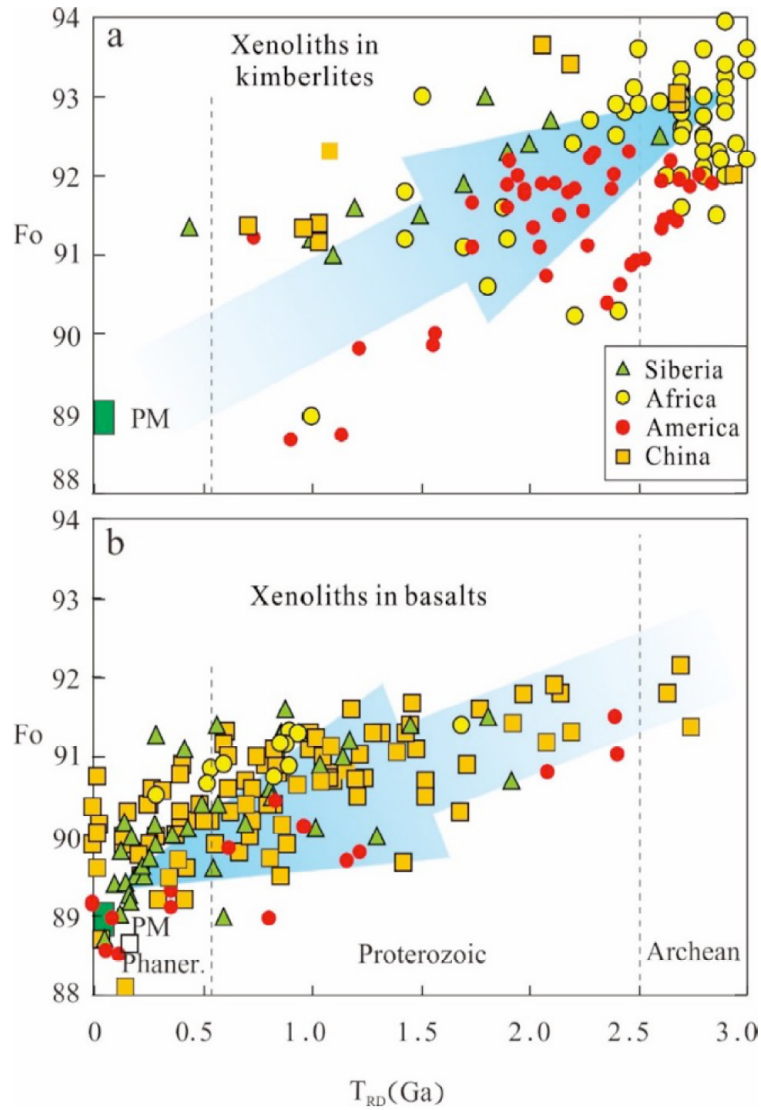
1897 residual phases after partial melting of normal mantle peridotite under different temperature
1898 and pressure conditions. The data points falling within the range of partial melting curves
1899 denote the residual of partial melting of normal mantle peridotite, whereas those falling
1900 outside the melting range do not represent the residual of normal mantle melting, but reflect
1901 the influence of melt metasomatism.

1902

1903 In particular in the typical ancient cratons of South Africa, Siberia and North
1904 America, mantle peridotites have a large range of SiO₂ contents with a significant
1905 portion being much higher than the composition range of normal mantle peridotites
1906 (Figure 21a). Such a feature indicates that these peridotites are not the pure remnants
1907 of partial melting of normal mantle peridotites, but have undergone various degrees
1908 of metasomatism with the introduction of silica-rich fluids or melts, probably related
1909 to subduction (e.g., [Bell et al., 2005](#); [Simon et al., 2007](#)). On the other hand, the
1910 common occurrence of kimberlites especially in Archean cratonic regions (Sparks,
1911 2013) and the addition of clinopyroxene, lherzolitic garnet and phlogopite etc.
1912 within the lithospheric mantle suggest another kind of metasomatism by volatile-rich
1913 and silica-poor melts, mostly associated with rising plumes (e.g., [Griffin et al., 2009](#);
1914 [Simon et al., 2007](#)).

1915 The Re-Os isotopic data of multiple sulfides in the global mantle peridotites also
1916 support the view that the subcontinental lithospheric mantle is widespread modified
1917 by peridotite-melt reaction. A large number of data show that most of the mantle
1918 peridotite xenoliths from the cratonic lithospheric mantle of Archean age have
1919 younger Re-depletion ages of Proterozoic to Cenozoic, which is well correlated with
1920 the propensity of Fo (Mg number) reduction in olivine (Figure 22). Both
1921 observations consistently reflect refertilization of the subcontinental lithospheric
1922 mantle by peridotite-melt reaction, with addition of Fe, Ca Al and Re to originally
1923 depleted protoliths (e.g., [An et al., 2017](#); [Aulbach et al., 2004](#); [Pearson, 1999](#); [Smith](#)

1924 & Boyd, 1987; Xu et al., 2008; Zhang et al., 2012). Therefore, the re-depletion
 1925 model ages of these peridotites do not represent the real formation ages of mantle
 1926 peridotites, but are the result of the multiple-phases of interactions between Archean
 1927 peridotites and melts (Shu et al., 2019; Zhang, 2009).



1928
 1929 **Figure 22.** Relationship between Re-depletion model age and Fo in olivine of peridotites in
 1930 global continental lithospheric mantle. Data sources: (Liu et al., 2015; Tang, Zhang, Ying,
 1931 Su, et al., 2013 and references therein). PM represents the primitive upper mantle.

1932

1933 The refertilization of the ancient depleted lithospheric mantle is mainly a bottom-up
1934 process as the upwelling of fertile asthenospheric material, and likely follows
1935 previously existing lithospheric weaknesses such as suture zones between ancient
1936 blocks or breaks in the Archean root (Foley, 2008; O'Reilly et al., 2001; Xiao &
1937 Zhang, 2011). Such kind of refertilization is indeed an asthenospherization of lower
1938 parts of the lithospheric mantle, which may be controlled by the topography of the
1939 lithosphere base (Foley, 2008). This process could result in a change in geochemical
1940 composition and properties (e.g., buoyancy, rheological strength, etc.) of the
1941 reworked part of the subcontinental lithospheric mantle, and thus potentially affect
1942 the stability and evolution of continents (e.g., Carlson et al., 2004; Chesley et al.,
1943 1999; Griffin et al., 2009).

1944 The widespread occurrence of reworking on the subcontinental lithospheric mantle
1945 via melt or fluid-induced metasomatism inevitably leads to enhanced water contents
1946 in the lithospheric mantle beneath continents (Peslier et al., 2017; Xia & Hao, 2013).
1947 This is evidenced by the mantle xenolith data, showing a large range of water
1948 concentrations in olivine for peridotites from several cratonic regions (Figure 10a).
1949 Although the water contents of olivine at near the base of the lithosphere (~200-km
1950 depth) in these regions are generally lower than that estimated for the asthenosphere
1951 (<10 ppm vs. ~30-70 ppm, Table 1), there do have cases of high water
1952 concentrations, such as locally beneath the Siberian craton (Figure 23). At shallower
1953 depths, i.e., ~120-150 km, anomalously high water contents (>50 ppm) in olivine
1954 appear within the lithospheric mantle of both the Kaapvaal and Siberian cratons,
1955 well exceeding the amount for the asthenosphere (Figure 23a) and inconsistent with
1956 the presumed dehydration nature of cratonic roots. The elevated water contents of
1957 olivine display positive trends with indices of metasomatism (such as modal
1958 proportion of clinopyroxene, Ni and Ti contents in peridotites) (Doucet et al., 2014;
1959 Jean et al., 2016), suggesting that the corresponding mantle xenoliths represent
1960 water-rich metasomatized peridotites rather than that of the typically dehydrated

cratonic mantle. On the other hand, the olivine from diamond inclusions in the mantle xenoliths from the Siberian craton has a much lower water content (Figure 23a), possibly due to the protection of diamonds for the inclusions from interactions with water-bearing metasomatic agents (Jean et al., 2016; Novella et al., 2015; Taylor et al., 2016). Therefore, water concentrations of olivine inclusions in diamonds are more representative for that of cratonic lithospheric mantle. Similar features are also observed for other peridotitic minerals, and the water contents in bulk-rock peridotites calculated from data measured for individual minerals show large differences in between metasomatized peridotites and those unaffected by metasomatism (Figure 23b).

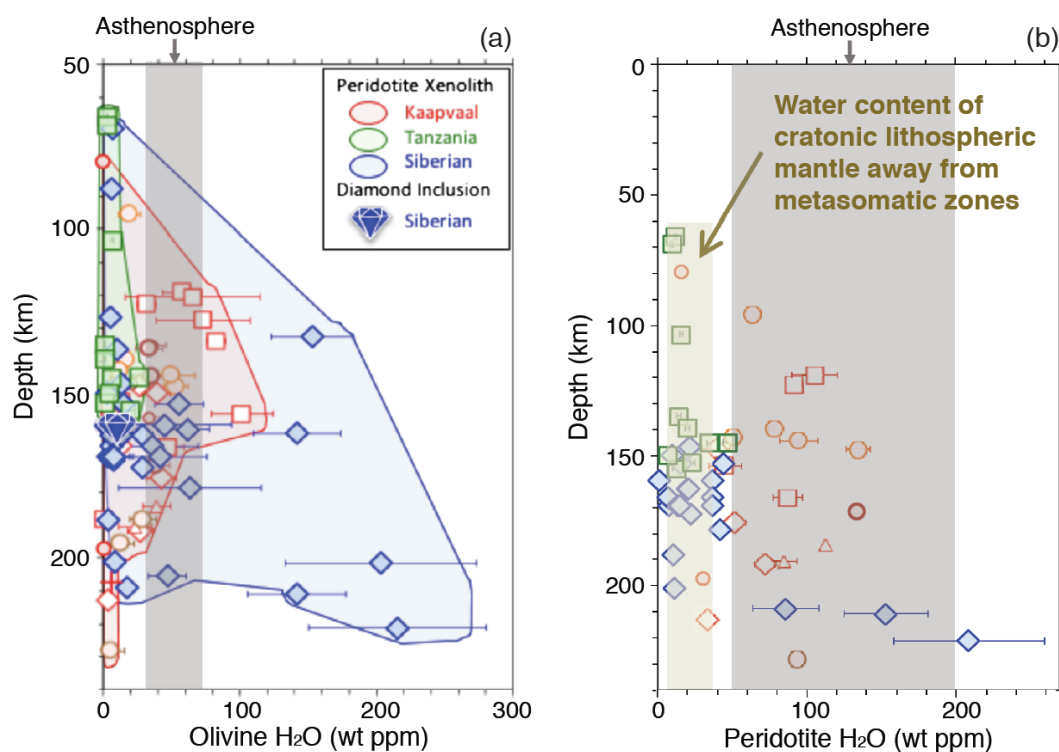


Figure 23. Water concentrations in olivine (a) and for bulk-rock peridotites (b) as a function of depth in the cratonic lithospheric for mantle xenoliths from the Kaapvaal, Siberian and Tanzanian cratons (modified from Peslier et al., 2017). Grey shaded areas represent the range of the corresponding water contents in the asthenosphere (Table 1).

1977 The water contents from xenoliths within subcontinental lithospheric mantle appear
1978 highly variable from region to region and also heterogeneous vertically (Figure 23),
1979 indicating complex and varying degrees of mantle metasomatism and thus
1980 reworking. The metasomatism-induced addition of water may have effects on the
1981 strength and rheological behavior of subcontinental lithospheric mantle. Such effects
1982 lie largely on the water concentration in olivine, the most abundant mineral of the
1983 upper mantle (>50% in volume). This is because even a trace amount of water
1984 weakens olivine (Dixon et al., 2004; Faul et al., 2016; Hirth & Kohlstedt, 1996;
1985 Karato, 2010), but water does not weaken clinopyroxene, and its weakening effect
1986 on orthopyroxene is complex (Gavrilenko et al., 2010; Ohuchi et al., 2011) and not
1987 well understood (Demouchy & Bolfan-Casanova, 2016). The water content of garnet
1988 is very limited compared with that in other phases of mantle peridotite (Demouchy
1989 & Bolfan-Casanova, 2016), and thus often not considered when evaluating the
1990 strength of the lithospheric mantle. It is worth to note that, although the large range
1991 of water concentrations in olivine of mantle xenoliths (Figure 23a) suggests high
1992 heterogeneity and complexity of lithospheric mantle reworking, primarily associated
1993 with the melting and metasomatic history of the mantle sampled by the xenoliths, it
1994 may not be indicative of large differences in the overall strength and rigidity of the
1995 cratonic lithospheric mantle, as the cratons do not show an enhanced instability with
1996 water contents of olivine.

1997 The typical cratonic lithospheric mantle is believed to remain relatively dry and
1998 strong (Peslier et al., 2017 and references therein). Taking the typical values of
1999 water contents in olivine from diamond inclusions (<10 ppm) for unaltered cratonic
2000 lithospheric mantle results in about one order of magnitude higher in viscosity at the
2001 base of the lithosphere than that of the asthenosphere (Figure 15c), consistent with
2002 the stability of most cratons. Moreover, seismic anisotropy observations show a
2003 dominant A-type fabric of olivine in the cratonic lithosphere (Baptiste & Tommasi,
2004 2014; Gung et al., 2003; Mainprice & Silver, 1993). Laboratory experimental results

2005 suggest that the A-type fabric of olivine is generally associated with a dry
2006 environment (Karato et al., 2008). All these together provide evidence for the
2007 general dry nature of the cratonic mantle lithosphere, and also indicate that, despite
2008 its common appearance among cratons, reworking by melt or fluid-induced
2009 metasomatism may be localized, possibly at lithospheric weaknesses (Peslier et al.,
2010 2017), and thus not alter the nature of the majority of the cratonic lithosphere. It is
2011 only in rare cases that severe reworking results in extremely high water contents and
2012 significant weakening of a large part of cratonic lithospheric mantle, leading to
2013 fundamental destruction of a craton. For instance, it was reported that the
2014 lithospheric mantle of the eastern NCC was highly hydrated (>1000 ppm) and
2015 metasomatized in the Early Cretaceous (~120 Ma) (e.g., Xia et al., 2013), a time
2016 period when this part of the craton was destroyed with a loss of more than 100 km of
2017 its mantle root (see 4.2.3 and 4.3).

2018 Complex metasomatism and reworking of continents is also manifested by the
2019 structural features and detailed fabrics of deformation in the lithospheric mantle. As
2020 mentioned before, continental lithosphere is characterized by large structural and
2021 rheological contrasts particularly between cratonic cores and surrounding mobile
2022 belts (4.1.3, Figure 16a-c). Such a characteristic represents the tectonic imprints of
2023 multiple phases of reworking mainly concentrated at weak zones in the lithosphere
2024 during the long-term evolution of continents, possibly superposed upon intrinsically
2025 different structural features associated with diverse continental formation processes
2026 (e.g., Begg et al., 2009; Chen, 2010; Schaeffer & Lebedev, 2014). Strong reworking
2027 especially in relatively weak continental lithosphere is evidenced by observations of
2028 localized softening and deformation to form mantle shear zones with various grain
2029 sizes in orogenic belts (e.g., Dickinson, 2004; Kaczmarek & Tommasi, 2011;
2030 Reuber et al., 1982), which often involves melt-rock reactions and fluid infiltration
2031 and thus further reduces the strength of the lithosphere (Dickinson, 2004). Moreover,
2032 the occurrence of earthquakes within the presumably strong and aseismic

lithospheric mantle beneath continents, e.g., the 2013 Mw 4.8 Wyoming earthquake at ~75-km depth (Prieto et al., 2017), deep seismicity below the Moho both along the Newport-Inglewood fault in southern California (Inbal et al., 2016) and in the Himalayan collision zone (Schulte-Pelkum et al., 2019), probably all reflects on-going weakening and reworking of the subcontinental mantle lithosphere in these areas.

Mobile belts surrounding cratons or tectonic boundary zones, which are mechanically weaker than cratonic interiors, generally experience more intensive reworking and exhibit lower-velocities or lower-resistivities, with sharp structural changes or distinct deformation patterns in the deep lithosphere compared with adjacent cratonic nuclei (e.g., Figure 16a-c). Experimental and theoretical studies indicate that, lithospheric weak zones could be long-lived structures, due to the extremely slow grain growth and healing of mantle rocks after being weakened (several 100 Myrs or more) compared to the fast weakening processes (in 1 Myrs or less) (e.g., Bercovici & Ricard, 2012; Chu & Korenaga, 2012). Therefore, pre-existing structures in the lithosphere have been the primary control on the tectono-thermal evolution and reworking of continents (Audet & Bürgmann, 2011; Buiter & Torsvik, 2014; Frizon de Lamotte et al., 2015; Heron et al., 2016; Thomas, 2006). The rheological weakness and mechanically anisotropic behavior of the pre-existing structures make them function as the sites of strain localization and intensive heating in the lithosphere during tectono-thermal events, leading to further weakening of these zones (Thomas, 2006; Tommasi et al., 2001; Vauchez et al., 1998). Such effects may repeatedly intensify the contrast in the lithospheric structure and properties across cratonic margins or tectonic boundary zones, and are considered to be responsible for the distinct present-day structural heterogeneities of continental lithosphere (Figure 16; Keranen & Klemperer, 2008; Schaeffer & Lebedev, 2014; Snyder et al., 2017; Zhu et al., 2011). This also well explains the observations that, during episodic assembly and break-up of continents in

association with the closure and opening of ocean basins, continental margins are repeatedly reworked with focused deformation and magmatism during subduction, collision and rifting, whereas continental cores remain largely intact (Buiter & Torsvik, 2014; Frizon de Lamotte et al., 2015; Houseman & Molnar, 2001; Li et al., 2008).

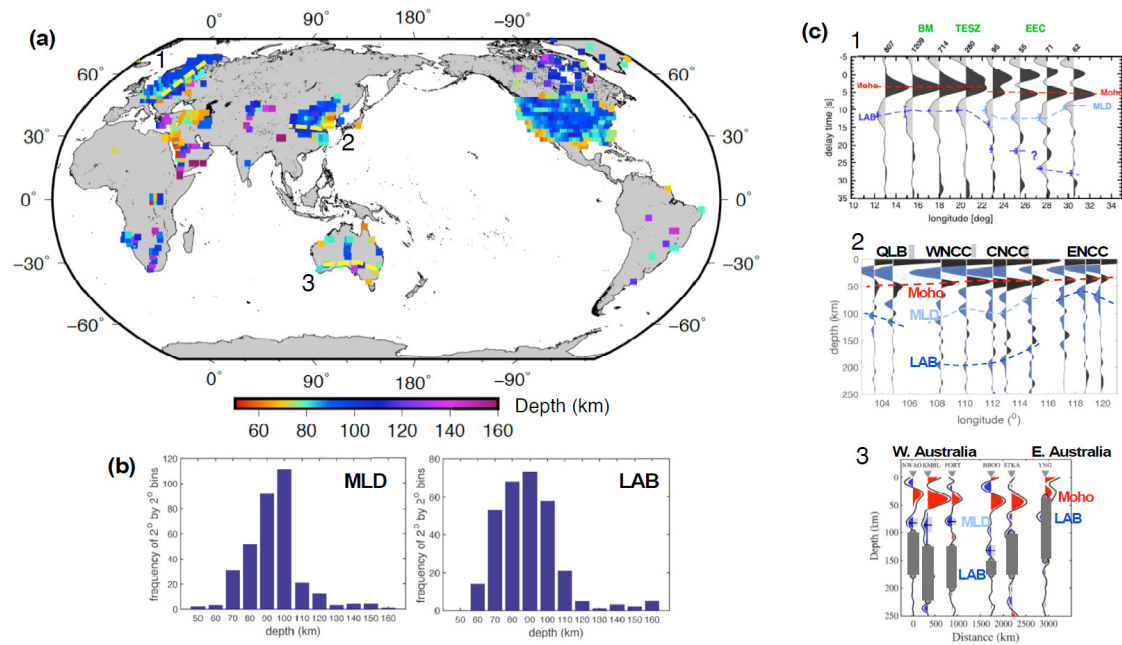


Figure 24. (a) Depth map of the discontinuity with a downward velocity decrease in the shallow upper mantle (≤ 160 km) beneath continents (modified from Chen, 2017). Only results from teleseismic converted wave (Sp or Ps) studies are considered to ensure similar resolutions, and recent studies, i.e., Yuan et al. (2017) for northwestern Namibia, Kennett and Sippl (2018) for central Australia, Chen et al. (2018) and Hopper and Fischer (2018) for U.S. are complemented to and Y. Zhang et al. (2019) for the North China Craton is used to update the dataset of Chen (2017). The locations of the three cross-sections in (c) are shown as yellow dashed lines; b) Spatial frequency of the depths in (a) but only for the interpreted MLD beneath cratonic regions (left) and the LAB beneath tectonically active regions (right); c) Three cross-sections of Sp waveforms: NE-SW oriented across the Trans-European Suture Zone (TESZ) (Knapmeyer-Endrun et al., 2017), E-W oriented across the North China Craton (modified from Chen et al., 2014), and E-W oriented in southern Australia

(modified from [Ford et al., 2010](#)). Moho, MLD and LAB are marked. These cross-sections show similar depths of the cratonic MLD and the LAB in adjacent tectonic regions.

In addition to reworking of cratonic margins and tectonic boundary zones that gives rise to significant lateral structural heterogeneities, continental evolution and reworking also result in marked vertical variations or layering of the structure and properties in not only the crust (e.g., Figure 20) but also the subcontinental lithospheric mantle. Recent seismic studies consistently reveal a sharp velocity reduction in a depth range of ~60-150 km but mostly clustered at ~70-100 km depth within the thick mantle root beneath cratonic regions (Figure 24; [Chen, 2017](#); [Fischer et al., 2010](#); [Selway et al., 2015](#) and references therein). The corresponding velocity discontinuity is thus named the mid-lithospheric discontinuity (MLD), marking the top of a relatively low-velocity layer (LVL) within the overall high-velocity cratonic lithospheric mantle. The common observations of the MLD and the underlying LVL beneath cratons indicates pronounced vertical structural variations or layering of continental lithospheric mantle ([Chen, 2017](#); [Yuan & Romanowicz, 2019](#) and references therein). The MLD is featured as a rather sharp discontinuity, with a shear-wave velocity reduction of several to over 10% generally within a 30-40 km depth range ([Selway et al., 2015](#)).

In cases, it was reported that the velocity drop at the MLD broadly coincides with vertical variations in other physical (e.g., seismic anisotropy, electrical resistance) or chemical properties (e.g., petrological characteristics) (e.g., [Chen et al., 2009](#); [Fichtner et al., 2010](#); [Wirth & Long, 2014](#)), possibly reflecting a same origin. In particular in the Kaapvaal craton, the structural layering of the lithospheric mantle observed seismically ([Sodoudi et al., 2013](#)) appears correlated with the vertical variations of both Mg# in olivine and shear-wave velocity calculated from whole-rock composition ([Griffin et al., 2009](#)), and also of the water content in

olivine that appears high (> 50 ppm) at $\sim 4\text{--}5$ GPa ($\sim 120\text{--}150$ km depth) and obviously decreases below ~ 5.5 GPa to almost dry (< 10 ppm) at the base of the lithosphere (Figure 10a, [Peslier et al., 2010, 2017](#)). Collectively, the structural feature of the MLD was typically attributed to the accumulations of hydrous or other volatile-rich minerals that are particularly stable at the MLD depths through melting or fluid-induced metasomatism (e.g., [Aulbach et al., 2017](#); [Saha et al., 2018](#); [Selway et al., 2015](#)), although other mechanisms were also proposed (e.g., [Karato et al., 2015](#); [Rader et al., 2015](#); [Thybo, 2006](#)). In combination with the geochemical observations showing widespread interactions between Archean peridotites and melts in cratonic regions (Figures 21–22), it may be reasonable to speculate that the velocity reduction and probably also other property variations at the MLD mainly results from the long-term multiple stages of refertilization of the lithospheric mantle, as previously suggested ([Aulbach et al., 2017](#); [Griffin et al., 2009](#)). It is possible that inherited fabrics related to the Archean formation of continental lithosphere may also contribute (e.g., [Chen et al., 2009](#); [Lee et al., 2011](#); [Rader et al., 2015](#)).

It is also interesting to note that both the depths and structural feature of the MLD beneath cratons are comparable to those of the LAB in tectonically active regions ([Calò et al., 2016](#); [Chen et al., 2014](#); [Foster et al., 2014](#); [Rychert et al., 2010](#); [Thybo, 2006](#)), even similar to the LAB beneath oceanic lithosphere (e.g., [Kawakatsu et al., 2009](#); [Olugboji et al., 2016](#)). Such observations probably reflect a genetic link between these discontinuities ([Chen, 2017](#)). A number of models have been proposed to relate of the cratonic MLD with the LAB beneath tectonic regions, such that a new and shallow LAB forms following the original MLD after the removal of the lower part of a weakened cratonic mantle root ([Aulbach et al., 2017](#); [Chen et al., 2014](#)), or that the LAB of a young and thin lithosphere gradually transforms to a MLD as the lithosphere progressively cools and thickens ([Rader et al., 2015](#)). In either model, the development of the MLD or the LAB is closely linked to the

evolution and reworking of continents, which is yet to be fully understood. In addition to the MLD commonly observed at ~70-100 km depth, recent studies also detect other deeper discontinuities with either velocity increase or decrease with depth within or immediately below the continental lithospheric mantle (e.g., Calò et al., 2016; Sodoudi et al., 2013; Wu et al., 2020), implying more complicated vertical structural variations beneath continents.

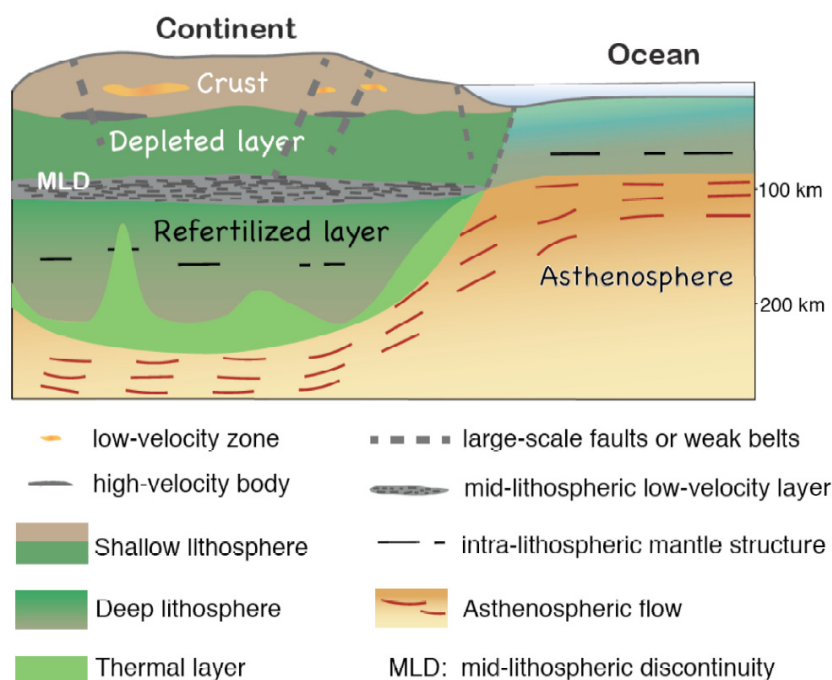


Figure 25. Conceptual model of continental lithosphere, showing lateral and vertical structural heterogeneities resulted from long-term evolution and reworking in comparison with oceanic lithosphere (modified from Yuan and Romanowicz, 2019).

Overall, it is the long history of evolution and particularly complex reworking of continents that result in the present-day striking structural heterogeneities, not only laterally but also vertically, of the continental lithosphere compared to its oceanic counterpart (Figure 25). In cratons, such heterogeneities likely mark mechanically weaknesses of various scales inside the overall strong cratonic lithosphere. The vertical heterogeneities, such as the weak layer topped by the MLD at ~70-100 km

depth, may behave similarly and play a similar role during deformation and magmatic processes as the laterally weak boundary zones discussed before (e.g., [Chen, 2017](#); [Hu et al., 2018](#)). Both these vertical and lateral weaknesses, once created, could have combined to exert significant impacts on the ensuing evolution and facilitate reworking of cratons.

4.2.4 Temporal and Spatial Extent of Continental Reworking

Reworking of continents occurs widely in both time and space. The reworking processes are mostly associated with the operation of plate tectonics, as reflected by the sharp increase in the reworking rate of continental crust (Figure 19b) and the teeming of UHT metamorphism in the Neoarchean (Figure 19c), a time period during which plate tectonics was thought to have become vigorous (e.g., [Dhuime et al., 2012](#); [Hawkesworth et al., 2016](#); [Sizova et al., 2010](#); [Tang et al., 2016](#)). The degree of continental crustal reworking appears to be well correlated with the evolution of supercontinents, showing increased reworking coeval with the supercontinent assembly (Figure 19b). The periods of intensified continental crust reworking during the supercontinent assembly witnessed the more frequent occurrence of deep crustal metamorphism (Figure 19c) and enhanced reworking of sedimentary materials as represented by elevated $\delta^{18}\text{O}$ of zircons ([Spencer et al., 2014](#)). Moreover, the U-Pb crystallization ages of detrital zircons over the Earth's history also peak at the same periods ([Voice et al., 2011](#)), which is considered to reflect better preservation of magmatic rocks generated in the late stage of subduction and collision associated with crustal thickening. These observations were interpreted to reflect more pronounced reworking of pre-existing continental crust during the periods of continental collision and development of supercontinents ([Hawkesworth et al., 2016](#)). On the other hand, more intensive magmatism with higher rates of juvenile crust generation happens during oceanic subduction before collision ([Clift et al., 2009](#); [Stern & Scholl, 2010](#)). However, it has been widely documented that continental crust is also destroyed by erosion, subduction and in

2179 cases delamination along subduction zones, at rates comparable to, or even greater
2180 than the rates of new crust generation ([Clift et al., 2009](#); [Scholl & von Huene, 2009](#);
2181 [Stern, 2011](#)). Collectively, both destruction and reworking of continental crust,
2182 which reshape the continents, mostly occur in the processes of oceanic subduction
2183 and continental collision during the assembly of supercontinents. Considering that
2184 the protection role of subcontinental lithospheric mantle to the overlying crust and
2185 the importance of crust-mantle coupling for the longevity of continents (see 4.1.2), it
2186 is expected that reworking and destruction of the subcontinental lithospheric mantle
2187 would be almost simultaneous to that of the continental crust.

2188 Spatially, reworking of continents preferentially takes place at continental margins,
2189 mostly along subduction and collision zones as indicated above, and to a lesser
2190 extent also happens at intracontinental zones and rifting margins. These reworked
2191 zones are usually pre-existing weaknesses (e.g., faults, ancient sutures) of
2192 continental lithosphere ([Audet & Bürgmann, 2011](#); [Bercovici & Ricard, 2012](#);
2193 [Buiter & Torsvik, 2014](#); [Frizon de Lamotte et al., 2015](#); [Heron et al., 2016](#);
2194 [Holdsworth et al., 2001](#)), as demonstrated before. During plate tectonic processes,
2195 the lithospheric fabrics and properties of the continental margins could be
2196 significantly altered, whereas the cratonic interior surrounded by these marginal
2197 zones are usually not noticeably affected. For example, the major part of the cratons
2198 in North America and South America remain rigid, thick and stable despite long
2199 periods of oceanic subduction to the west (Figure 16a, [Carlson et al., 2005](#)).
2200 Continental rifting also mostly occurs along tectonic belts that wrap around cratonic
2201 cores, such as the two branches of the East Africa rift system encircling the
2202 Tanzanian Craton ([Fletcher et al., 2018](#)), the Yinchuan-Hetao and Fenwei rift
2203 systems surrounding the stable Ordos block of the western NCC ([Zhang et al., 1998](#)),
2204 and the Baikal rift developed at around the southern boundary of the Siberian Craton
2205 ([Logatchev & Florensov, 1978](#)). And in many, if not all, cases of oceanic opening,
2206 for examples for the Atlantic and Indian Oceans, passive margins break up often

2207 along former sutures with or without the help from rising plumes (Buiter & Torsvik,
2208 2014; Frizon de Lamotte et al., 2015). Moreover, as mentioned before, although
2209 reworking of the lithospheric mantle by melt- or fluid-induced metasomatism is
2210 commonly observed and results in elevated water contents in stable cratons (Figure
2211 23), it does not obviously affect the overall nature of the cratonic lithosphere. This
2212 could be because such kind of metasomatism more focuses at pre-existing
2213 weaknesses (Foley, 2008; Peslier et al., 2017) or intralithospheric depths, such as the
2214 MLD layer that does not directly contact with and thus is not easily affected and
2215 weakened by the convecting asthenosphere (Figure 25).

2216 Although continental reworking is usually concentrated at lithospheric weaknesses,
2217 in specific cases it does happen in cratonic regions, resulting in reactivation and
2218 modification, even destruction of the presumably strong cratonic lithosphere.
2219 Following previous studies (e.g., Carlson et al., 2005; Wu et al., 2008; Zhu et al.,
2220 2011), here the phrase of craton destruction or decratonization refers to a kind of
2221 geological phenomena that both the lithospheric mantle and the crust of a craton are
2222 severely reworked, such that the craton loses its intrinsic stability. As demonstrated
2223 in 4.2.1, the western North American craton especially Wyoming craton, the
2224 Brazilian craton in South America and the NCC in East Asia are such examples that
2225 have experienced at least partial destruction since the Mesozoic.

2226 The NCC is considered to be the most significantly destroyed craton in the world
2227 (Carlson et al., 2005; Zhu et al., 2011). After its formation at ~1.85 Ga by the
2228 amalgamation of the eastern and western blocks (eastern and western NCC) of
2229 Archean ages along the Trans-North China Orogen (central NCC) (Zhao et al., 2001,
2230 2005), the NCC was not noticeably disturbed and remained stable like other typical
2231 cratons until the Mesozoic. However, severe reworking of the eastern NCC, as
2232 manifested by significant lithospheric extension with the formation of widespread
2233 metamorphic core complexes, pull-part basins and grabens, intensive magmatism
2234 and large-scale gold mineralization, took place in the early Cretaceous (~135-115

Ma), leading to vital destruction of this part of the craton (e.g., [F. Y. Wu et al., 2019](#); [Zhu et al., 2012a](#)). It was suggested that the eastern NCC lost more than 100 km of its mantle root and its crust was also thinned, chemically modified and weakened during the destruction, whereas the lithosphere of the central and western NCC was only locally thinned and modified and has largely retained its cratonic nature over the long-term evolution (e.g., [Chen, 2010](#); [Xu, 2001](#); [Zhu et al., 2011](#)).

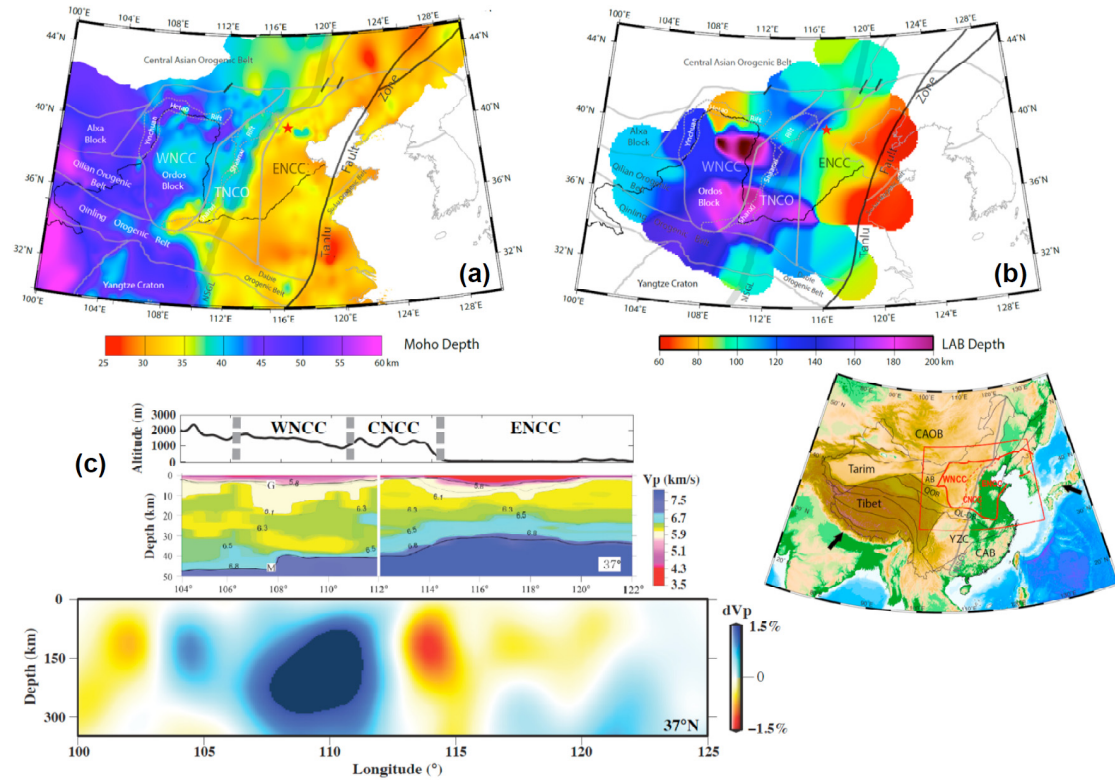


Figure 26. Depth distributions of the Moho (a) and the LAB (b) in the NCC and crustal and upper mantle P-wave velocity structure together with altitude along 37°N latitude across the craton (c), showing large differences in crustal and lithospheric thickness and structure and topography as well between the eastern NCC (ENCC) and the central (CNCC or TNCO) - western NCC (WNCC). The Moho depth data used in (a) are from [Wei et al. \(2015, 2016\)](#); b) is modified from [Y. Zhang et al. \(2019\)](#). The crustal and upper mantle velocity models in (c) are from [Zheng et al. \(2017\)](#) and [Xu et al. \(2018\)](#), respectively. G – base of sediments; M – Moho. Inset shows the distinct E-W difference in topography (low land in the east and plateaus or mountains in the west separated roughly by the North-South Gravity Lineament,

or in brief, NSGL) in eastern China, which broadly coincides with the deep structural variations as observed in the NCC (a-c). Red lines outline the NCC and the spatial range of (a,b). AB – Alxa block; CAB – Cathaysia block; CAO – Central Asian Orogenic Belt; QL-DB – Qinling-Dabie Orogenic Belt; QOB – Qilian Orogenic Belt; YZC – Yangtze Craton.

Today the eastern NCC shows a thin crust (<35 km) and lithosphere (mostly <100 km) with a slow, fertile and young lithospheric mantle, in contrast to the thicker crust (~35-50 km) and generally fast, thick and stable mantle root with localized thinning and modification in the central and western NCC (Figure 26a-c) and also differing from the crustal and lithospheric structure of typical cratons in the world (e.g., Table 1). It is interesting to note that the characteristic variation of surface topography is broadly concordant with the E-W difference in the crustal and lithospheric structure (Figure 26) and associated spatially uneven reworking and destruction of the NCC (Chen, 2010; Xu, 2001; Zhu et al., 2011), suggesting the involvement of the entire lithosphere from the surface to the base during the craton destruction.

The Wyoming craton in western U.S. was also reported to have considerably reworked and partially destroyed during the Late Cretaceous to Paleocene Laramide orogeny and later processes, with a significant portion of its lower lithosphere eroded and partially replaced by juvenile mantle (Figure 16a-b; Carlson et al., 2004; Dave & Li, 2016; Snyder et al., 2017). Similarly, the lithosphere of the western Brazilian craton was documented to have been thinned and destroyed associated with the Cenozoic Nazca plate subduction (Beck & Zandt, 2002), but less information is available.

The cratons that have experienced various degrees of destruction since the Mesozoic are all along the circum-Pacific subduction zones, and the reworking and destruction

of their cratonic lithosphere are suggested to be triggered largely by oceanic subduction (e.g., [Beck & Zandt, 2002](#); [Snyder et al., 2017](#); [F. Y. Wu et al., 2019](#); [Zhu et al., 2011](#)). This will be discussed later in 4.3. Recent studies on the Wyoming craton and NCC suggest that the destruction of these cratons may have been closely related to a rapid change of subduction regime from an early flat or shallow-angle subduction to a later steep subduction following fast trench retreat, accompanying intensive lithospheric deformation from compressional to dominantly extensional, infiltration of large volumes of fluids and voluminous magmatism on the overlying continental lithosphere (e.g., [F. Y. Wu et al., 2019](#); [Yonkee & Weil, 2015](#)). Although the details need further investigation, it indicates that destruction of cratons may not take place casually and evenly in time and space, but probably happen with specific conditions or features of plate tectonics, particularly of oceanic subduction. That means that craton destruction would be temporarily and spatially confined, consistent with less such observations than those of the long-term stability and preservation of cratons ([Carlson et al., 2005](#)).

4.3. Mechanisms of Continental Reworking

Two main mechanisms or dynamic triggers have been proposed for the reworking of continents, in particular cratons. One is oceanic subduction, and the other is mantle plume activity, representing processes at plate boundaries and underneath plates, respectively. The key factors dominating these processes and their effects on the cratonic stability are, however, still controversial.

4.3.1. Mantle Plume Perspective

It has been proposed that mantle plume impingement can cause thinning, refertilization and destabilization of the continental lithosphere through thermo-mechanical-magmatic erosion (e.g., [Foley, 2008](#); [Lee et al., 2011](#)). Numerical simulation studies suggest that a typical thick Archean lithosphere cannot be thinned significantly via thermomechanical erosion by a hot mantle plume over a

2305 short period of time (<100-200 Ma, [Petitjean et al., 2006](#); [Wang et al., 2015](#)). For a
2306 more effective lithospheric erosion and refertilization, sufficient amounts of melts
2307 are required. However, such a process is largely suppressed beneath cratons with
2308 thick lithospheric roots. This is because 1) mantle plumes are preferentially
2309 deflected away to areas of thin lithosphere, e.g., craton margins compared to the
2310 craton interior, making the interactions between mantle plumes and thick cratonic
2311 root short-lived and less intensive and hence preventing erosion of the thick root
2312 from below ([Foley, 2008](#)); and 2) decompression melting is greatly reduced beneath
2313 thick cratonic mantle root, due to relatively high pressure and the lack of adequate
2314 space for decompression above the solidus ([Lee et al., 2011](#)). Therefore, the
2315 influence of mantle plumes on thick lithosphere of Archean cratons by means of
2316 thermomagmatic erosion is expected to be limited, and may not noticeably
2317 contribute to craton destruction.

2318 Structurally heterogeneities commonly presented in cratonic lithosphere may help to
2319 enhance the effects of mantle plumes. It has been reported that laterally weak belts
2320 in continental lithosphere are often the areas of intense heating and strain
2321 concentration during tectono-thermal events (e.g., [Tommasi et al., 2001](#)). The weak
2322 layer topped with the MLD within cratonic lithospheric mantle was also suggested
2323 to be the focus of ductile deformation at mantle depths ([Chen, 2017](#); [Prieto et al.,](#)
2324 [2017](#)). A recent geodynamic study proposed that energetically rising mantle plumes
2325 could preferentially concentrate to pre-existing weak belts in stable cratonic regions
2326 and trigger the removal of the lower part of the thick lithosphere by progressively
2327 peeling off the cratonic root along the weak MLD layer, causing widespread surface
2328 uplift and volcanism ([Hu et al., 2018](#)). Such a process and later vertical accretion
2329 and thickening of the lithosphere were invoked to link the evolution of cratons with
2330 mantle plume activities in terms of plume-lithosphere interaction, which indeed well
2331 explains the kimberlite volcanism, sedimentation and unroofing history of the
2332 western Gondwana cratons since the Cretaceous and the present-day crustal and

2333 mantle structure of the region (Hu et al., 2018). Seismic observations in South
 2334 Africa, a region that was once part of western Gondwana, further show that the
 2335 mantle plume-related kimberlite volcanism and corresponding lithospheric
 2336 modifications apparently cluster at relatively weak and low-velocity belts within
 2337 cratons or craton margins, without changing the lithospheric structural coherency
 2338 and long-term stability of the craton cores (Begg et al., 2009; Griffin et al., 2009).
 2339 Such a feature is also present in North America where diamond-bearing and
 2340 non-diamondiferous kimberlites tend to occur within or at the boundaries or
 2341 surrounding areas of the high-velocity cores of cratons with various degrees of
 2342 velocity reduction (Figure 16a; Schaeffer & Lebedev, 2014), suggesting lithospheric
 2343 reworking to different extents on relatively weaker parts of the lithosphere but
 2344 without affecting the overall structure and nature of the craton interior.

2345 Indeed, there is little evidence for any Archean craton having been destroyed by
 2346 underlying mantle plumes, even superplumes (Lee et al., 2011; Wu et al., 2014). In
 2347 addition to the western Gondwana cratons and those in North America mentioned
 2348 above, a plenty of other cratons in the world, such as the Siberian craton (Howarth et
 2349 al., 2014; Reichow et al., 2009), Indian craton (Chalapathi Rao et al., 2013;
 2350 Lehmann et al., 2010), Eastern European craton (Downes et al., 2005; Wu et al.,
 2351 2013), Tarim craton (Xu et al., 2014), western Yangtze craton (Xu et al., 2004), etc.,
 2352 which all have been noticeably affected by plume activities with or without
 2353 significant lithospheric thinning, remain rigid and stable today. This indicates that
 2354 mantle plumes may not be efficient in causing severe refertilization and
 2355 destabilization of cratons, even being capable of inducing marked thinning of
 2356 cratonic lithosphere by making use of both lateral and vertical within-lithosphere
 2357 weaknesses (Figure 27a). Probably the accretion of remnant mantle plume materials
 2358 from below could even result in a rapid thickening of the thinned lithosphere in the
 2359 wake of the mantle plume activity, as suggested in some cratonic regions of eastern

Europe and western Gondwana (e.g., Hu et al., 2018; Wu et al., 2014; Yuan et al., 2017).

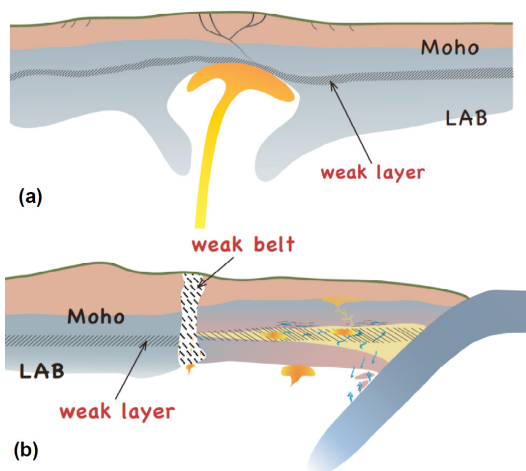


Figure 27. Schematic models of lithospheric delamination and thinning caused by plume-lithosphere interaction (a) and lithospheric destruction of a craton caused by oceanic subduction (b). In (a), the cratonic lithosphere is not severely refertilized and destabilized by the plume, although delamination of the lower part of the cratonic lithosphere may happen along the MLD-topped weak layer, caused by the upwelling of the plume along a horizontal weak belt within the cratonic lithosphere. After delamination, melt-depleted plume materials could accrete from below to the bottom of the thinned lithosphere and result in a rapid lithospheric thickening in the wake of the plume activity. Modified from Hu et al. (2018). In (b), the composition and properties of the cratonic lithosphere is greatly changed during the long-term oceanic subduction. The lower part of the lithospheric mantle is severely metasomatized via infiltration of fluids released by subducting slabs and melts in the mantle wedge. The portion that is surrounded by the MLD-topped weak layer and a major weak belt in the lithosphere is eventually destroyed by rapid erosion and/or delamination. The upper part of the lithospheric mantle and the crust are also modified and weakened by subduction-related magmatic and deformation processes, especially after delamination.

4.3.2. Plate Tectonics Perspective

Compared with mantle plume activities, plate tectonic processes are more efficient for reworking as well as accretion of continents (see section 3 and also (Stern & Scholl, 2010; Tang et al., 2016), due largely to the vigorous recycling of water and other volatiles and involvement of more significant deformation and metamorphism.

Water abundance or accessibility of fluids is probably the most important factor in controlling the style, degree and process of continental reworking. For example, fluid flows and associated fluid-rock interactions are of central importance in controlling the reactivation of shear zones and fault systems as well as deep crustal deformation and metamorphism during orogenic processes (Austrheim, 1998; Cartwright et al., 2000; Stewart et al., 2000). In particular, fluid is required for efficient eclogitization, and thus accessibility of fluids is key for whether or not crustal roots can survive from delamination to arrest orogenic collapse (Leech, 2001). Moreover, the presence of water promotes partial melting and facilitates melt- or fluid-induced metasomatism to modify the composition and affect the density and rheology of subcontinental lithospheric mantle (Karato, 2010; Peslier et al., 2017; Tang, Zhang, Santosh, et al., 2013), which are key factors to influence the stability and longevity of cratons. Large amounts of water and easy accessibility of fluids are mostly favored at convergent boundaries, especially in subduction zones (Cai et al., 2018; Dixon et al., 2002; Hirschmann, 2006; Karato, 2010). Moreover, the prevailing oxidation conditions above subducting slabs were also suggested experimentally to be an important factor in softening mantle peridotites (Cline II et al., 2018). These features thus make subduction zones the most significant sites of both creation of juvenile continental crust and loss and reworking of pre-existing one over other tectonic settings (Clift et al., 2009; Hawkesworth et al., 2016; Stern & Scholl, 2010).

Another main difference between subduction processes and mantle plume activities in affecting continental evolution is probably their different durations in function. Mantle plume activities do not focus on the same continental region for a sufficient

long period. Considering a typical plate speed of 5 cm/yr, the distance from the mantle plume to the original site of plume impingement after 50 Ma would be 2500 km, which is too far for the mantle plume's effects to remain on the lithosphere of the original site. On the other hand, subduction zones can be much longer-lived along a continental margin and the subduction processes can continuously affect the physical and chemical properties and thus control deformation of the overlying continental lithosphere. For instance, the eastern margin of East Asia has been an active continental margin associated with Paleo-Pacific subduction since ~200 Ma (Wu, Li, et al., 2007; Xu et al., 2013), and the Cordilleran active continental margin in eastern Pacific started in Late Triassic or even earlier (Barth et al., 2011; Boschman et al., 2018; Riggs et al., 2016). These suggest that both continental regions have been influenced by oceanic subduction in the Pacific tectonic domain for at least ~200 Ma. If considering earlier subduction events that may have also imposed effects on the two regions, e.g., the Paleo-Asian ocean subduction from north and Paleo-Tethyan ocean subduction from south beneath East Asia during Paleozoic to early Mesozoic (Meng & Zhang, 1999; Xiao et al., 2015; Zhao et al., 2018), and the late Permian-early Triassic Sonoma orogeny in Cordillera (Dickinson, 2004), the duration of subduction influence there could be much longer. The region of South Eurasia along the Tethys belt has also experienced long-term ocean subduction and repeated collision and accretion of continental ribbons from Gondwana since the Paleozoic (Wan et al., 2019). A longer period of subduction and associated processes would lead to larger volumes of water or fluids released from subducting slabs, and are expected to exert stronger impacts on the overlying continental lithosphere, not only margins but also interiors. This may explain why significant deformation and reworking of continents including some cratons have occurred and even are on-going processes today in the circum-Pacific and Tethys domains (Figure 17).

Similar to the mantle plume case, structural heterogeneities in the lithosphere may also significantly influence the extent and processes of the subduction-associated reworking of continents. On the one hand, both lateral (e.g., faults, boundary zones) and vertical weaknesses (e.g., decollements, MLD layer) could intensify and speed up the thermo-chemical-mechanical modification of the continental lithosphere by providing paths for the infiltration of fluids and melts and concentrating deformation due to their weaker rheology (e.g., [Liu et al., 2018a](#); [Peslier et al., 2017](#); [Wang et al., 2018](#)). Moreover, the presence of lithospheric weaknesses would promote mechanical decoupling between juxtaposed tectonic units or between the upper and lower parts of the continental lithosphere during the reworking process (e.g., [Heron et al., 2016](#); [Lenardic et al., 2003](#); [Liao & Gerya, 2014](#)). For a generally short period (e.g., < 30-50 Ma comparable to the duration of a plume activity) or a limited influence of subduction on the interior of continents or core parts of cratons (e.g., a craton being separated from a subduction zone by a wide marginal belt or the cratonic crust and upper lithospheric mantle separated from convecting asthenosphere by the lower mantle root), these effects of structural heterogeneities on continental reworking are essentially similar to those in the mantle plume-lithosphere interactions. In such cases, the lithospheric reworking is primarily intensified at the weaknesses themselves, and thus these weaknesses function as buffer zones to protect cratons from tectonic deformation and modification (e.g., [Lenardic et al., 2003](#); [Zhu et al., 2011](#)).

However, with a longer period and more continuous and stronger influence of oceanic subduction, lithospheric weaknesses appear to fail in preventing craton from significant reworking to destruction (e.g., the NCC, Wyoming craton, etc.). Rather, the major weaknesses in the lithosphere may control the process, degree and spatial extent of craton destruction (Figure 27b). Under the influence of long-lived subduction, the overlying continental lithosphere could be significantly reworked, such that the lithosphere of the trench-side mobile belt is largely destroyed and the

cratonic lithosphere is directly exposed to the subduction. The lower part of the cratonic mantle root may thus be strongly metasomatized from below by melts and fluids sourced from the subducting slab, and the weak MLD layer may be further weakened and enlarged by hydrous inflow from nearby asthenosphere in the mantle wedge, as suggested by numerical modeling results (e.g., [Liu et al., 2018a](#); [Wang et al., 2018](#)). This simultaneous reworking both in the middle and lower parts of the cratonic lithosphere is expected to hasten gravitational instability and induce a rapid delamination or whole-sale erosion of the lower mantle root along the MLD layer. It is worth noting that after the loss of the lower mantle root, a new LAB could develop at the previous MLD depths, and the overlying original upper lithospheric mantle and the crust may be heated and modified by the hot rising asthenospheric mantle as the subduction process continues (Figure 27b, [Chen et al., 2014](#); [Liu et al., 2018b](#)). On the other hand, such lithospheric reworking and destruction are possibly spatially confined by a major vertically extended weak belt within the upper continental plate, and the hinterland to the other side may not be significantly modified, due probably to both the protection effect of the weak belt and the fading away of the subduction influence (Figure 27b).

Overall, under the long-lived and strong influence of subduction and important effects of pre-existing lithospheric weaknesses, a craton could be severely modified even destroyed but likely with a spatially uneven reworking and destruction (Figure 27b). This explains the sharp differences in both tectonic processes (e.g., [F. Y. Wu et al., 2019](#); [Xu, 2001](#); [Zhu et al., 2011](#)) and structure from the surface to the base of the lithosphere between the eastern and central-western NCC (Figure 26; [Chen, 2010](#); [Wei et al., 2015](#); [Xu et al., 2018](#); [Y. Zhang et al., 2019](#); [Zheng et al., 2017](#)), and may also be responsible for the similar observations across the boundaries of distinctly different structures and/or deformation in western North America, including the Wyoming craton (Figure 16a a-b). The scenario proposed in Figure 27b is consistent with the observed similar depths of the MLD in stable cratonic

regions and the LAB in adjacent destroyed cratonic parts or tectonic regions (Figure 24, [Chen, 2017](#); [Thybo, 2006](#) and references therein).

In both cases of the NCC and the western North American craton, the MLD layer is thought to be the key horizontally extended weakness within the lithosphere affecting the destruction of the cratons (e.g., [Chen et al., 2014](#); [Liu et al., 2018a](#); [Wang et al., 2018](#)). The effects of the MLD layer to facilitate decoupling and delamination of the lower mantle root from the upper part could be particularly pronounced in the compressional setting (e.g., [Gorczyk et al., 2012](#); [Wang et al., 2018](#)) during the earlier flat oceanic subduction beneath both regions (e.g., [F. Y. Wu et al., 2019](#); [Yonkee & Weil, 2015](#)). It is also possible that the weak lower crust with compressional thickening and eclogitization may further aid the deformation and destruction of the cratonic lithosphere (e.g., [Bird, 1979](#); [Le Pourhiet et al., 2006](#); [Wang et al., 2018](#)). As for the major vertically extended weaknesses, the Paleoproterozoic Trans-North China Orogen (central NCC) that sutured the Archean western and eastern NCC may be reactivated and play an important role in controlling the spatial extent of the craton destruction, as all the sharp E-W changes in topography, gravity (marked by the North South Gravity Lineament, or NSGL) and crustal and lithospheric structures spatially coincide with this belt (Figure 26). In the western North America especially around the Wyoming craton, large velocity gradients in the shallow upper mantle (100-150 km depth) and the boundary of stable cratonic core appear roughly following the Paleoproterozoic Trans-Hudson Orogen (Figure 16a-b), indicating a possibly similar role of the orogenic belt to the Trans-North China Orogen during the destruction of the western North American craton.

Overall, the combination of current observations of continental reworking and destruction of cratons and results of numerical modeling suggests that both processes at plate boundaries (i.e., plate tectonics) and underneath plates (e.g., mantle plume activities) can cause modifications of the continental lithosphere to

various degrees, but mostly at around continental margins or lithospheric weak zones. However, specific plate tectonic processes, in particular long-lasting oceanic subduction, may induce significant softening and deformation of both the cratonic crust and lithospheric mantle by involving great amounts of water and other volatiles and large tectonic stresses. Further due to the important effects of reactivated pre-existing lithospheric weaknesses, these processes can eventually lead to severe but spatially heterogeneous reworking and destruction of cratons.

5. Discussion and Conclusions

5.1. Origin of Continents

As discussed in Section 2, both the island arc and oceanic plateau models can be applied to interpret the formation of Archean granite-greenstone terranes, but neither of them can satisfactorily explain all features of Archean continental cratons. For example, the island arc model under a plate tectonic regime cannot reasonably explain the following features of Archean cratons:

(1) Bimodal volcanic assemblages in the Archean greenstone terranes. In the Archean greenstones, common volcanic rock associations are bimodal, where basaltic and ultramafic rocks are associated with dacite and rhyolite, without much andesite. They are different from Phanerozoic volcanic arc assemblages which are commonly unimodal with andesite as the most typical volcanic-rock type in many mature magmatic arcs.

(2) Widespread presence of komatiites and komatiitic rocks in the Archean greenstone terranes. Plate tectonics is incompetent to explain the origin of these Archean komatiites because their formation needed a melting process that occurred at 1600-1900°C. Most Archean greenstones contain komatiites. Komatiites is characterized by high MgO (>18%), which requires at least 40-60% partial melting of the mantle. Such high degree partial melting of the mantle requires the partial melting temperatures at 1600-1900°C. Such high temperature conditions are not

2546 common in island arc environments, though minor komatiites with high silicon
2547 contents and hydration may have been produced in subduction zones.

2548 (3) TTG gneisses making up 60~70% of the basement exposure in Archean terranes.
2549 In major Archean cratons, similar-aged TTG gneisses are exposed over a whole
2550 craton and do not show any systematic progression in age across the 500-1000 km
2551 wide, all emplaced within a very short period. This is inconsistent with a
2552 successively-accreted arc model in the plate tectonics context.

2553 (4) Mass-balance problem with the Archean TTGs that make up 60-70% exposure of
2554 Archean cratons. Due to their high LREE/HREE ratios, high large ion lithophile
2555 element contents and negative Nb–Ta–Ti anomalies, Archean TTG rocks could be
2556 either derived from the partial melting of eclogites or rutile-bearing garnet
2557 amphibolites of subducted oceanic crust, or generated by melting the base of thick
2558 basaltic plateaus above mantle plumes, leaving behind restites containing pyroxene,
2559 garnet, and rutile ([Bédard, 2006](#)). However, modern petrological experiments have
2560 demonstrated that if TTG rocks were formed by partial melting of eclogites or
2561 garnet-/rutile-bearing amphibolites, the partial melting degree should be lower than
2562 30%; otherwise, the resultant TTG rocks would not possess above geochemical
2563 features. If the partial melting degree is no higher than 30%, it requires that the
2564 actual volume of eclogites or garnet-/rutile-bearing amphibolites is three times of the
2565 volume of TTG rocks, which would create a mass-balance problem with the
2566 Archean TTGs that make up 60-70% exposure of Archean cratons, especially
2567 considering the difficulty of extracting such a large volume of TTG melts from
2568 subducting slabs within such a short period.

2569 (5) Anticlockwise P-T paths involving isobaric cooling reconstructed for many
2570 Archean cratons. Available data show that the metamorphic evolution of Archean
2571 rocks from many Archean cratons is characterized by anticlockwise P-T paths
2572 involving isobaric cooling ([Ge et al., 2003](#); [Halpin & Reid, 2016](#); [Jayananda et al.,](#)

2573 2000; Kamber et al., 1996; Kramers et al., 2001; Maas & Henry, 2002; Mvondo et
2574 al., 2017; Percival, 1994; Raith et al., 1990, 1999; Rollinson, 1989; Sandiford, 1985;
2575 Tsunogae et al., 1992, 1999; Zhao et al., 1998, 2001, 2005; Zulbati & Harley, 2007),
2576 which reflect the metamorphism related to the intrusion and underplating of large
2577 amounts of mantle-derived magmas (Bohlen, 1991). Although anticlockwise P-T
2578 paths involving isobaric cooling may also characterize the metamorphism occurring
2579 at the root of magmatic arcs or under back-arc basin setting, it is argued that such
2580 metamorphism should be paired with the relatively high pressure metamorphism of
2581 subducted zones that is characterized by clockwise P-T paths involving isothermal
2582 decompression, and they together form the paired metamorphic belts like what we
2583 have observed in modern magmatic arcs (Brown, 2006, 2008; Brown et al., 2020).
2584 Brown (Brown, 2008) argued that paired metamorphic belts could be regarded as a
2585 hallmark for tracing plate tectonics in the early history of the Earth. This is not the
2586 case in many Archean cratons where the Archean metamorphism is characterized by
2587 anticlockwise P-T paths involving isobaric cooling, without any clockwise P-T paths
2588 involving isothermal decompression to form paired metamorphic belts.

2589 (6) The dominant structural patterns of Archean cratons are gneiss domes
2590 (dome-and-keel structures), which do not resemble linear orogenic belts that typify
2591 Proterozoic and Phanerozoic accretionary (subduction) orogens that resulted from
2592 metamorphosed and deformed continent margin arcs.

2593 (7) Absence of ophiolites and ultra-high pressure (UHP rocks) in Archean cratons.
2594 Ophiolites are an unequivocal index of plate tectonic activity as they are fragments
2595 of oceanic lithosphere tectonically emplaced on continental crust through horizontal
2596 movements, but evidence for Archean ophiolites is sparse and often controversial. It
2597 is the same case with UHP rocks that are common in Phanerozoic and even
2598 Proterozoic arc terranes, but have not been reported with reliable Archean
2599 metamorphic ages from Archean terrains.

In summary, Archean cratons do not exhibit typical lithotectonic elements that are observed in Phanerozoic island arcs. In contrast, although oceanic plateaus formed by mantle plumes fail to provide enough H₂O for the partial melting of basaltic rocks to form TTG magmas, the mantle plume-driven oceanic plateau model can well explain: (1) the exceptionally large exposure of TTG and granitoid intrusions that were emplaced over a short time period without systematic age progression across a craton-scale; 2) the presence of MgO-rich komatiitic melts with eruption temperatures as high as 1650°C; 3) bimodal volcanic assemblages; 4) dominant diapirism-related domal structures; 5) metamorphism (with anticlockwise P-T paths involving isobaric cooling) related to the intrusion and underplating of large amounts of mantle-derived magmas; and (6) affinities of mafic rocks (metamorphosed to be amphibolites and mafic granulites) to continental tholeiitic basalts. Taken together, we favor a mantle plume-driven oceanic plateau model for the formation of Archean felsic continents. In our view, felsic continents appeared before plate tectonics started on our planet, and it was just felsic continents that created favorable conditions for initialing plate tectonics through subduction of a dense oceanic crust below a buoyant continental crust. In this sense, modern-style plate tectonics contributed little to the formation of ancient continents, but it played an important role in the accretion and reworking of continents that will be discussed in the next two sections.

5.2. Growth of Continents

Through the previous review of major geological events leading to the formation and accretion of the five major continents in the world, we can summarize some common basic laws for craton formation and continental growth. It is obvious that each continent was composed of several Archean cratonic nucleuses welded by post-Archean orogenic belts. The Archean cratons were formed by older cores, i.e. cratonic nucleuses, which were amalgamated together along Proterozoic orogenic

belts. Although there is controversy on the origin of continents (see Section 2), it is evident that small pieces of early Archean nucleuses joined together to form larger Archean provinces through tectonic processes similar to terrane accretion in Phanerozoic orogenic systems. The accretionary processes of Archean cratons were best illustrated by the North American continent where Slave, Rae, Hearne, and Wyoming cratons each grew on its margin by oceanic subduction and arc accretion, and subsequently collided together to form a larger Archean province.

The Archean nucleuses grew laterally through arc magmatism in the Paleoproterozoic, which happened in all the continents worldwide. Through the subduction and accretionary processes, the continents grew progressively. This kind of enlargement of continents is well recorded in the South America, Australia and South Africa continents (Figs. 10-12). Paleoproterozoic (2.1-1.8 Ga) continent-continent collisional orogeny happened globally, which led to the formation of the Earth's first supercontinent Columbia/Nuna (Zhao et al., 2002). In the North America continent, Paleoproterozoic (~1.8 Ga) high-pressure, low-temperature collisional metamorphism and crustal layering in both structure and deformation comparable to the Himalaya orogeny was discovered in the Trans-Hudson orogen, which implies that modern-style plate tectonic processes featuring deep continental subduction and subsequent extensional collapse of an orogen occurred at least about 1800 million years ago (Darbyshire et al., 2017; Weller & St-Onge, 2017). Similar collisional process has also been well-documented in the Paleoproterozoic Trans-North China Orogen in the North China Craton (Zhao et al., 2012).

Two contrasting orogenic systems (external and internal) were proposed to describe the global Phanerozoic orogens (Collins et al., 2011), of which continental accretion mainly occurs in the external orogenic systems, also known as accretionary orogens that are major sites for Phanerozoic continental growth, particularly important for the enlargement of the Eurasia, North America, South

America and Australia continents during Phanerozoic time. Growth of giant subduction-accretion complexes, slab roll-back, oceanic ridge subduction and formation of intra-oceanic subduction systems are major processes that lead to continental growth during accretionary orogenesis (Jahn et al., 2000; Şengör et al., 1993; Xiao et al., 2015). These have been well illustrated in the Altaids in Central Asia, the Cordillera in North America, the Andes in South America and the Tasmanides in Australia.

We propose that accretionary processes in ocean-continent convergent margins have been playing important roles in the formation and growth of the global continents since Archean when the size of continents was small. In contrast, modern-style continent-continent collisional orogeny, marked by deep subduction of continental lithosphere, might have occurred much later since the Paleoproterozoic (1.9-1.8 Ga) when the continents grew to considerable size through earlier accretionary processes. The collisional orogeny is likely a hallmark for the change from Archean-style plate tectonics to modern-style plate tectonics. In the early Earth, accretionary processes were the major mechanism for continental growth, while both accretionary and collisional orogenesis have been important in shaping the Earth. The secular change of plate tectonics style has changed the behavior of Earth's lithosphere, which in turn affects the mechanism and rates of continental growth.

5.3. Reworking of Continents

5.3.1. Continental Reworking vs. Continental Growth

The generation, growth (accretion), reworking and destruction of continents are mutually correlated over time. At present, only a small volume (<25%) of the continental crust is older than ~3.0 Ga (e.g., Belousova et al., 2010; Korenaga, 2018; Voice et al., 2011), whereas about 60-80% of the present volume of the continental crust may have formed after 3.0 Ga (Campbell, 2003; Dhuime et al., 2012; Pujol et al., 2013). This means that significant volumes of old crust have been destroyed,

2682 accompanying obvious variations in the rates of growth and reworking of the
2683 continental crust since ~ 3 Ga (e.g., [Dhuime et al., 2018](#); [Hawkesworth et al., 2020](#)
2684 and references therein). In particular, dramatic increases in the rates of reworking
2685 and destruction and simultaneous reduction in the rates of net growth of the
2686 continental crust took place during Neoarchean time (3.0-2.5 Ga), coeval with the
2687 marked changes in the global tectonics. For instance, with the continuous cooling of
2688 the Earth since ~ 3.0 Ga ([Korenaga, 2013](#)), the crust and lithosphere of continents
2689 could have attained a certain rigidity in the Neoarchean, as reflected by the
2690 formation of the oldest major sedimentary basins (~ 2.8 Ga) and oldest regional dyke
2691 swarms (~ 2.6 Ga) ([Cawood et al., 2018](#)). The appearance of the oldest granulite
2692 (Holder et al., 2019) coincided with the gradual increase in the thickness and
2693 buoyancy of the continental crust as a result of a compositional change from mafic
2694 to more felsic in the Neoarchean ([Dhuime et al., 2018](#); [Tang et al., 2016](#)). Such a
2695 coincidence suggests that it was probably till the Neoarchean that the continental
2696 crust was sufficiently strong to sustain crustal thickening and deep-crustal
2697 metamorphism. This may explain the rapid emergence of UHT metamorphism since
2698 ~ 2.8 Ga (Figure 19c). The strong and rigid continental crust and stabilized
2699 lithosphere in the Neoarchean would have facilitated the onset of plate tectonics as
2700 the dominant global regime, leading to the reduction in the net crustal growth and
2701 the development of the supercontinents/supercratons, as reflected by the dramatical
2702 increases in the rates at which differentiated continental crust was reworked and
2703 destroyed ([Hawkesworth et al., 2020](#)).

2704 The development and continuous operation of plate tectonics over time is thought to
2705 generally increase the destruction and reworking rates and in turn reduce the growth
2706 rates of continental crust, with much less effects on the overall rate of crustal
2707 generation ([Dhuime et al., 2018](#); [Hawkesworth et al., 2020](#)). This is largely
2708 attributed to the widespread subduction and associated tectonic processes. In
2709 addition to this long-term trend, it has demonstrated that the degree of continental

crustal reworking exhibits shorter-period variations, closely associated with the evolution of supercontinents (Figure 19b, also see 4.2.4). However, it is still unclear whether or not the sharp changes of the continental crust at ~3.0-2.5 Ga accompanied similar changes in the continental lithospheric mantle, since the origin, timing and formation processes of the mantle lithosphere and its link with the crustal formation during the early Earth remain unknown or controversial (e.g., [Gerya, 2014](#); [Perchuk et al., 2020](#) and references therein). On the other hand, in the later evolution of continents under the plate tectonics regime, during which strong crust-mantle coupling has proven to be a pre-request for the rigidity and long-term stability of continental lithosphere (see 4.1.2), the growth, reworking and destruction of the continental lithospheric mantle would closely link to that of the continental crust in both time and space.

5.3.2. Cratons vs. Orogens

Under the plate tectonics regime, the processes of generation, accretion, reworking and destruction of continents took place mostly at convergent plate margins during the development of accretional and collisional orogens ([Clift et al., 2009](#); [Hawkesworth et al., 2016, 2020](#); [Stern & Scholl, 2010](#)). Orogenic processes in the Precambrian played essential roles in shaping the lithosphere of cratons, which differs in structure and properties from that of Phanerozoic orogens/tectonic belts (see 4.1, Table 1). Temperature is considered the most significant factor responsible for the differences between Precambrian and Phanerozoic orogens and thus between old cratons and young tectonic belts. In the late Archean and early Proterozoic (>1.6 Ga), during which most cratons developed without modern analogues ([Arndt et al., 2009](#); [Eaton & Claire Perry, 2013](#); [Lee et al., 2011](#)), high mantle temperatures (~150–250 degrees Celsius) than the present-day values ([Herzberg et al., 2010](#); [Korenaga, 2013](#)) resulted in hot orogens characterized by higher-degree mantle melting, weaker crust and upper mantle, distributed shortening, high- to intermediate-temperature metamorphism, and efficient elimination of high-density,

low-viscosity lithologies (Arndt et al., 2009; Chardon et al., 2009; Condie, 2007; Gerya, 2014). The continental lithosphere established at such old orogens appears to be sufficiently buoyant and strong to survive from mantle erosion and tectonic disturbance as the Earth cools (Eaton & Claire Perry, 2013; Perchuk et al., 2020). In contrast, Neoproterozoic to Phanerozoic orogens are typically cold orogens with temperatures too low (<150 degree than the present-day values) to produce craton-type of lithosphere, but favorable for the stabilization of continental subduction and generation of UHP metamorphic complexes that are nearly absent in the Precambrian (Ernst et al., 1997; Gerya, 2014; Guillot et al., 2008).

Despite the large differences, there are some observations on the commonalities between structures produced by Phanerozoic orogens and those preserved within old, cratonic lithosphere, based on which comparable tectonic processes have been suggested among orogens of Precambrian and Phanerozoic ages. As mentioned in 4.2.2, the common features of layering in the crustal structure and deformation have led to the suggestion that similar mid-lower crustal flow may have taken place in both the Mesoproterozoic Grenville and Paleoproterozoic Trans-Hudson orogens and the present-day Himalayan-Tibetan orogen, probably under sufficiently high temperature conditions that made the crust much weaker than usual, as indicated by geophysical observations (Bai et al., 2010; Darbyshire et al., 2017; Liu et al., 2014; Pawlak et al., 2012; Petrescu et al., 2016). Considering the gradual cooling of the Earth, it is expected that such kind of high-temperature conditions might be more frequently met in the Precambrian than the Phanerozoic to present day. It is also proposed based on geodynamic modeling (e.g., Betts et al., 2015; Cooper & Miller, 2014) that modern terrane accretion, such as the Paleozoic accretion of the Selwyn block to the Gondwana margin in SE Australia (Cayley, 2011; Foster & Gray, 2000) and the ongoing accretion of the Yakutat terrane in the eastern end of the Aleutian subduction zone (Colpron et al., 2007; Eberhart-Phillips et al., 2006), introduces features reminiscent of the internal dipping structures (such as dipping MLDs)

widely observed in the shallow cratonic lithospheric mantle (Copeland et al., 2017). Therefore, the dipping structures observed beneath cratonic regions are considered a kind of tectonic imprints of Precambrian accretionary orogens (e.g., Bostock, 1998; Chen et al., 2009; Snyder et al., 2017 and references therein), which contribute strongly to the assembly and stabilization of cratons and growth of continents owing to their high production rates of juvenile crust compared to Phanerozoic accretional orogens (Chardon et al., 2009; Condie, 2007). However, to what extent Precambrian accretionary orogens are comparable in terms of tectonic regime and processes to modern counterparts is still an open question.

5.3.3. Lithospheric Processes vs. Mantle Dynamics

Lithospheric processes especially at orogens of various styles and ages, which are responsible for the formation and long-term evolution of continents, have been increasingly evidenced to be largely controlled by and strongly interact with sublithospheric mantle dynamics (e.g., Chen et al., 2019; Copeland et al., 2017; Faccenna et al., 2013; Handy et al., 2010). Under the plate tectonic regime, variations in crustal and lithospheric deformation, magmatic activity and surface topography, or collectively in the pattern of orogeny in different orogens, and also episodic changes along a single orogenic belt at convergent plate margins, are often attributed to different morphologies of the subducting slabs and slab-mantle interactions at depth. Typically the subduction dynamics in the upper mantle, such as trench retreat or advance, slab flattening or steepening, continuous subduction or break-off, slab stagnating in the mantle transition zone or penetrating into the lower mantle, etc., is considered of key importance in determining the orogenic style in the overlying plate, based on the studies of both circum-Pacific (Copeland et al., 2017; Horton et al., 2016; Li & Li, 2007; Yang et al., 2018) and Tethyan orogens (Handy et al., 2010; Li et al., 2011; Mouthereau et al., 2012). Recent geological and geophysical observations and geodynamic modeling have further explored the significant roles of slab subduction in the lower mantle in driving plate motion and

2794 shaping orogens on the surface, with particular emphasizes on the different tectonic
2795 responses of the overlying continental lithosphere to slab-upper mantle and
2796 slab-lower mantle interactions (e.g., [Chen et al., 2019](#); [Faccenna et al., 2013](#);
2797 [Schellart, 2017](#)). It has been suggested that the driving forces provided by
2798 subducting slabs function differently in the upper and whole (upper + lower) mantle
2799 subduction systems, which may result in distinct patterns of orogeny ([Conrad &](#)
2800 [Lithgow-Bertelloni, 2004](#); [Faccenna et al., 2013](#)). In case of an upper mantle
2801 subduction, the pull force that the subducting slab exerts directly on the surface plate
2802 dominates in the system, such that the overriding plate moves in the same horizontal
2803 direction as the subducting slab and slab rollback/trench retreat leads to extensional
2804 deformation in the overriding plate without obvious crustal thickening ([Faccenna et](#)
2805 [al., 2013](#)). This indeed explains the main features of the Cenozoic Mediterranean
2806 mobile belt ([Faccenna et al., 2014](#); [Jolivet et al., 2003](#)) where seismic tomography
2807 shows that high-velocity slabs are mainly confined in the upper mantle (e.g, [Zhu et](#)
2808 [al., 2012a](#)). In case of a slab penetrating to the more viscous lower mantle, on the
2809 other hand, the down-going slab exerts indirect suction force on the surface plate by
2810 exciting mantle circulations through viscous coupling. The slab suction force is
2811 thought to play a more important role than slab pull in this subduction system,
2812 inducing opposite horizontal movements of the overlying plate and subducting slab,
2813 with compressional deformation and obvious thickening of the crust in the
2814 overriding plate ([Faccenna et al., 2013](#)). Such a scenario is consistent with the
2815 observations at a number of orogens controlled by whole-mantle subduction,
2816 typically the Himalaya-Tibet and Central Andes (e.g., [Allmendinger et al., 1997](#);
2817 [Hatzfeld & Molnar, 2010](#)). The differences in the upper- and whole-mantle
2818 subduction dynamics and corresponding lithospheric responses have been invoked
2819 not only to decipher the distinct characteristics of orogens (e.g, [Faccenna et al.,](#)
2820 [2013](#)), but also to understand the temporal variations of lithospheric tectonics in a

2821 single orogenic system, such as the Andes during the Mesozoic-Cenozoic evolution
 2822 (e.g, [Chen et al., 2019](#); [Schellart, 2017](#)).

2823 In addition to slab subduction at depth, other mantle processes, particularly plume
 2824 upwelling, have also been widely investigated and suggested to have played
 2825 important roles in the growth of Archean cratonic mantle keels (e.g., [Arndt et al.,](#)
 2826 [2009](#); [Griffin et al., 2003](#); [Stein & Hofmann, 1994](#)) and exerted considerable
 2827 impacts on the later growth and reworking of continents (e.g., [Chen et al., 2020](#); [Hu](#)
 2828 [et al., 2018](#); [Wang et al., 2015](#); [Wu et al., 2014](#); [Yuan et al., 2017](#)). As demonstrated
 2829 in 4.3.1, rising plumes help to speed up the thinning and in some cases later
 2830 thickening of cratonic lithosphere, especially at pre-existing lithospheric weak zones
 2831 ([Hu et al., 2018](#); [Wang et al., 2015](#)), although plume impingement alone appears
 2832 incapable of contributing to an efficient weakening and destruction of stable cratons.

2833 It is also suggested that strong interactions between plumes and overlying plates
 2834 could result in an acceleration of plate motion by reducing the
 2835 lithosphere-asthenosphere coupling ([Kumar et al., 2007](#)), or trigger rifting and even
 2836 break-up of continents with the help of lithospheric weaknesses ([Buiter & Torsvik,](#)
 2837 [2014](#); [Frizon de Lamotte et al., 2015](#)), or both. This has been invoked to explain the
 2838 globally fastest plate motion ([Müller et al., 2016](#)) and longest continental rift system
 2839 ([Brune et al., 2017](#)) coeval in the early Cretaceous (~140-120 Ma) over the past 200
 2840 Myrs, for this time period was characterized by significantly enhanced plume
 2841 activities and mantle temperature ([Humler et al., 1999](#)). Moreover, the coupling
 2842 between superplume and supercontinent cycles throughout the geological history
 2843 (e.g., [Li & Zhong, 2009](#); [Li et al., 2019](#)) further indicates that the lithosphere-plume
 2844 interactions and strong influences of plume activities on the structure and tectonics
 2845 of continents not only are evident in the recent short era, but also persist during the
 2846 Earth's long-term evolution. Indeed, an integration of various observations on plate
 2847 and plume tectonics and their interactions at multiple time-space scales would help

to gain deeper insight into the correlation between lithospheric processes and mantle dynamics and the co-evolution of the shallow and deep Earth (Chen et al., 2020).

5.4. A Scenario for the Formation, Accretion and Reworking of Continents

On the basis of the above discussion, we propose the following scenario for the formation, accretion and reworking/destruction of continents:

- (1) **Formation of continents:** During the Eoarchean-Mesoarchean time when plate tectonics had not started on our planet, felsic continental crust was most likely originated from oceanic plateaus formed by mantle plumes that were originated from the core-mantle boundary due to tremendous accumulation of radioactive heat in the ~200 km thick D'' layer following the formation of core-mantle-crust and associated magma ocean event at about 4.45 Ga. In many Archean cratons, TTG rocks were several hundred million years younger than greenstones that are considered to have formed from oceanic island basalts (OIB), indicating that the dominant ultramafic-mafic and minor felsic volcanic rocks (greenstones) and TTG rocks in the Archean cratons were not the products of a single mantle plume event. For this reason, we favor a two-stage model for the formation of Archean felsic continents, which is shown in Figure 28a-c. As shown in Figure 28a-b, the first stage represented the formation of an oceanic plateau by an early mantle plume. When the total heat from the accumulation of radioactive decay in the D'' layer at the core-mantle boundary and released from the outer core reached a critical value, causing partial melting of the mantle material, a plume was induced with the upwelling of the molten mantle material. During the ascent, the plume would trap large amounts of mantle material to enlarge itself as a mushroom-shaped body that had a huge head with a long and narrow tail connecting to a magma chamber at the core-mantle boundary (Figure 28a). When the huge head reached the base of lithosphere, it became a flattened

mushroom shape and then experienced decompressional partial melting to form basaltic magmas. The basaltic magmas erupted on the surface within a very short period (< 1 Ma), forming oceanic plateaus with diameters ranging from 1000-2000 km on ocean floors (Figure 28b).

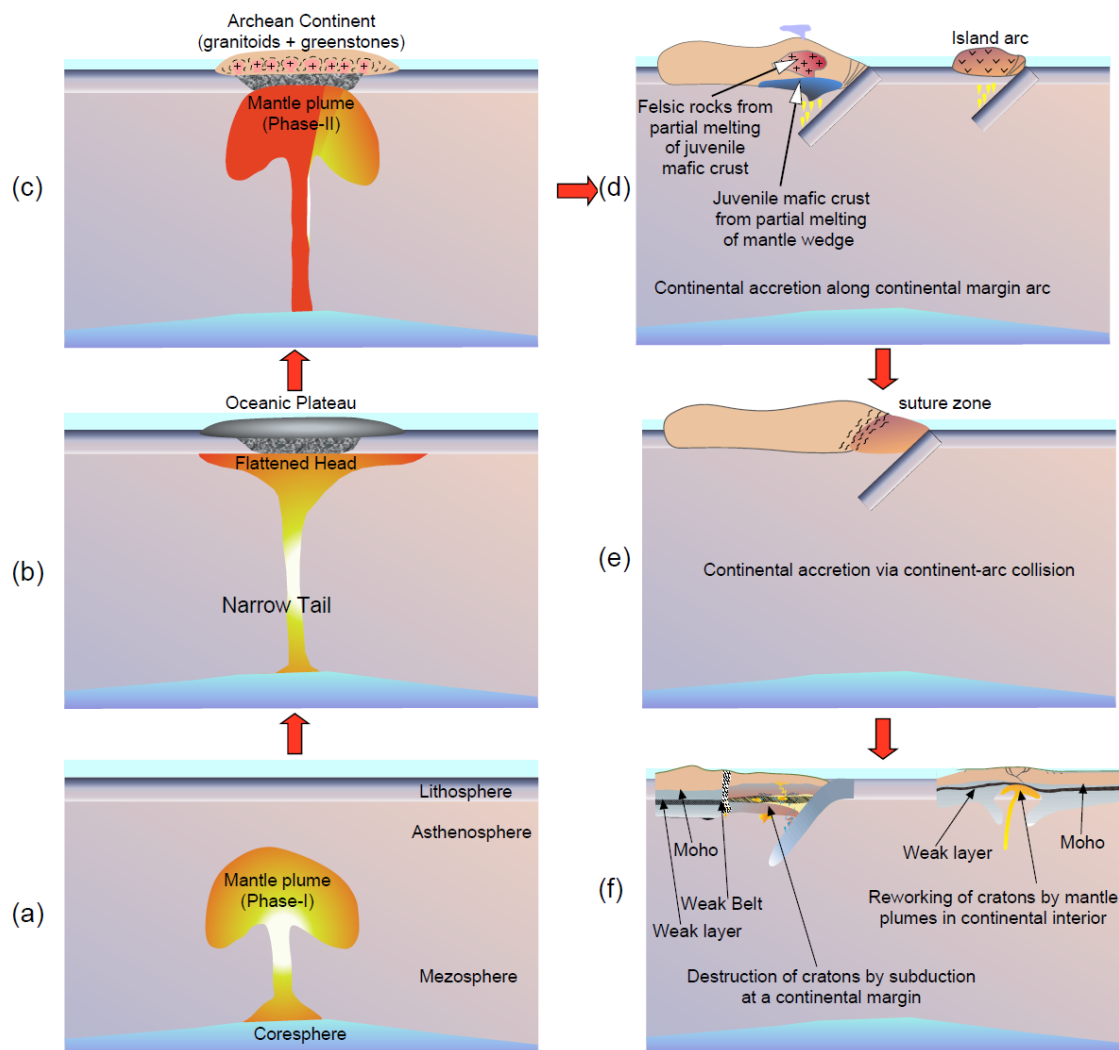


Figure 28. Schematic cartoons showing proposed geological models for the origin, accretion and reworking of continents.

At the later stage when the narrow tail of the plume reached the base of lithosphere, the molten material from the tail erupted on the surface, forming high-temperature ($\sim 1600^{\circ}\text{C}$) komatiites that are important components of

Archean greenstones. Meanwhile, the high-temperature komatiitic magmas may have also caused the partial melting of mafic oceanic crust to form minor TTG rocks, like minor 2.75-2.65 Ga TTG rocks from the North China Craton. The first stage would end when all mantle magmas were consumed from the chamber at the core-mantle boundary. The second stage represented the partial melting of the base of the oceanic plateau to form TTG magmas, possibly caused by a later mantle plume (Figure 28c). At the second stage, when another mantle plume reached the base of the oceanic plateau, it would cause extensive metamorphism, forming greenstones, amphibolites and garnet-bearing granulites from the metamorphosed upper, middle and lower crust of the oceanic plateau, respectively. The mantle plume would also cause partial melting of the lower crust of the oceanic plateau to form TTG magmas. Driven by density difference, the light TTG magmas would rise and the heavy greenstones would sink down (sagduction), forming unique dome-and-Keel structures in Archean cratons in which the diapiric TTG domes were surrounded by sinking down greenstone belts (Figure 28c). When the mantle plume ceased to provide magmas, the heating stopped and the metamorphic crust experienced cooling without variations in the crustal thickness, leading to the metamorphism characterized by an anticlockwise P-T path involving isobaric cooling. Therefore, the oceanic plateau model can not only reasonably interpret the formation of Archean TTG and greenstones, but also satisfactorily explain the metamorphic and structural features of Archean cratons.

(2) ***Accretion of continents***: Once felsic continents developed from oceanic plateaus, they become continental nucleuses of continental cratons in the early stage. In the following stage, the density difference between felsic continental crust and oceanic crust may have induced subduction of the oceanic lithosphere beneath the continental lithosphere, which may indicate

the start of modern-style plate tectonics in our planet. Subduction zones along the margins of continents are the main sites for docking various terranes including island arcs, seamounts and oceanic plateaus, and micro-continental blocks, which are emplaced into, and/or connected by, accretionary complexes formed by the subduction zones. These long-lived geodynamic processes are mainly characterized by multiple phases of orogeny, sometimes with orogen-scale oroclinal bending long linear arcs and/or continental ribbons, generating outside large-scale accretion or massive growth of continental cratons as discussed in Section 3. When an oceanic slab is subducted to a deep level, large amounts of H₂O-dominant fluids would be released out and enter into the mantle wedge, leading to the partial melting of the mantle wedge, producing basaltic magmas. The underplating of basaltic magmas lead to addition of a juvenile mafic crust to the base of upper plates, including continental lithosphere and intra-oceanic arcs (Figure 28d). Some of the basaltic magmas derived from the partial melting of the mantle wedge may also ascend to the surface along deep fractures or faults, forming basalts and andesites due to felsic continental crustal contamination during the ascent, forming continental marginal volcanic arcs (Figure 28d). In many long-live subduction zones, the juvenile mafic crust above the mantle wedge will be heated and undergo partial melting, producing calc-alkaline magmas that are emplaced into the crust to form felsic plutons, leading to continental marginal accretion (Figure 28d). During Proterozoic and especially Phanerozoic times, the accretion or growth of continents may also result from early stage of continent-continent collision or continent-arc collision (Figure 28e).

(3) ***Reworking or destruction of continents***: While juvenile continental crustal material was extracted from the mantle wedge in subduction zones, leading to the outside accretion/outgrowth of continents, the base of the continental

lithosphere may experience softening, thinning and delamination due to the vigorous infiltration and recycling of H₂O-dominant fluids (released out from subducted slabs) along weak layers or weak belts, leading to the widespread reworking and even destruction of continental lithosphere (Figure 28f). Minor reworking or modification of continental lithosphere may also occur in the interiors of continents due to thermo-mechanical-magmatic erosion by mantle plumes (Figure 28f).

5.5. Conclusions

(1) Archean continents with felsic crust must have been originated either from island arcs under a plate tectonic regime or from oceanic plateaus derived from mantle plume.

(2) The island arc model can well explain the formation of Archean TTG rocks, of which the high-pressure-type TTG rocks are considered to have been derived from the partial melting of subducted slabs, whereas the low-pressure-type TTG rocks (equivalent to calc-alkaline granitoids) were derived from the partial melting of juvenile basaltic crust which itself formed by the partial melting of the mantle wedge with addition of fluids released from the subducted slabs. However, the island arc model is in failure to explain the absence of andesites from the Archean greenstone terranes, the presence of komatiites with temperatures of 1600°C, nearly coeval emplacement of TTG plutons on a cratonic scale, dome-and-keel structures and anticlockwise P-T paths involving isobaric cooling that characterize the deformation and metamorphism of Archean continental cratons.

(3) The mantle-plume oceanic plateau model can reasonably interpret the origins of both Archean greenstones and TTG rocks, of which the tholeiites and komatiites from the greenstones were derived from partial melting of the head and tail of a mantle plume, respectively, the felsic dacite, rhyolitic dacite and

2970 rhyolite from the greenstone were derived from the partial melting of the crust,
2971 and TTG rocks were derived from the partial melting of basaltic rocks from the
2972 lower part of oceanic plateau, though oceanic plateaus seem to be difficult to
2973 provide enough H₂O for the aqueous partial melting of basaltic rocks to form
2974 TTG magmas. In addition, the oceanic plateau model can also well interpret the
2975 Archean dome-and-keel structure, anticlockwise P-T paths, and absence of
2976 blueschist and paired metamorphic belts.

2977 (4) Since plate tectonics appeared in Earth, Archean continental nucleuses
2978 underwent accretion or growth along their margins through the subduction of
2979 oceanic lithosphere, and accretionary processes involving juvenile arc formation
2980 and arc accretion were the major mechanism for continental growth in the early
2981 earth's history.

2982 (5) Archean nucleuses grew laterally through arc magmatism and amalgamation
2983 during Paleoproterozoic to form sizeable landmass. Globally
2984 continent-continental collisional orogeny happened since Paleoproterozoic
2985 (2.1-1.8 Ga), which led to the formation of the Earth's first supercontinent Nuna.
2986 Phanerozoic continental growth is best illustrated in the Central Asia, the North
2987 America Cordillera and the Tasmanides of East Australia.

2988 (6) Growth of giant subduction-accretion complexes, slab roll-back, oceanic
2989 ridge subduction and formation of intra-oceanic subduction systems are major
2990 processes that lead to continental growth during accretionary orogenesis. The
2991 collisional orogeny is likely a hallmark for the change from Archean-style plate
2992 tectonics (accretion) to modern-style plate tectonics (accretion and collision).

2993 (7) In addition to lateral accretion or growth along their margins, continental
2994 lithosphere also experiences episodic reworking throughout its evolution history,
2995 resulting in ubiquitous lateral and vertical structural heterogeneities. This and the

2996 intrinsic chemical buoyancy and high strength of both the crust and mantle
2997 lithosphere are essential factors for the longevity and stability of continents.

2998 (8) Reworking of continents has become increasingly significant but with
2999 simultaneous reduction in the rates of continental growth since the operation of
3000 plate tectonics at ~3.0-2.5 Ga, mostly associated with oceanic subduction and
3001 continental collision and related mantle processes at depth during the assembly
3002 of supercontinents.

3003 (9) Usually reworking is concentrated at lithospheric weaknesses in either
3004 continental margins or interiors, which does not affect the overall stability of
3005 continents. However, significant reworking does happen in presumably stable
3006 cratonic regions, resulting in severe reactivation and modification, even
3007 destruction of the strong cratonic lithosphere.

3008 (10) Destruction of cratons is largely attributed to long-lasting oceanic
3009 subductions that could induce marked softening and deformation of the cratonic
3010 lithosphere by involving vigorous recycling of water and other volatiles and
3011 large tectonic stresses. Plume activities underneath plates play a relatively minor
3012 role in continental reworking and destruction, though in cases do affect plate
3013 motion and the evolution of cratonic lithosphere.

3014 **Acknowledgements**

3015 This study was financially supported by National Science Foundation of China
3016 (NSFC) grant numbers 41688103, 41890831, 41888101, and 41725014.

3017 **Conflict of Interest**

3018 The authors declare no competing interests.

3019 **Data Availability Statement**

No new data were used in the review article, which is based on existing data from previously published sources. The sources of the public or published data used in the figures are detailed in the legend.

References

- Abbott, D. (1996). Plumes and hotspots as sources of greenstone belts. *Lithos*, 37(2), 113-127. [https://doi.org/10.1016/0024-4937\(95\)00032-1](https://doi.org/10.1016/0024-4937(95)00032-1)
- Abbott, D., & Mooney, W. (1995). The structural and geochemical evolution of the continental crust: Support for the oceanic plateau model of continental growth. *Reviews of Geophysics*, 33(S1), 231-242. <https://doi.org/10.1029/95RG00551>
- Aitken, A. R. A., Quentin de Gromard, R., Joly, A., Howard, H. M., & Smithies, R. H. (2019). Thermal, rheological and kinematic conditions for channelized lower crustal flow in a threshold example. *Tectonophysics*, 753, 63-78. <https://doi.org/10.1016/j.tecto.2019.01.002>
- Aleinikoff, J. N., Reed, J. C., & Wooden, J. L. (1993). Lead isotopic evidence for the origin of Paleo- and Mesoproterozoic rocks of the Colorado Province, U.S.A. *Precambrian Research*, 63(1), 97-122. [https://doi.org/10.1016/0301-9268\(93\)90007-O](https://doi.org/10.1016/0301-9268(93)90007-O)
- Allen, M. B., & Armstrong, H. A. (2008). Arabia–Eurasia collision and the forcing of mid-Cenozoic global cooling. *Palaeogeography, Palaeoclimatology, Palaeoecology*, 265(1), 52-58. <https://doi.org/10.1016/j.palaeo.2008.04.021>
- Allmendinger, R. W., Jordan, T. E., Kay, S. M., & ISACKS, B. L. (1997). The evolution of the Altiplano-Puna Plateau of the Central Andes. *Annual Review of Earth and Planetary Sciences*, 25(1), 139-174. <https://doi.org/10.1146/annurev.earth.25.1.139>
- Amato, J. M., Boullion, A. O., Serna, A. M., Sanders, A. E., Farmer, G. L., Gehrels, G. E., et al. (2008). Evolution of the Mazatzal province and the timing of the Mazatzal orogeny: Insights from U-Pb geochronology and geochemistry of igneous and metasedimentary rocks in southern New Mexico. *GSA Bulletin*, 120(3-4), 328-346. <https://doi.org/10.1130/b26200.1>
- An, Y., Huang, J.-X., Griffin, W. L., Liu, C., & Huang, F. (2017). Isotopic composition of Mg and Fe in garnet peridotites from the Kaapvaal and Siberian cratons. *Geochimica et Cosmochimica Acta*, 200, 167-185.

3051 <https://doi.org/10.1016/j.gca.2016.11.041>

3052 Anhaeusser, C. R., & Wilson, J. F. (1981). The granitic–gneiss greenstone shield. In D. R.

3053 Hunter (Ed.), *Precambrian of The Southern Hemisphere* (pp. 423-499). Amsterdam:

3054 Elsevier.

3055 Armijo, R., Tapponnier, P., Mercier, J. L., & Han, T.-L. (1986). Quaternary extension in

3056 southern Tibet: Field observations and tectonic implications. *Journal of*

3057 *Geophysical Research: Solid Earth*, 91(B14), 13803-13872.

3058 <https://doi.org/10.1029/JB091iB14p13803>

3059 Armstrong, R. L., Harmon, R. S., Moorbath, S. E., & Windley, B. F. (1981). Radiogenic

3060 isotopes: the case for crustal recycling on a near-steady-state no-continental-growth

3061 Earth. *Philosophical Transactions of the Royal Society of London. Series A,*

3062 *Mathematical and Physical Sciences*, 301(1461), 443-472.

3063 <https://doi.org/10.1098/rsta.1981.0122>

3064 Arndt, N., Lesher, C. M., & Barnes, S. J. (2008). *Komatiite*. New York: Cambridge

3065 University Press.

3066 Arndt, N. T. (2013). The formation and evolution of the continental crust. *Geochemical*

3067 *Perspectives*, 2(3), 405-533. <https://doi.org/10.7185/geochempersp.2.3>

3068 Arndt, N. T., Coltice, N., Helmstaedt, H., & Gregoire, M. (2009). Origin of Archean

3069 subcontinental lithospheric mantle: Some petrological constraints. *Lithos*, 109(1),

3070 61-71. <https://doi.org/10.1016/j.lithos.2008.10.019>

3071 Artemieva, I. M. (2009). The continental lithosphere: Reconciling thermal, seismic, and

3072 petrologic data. *Lithos*, 109(1), 23-46. <https://doi.org/10.1016/j.lithos.2008.09.015>

3073 Arth, J. G., & Barker, F. (1976). Rare-earth partitioning between hornblende and dacitic

3074 liquid and implications for the genesis of trondhjemitic-tonalitic magmas. *Geology*,

3075 4(9), 534-536. [https://doi.org/10.1130/0091-7613\(1976\)4<534:rpbhad>2.0.co;2](https://doi.org/10.1130/0091-7613(1976)4<534:rpbhad>2.0.co;2)

3076 Arth, J. G., Barker, F., Peterman, Z. E., & Friedman, I. (1978). Geochemistry of the

3077 gabbro-diorite-tonalite-trondhjemitic suite of southwest Finland and its implications

3078 for the origin of tonalitic and trondhjemitic magmas. *Journal of Petrology*, 19(2),

3079 289-316. <https://doi.org/10.1093/petrology/19.2.289>

3080 Audet, P., & Bürgmann, R. (2011). Dominant role of tectonic inheritance in supercontinent

3081 cycles. *Nature Geoscience*, 4(3), 184-187. <https://doi.org/10.1038/ngeo1080>

3082 Aulbach, S., Griffin, W. L., Pearson, N. J., O'Reilly, S. Y., Kivi, K., & Doyle, B. J. (2004).

3083 Mantle formation and evolution, Slave Craton: constraints from HSE abundances

3084 and Re-Os isotope systematics of sulfide inclusions in mantle xenocrysts. *Chemical*
3085 *Geology*, 208(1-4), 61-88. <https://doi.org/10.1016/j.chemgeo.2004.04.006>

3086 Aulbach, S., Massuyeau, M., & Gaillard, F. (2017). Origins of cratonic mantle
3087 discontinuities: A view from petrology, geochemistry and thermodynamic models.
3088 *Lithos*, 268-271, 364-382. <http://dx.doi.org/10.1016/j.lithos.2016.11.004>

3089 Austrheim, H. (1998). Influence of fluid and deformation on metamorphism of the deep
3090 crust and consequences for the geodynamics of collision zones. In B. R. Hacker & J.
3091 G. Liou (Eds.), *When Continents Collide: Geodynamics and Geochemistry of*
3092 *Ultrahigh-Pressure Rocks* (pp. 297-323). Dordrecht: Springer Netherlands.

3093 Avouac, J. P., Tapponnier, P., Bai, M., You, H., & Wang, G. (1993). Active thrusting and
3094 folding along the northern Tien Shan and Late Cenozoic rotation of the Tarim
3095 relative to Dzungaria and Kazakhstan. *Journal of Geophysical Research: Solid*
3096 *Earth*, 98(B4), 6755-6804. <https://doi.org/10.1029/92JB01963>

3097 Bédard, J. H. (2006). A catalytic delamination-driven model for coupled genesis of
3098 Archaean crust and sub-continental lithospheric mantle. *Geochimica et*
3099 *Cosmochimica Acta*, 70(5), 1188-1214. <https://doi.org/10.1016/j.gca.2005.11.008>

3100 Bédard, J. H. (2018). Stagnant lids and mantle overturns: Implications for Archaean
3101 tectonics, magmagenesis, crustal growth, mantle evolution, and the start of plate
3102 tectonics. *Geoscience Frontiers*, 9(1), 19-49.
3103 <https://doi.org/10.1016/j.gsf.2017.01.005>

3104 Bai, D., Unsworth, M. J., Meju, M. A., Ma, X., Teng, J., Kong, X., et al. (2010). Crustal
3105 deformation of the eastern Tibetan plateau revealed by magnetotelluric imaging.
3106 *Nature Geoscience*, 3(5), 358-362. <https://doi.org/10.1038/ngeo830>

3107 Baldwin, J. A., Bowring, S. A., & Williams, M. L. (2003). Petrological and
3108 geochronological constraints on high pressure, high temperature metamorphism in
3109 the Snowbird tectonic zone, Canada. *Journal of Metamorphic Geology*, 21(1), 81-98.
3110 <https://doi.org/10.1046/j.1525-1314.2003.00413.x>

3111 Baldwin, J. A., Bowring, S. A., Williams, M. L., & Williams, I. S. (2004). Eclogites of the
3112 Snowbird tectonic zone: petrological and U-Pb geochronological evidence for
3113 Paleoproterozoic high-pressure metamorphism in the western Canadian Shield.
3114 *Contributions to Mineralogy and Petrology*, 147(5), 528-548.
3115 <https://doi.org/10.1007/s00410-004-0572-4>

3116 Baptiste, V., & Tommasi, A. (2014). Petrophysical constraints on the seismic properties of

3117 the Kaapvaal craton mantle root. *Solid Earth*, 5, 1-19.
 3118 <https://doi.org/10.5194/se-5-45-2014>

3119 Barbosa, J. S. F., & Sabaté, P. (2004). Archean and Paleoproterozoic crust of the São
 3120 Francisco Craton, Bahia, Brazil: geodynamic features. *Precambrian Research*,
 3121 133(1), 1-27. <https://doi.org/10.1016/j.precamres.2004.03.001>

3122 Barker, F. (1979). Trondhjemite: Definition, environment and hypotheses of origin. In F.
 3123 Barker (Ed.), *Trondhjemites, Dacites, and Related rocks* (Vol. 6, pp. 1-12).
 3124 Amsterdam: Elsevier.

3125 Barker, F., & Arth, J. G. (1976). Generation of trondhjemitic-tonalitic liquids and Archean
 3126 bimodal trondhjemite-basalt suites. *Geology*, 4(10), 596-600.
 3127 [https://doi.org/10.1130/0091-7613\(1976\)4<596:gotlaa>2.0.co;2](https://doi.org/10.1130/0091-7613(1976)4<596:gotlaa>2.0.co;2)

3128 Barley, M. E., Loader, S. E., & McNaughton, N. J. (1998). 3430 to 3417 Ma calc-alkaline
 3129 volcanism in the McPhee Dome and Kelly Belt, and growth of the eastern Pilbara
 3130 Craton. *Precambrian Research*, 88(1), 3-23.
 3131 [https://doi.org/10.1016/S0301-9268\(97\)00061-2](https://doi.org/10.1016/S0301-9268(97)00061-2)

3132 Barovich, K. M., Patchett, P. J., Peterman, Z. E., & Sims, P. K. (1989). Nd isotopes and the
 3133 origin of 1.9-1.7 Ga Penokean continental crust of the Lake Superior region. *GSA*
 3134 *Bulletin*, 101(3), 333-338.
 3135 [https://doi.org/10.1130/0016-7606\(1989\)101<0333:niatoo>2.3.co;2](https://doi.org/10.1130/0016-7606(1989)101<0333:niatoo>2.3.co;2)

3136 Barth, A. P., Walker, J. D., Wooden, J. L., Riggs, N. R., & Schweickert, R. A. (2011). Birth
 3137 of the Sierra Nevada magmatic arc: Early Mesozoic plutonism and volcanism in the
 3138 east-central Sierra Nevada of California. *Geosphere*, 7(4), 877-897.
 3139 <https://doi.org/10.1130/ges00661.1>

3140 Beck, S. L., & Zandt, G. (2002). The nature of orogenic crust in the central Andes. *Journal*
 3141 *of Geophysical Research: Solid Earth*, 107(B10), 2230.
 3142 <https://doi.org/10.1029/2000JB000124>

3143 Begg, G. C., Griffin, W. L., Natapov, L. M., O'Reilly, S. Y., Grand, S. P., O'Neill, C. J., et al.
 3144 (2009). The lithospheric architecture of Africa: Seismic tomography, mantle
 3145 petrology, and tectonic evolution. *Geosphere*, 5(1), 23-50.
 3146 <https://doi.org/10.1130/ges00179.1>

3147 Bell, D. R., Grégoire, M., Grove, T. L., Chatterjee, N., Carlson, R. W., & Buseck, P. R.
 3148 (2005). Silica and volatile-element metasomatism of Archean mantle: a
 3149 xenolith-scale example from the Kaapvaal Craton. *Contributions to Mineralogy and*

3150 *Petrology*, 150(3), 251-267. <https://doi.org/10.1007/s00410-005-0673-8>

3151 Belousova, E. A., Kostitsyn, Y. A., Griffin, W. L., Begg, G. C., O'Reilly, S. Y., & Pearson, N.
3152 J. (2010). The growth of the continental crust: Constraints from zircon Hf-isotope
3153 data. *Lithos*, 119(3), 457-466. <https://doi.org/10.1016/j.lithos.2010.07.024>

3154 Bercovici, D., & Ricard, Y. (2012). Mechanisms for the generation of plate tectonics by
3155 two-phase grain-damage and pinning. *Physics of the Earth and Planetary Interiors*,
3156 202-203, 27-55. <https://doi.org/10.1016/j.pepi.2012.05.003>

3157 Berman, R. G., Davis, W. J., & Pehrsson, S. (2007). Collisional Snowbird tectonic zone
3158 resurrected: Growth of Laurentia during the 1.9 Ga accretionary phase of the
3159 Hudsonian orogeny. *Geology*, 35(10), 911-914. <https://doi.org/10.1130/g23771a.1>

3160 Betts, P. G., Giles, D., Lister, G. S., & Frick, L. R. (2002). Evolution of the Australian
3161 lithosphere. *Australian Journal of Earth Sciences*, 49(4), 661-695.
3162 <https://doi.org/10.1046/j.1440-0952.2002.00948.x>

3163 Betts, P. G., Moresi, L., Miller, M. S., & Willis, D. (2015). Geodynamics of oceanic plateau
3164 and plume head accretion and their role in Phanerozoic orogenic systems of China.
3165 *Geoscience Frontiers*, 6(1), 49-59. <https://doi.org/10.1016/j.gsf.2014.07.002>

3166 Bickford, M. E., Collerson, K. D., Lewry, J. F., Van Schmus, W. R., & Chiarenzelli, J. R.
3167 (1990). Proterozoic collisional tectonism in the Trans-Hudson orogen,
3168 Saskatchewan. *Geology*, 18(1), 14-18.
3169 [https://doi.org/10.1130/0091-7613\(1990\)018<0014:pctitt>2.3.co;2](https://doi.org/10.1130/0091-7613(1990)018<0014:pctitt>2.3.co;2)

3170 Bird, P. (1979). Continental delamination and the Colorado Plateau. *Journal of Geophysical*
3171 *Research: Solid Earth*, 84(B13), 7561-7571.
3172 <https://doi.org/10.1029/JB084iB13p07561>

3173 Bogdanova, S. V., Bingen, B., Gorbatshev, R., Kheraskova, T. N., Kozlov, V. I., Puchkov, V.
3174 N., et al. (2008). The East European Craton (Baltica) before and during the
3175 assembly of Rodinia. *Precambrian Research*, 160(1), 23-45.
3176 <https://doi.org/10.1016/j.precamres.2007.04.024>

3177 Bohlen, S. R. (1991). On the formation of granulites. *Journal of Metamorphic Geology*, 9(3),
3178 223-229. <https://doi.org/10.1111/j.1525-1314.1991.tb00518.x>

3179 Boschman, L. M., van Hinsbergen, D. J. J., Kimbrough, D. L., Langereis, C. G., & Spakman,
3180 W. (2018). The dynamic history of 220 million years of subduction below Mexico:
3181 A correlation between slab geometry and overriding plate deformation based on
3182 geology, paleomagnetism, and seismic tomography. *Geochemistry, Geophysics*,

3183 *Geosystems*, 19(12), 4649-4672. <https://doi.org/10.1029/2018GC007739>

3184 Bostock, M. (1998). Mantle Stratigraphy and evolution of the Slav province. *Journal of*
 3185 *Geophysical Research*, 1032, 21183-21200. <https://doi.org/10.1029/98JB01069>

3186 Bowring, S. A., & Podosek, F. A. (1989). Nd isotopic evidence from Wopmay Orogen for
 3187 2.0–2.4 Ga crust in western North America. *Earth and Planetary Science Letters*,
 3188 94(3), 217-230. [https://doi.org/10.1016/0012-821X\(89\)90141-6](https://doi.org/10.1016/0012-821X(89)90141-6)

3189 Bowring, S. A., & Williams, I. S. (1999). Priscoan (4.00–4.03 Ga) orthogneisses from
 3190 northwestern Canada. *Contributions to Mineralogy and Petrology*, 134(1), 3-16.
 3191 <https://doi.org/10.1007/s004100050465>

3192 Boyd, F. R. (1989). Compositional distinction between oceanic and cratonic lithosphere.
 3193 *Earth and Planetary Science Letters*, 96(1-2), 15-26.
 3194 [https://doi.org/10.1016/0012-821X\(89\)90120-9](https://doi.org/10.1016/0012-821X(89)90120-9)

3195 Brito Neves, B. B. d., Campos Neto, M. d. C., & Fuck, R. A. (1999). From Rodinia to
 3196 western Gondwana: An approach to the Brasiliano-Pan African cycle and orogenic
 3197 collage. *Episodes*, 22(3), 155-166. <https://doi.org/10.18814/epiugs/1999/v22i3/002>

3198 Brodholt, J. (2013). Water may be a damp squib. *Nature*, 498(7453), 181-182.
 3199 <https://doi.org/10.1038/498181a>

3200 Bronner, A., Sauter, D., Manatschal, G., Péron-Pinvidic, G., & Munschy, M. (2011).
 3201 Magmatic breakup as an explanation for magnetic anomalies at magma-poor rifted
 3202 margins. *Nature Geoscience*, 4(8), 549-553. <https://doi.org/10.1038/ngeo1201>

3203 Brown, H. (1949). Rare gases and the formation of the Earth's atmosphere. In G. Kuiper
 3204 (Ed.), *The Atmosphere of the Earth and Planets* (pp. 258-266). Chicago: Univ.
 3205 Chicago Press.

3206 Brown, M. (1993). P–T–t evolution of orogenic belts and the causes of regional
 3207 metamorphism. *Journal of the Geological Society*, 150(2), 227-241.
 3208 <https://doi.org/10.1144/gsjgs.150.2.0227>

3209 Brown, M. (2006). Duality of thermal regimes is the distinctive characteristic of plate
 3210 tectonics since the Neoproterozoic. *Geology*, 34(11), 961-964.
 3211 <https://doi.org/10.1130/g22853a.1>

3212 Brown, M. (2008). Characteristic thermal regimes of plate tectonics and their metamorphic
 3213 imprint throughout Earth history. In K. C. Condie & V. Pease (Eds.), *When Did*
 3214 *Plate Tectonics Begin on Planet Earth?* (Vol. 440, pp. 97-128): Geological Society
 3215 of America Special Paper.

3216 Brown, M., & Johnson, T. (2018). Secular change in metamorphism and the onset of global
3217 plate tectonics. *American Mineralogist*, 103(2), 181-196.
3218 <https://doi.org/10.2138/am-2018-6166>

3219 Brown, M., Johnson, T., & Gardiner, N. J. (2020). Plate tectonics and the Archean earth.
3220 *Annual Review of Earth and Planetary Sciences*, 48(1), 291-320.
3221 <https://doi.org/10.1146/annurev-earth-081619-052705>

3222 Brune, S., Williams, S. E., & Müller, R. D. (2017). Potential links between continental
3223 rifting, CO₂ degassing and climate change through time. *Nature Geoscience*, 10(12),
3224 941-946. <https://doi.org/10.1038/s41561-017-0003-6>

3225 Buitert, S. J. H., & Torsvik, T. H. (2014). A review of Wilson cycle plate margins: A role for
3226 mantle plumes in continental break-up along sutures? *Gondwana Research*, 26(2),
3227 627-653. <https://doi.org/10.1016/j.gr.2014.02.007>

3228 Burov, E. B., & Diament, M. (1995). The effective elastic thickness (T_e) of continental
3229 lithosphere: What does it really mean? *Journal of Geophysical Research: Solid*
3230 *Earth*, 100(B3), 3905-3927. <https://doi.org/10.1029/94JB02770>

3231 Cai, C., Wiens, D. A., Shen, W., & Eimer, M. (2018). Water input into the Mariana
3232 subduction zone estimated from ocean-bottom seismic data. *Nature*, 563(7731),
3233 389-392. <http://dx.doi.org/10.1038/s41586-018-0655-4>

3234 Calò, M., Bodin, T., & Romanowicz, B. (2016). Layered structure in the upper mantle
3235 across North America from joint inversion of long and short period seismic data.
3236 *Earth and Planetary Science Letters*, 449, 164-175.
3237 <https://doi.org/10.1016/j.epsl.2016.05.054>

3238 Calvès, G., Schwab, A. M., Huuse, M., Clift, P. D., Gaina, C., Jolley, D., et al. (2011).
3239 Seismic volcanostratigraphy of the western Indian rifted margin: The pre-Deccan
3240 igneous province. *Journal of Geophysical Research: Solid Earth*, 116(B1).
3241 <https://doi.org/10.1029/2010JB000862>

3242 Calvert, A. J., & Doublier, M. P. (2018). Archaean continental spreading inferred from
3243 seismic images of the Yilgarn Craton. *Nature Geoscience*, 11(7), 526-530.
3244 <https://doi.org/10.1038/s41561-018-0138-0>

3245 Campbell, I. H. (2003). Constraints on continental growth models from Nb/U ratios in the
3246 3.5 Ga Barberton and other Archaean basalt-komatiite suites. *American Journal of*
3247 *Science*, 303(4), 319-351. <http://dx.doi.org/10.2475/ajs.303.4.319>

3248 Campbell, I. H. (2005). Large igneous provinces and the mantle plume hypothesis. *Elements*,

3249 *l*(5), 265-269. <http://dx.doi.org/10.2113/gselements.1.5.265>

3250 Campbell, I. H., & Griffiths, R. W. (1990). Implications of mantle plume structure for the
 3251 evolution of flood basalts. *Earth and Planetary Science Letters*, 99(1), 79-93.
 3252 [https://doi.org/10.1016/0012-821X\(90\)90072-6](https://doi.org/10.1016/0012-821X(90)90072-6)

3253 Campbell, I. H., & Griffiths, R. W. (1992). The changing nature of mantle hotspots through
 3254 time: Implications for the chemical evolution of the mantle. *The Journal of Geology*,
 3255 100(5), 497-523. <http://dx.doi.org/10.1086/629605>

3256 Campbell, I. H., Griffiths, R. W., & Hill, R. I. (1989). Melting in an Archaean mantle plume:
 3257 heads it's basalts, tails it's komatiites. *Nature*, 339(6227), 697-699.
 3258 <http://dx.doi.org/10.1038/339697a0>

3259 Campbell, I. H., & Hill, R. I. (1988). A two-stage model for the formation of the
 3260 granite-greenstone terrains of the Kalgoorlie-Norseman area, Western Australia.
 3261 *Earth and Planetary Science Letters*, 90(1), 11-25.
 3262 [https://doi.org/10.1016/0012-821X\(88\)90107-0](https://doi.org/10.1016/0012-821X(88)90107-0)

3263 Campbell, I. H., & Taylor, S. R. (1983). No water, no granites - No oceans, no continents.
 3264 *Geophysical Research Letters*, 10(11), 1061-1064.
 3265 <https://doi.org/10.1029/GL010i011p01061>

3266 Canil, D. (2008). Canada's craton: A bottoms-up view. *GSA Today*, 18(6), 4-10.
 3267 <http://dx.doi.org/10.1130/GSAT01806A.1>

3268 Capitanio, F. A., Morra, G., Goes, S., Weinberg, R. F., & Moresi, L. (2010). India–Asia
 3269 convergence driven by the subduction of the Greater Indian continent. *Nature*
 3270 *Geoscience*, 3(2), 136-139. <http://dx.doi.org/10.1038/ngeo725>

3271 Carlson, R. L., & Raskin, G. S. (1984). Density of the ocean crust. *Nature*, 311(5986),
 3272 555-558. <http://dx.doi.org/10.1038/311555a0>

3273 Carlson, R. W., Irving, A. J., Schulze, D. J., & Hearn, B. C. (2004). Timing of Precambrian
 3274 melt depletion and Phanerozoic refertilization events in the lithospheric mantle of
 3275 the Wyoming Craton and adjacent Central Plains Orogen. *Lithos*, 77(1-4), 453-472.
 3276 <http://dx.doi.org/10.1016/j.lithos.2004.03.030>

3277 Carlson, R. W., Pearson, D. G., & James, D. E. (2005). Physical, chemical, and
 3278 chronological characteristics of continental mantle. *Reviews of Geophysics*,
 3279 43(DG1001). <http://dx.doi.org/10.1029/2004RG000156>

3280 Cartwright, I., Buick, I., & Vry, J. (2000). The time-integrated history of crustal fluid flow:
 3281 Reynolds Range, central Australia. *Journal of Geochemical Exploration*, 69-70,

3282 353-357. [https://doi.org/10.1016/S0375-6742\(00\)00091-1](https://doi.org/10.1016/S0375-6742(00)00091-1)

3283 Cawood, P. A. (2020). Metamorphic rocks and plate tectonics. *Science Bulletin*, 65(12),

3284 968-969. <https://doi.org/10.1016/j.scib.2020.02.016>

3285 Cawood, P. A., Hawkesworth, C. J., Pisarevsky, S. A., Dhuime, B., Capitanio, F. A., &

3286 Nebel, O. (2018). Geological archive of the onset of plate tectonics. *Philos Trans A*

3287 *Math Phys Eng Sci*, 376(2132). <https://doi.org/10.1098/rsta.2017.0405>

3288 Cawood, P. A., Pisarevsky, S. A., & Leitch, E. C. (2011). Unraveling the New England

3289 orocline, east Gondwana accretionary margin. *Tectonics*, 30(5).

3290 <https://doi.org/10.1029/2011TC002864>

3291 Cayley, R. A. (2011). Exotic crustal block accretion to the eastern Gondwanaland margin in

3292 the Late Cambrian–Tasmania, the Selwyn Block, and implications for the

3293 Cambrian–Silurian evolution of the Ross, Delamerian, and Lachlan orogens.

3294 *Gondwana Research*, 19(3), 628-649. <https://doi.org/10.1016/j.gr.2010.11.013>

3295 Chalapathi Rao, N. V., Wu, F.-Y., Mitchell, R. H., Li, Q.-L., & Lehmann, B. (2013).

3296 Mesoproterozoic U–Pb ages, trace element and Sr–Nd isotopic composition of

3297 perovskite from kimberlites of the Eastern Dharwar craton, southern India: Distinct

3298 mantle sources and a widespread 1.1Ga tectonomagmatic event. *Chemical Geology*,

3299 353, 48-64. <https://doi.org/10.1016/j.chemgeo.2012.04.023>

3300 Chamberlain, K. R., Frost, C. D., & Frost, B. R. (2003). Early Archean to Mesoproterozoic

3301 evolution of the Wyoming Province: Archean origins to modern lithospheric

3302 architecture. *Canadian Journal of Earth Sciences*, 40(10), 1357-1374.

3303 <http://dx.doi.org/10.1139/e03-054>

3304 Chardon, D., Gapais, D., & Cagnard, F. (2009). Flow of ultra-hot orogens: A view from the

3305 Precambrian, clues for the Phanerozoic. *Tectonophysics*, 477(3), 105-118.

3306 <https://doi.org/10.1016/j.tecto.2009.03.008>

3307 Chen, C.-W., Rondenay, S., Evans, R. L., & Snyder, D. B. (2009). Geophysical detection of

3308 relict metasomatism from an Archean (~3.5 Ga) subduction zone. *Science*,

3309 326(5956), 1089-1091. <http://dx.doi.org/10.1126/science.1178477>

3310 Chen, C., Gilbert, H., Fischer, K. M., Andronicos, C. L., Pavlis, G. L., Hamburger, M. W., et

3311 al. (2018). Lithospheric discontinuities beneath the U.S. Midcontinent – signatures

3312 of Proterozoic terrane accretion and failed rifting. *Earth and Planetary Science*

3313 *Letters*, 481, 223-235. <https://doi.org/10.1016/j.epsl.2017.10.033>

3314 Chen, L. (2010). Concordant structural variations from the surface to the base of the upper

mantle in the North China Craton and its tectonic implications. *Lithos*, 120(1–2), 96-115. <http://dx.doi.org/10.1016/j.lithos.2009.12.007>

Chen, L. (2017). Layering of subcontinental lithospheric mantle. *Science Bulletin*, 62(14), 1030-1034. <https://doi.org/10.1016/j.scib.2017.06.003>

Chen, L., Jiang, M., Yang, J., Wei, Z., Liu, C., & Ling, Y. (2014). Presence of an intralithospheric discontinuity in the central and western North China Craton: Implications for destruction of the craton. *Geology*, 42(3), 223-226. <http://dx.doi.org/10.1130/g35010.1>

Chen, L., Wang, X., Liang, X., Wan, B., & Liu, L. (2020). Subduction tectonics vs. Plume tectonics—Discussion on driving forces for plate motion. *Science China Earth Sciences*, 63(3), 315-328. <https://doi.org/10.1007/s11430-019-9538-2>

Chen, Y., Gu, Y. J., Dokht, R. M. H., & Sacchi, M. D. (2015). Crustal imprints of Precambrian orogenesis in western Laurentia. *Journal of Geophysical Research: Solid Earth*, 120(10), 6993-7012. <https://doi.org/10.1002/2014JB011353>

Chen, Y. W., Wu, J., & Suppe, J. (2019). Southward propagation of Nazca subduction along the Andes. *Nature*, 565(7740), 441-447. <https://doi.org/10.1038/s41586-018-0860-1>

Cheng, C., Chen, L., Yao, H., Jiang, M., & Wang, B. (2013). Distinct variations of crustal shear wave velocity structure and radial anisotropy beneath the North China Craton and tectonic implications. *Gondwana Research*, 23(1), 25-38. <https://doi.org/10.1016/j.gr.2012.02.014>

Chesley, J. T., Rudnick, R. L., & Lee, C. T. (1999). Re-Os systematics of mantle xenoliths from the East African Rift: Age, structure, and history of the Tanzanian craton. *Geochimica et Cosmochimica Acta*, 63(7-8), 1203-1217. [https://doi.org/10.1016/S0016-7037\(99\)00004-6](https://doi.org/10.1016/S0016-7037(99)00004-6)

Chopin, C. (1984). Coesite and pure pyrope in high-grade blueschists of the Western Alps: a first record and some consequences. *Contributions to Mineralogy and Petrology*, 86(2), 107-118. <https://doi.org/10.1007/BF00381838>

Christensen, N. I., & Mooney, W. D. (1995). Seismic velocity structure and composition of the continental crust: A global view. *Journal of Geophysical Research: Solid Earth*, 100(B6), 9761-9788. <https://doi.org/10.1029/95JB00259>

Chu, X., & Korenaga, J. (2012). Olivine rheology, shear stress, and grain growth in the lithospheric mantle: Geological constraints from the Kaapvaal craton. *Earth and Planetary Science Letters*, 333-334, 52-62.

- 3348 <https://doi.org/10.1016/j.epsl.2012.04.019>
- 3349 Chu, Y., Lin, W., Faure, M., Xue, Z., Ji, W., & Feng, Z. (2019). Cretaceous episodic
 3350 extension in the south China block, east Asia: Evidence from the Yuechengling
 3351 massif of central south China. *Tectonics*, 38(10), 3675-3702.
 3352 <https://doi.org/10.1029/2019TC005516>
- 3353 Chulick, G. S., Detweiler, S., & Mooney, W. D. (2013). Seismic structure of the crust and
 3354 uppermost mantle of South America and surrounding oceanic basins. *Journal of*
 3355 *South American Earth Sciences*, 42, 260-276.
 3356 <https://doi.org/10.1016/j.jsames.2012.06.002>
- 3357 Claesson, S., Bogdanova, S. V., Bibikova, E. V., & Gorbatshev, R. (2001). Isotopic
 3358 evidence for Palaeoproterozoic accretion in the basement of the East European
 3359 Craton. *Tectonophysics*, 339(1), 1-18.
 3360 [https://doi.org/10.1016/S0040-1951\(01\)00031-2](https://doi.org/10.1016/S0040-1951(01)00031-2)
- 3361 Clark, C., Fitzsimons, I. C. W., Healy, D., & Harley, S. L. (2011). How does the continental
 3362 crust get really hot? *Elements*, 7(4), 235-240.
 3363 <https://doi.org/10.2113/gselements.7.4.235>
- 3364 Clark, C., Taylor, R. J. M., Kylander-Clark, A. R. C., & Hacker, Bradley R. (2018).
 3365 Prolonged (>100 Ma) ultrahigh temperature metamorphism in the Napier Complex,
 3366 East Antarctica: A petrochronological investigation of Earth's hottest crust. *Journal*
 3367 *of Metamorphic Geology*, 36(9), 1117-1139. <https://doi.org/10.1111/jmg.12430>
- 3368 Clift, P. D., Schouten, H., & Vannucchi, P. (2009). Arc-continent collisions, sediment
 3369 recycling and the maintenance of the continental crust. *Geological Society, London,*
 3370 *Special Publications*, 318(1), 75-103. <https://doi.org/10.1144/sp318.3>
- 3371 Cline II, C. J., Faul, U. H., David, E. C., Berry, A. J., & Jackson, I. (2018).
 3372 Redox-influenced seismic properties of upper-mantle olivine. *Nature*, 555(7696),
 3373 355-358. <https://doi.org/10.1038/nature25764>
- 3374 Coffin, M. F., & Eldholm, O. (1994). Large igneous provinces: Crustal structure,
 3375 dimensions, and external consequences. *Reviews of Geophysics*, 32(1), 1-36.
 3376 <https://doi.org/10.1029/93RG02508>
- 3377 Collins, W. J., Belousova, E. A., Kemp, A. I. S., & Murphy, J. B. (2011). Two contrasting
 3378 Phanerozoic orogenic systems revealed by hafnium isotope data. *Nature Geoscience*,
 3379 4(5), 333-337. <https://doi.org/10.1038/ngeo1127>
- 3380 Collins, W. J., Van Kranendonk, M. J., & Teyssier, C. (1998). Partial convective overturn of

3381 Archaean crust in the east Pilbara Craton, Western Australia: driving mechanisms
 3382 and tectonic implications. *Journal of Structural Geology*, 20(9), 1405-1424.
 3383 [https://doi.org/10.1016/S0191-8141\(98\)00073-X](https://doi.org/10.1016/S0191-8141(98)00073-X)

3384 Colpron, M., Nelson, J., & Murphy, D. (2007). Northern Cordilleran terranes and their
 3385 interactions through time. *GSA Today*, 17, 4.
 3386 <https://doi.org/10.1130/GSAT01704-5A.1>

3387 Condie, K. C. (1975). Mantle-plume model for the origin of Archaean greenstone belts
 3388 based on trace element distributions. *Nature*, 258(5534), 413-414.
 3389 <https://doi.org/10.1038/258413a0>

3390 Condie, K. C. (1994). Greenstones through time. In K. C. Condie (Ed.), *Archean Crustal*
 3391 *Evolution* (Vol. 11, pp. 85-120). Amsterdam: Elsevier.

3392 Condie, Kent C. (1997). Contrasting sources for upper and lower continental crust: The
 3393 greenstone connection. *The Journal of Geology*, 105(6), 729-736.
 3394 <https://doi.org/10.1086/515980>

3395 Condie, K. C. (2001). *Mantle plumes and their record in earth history*. Cambridge:
 3396 Cambridge University Press.

3397 Condie, K. C. (2005). TTGs and adakites: are they both slab melts? *Lithos*, 80(1), 33-44.
 3398 <https://doi.org/10.1016/j.lithos.2003.11.001>

3399 Condie, K. C. (2007). Accretionary orogens in space and time. *Geological Society of*
 3400 *America Memoir*, 200, 145-158. [https://doi.org/10.1130/2007.1200\(09\)](https://doi.org/10.1130/2007.1200(09))

3401 Condie, K. C. (2014). How to make a continent: thirty-five years of TTG research. In Y.
 3402 Dilek & H. Furnes (Eds.), *Evolution of Archean Crust and Early Life. Modern*
 3403 *Approaches in Solid Earth Sciences* (Vol. 7, pp. 179-193). Dordrecht: Springer.

3404 Coney, P. J. (1980). Cordilleran metamorphic core complexes: An overview. *Geological*
 3405 *Society of America Memoirs*, 153, 7-31. <https://doi.org/10.1130/MEM153-p7>

3406 Coney, P. J. (1992). The lachlan belt of eastern Australia and circum-Pacific tectonic
 3407 evolution. *Tectonophysics*, 214(1), 1-25.
 3408 [https://doi.org/10.1016/0040-1951\(92\)90187-B](https://doi.org/10.1016/0040-1951(92)90187-B)

3409 Connelly, J. N., & Ryan, B. (1996). Late Archean evolution of the Nain Province, Nain,
 3410 Labrador: imprint of a collision. *Canadian Journal of Earth Sciences*, 33(9),
 3411 1325-1342. <https://doi.org/10.1139/e96-100>

3412 Conrad, C., & Lithgow-Bertelloni, C. (2004). The temporal evolution of plate driving forces:
 3413 Importance of "slab suction"versus "slab pull"during the Cenozoic. *Journal of*

3414 *Geophysical Research*, 109. <https://doi.org/10.1029/2004JB002991>

3415 Cook, F. A. (2011). Multiple arc development in the Paleoproterozoic Wopmay orogen,
 3416 northwest Canada. In D. Brown & P. D. Ryan (Eds.), *Arc-Continent Collision* (pp.
 3417 403-427). Berlin, Heidelberg: Springer.

3418 Cooper, C. M., & Miller, M. S. (2014). Craton formation: Internal structure inherited from
 3419 closing of the early oceans. *Lithosphere*, 6(1), 35-42. <https://doi.org/10.1130/L321.1>

3420 Copeland, P., Currie, C. A., Lawton, T. F., & Murphy, M. A. (2017). Location, location,
 3421 location: The variable lifespan of the Laramide orogeny. *Geology*, 45(5), 223-226.
 3422 <https://doi.org/10.1130/G38810.1>

3423 Cordani, U. G., & Sato, K. (1999). Crustal evolution of the south American platform, based
 3424 on Nd isotopic systematics on granitoid rocks. *Episodes*, 22(3), 167-173.
 3425 <https://doi.org/10.18814/epiugs/1999/v22i3/003>

3426 Cordani, U. G., & Teixeira, W. (2007). Proterozoic accretionary belts in the Amazonian
 3427 Craton. In R. D. J. Hatcher, M. P. Carlson, J. H. McBride & J. R. Martínez-Catalán
 3428 (Eds.), *4-D Framework of Continental Crust* (Vol. 200, pp. 297-320): Geological
 3429 Society of America Memoir.

3430 Corrigan, D., Hajnal, Z., Németh, B., & Lucas, S. B. (2005). Tectonic framework of a
 3431 Paleoproterozoic arc-continent to continent-continent collisional zone,
 3432 Trans-Hudson Orogen, from geological and seismic reflection studies. *Canadian*
 3433 *Journal of Earth Sciences*, 42(4), 421-434. <https://doi.org/10.1139/e05-025>

3434 Corrigan, D., Pehrsson, S., Wodicka, N., & de Kemp, E. (2009). The Palaeoproterozoic
 3435 Trans-Hudson Orogen: a prototype of modern accretionary processes. *Geological*
 3436 *Society, London, Special Publications*, 327(1), 457-479.
 3437 <https://doi.org/10.1144/sp327.19>

3438 Dèzes, P., Schmid, S. M., & Ziegler, P. A. (2004). Evolution of the European Cenozoic rift
 3439 system: interaction of the Alpine and Pyrenean orogens with their foreland
 3440 lithosphere. *Tectonophysics*, 389(1), 1-33.
 3441 <https://doi.org/10.1016/j.tecto.2004.06.011>

3442 Daigneault, R., Mueller, W. U., & Chown, E. H. (2002). Oblique Archean subduction:
 3443 accretion and exhumation of an oceanic arc during dextral transpression, Southern
 3444 Volcanic Zone, Abitibi Subprovince Canada. *Precambrian Research*, 115(1),
 3445 261-290. [https://doi.org/10.1016/S0301-9268\(02\)00012-8](https://doi.org/10.1016/S0301-9268(02)00012-8)

3446 Darbyshire, F. A., Bastow, I. D., Petrescu, L., Gilligan, A., & Thompson, D. A. (2017). A

3447 tale of two orogens: Crustal processes in the Proterozoic Trans-Hudson and
 3448 Grenville Orogens, eastern Canada. *Tectonics*, 36(8), 1633-1659.
 3449 <https://doi.org/10.1002/2017TC004479>
 3450 Dave, R., & Li, A. (2016). Destruction of the Wyoming craton: Seismic evidence and
 3451 geodynamic processes. *Geology*, 44(11), 883-886. <https://doi.org/10.1130/g38147.1>
 3452 De Waele, B., Johnson, S. P., & Pisarevsky, S. A. (2008). Palaeoproterozoic to
 3453 Neoproterozoic growth and evolution of the eastern Congo Craton: Its role in the
 3454 Rodinia puzzle. *Precambrian Research*, 160(1), 127-141.
 3455 <https://doi.org/10.1016/j.precamres.2007.04.020>
 3456 de Wit, M. J. (1998). On Archean granites, greenstones, cratons and tectonics: does the
 3457 evidence demand a verdict? *Precambrian Research*, 91(1), 181-226.
 3458 [https://doi.org/10.1016/S0301-9268\(98\)00043-6](https://doi.org/10.1016/S0301-9268(98)00043-6)
 3459 Deen, T. J., Griffin, W. L., Begg, G., O'Reilly, S. Y., Natapov, L. M., & Hronsky, J. (2006).
 3460 Thermal and compositional structure of the subcontinental lithospheric mantle:
 3461 Derivation from shear wave seismic tomography. *Geochemistry, Geophysics,*
 3462 *Geosystems*, 7(7). <https://doi.org/10.1029/2005GC001120>
 3463 Delph, J. R., & Porter, R. C. (2015). Crustal structure beneath southern Africa: insight into
 3464 how tectonic events affect the Mohorovičić discontinuity. *Geophysical Journal*
 3465 *International*, 200(1), 254-264. <https://doi.org/10.1093/gji/ggu376>
 3466 Demouchy, S., & Bolfan-Casanova, N. (2016). Distribution and transport of hydrogen in the
 3467 lithospheric mantle: A review. *Lithos*, 240-243, 402-425.
 3468 <https://doi.org/10.1016/j.lithos.2015.11.012>
 3469 Desrochers, J.-P., Hubert, C., Ludden, J. N., & Pilote, P. (1993). Accretion of Archean
 3470 oceanic plateau fragments in the Abitibi, greenstone belt, Canada. *Geology*, 21(5),
 3471 451-454. [https://doi.org/10.1130/0091-7613\(1993\)021<0451:aoaopf>2.3.co;2](https://doi.org/10.1130/0091-7613(1993)021<0451:aoaopf>2.3.co;2)
 3472 Dhuime, B., Hawkesworth, C. J., Cawood, P. A., & Storey, C. D. (2012). A change in the
 3473 geodynamics of continental growth 3 billion years ago. *Science*, 335(6074),
 3474 1334-1336. <https://doi.org/10.1126/science.1216066>
 3475 Dhuime, B., Hawkesworth, C. J., Delavault, H., & Cawood, P. A. (2018). Rates of
 3476 generation and destruction of the continental crust: implications for continental
 3477 growth. *Philos Trans A Math Phys Eng Sci*, 376(2132).
 3478 <https://doi.org/10.1098/rsta.2017.0403>
 3479 Dick, H. J. B., Lin, J., & Schouten, H. (2003). An ultraslow-spreading class of ocean ridge.

3480 *Nature*, 426(6965), 405-412. <https://doi.org/10.1038/nature02128>

3481 Dickinson, W. R. (2004). Evolution of the north American Cordillera. *Annual Review of*
3482 *Earth and Planetary Sciences*, 32(1), 13-45.
3483 <https://doi.org/10.1146/annurev.earth.32.101802.120257>

3484 Dickinson, W. R. (2008). Accretionary Mesozoic–Cenozoic expansion of the Cordilleran
3485 continental margin in California and adjacent Oregon. *Geosphere*, 4(2), 329-353.
3486 <https://doi.org/10.1130/ges00105.1>

3487 Dickinson, W. R., & Snyder, W. S. (1979). Geometry of subducted slabs related to San
3488 Andreas transform. *The Journal of Geology*, 87(6), 609-627.
3489 <https://doi.org/10.1086/628456>

3490 Ding, L., Kapp, P., & Wan, X. (2005). Paleocene–Eocene record of ophiolite obduction and
3491 initial India-Asia collision, south central Tibet. *Tectonics*, 24(3).
3492 <https://doi.org/10.1029/2004TC001729>

3493 Dixon, J. E., Dixon, T. H., Bell, D. R., & Malservisi, R. (2004). Lateral variation in upper
3494 mantle viscosity: role of water. *Earth and Planetary Science Letters*, 222(2),
3495 451-467. <https://doi.org/10.1016/j.epsl.2004.03.022>

3496 Dixon, J. E., Leist, L., Langmuir, C., & Schilling, J.-G. (2002). Recycled dehydrated
3497 lithosphere observed in plume-influenced mid-ocean-ridge basalt. *Nature*,
3498 420(6914), 385-389. <https://doi.org/10.1038/nature01215>

3499 Doin, M.-P., Fleitout, L., & Christensen, U. (1997). Mantle convection and stability of
3500 depleted and undepleted continental lithosphere. *Journal of Geophysical Research:*
3501 *Solid Earth*, 102(B2), 2771-2787. <https://doi.org/10.1029/96JB03271>

3502 Doucet, L. S., Ionov, D. A., Golovin, A. V., & Pokhilenko, N. P. (2012). Depth, degrees and
3503 tectonic settings of mantle melting during craton formation: inferences from major
3504 and trace element compositions of spinel harzburgite xenoliths from the Udachnaya
3505 kimberlite, central Siberia. *Earth and Planetary Science Letters*, 359-360, 206-218.
3506 <https://doi.org/10.1016/j.epsl.2012.10.001>

3507 Doucet, L. S., Peslier, A. H., Ionov, D. A., Brandon, A. D., Golovin, A. V., Goncharov, A. G.,
3508 et al. (2014). High water contents in the Siberian cratonic mantle linked to
3509 metasomatism: An FTIR study of Udachnaya peridotite xenoliths. *Geochimica et*
3510 *Cosmochimica Acta*, 137, 159-187. <https://doi.org/10.1016/j.gca.2014.04.011>

3511 Downes, H., Balaganskaya, E., Beard, A., Liferovich, R., & Demaiffe, D. (2005).
3512 Petrogenetic processes in the ultramafic, alkaline and carbonatitic magmatism in the

3513 Kola Alkaline Province: A review. *Lithos*, 85(1-4), 48-75.
 3514 <https://doi.org/10.1016/j.lithos.2005.03.020>

3515 Drummond, B. J. (1988). A review of crust/upper mantle structure in the Precambrian areas
 3516 of Australia and implications for Precambrian crustal evolution. *Precambrian*
 3517 *Research*, 40-41, 101-116. [https://doi.org/10.1016/0301-9268\(88\)90063-0](https://doi.org/10.1016/0301-9268(88)90063-0)

3518 Durrheim, R. J., & Mooney, W. D. (1994). Evolution of the Precambrian lithosphere:
 3519 Seismological and geochemical constraints. *Journal of Geophysical Research: Solid*
 3520 *Earth*, 99(B8), 15359-15374. <https://doi.org/10.1029/94JB00138>

3521 Eaton, D. W., & Claire Perry, H. K. (2013). Ephemeral isopycnicity of cratonic mantle keels.
 3522 *Nature Geoscience*, 6(11), 967-970. <https://doi.org/10.1038/ngeo1950>

3523 Eberhart-Phillips, D., Christensen, D. H., Brocher, T. M., Hansen, R., Ruppert, N. A.,
 3524 Haeussler, P. J., et al. (2006). Imaging the transition from Aleutian subduction to
 3525 Yakutat collision in central Alaska, with local earthquakes and active source data.
 3526 *Journal of Geophysical Research: Solid Earth*, 111(B11).
 3527 <https://doi.org/10.1029/2005JB004240>

3528 Elkins-Tanton, L. T. (2012). Magma Oceans in the Inner Solar System. *Annual Review of*
 3529 *Earth and Planetary Sciences*, 40(1), 113-139.
 3530 <https://doi.org/10.1146/annurev-earth-042711-105503>

3531 Ernst, R. E. (2014). Oceanic LIPs: oceanic plateaus and ocean-basin flood basalts and their
 3532 remnants through time. In R. E. Ernst (Ed.), *Large Igneous Provinces* (pp. 90-110).
 3533 Cambridge: Cambridge University Press.

3534 Ernst, R. E., & Buchan, K. L. (2003). Recognizing Mantle Plumes in the Geological Record.
 3535 *Annual Review of Earth and Planetary Sciences*, 31(1), 469-523.
 3536 <https://doi.org/10.1146/annurev.earth.31.100901.145500>

3537 Ernst, W. G., & Liou, J. G. (1995). Contrasting plate-tectonic styles of the
 3538 Qinling-Dabie-Sulu and Franciscan metamorphic belts. *Geology*, 23(4), 353-356.
 3539 [https://doi.org/10.1130/0091-7613\(1995\)023<0353:cptsot>2.3.co;2](https://doi.org/10.1130/0091-7613(1995)023<0353:cptsot>2.3.co;2)

3540 Ernst, W. G., Maruyama, S., & Wallis, S. (1997). Buoyancy-driven, rapid exhumation of
 3541 ultrahigh-pressure metamorphosed continental crust. *Proceedings of the National*
 3542 *Academy of Sciences*, 94(18), 9532-9537. <https://doi.org/10.1073/pnas.94.18.9532>

3543 Faccenna, C., Becker, T., Conrad, C., & Husson, L. (2013). Mountain building and mantle
 3544 dynamics. *Tectonics*, 32. <https://doi.org/10.1029/2012TC003176>

3545 Faccenna, C., Becker, T. W., Auer, L., Billi, A., Boschi, L., Brun, J. P., et al. (2014). Mantle

3546 dynamics in the Mediterranean. *Reviews of Geophysics*, 52(3), 283-332.
3547 <https://doi.org/10.1002/2013RG000444>

3548 Fan, X., & Chen, Q. F. (2019). Seismic constraints on the magmatic system beneath the
3549 Changbaishan volcano: Insight into its origin and regional tectonics. *Journal of*
3550 *Geophysical Research: Solid Earth*, 124(2), 2003-2024.
3551 <https://doi.org/10.1029/2018JB016288>

3552 Farley, K. A., Natland, J. H., & Craig, H. (1992). Binary mixing of enriched and undegassed
3553 (primitive?) mantle components (He, Sr, Nd, Pb) in Samoan lavas. *Earth and*
3554 *Planetary Science Letters*, 111(1), 183-199.
3555 [https://doi.org/10.1016/0012-821X\(92\)90178-X](https://doi.org/10.1016/0012-821X(92)90178-X)

3556 Faul, U. H., Cline, C. J., David, E. C., Berry, A. J., & Jackson, I. (2016). Titanium-hydroxyl
3557 defect-controlled rheology of the Earth's upper mantle. *Earth and Planetary Science*
3558 *Letters*, 452, 227-237. <https://doi.org/10.1016/j.epsl.2016.07.016>

3559 Fei, H., Wiedenbeck, M., Yamazaki, D., & Katsura, T. (2013). Small effect of water on
3560 upper-mantle rheology based on silicon self-diffusion coefficients. *Nature*,
3561 498(7453), 213-215. <https://doi.org/10.1038/nature12193>

3562 Fergusson, C. L., & Henderson, R. A. (2015). Early Palaeozoic continental growth in the
3563 Tasmanides of northeast Gondwana and its implications for Rodinia assembly and
3564 rifting. *Gondwana Research*, 28(3), 933-953.
3565 <https://doi.org/10.1016/j.gr.2015.04.001>

3566 Fichtner, A., Kennett, B. L. N., Igel, H., & Bunge, H.-P. (2010). Full waveform tomography
3567 for radially anisotropic structure: New insights into present and past states of the
3568 Australasian upper mantle. *Earth and Planetary Science Letters*, 290(3), 270-280.
3569 <https://doi.org/10.1016/j.epsl.2009.12.003>

3570 Fischer, K. M. (2002). Waning buoyancy in the crustal roots of old mountains. *Nature*,
3571 417(6892), 933-936. <https://doi.org/10.1038/nature00855>

3572 Fischer, K. M., Ford, H. A., Abt, D. L., & Rychert, C. A. (2010). The
3573 lithosphere-asthenosphere boundary. *Annual Review of Earth and Planetary*
3574 *Sciences*, 38(1), 551-575. <https://doi.org/10.1146/annurev-earth-040809-152438>

3575 Fishwick, S., Heintz, M., Kennett, B. L. N., Reading, A. M., & Yoshizawa, K. (2008). Steps
3576 in lithospheric thickness within eastern Australia, evidence from surface wave
3577 tomography. *Tectonics*, 27(4), TC4009. <https://doi.org/10.1029/2007TC002116>

3578 Fletcher, A. W., Abdelsalam, M. G., Emishaw, L., Atekwana, E. A., Laó-Dávila, D. A., &

3579 Ismail, A. (2018). Lithospheric controls on the rifting of the Tanzanian craton at the
 3580 Eyasi basin, eastern branch of the East African Rift System. *Tectonics*, 37(9),
 3581 2818-2832. <https://doi.org/10.1029/2018TC005065>

3582 Foden, J., Elburg, M A., Dougherty-Page, J., & Burt, A. (2006). The timing and duration of
 3583 the Delamerian orogeny: Correlation with the Ross orogen and implications for
 3584 Gondwana assembly. *The Journal of Geology*, 114(2), 189-210.
 3585 <https://doi.org/10.1086/499570>

3586 Foley, S. F. (2008). Rejuvenation and erosion of the cratonic lithosphere. *Nature Geoscience*,
 3587 1(8), 503-510. <http://dx.doi.org/10.1038/ngeo261>

3588 Ford, H. A., Fischer, K. M., Abt, D. L., Rychert, C. A., & Elkins-Tanton, L. T. (2010). The
 3589 lithosphere–asthenosphere boundary and cratonic lithospheric layering beneath
 3590 Australia from Sp wave imaging. *Earth and Planetary Science Letters*, 300(3),
 3591 299-310. <https://doi.org/10.1016/j.epsl.2010.10.007>

3592 Foster, D. A., & Gray, D. R. (2000). Evolution and structure of the Lachlan fold belt (orogen)
 3593 of eastern Australia. *Annual Review of Earth and Planetary Sciences*, 28(1), 47-80.
 3594 <https://doi.org/10.1146/annurev.earth.28.1.47>

3595 Foster, K., Dueker, K., Schmandt, B., & Yuan, H. (2014). A sharp cratonic
 3596 lithosphere–asthenosphere boundary beneath the American Midwest and its relation
 3597 to mantle flow. *Earth and Planetary Science Letters*, 402, 82-89.
 3598 <https://doi.org/10.1016/j.epsl.2013.11.018>

3599 François, T., Burov, E., Meyer, B., & Agard, P. (2013). Surface topography as key constraint
 3600 on thermo-rheological structure of stable cratons. *Tectonophysics*, 602, 106-123.
 3601 <https://doi.org/10.1016/j.tecto.2012.10.009>

3602 French, S. W., Fischer, K. M., Syracuse, E. M., & Wyssession, M. E. (2009). Crustal
 3603 structure beneath the Florida-to-Edmonton broadband seismometer array.
 3604 *Geophysical Research Letters*, 36(8). <https://doi.org/10.1029/2008GL036331>

3605 Frisch, W., Meschede, M., & Blakey, R. C. (2011). *Plate tectonics: Continental drift and*
 3606 *mountain building*. Heidelberg: Springer, Berlin, Heidelberg.

3607 Fritz, H., Abdelsalam, M., Ali, K. A., Bingen, B., Collins, A. S., Fowler, A. R., et al. (2013).
 3608 Orogen styles in the east African orogen: A review of the Neoproterozoic to
 3609 Cambrian tectonic evolution. *Journal of African Earth Sciences*, 86, 65-106.
 3610 <https://doi.org/10.1016/j.jafrearsci.2013.06.004>

3611 Frizon de Lamotte, D., Fourdan, B., Leleu, S., Leparmentier, F., & de Clarens, P. (2015).

3612 Style of rifting and the stages of Pangea breakup. *Tectonics*, 34(5), 1009-1029.
3613 <https://doi.org/10.1002/2014TC003760>

3614 Frost, C. D., Fruchey, B. L., Chamberlain, K. R., & Frost, B. R. (2006). Archean crustal
3615 growth by lateral accretion of juvenile supracrustal belts in the south-central
3616 Wyoming Province. *Canadian Journal of Earth Sciences*, 43(10), 1533-1555.
3617 <https://doi.org/10.1139/e06-092>

3618 Furnes, H., Rosing, M., Dilek, Y., & de Wit, M. (2009). Isua supracrustal belt
3619 (Greenland)—A vestige of a 3.8 Ga suprasubduction zone ophiolite, and the
3620 implications for Archean geology. *Lithos*, 113(1), 115-132.
3621 <https://doi.org/10.1016/j.lithos.2009.03.043>

3622 Furumoto, A. S., Webb, J. P., Odegard, M. E., & Hussong, D. M. (1976). Seismic studies on
3623 the Ontong Java Plateau, 1970. *Tectonophysics*, 34(1), 71-90.
3624 [https://doi.org/10.1016/0040-1951\(76\)90177-3](https://doi.org/10.1016/0040-1951(76)90177-3)

3625 Fyfe, W. S. (1978). The evolution of the earth's crust: Modern plate tectonics to ancient hot
3626 spot tectonics? *Chemical Geology*, 23(1), 89-114.
3627 [https://doi.org/10.1016/0009-2541\(78\)90068-2](https://doi.org/10.1016/0009-2541(78)90068-2)

3628 Galer, S. J. G. (1991). Interrelationships between continental freeboard, tectonics and mantle
3629 temperature. *Earth and Planetary Science Letters*, 105(1), 214-228.
3630 [https://doi.org/10.1016/0012-821X\(91\)90132-2](https://doi.org/10.1016/0012-821X(91)90132-2)

3631 Ganne, J., De Andrade, V., Weinberg, R. F., Vidal, O., Dubacq, B., Kagambega, N., et al.
3632 (2012). Modern-style plate subduction preserved in the Palaeoproterozoic West
3633 African craton. *Nature Geoscience*, 5(1), 60-65. <https://doi.org/10.1038/ngeo1321>

3634 Gao, J., Wu, S., McIntosh, K., Mi, L., Yao, B., Chen, Z., et al. (2015). The continent–ocean
3635 transition at the mid-northern margin of the South China Sea. *Tectonophysics*, 654,
3636 1-19. <https://doi.org/10.1016/j.tecto.2015.03.003>

3637 Gao, Y., Chen, L., Wang, X., & Ai, Y. (2019). Complex lithospheric deformation in eastern
3638 and northeastern Tibet from shear wave splitting observations and its geodynamic
3639 implications. *Journal of Geophysical Research: Solid Earth*, 124(10), 10331-10346.
3640 <https://doi.org/10.1029/2018JB017081>

3641 Gaucher, C., Frei, R., Chemale, F., Frei, D., Bossi, J., Martínez, G., et al. (2011).
3642 Mesoproterozoic evolution of the Río de la Plata Craton in Uruguay: at the heart of
3643 Rodinia? *International Journal of Earth Sciences*, 100(2), 273-288.
3644 <https://doi.org/10.1007/s00531-010-0562-x>

- 3645 Gaul, O. F., Griffin, W. L., O'Reilly, S. Y., & Pearson, N. J. (2000). Mapping olivine
3646 composition in the lithospheric mantle. *Earth and Planetary Science Letters*,
3647 182(3-4), 223-235. [https://doi.org/10.1016/S0012-821X\(00\)00243-0](https://doi.org/10.1016/S0012-821X(00)00243-0)
- 3648 Gavrilenko, P., Ballaran, T. B., & Keppler, H. (2010). The effect of Al and water on the
3649 compressibility of diopside. *American Mineralogist*, 95(4), 608-616.
3650 <https://doi.org/10.2138/am.2010.3400>
- 3651 Ge, W., Zhao, G., Sun, D., Wu, F., & Lin, Q. (2003). Metamorphic P-T Path of the Southern
3652 Jilin complex: Implications for tectonic evolution of the Eastern block of the North
3653 China craton. *International Geology Review*, 45(11), 1029-1043.
3654 <https://doi.org/10.2747/0020-6814.45.11.1029>
- 3655 Gerya, T. (2014). Precambrian geodynamics: Concepts and models. *Gondwana Research*,
3656 25(2), 442-463. <https://doi.org/10.1016/j.gr.2012.11.008>
- 3657 Gibb, R. A., & Walcott, R. I. (1971). A precambrian suture in the Canadian shield. *Earth and*
3658 *Planetary Science Letters*, 10(4), 417-422.
3659 [https://doi.org/10.1016/0012-821X\(71\)90090-2](https://doi.org/10.1016/0012-821X(71)90090-2)
- 3660 Gilbert, M. C. (1983). Timing and chemistry of igneous events associated with the Southern
3661 Oklahoma Aulacogen. *Tectonophysics*, 94(1), 439-455.
3662 [https://doi.org/10.1016/0040-1951\(83\)90028-8](https://doi.org/10.1016/0040-1951(83)90028-8)
- 3663 Gladkochub, D., Pisarevsky, S., Donskaya, T., Natapov, L., Mazukabzov, A., Stanevich, A.,
3664 et al. (2006). The Siberian craton and its evolution in terms of the Rodinia
3665 hypothesis. *Episodes*, 29(3), 169-174.
3666 <https://doi.org/10.18814/epiugs/2006/v29i3/002>
- 3667 Glen, R. A. (2005). The Tasmanides of eastern Australia. *Terrane Processes at the Margins*
3668 *of Gondwana, Special Publication* 246, 23-96.
3669 <https://doi.org/10.1144/gsl.sp.2005.246.01.02>
- 3670 Gorczyk, W., Hobbs, B., & Gerya, T. (2012). Initiation of Rayleigh–Taylor instabilities in
3671 intra-cratonic settings. *Tectonophysics*, 514-517, 146-155.
3672 <https://doi.org/10.1016/j.tecto.2011.10.016>
- 3673 Gornova, M. A., Belyaev, V. A., & Belozeroval, O. Y. (2013). Textures and geochemistry of
3674 the Saramta peridotites (Siberian craton): Melting and refertilization during early
3675 evolution of the continental lithospheric mantle. *Journal of Asian Earth Sciences*,
3676 62, 4-17. <http://dx.doi.org/10.1016/j.jseaes.2012.10.004>
- 3677 Goscombe, B., Gray, D., & Hand, M. (2004). Variation in metamorphic style along the

3678 northern margin of the Damara orogen, Namibia. *Journal of Petrology*, 45(6),
3679 1261-1295. <https://doi.org/10.1093/petrology/egh013>

3680 Greber, N. D., Dauphas, N., Bekker, A., Ptáček, M. P., Bindeman, I. N., & Hofmann, A.
3681 (2017). Titanium isotopic evidence for felsic crust and plate tectonics 3.5 billion
3682 years ago. *Science*, 357(6357), 1271-1274. <https://doi.org/10.1126/science.aan8086>

3683 Green, J. C. (1983). Geologic and geochemical evidence for the nature and development of
3684 the middle proterozoic (keweenawan) midcontinent Rift of north america.
3685 *Tectonophysics*, 94(1), 413-437. [https://doi.org/10.1016/0040-1951\(83\)90027-6](https://doi.org/10.1016/0040-1951(83)90027-6)

3686 Grenville, A. J. C. (1922). The primitive crust of the earth. *Nature*, 110(2755), 249-249.
3687 <https://doi.org/10.1038/110249a0>

3688 Griffin, W. L., O'Reilly, S. Y., Afonso, J. C., & Begg, G. C. (2009). The composition and
3689 evolution of lithospheric mantle: a re-evaluation and its tectonic implications.
3690 *Journal of Petrology*, 50(7), 1185-1204. <https://doi.org/10.1093/petrology/egn033>

3691 Griffin, W. L., O'Reilly, S. Y., & Ryan, C. G. (1999). The composition and origin of
3692 sub-continental lithospheric mantle. In Y. Fei, C. M. BertKa & B. O. Mysen (Eds.),
3693 *Mantle Petrology: Field Observations and High-Pressure Experimentation. A*
3694 *Tribute to Francis R. (Joe) Boyd*. (Vol. Geochem. Soc. Spec. Publ, vol. 6, pp. 13-45).
3695 Houston: The Geochemical Society.

3696 Griffin, W. L., O'Reilly, S. Y., Abe, N., Aulbach, S., Davies, R. M., Pearson, N. J., et al.
3697 (2003). The origin and evolution of Archean lithospheric mantle. *Precambrian*
3698 *Research*, 127(1), 19-41. [https://doi.org/10.1016/S0301-9268\(03\)00180-3](https://doi.org/10.1016/S0301-9268(03)00180-3)

3699 Grosch, E. G., & Slama, J. (2017). Evidence for 3.3-billion-year-old oceanic crust in the
3700 Barberton greenstone belt, South Africa. *Geology*, 45(8), 695-698.
3701 <https://doi.org/10.1130/g39035.1>

3702 Guillot, S., Mahéo, G., de Sigoyer, J., Hattori, K. H., & Pêcher, A. (2008). Tethyan and
3703 Indian subduction viewed from the Himalayan high- to ultrahigh-pressure
3704 metamorphic rocks. *Tectonophysics*, 451(1), 225-241.
3705 <https://doi.org/10.1016/j.tecto.2007.11.059>

3706 Guitreau, M., Blichert-Toft, J., Mojzsis, S. J., Roth, A. S. G., Bourdon, B., Cates, N. L., et al.
3707 (2014). Lu–Hf isotope systematics of the Hadean–Eoarchean Acasta Gneiss
3708 Complex (Northwest Territories, Canada). *Geochimica et Cosmochimica Acta*, 135,
3709 251-269. <https://doi.org/10.1016/j.gca.2014.03.039>

3710 Gung, Y., Panning, M., & Romanowicz, B. (2003). Global anisotropy and the thickness of

3711 continents. *Nature*, 422(6933), 707-711. <https://doi.org/10.1038/nature01559>

3712 Guo, Z. T., Ruddiman, W. F., Hao, Q. Z., Wu, H. B., Qiao, Y. S., Zhu, R. X., et al. (2002).
 3713 Onset of Asian desertification by 22 Myr ago inferred from loess deposits in China.
 3714 *Nature*, 416(6877), 159-163. <https://doi.org/10.1038/416159a>

3715 Hölttä, P., & Paavola, J. (2000). P–T–t development of Archaean granulites in Varpaisjärvi,
 3716 Central Finland: I. Effects of multiple metamorphism on the reaction history of
 3717 mafic rocks. *Lithos*, 50(1), 97-120. [https://doi.org/10.1016/S0024-4937\(99\)00056-0](https://doi.org/10.1016/S0024-4937(99)00056-0)

3718 Hacker, B. R., Kelemen, P. B., & Behn, M. D. (2015). Continental lower crust. *Annual*
 3719 *Review of Earth and Planetary Sciences*, 43(1), 167-205.
 3720 <https://doi.org/10.1146/annurev-earth-050212-124117>

3721 Hallberg, J. A., & Glikson, A. Y. (1981). Archaean granite–greenstone terranes of western
 3722 Australia. In D. R. Hunter (Ed.), *Precambrian of The Southern Hemisphere* (Vol. 2,
 3723 pp. 33-103). Amsterdam: Elsevier.

3724 Halpin, J. A., & Reid, A. J. (2016). Earliest Paleoproterozoic high-grade metamorphism and
 3725 orogenesis in the Gawler Craton, South Australia: The southern cousin in the Rae
 3726 family? *Precambrian Research*, 276, 123-144.
 3727 <https://doi.org/10.1016/j.precamres.2016.02.001>

3728 Hamilton, W. B. (1998). Archean magmatism and deformation were not products of plate
 3729 tectonics. *Precambrian Research*, 91(1), 143-179.
 3730 [https://doi.org/10.1016/S0301-9268\(98\)00042-4](https://doi.org/10.1016/S0301-9268(98)00042-4)

3731 Hamilton, W. B. (2007). Earth's first two billion years—The era of internally mobile crust.
 3732 *Geological Society of America Memoir* 200, 233-296.
 3733 [https://doi.org/10.1130/2007.1200\(13\)](https://doi.org/10.1130/2007.1200(13))

3734 Hamilton, W. B. (2011). Plate tectonics began in Neoproterozoic time, and plumes from
 3735 deep mantle have never operated. *Lithos*, 123(1), 1-20.
 3736 <https://doi.org/10.1016/j.lithos.2010.12.007>

3737 Hamilton, W. B. (2019). Toward a myth-free geodynamic history of Earth and its neighbors.
 3738 *Earth-Science Reviews*, 198, 102905.
 3739 <https://doi.org/10.1016/j.earscirev.2019.102905>

3740 Hand, M., & Sandiford, M. (1999). Intraplate deformation in central Australia, the link
 3741 between subsidence and fault reactivation. *Tectonophysics*, 305(1), 121-140.
 3742 [https://doi.org/10.1016/S0040-1951\(99\)00009-8](https://doi.org/10.1016/S0040-1951(99)00009-8)

3743 Handy, M. R., M. Schmid, S., Bousquet, R., Kissling, E., & Bernoulli, D. (2010).

3744 Reconciling plate-tectonic reconstructions of Alpine Tethys with the
 3745 geological–geophysical record of spreading and subduction in the Alps.
 3746 *Earth-Science Reviews*, 102(3), 121-158.
 3747 <https://doi.org/10.1016/j.earscirev.2010.06.002>
 3748 Hanmer, S., Parrish, R., Williams, M., & Kopf, C. (1994). Striding-Athabasca mylonite zone:
 3749 Complex Archean deep-crustal deformation in the East Athabasca mylonite triangle,
 3750 northern Saskatchewan. *Canadian Journal of Earth Sciences*, 31(8), 1287-1300.
 3751 <https://doi.org/10.1139/e94-111>
 3752 Harley, S. L. (1988). Proterozoic granulites from the Rauer Group, East Antarctica. I.
 3753 Decompressional pressure-temperature paths deduced from mafic and felsic
 3754 gneisses. *Journal of Petrology*, 29(5), 1059-1095.
 3755 <https://doi.org/10.1093/petrology/29.5.1059>
 3756 Harley, S. L. (1989). The origins of granulites: a metamorphic perspective. *Geological*
 3757 *Magazine*, 126(3), 215-247. <https://doi.org/10.1017/S0016756800022330>
 3758 Harrington, H. J., & Korsch, R. J. (1985). Tectonic model for the Devonian to middle
 3759 Permian of the New England Orogen. *Australian Journal of Earth Sciences*, 32(2),
 3760 163-179. <https://doi.org/10.1080/08120098508729322>
 3761 Harrison, T. M. (2009). The Hadean crust: Evidence from >4 Ga zircons. *Annual Review of*
 3762 *Earth and Planetary Sciences*, 37(1), 479-505.
 3763 <https://doi.org/10.1146/annurev.earth.031208.100151>
 3764 Hart, S. R., Hauri, E. H., Oschmann, L. A., & Whitehead, J. A. (1992). Mantle plumes and
 3765 entrainment: Isotopic evidence. *Science*, 256(5056), 517-520.
 3766 <https://doi.org/10.1126/science.256.5056.517>
 3767 Hartlaub, R. P., Chacko, T., Heaman, L. M., Creaser, R. A., Ashton, K. E., & Simonetti, A.
 3768 (2005). Ancient (Meso- to Paleoproterozoic) crust in the Rae Province, Canada:
 3769 Evidence from Sm–Nd and U–Pb constraints. *Precambrian Research*, 141(3),
 3770 137-153. <https://doi.org/10.1016/j.precamres.2005.09.001>
 3771 Hastie, A. R., Fitton, J. G., Bromiley, G. D., Butler, I. B., & Odling, N. W. A. (2016). The
 3772 origin of Earth's first continents and the onset of plate tectonics. *Geology*, 44(10),
 3773 855-858. <https://doi.org/10.1130/g38226.1>
 3774 Hastie, A. R., Kerr, A. C., McDonald, I., Mitchell, S. F., Pearce, J. A., Millar, I. L., et al.
 3775 (2010). Geochronology, geochemistry and petrogenesis of rhyodacite lavas in
 3776 eastern Jamaica: A new adakite subgroup analogous to early Archaean continental

3777 crust? *Chemical Geology*, 276(3), 344-359.
 3778 <https://doi.org/10.1016/j.chemgeo.2010.07.002>

3779 Hatcher, R. D. (2010). The Appalachian orogen: A brief summary. In R. P. Tollo, M. J.
 3780 Bartholomew, J. P. Hibbard & P. M. Karabinos (Eds.), *From Rodinia to Pangea:*
 3781 *The Lithotectonic Record of the Appalachian Region* (Vol. 206, pp. 1-19):
 3782 Geological Society of America.

3783 Hatzfeld, D., & Molnar, P. (2010). Comparisons of the kinematics and deep structures of the
 3784 Zagros and Himalaya and of the Iranian and Tibetan Plateaus and geodynamic
 3785 implications. *Reviews of Geophysics*, 48. <https://doi.org/10.1029/2009RG000304>

3786 Hawkesworth, C., Cawood, P. A., & Dhuime, B. (2020). The evolution of the continental
 3787 crust and the onset of plate tectonics. *Frontiers in earth science*, 8, 326.
 3788 <https://doi.org/10.3389/feart.2020.00326>

3789 Hawkesworth, C. J., Cawood, P. A., & Dhuime, B. (2016). Tectonics and crustal evolution.
 3790 *GSA Today*, 26(9), 4-11. <https://doi.org/10.1130/GSATG272A.1>

3791 Hawkesworth, C. J., Dhuime, B., Pietranik, A. B., Cawood, P. A., Kemp, A. I. S., & Storey,
 3792 C. D. (2010). The generation and evolution of the continental crust. *Journal of the*
 3793 *Geological Society*, 167(2), 229-248. <https://doi.org/10.1144/0016-76492009-072>

3794 Helmstaedt, H. (2009). Crust–mantle coupling revisited: The Archean Slave craton, NWT,
 3795 Canada. *Lithos*, 112, 1055-1068. <https://doi.org/10.1016/j.lithos.2009.04.046>

3796 Heron, P. J., Pysklywec, R. N., & Stephenson, R. (2016). Lasting mantle scars lead to
 3797 perennial plate tectonics. *Nature Communications*, 7(1), 11834.
 3798 <https://doi.org/10.1038/ncomms11834>

3799 Herzberg, C. (2004). Geodynamic information in peridotite petrology. *Journal of Petrology*,
 3800 45(12), 2507-2530. <https://doi.org/10.1093/petrology/egh039>

3801 Herzberg, C., Condie, K., & Korenaga, J. (2010). Thermal history of the Earth and its
 3802 petrological expression. *Earth and Planetary Science Letters*, 292(1), 79-88.
 3803 <https://doi.org/10.1016/j.epsl.2010.01.022>

3804 Hetényi, G., Cattin, R., Brunet, F., Bollinger, L., Vergne, J., Nábělek, J. L., et al. (2007).
 3805 Density distribution of the India plate beneath the Tibetan plateau: Geophysical and
 3806 petrological constraints on the kinetics of lower-crustal eclogitization. *Earth and*
 3807 *Planetary Science Letters*, 264(1), 226-244.
 3808 <https://doi.org/10.1016/j.epsl.2007.09.036>

3809 Hibbard, J. (2000). Docking Carolina: Mid-Paleozoic accretion in the southern

3810 Appalachians. *Geology*, 28(2), 127-130.
 3811 [https://doi.org/10.1130/0091-7613\(2000\)28<127:dcma>2.0.co;2](https://doi.org/10.1130/0091-7613(2000)28<127:dcma>2.0.co;2)
 3812 Hieronymus, C. F., Shomali, Z. H., & Pedersen, L. B. (2007). A dynamical model for
 3813 generating sharp seismic velocity contrasts underneath continents: Application to
 3814 the Sorgenfrei–Tornquist Zone. *Earth and Planetary Science Letters*, 262(1), 77-91.
 3815 <https://doi.org/10.1016/j.epsl.2007.07.043>
 3816 Hill, R. I. (1993). Mantle plumes and continental tectonics. *Lithos*, 30(3), 193-206.
 3817 [https://doi.org/10.1016/0024-4937\(93\)90035-B](https://doi.org/10.1016/0024-4937(93)90035-B)
 3818 Hill, R. I., Campbell, I. H., Davies, G. F., & Griffiths, R. W. (1992). Mantle Plumes and
 3819 Continental Tectonics. *Science*, 256(5054), 186-193.
 3820 <https://doi.org/10.1126/science.256.5054.186>
 3821 Hirschmann, M. M. (2006). Water, melting, and the deep earth H₂O cycle. *Annual Review of*
 3822 *Earth and Planetary Sciences*, 34(1), 629-653.
 3823 <https://doi.org/10.1146/annurev.earth.34.031405.125211>
 3824 Hirth, G., & Kohlstedt, D. L. (1996). Water in the oceanic upper mantle: implications for
 3825 rheology, melt extraction and the evolution of the lithosphere. *Earth and Planetary*
 3826 *Science Letters*, 144(1), 93-108. [https://doi.org/10.1016/0012-821X\(96\)00154-9](https://doi.org/10.1016/0012-821X(96)00154-9)
 3827 Hoffman, P. F. (1988). United plates of America, the birth of a craton: Early Proterozoic
 3828 assembly and growth of Laurentia. *Annual Review of Earth and Planetary Sciences*,
 3829 16(1), 543-603. <https://doi.org/10.1146/annurev.earth.16.050188.002551>
 3830 Holdsworth, R. E., Handa, M., Miller, J. A., & Buick, I. S. (2001). Continental reactivation
 3831 and reworking: an introduction. *Geological Society, London, Special Publications*,
 3832 184(1), 1-12. <https://doi.org/10.1144/gsl.sp.2001.184.01.01>
 3833 Holm, D. K., Van Schmus, W. R., MacNeill, L. C., Boerboom, T. J., Schweitzer, D., &
 3834 Schneider, D. (2005). U-Pb zircon geochronology of Paleoproterozoic plutons from
 3835 the northern midcontinent, USA: Evidence for subduction flip and continued
 3836 convergence after geon 18 Penokean orogenesis. *GSA Bulletin*, 117(3-4), 259-275.
 3837 <https://doi.org/10.1130/b25395.1>
 3838 Hopper, E., & Fischer, K. M. (2018). The changing face of the lithosphere-asthenosphere
 3839 boundary: Imaging continental scale patterns in upper mantle structure across the
 3840 contiguous U.S. With Sp converted waves. *Geochemistry, Geophysics, Geosystems*,
 3841 19(8), 2593-2614. <https://doi.org/10.1029/2018GC007476>
 3842 Horton, F., Hacker, B., Kylander-Clark, A., Holder, R., & Jöns, N. (2016). Focused

3843 radiogenic heating of middle crust caused ultrahigh temperatures in southern
 3844 Madagascar. *Tectonics*, 35(2), 293-314. <https://doi.org/10.1002/2015TC004040>
 3845 Houseman, G., & Molnar, P. (2001). Mechanisms of lithospheric rejuvenation associated
 3846 with continental orogeny. *Geological Society, London, Special Publications*, 184(1),
 3847 13-38. <https://doi.org/10.1144/gsl.sp.2001.184.01.02>
 3848 Howarth, G. H., Barry, P. H., Pernet-Fisher, J. F., Baziotis, I. P., Pokhilenko, N. P.,
 3849 Pokhilenko, L. N., et al. (2014). Superplume metasomatism: Evidence from
 3850 Siberian mantle xenoliths. *Lithos*, 184-187, 209-224.
 3851 <https://doi.org/10.1016/j.lithos.2013.09.006>
 3852 Hu, J., Liu, L., Faccenda, M., Zhou, Q., Fischer, K. M., Marshak, S., et al. (2018).
 3853 Modification of the Western Gondwana craton by plume–lithosphere interaction.
 3854 *Nature Geoscience*, 11(3), 203-210. <https://doi.org/10.1038/s41561-018-0064-1>
 3855 Huang, H.-H., Lin, F.-C., Schmandt, B., Farrell, J., Smith, R. B., & Tsai, V. C. (2015). The
 3856 Yellowstone magmatic system from the mantle plume to the upper crust. *Science*,
 3857 348(6236), 773-776. <https://doi.org/10.1126/science.aaa5648>
 3858 Humlera, E., Langmuirb, C., & Dauxc, V. (1999). Depth versus age: new perspectives from
 3859 the chemical compositions of ancient crust. *Earth and Planetary Science Letters*,
 3860 173(1), 7-23. [https://doi.org/10.1016/S0012-821X\(99\)00218-6](https://doi.org/10.1016/S0012-821X(99)00218-6)
 3861 Hynes, A., & Rivers, T. (2010). Protracted continental collision — evidence from the
 3862 Grenville Orogen. *Canadian Journal of Earth Sciences*, 47(5), 591-620.
 3863 <https://doi.org/10.1139/e10-003>
 3864 Inbal, A., Ampuero, J. P., & Clayton, R. W. (2016). Localized seismic deformation in the
 3865 upper mantle revealed by dense seismic arrays. *Science*, 354(6308), 88-92.
 3866 <https://doi.org/10.1126/science.aaf1370>
 3867 Jackson, S. L., & Fyon, J. A. (1991). The western Abitibi subprovince in Ontario. In P. C.
 3868 Thurston (Ed.), *Geology of Ontario, Ontario Geological Survey Special Paper 4*
 3869 (Vol. 4, pp. 405-482).
 3870 Jacobs, J., Pisarevsky, S., Thomas, R. J., & Becker, T. (2008). The Kalahari craton during
 3871 the assembly and dispersal of Rodinia. *Precambrian Research*, 160(1), 142-158.
 3872 <https://doi.org/10.1016/j.precamres.2007.04.022>
 3873 Jahn, B. M., Glikson, A. Y., Peucat, J. J., & Hickman, A. H. (1981). REE geochemistry and
 3874 isotopic data of Archean silicic volcanics and granitoids from the Pilbara Block,
 3875 Western Australia: implications for the early crustal evolution. *Geochimica et*

3876 *Cosmochimica Acta*, 45(9), 1633-1652.
3877 [https://doi.org/10.1016/S0016-7037\(81\)80002-6](https://doi.org/10.1016/S0016-7037(81)80002-6)
3878 Jahn, B. M., Wu, F., & Chen, B. (2000). Granitoids of the Central Asian Orogenic Belt and
3879 continental growth in the Phanerozoic. *Earth and Environmental Science*
3880 *Transactions of the Royal Society of Edinburgh*, 91(1-2), 181-193.
3881 <https://doi.org/10.1017/S0263593300007367>
3882 James, D. E., Fouch, M. J., VanDecar, J. C., van der Lee, S., & Group, K. S. (2001).
3883 Tectospheric structure beneath southern Africa. *Geophysical Research Letters*,
3884 28(13), 2485-2488. <https://doi.org/10.1029/2000GL012578>
3885 Jaupart, C., & Mareschal, J. C. (2015). Heat flow and thermal structure of the lithosphere. In
3886 G. Schubert (Ed.), *Treatise on Geophysics (Second Edition)* (pp. 217-253). Oxford:
3887 Elsevier.
3888 Jayananda, M., Moyen, J. F., Martin, H., Peucat, J. J., Auvray, B., & Mahabaleswar, B.
3889 (2000). Late Archaean (2550–2520 Ma) juvenile magmatism in the Eastern
3890 Dharwar craton, southern India: constraints from geochronology, Nd–Sr isotopes
3891 and whole rock geochemistry. *Precambrian Research*, 99(3), 225-254.
3892 [https://doi.org/10.1016/S0301-9268\(99\)00063-7](https://doi.org/10.1016/S0301-9268(99)00063-7)
3893 Jean, M. M., Taylor, L. A., Howarth, G. H., Peslier, A. H., Fedele, L., Bodnar, R. J., et al.
3894 (2016). Olivine inclusions in Siberian diamonds and mantle xenoliths: Contrasting
3895 water and trace-element contents. *Lithos*, 265, 31-41.
3896 <https://doi.org/10.1016/j.lithos.2016.07.023>
3897 Jiao, S., Fitzsimons, I. C. W., Zi, J.-W., Evans, N. J., McDonald, B. J., & Guo, J. (2020).
3898 Texturally controlled U–Th–Pb monazite geochronology reveals Paleoproterozoic
3899 UHT metamorphic evolution in the Khondalite belt, North China Craton. *Journal of*
3900 *Petrology*, 61(1). <https://doi.org/10.1093/petrology/egaa023>
3901 Johnson, T. E., Brown, M., Gardiner, N. J., Kirkland, C. L., & Smithies, R. H. (2017).
3902 Earth's first stable continents did not form by subduction. *Nature*, 543(7644),
3903 239-242. <https://doi.org/10.1038/nature21383>
3904 Johnston, S. T. (2001). The Great Alaskan Terrane Wreck: reconciliation of paleomagnetic
3905 and geological data in the northern Cordillera. *Earth and Planetary Science Letters*,
3906 193(3), 259-272. [https://doi.org/10.1016/S0012-821X\(01\)00516-7](https://doi.org/10.1016/S0012-821X(01)00516-7)
3907 Johnston, S. T. (2008). The Cordilleran ribbon continent of North America. *Annual Review*
3908 *of Earth and Planetary Sciences*, 36(1), 495-530.

3909 <https://doi.org/10.1146/annurev.earth.36.031207.124331>

3910 Jolivet, L., Faccenna, C., Becker, T., Tesauro, M., Sternai, P., & Bouilhol, P. (2018). Mantle
 3911 flow and deforming continents: From India-Asia convergence to Pacific subduction.
 3912 *Tectonics*, 37(9), 2887-2914. <https://doi.org/10.1029/2018TC005036>

3913 Jolivet, L., Faccenna, C., Goff , B., Burov, E., & Agard, P. (2003). Subduction tectonics and
 3914 exhumation of high-pressure metamorphic rocks in the Mediterranean orogens.
 3915 *American Journal of Science*, 303(5), 353-409.
 3916 <https://doi.org/10.2475/ajs.303.5.353>

3917 Jordan, T. E., Isacks, B. L., Allmendinger, R. W., Brewer, J. A., Ramos, V. A., & Ando, C. J.
 3918 (1983). Andean tectonics related to geometry of subducted Nazca plate. *GSA*
 3919 *Bulletin*, 94(3), 341-361.
 3920 [https://doi.org/10.1130/0016-7606\(1983\)94<341:atrtgo>2.0.co;2](https://doi.org/10.1130/0016-7606(1983)94<341:atrtgo>2.0.co;2)

3921 Jordan, T. H. (1978). Composition and development of the continental tectosphere. *Nature*,
 3922 274(5671), 544-548. <https://doi.org/10.1038/274544a0>

3923 Jordan, T. H. (1988). Structure and formation of the continental tectosphere. *Journal of*
 3924 *Petrology*, Special Volume(1), 11-37.
 3925 https://doi.org/10.1093/petrology/Special_Volume.1.11

3926 Kaczmarek, M.-A., & Tommasi, A. (2011). Anatomy of an extensional shear zone in the
 3927 mantle, Lanzo massif, Italy. *Geochemistry, Geophysics, Geosystems*, 12(8).
 3928 <https://doi.org/10.1029/2011GC003627>

3929 Kamber, B. S., Biino, G. G., Wijbrans, J. R., Davies, G. R., & Villa, I. M. (1996). Archaean
 3930 granulites of the Limpopo belt, Zimbabwe: One slow exhumation or two rapid
 3931 events? *Tectonics*, 15(6), 1414-1430. <https://doi.org/10.1029/96TC00850>

3932 Karabinos, P., Samson, S. D., Hepburn, J. C., & Stoll, H. M. (1998). Taconian orogeny in
 3933 the New England Appalachians: Collision between Laurentia and the Shelburne
 3934 Falls arc. *Geology*, 26(3), 215-218.
 3935 [https://doi.org/10.1130/0091-7613\(1998\)026<0215:toitne>2.3.co;2](https://doi.org/10.1130/0091-7613(1998)026<0215:toitne>2.3.co;2)

3936 Karato, S.-i. (2010). Rheology of the deep upper mantle and its implications for the
 3937 preservation of the continental roots: A review. *Tectonophysics*, 481(1), 82-98.
 3938 <https://doi.org/10.1016/j.tecto.2009.04.011>

3939 Karato, S.-i., Jung, H., Katayama, I., & Skemer, P. (2008). Geodynamic significance of
 3940 seismic anisotropy of the upper mantle: New insights from laboratory studies.
 3941 *Annual Review of Earth and Planetary Sciences*, 36(1), 59-95.

- 3942 <https://doi.org/10.1146/annurev.earth.36.031207.124120>
- 3943 Karato, S.-i., Olugboji, T., & Park, J. (2015). Mechanisms and geologic significance of the
 3944 mid-lithosphere discontinuity in the continents. *Nature Geoscience*, 8(7), 509-514.
 3945 <https://doi.org/10.1038/ngeo2462>
- 3946 Karlstrom, K. E., & Bowring, S. A. (1988). Early Proterozoic assembly of
 3947 tectonostratigraphic terranes in Southwestern North America. *The Journal of*
 3948 *Geology*, 96(5), 561-576. <https://doi.org/10.1086/629252>
- 3949 Kawakatsu, H., Kumar, P., Takei, Y., Shinohara, M., Kanazawa, T., Araki, E., et al. (2009).
 3950 Seismic evidence for sharp lithosphere-asthenosphere boundaries of oceanic plates.
 3951 *Science*, 324(5926), 499-502. <https://doi.org/10.1126/science.1169499>
- 3952 Keller, G. R., & Stephenson, R. A. (2007). The southern Oklahoma and Dniepr-Donets
 3953 aulacogens: A comparative analysis. In R. D. Hatcher, Jr., M. P. Carlson, J. H.
 3954 McBride & J. R. M. Catalán (Eds.), *4-D Framework of Continental Crust* (Vol. 200,
 3955 pp. 127-143): Geological Society of America Memoirs.
- 3956 Kelsey, D. E. (2008). On ultrahigh-temperature crustal metamorphism. *Gondwana Research*,
 3957 13(1), 1-29. <https://doi.org/10.1016/j.gr.2007.06.001>
- 3958 Kennett, B. L. N., & Sippl, C. (2018). Lithospheric discontinuities in Central Australia.
 3959 *Tectonophysics*, 744, 10-22. <https://doi.org/10.1016/j.tecto.2018.06.008>
- 3960 Kent, R. W., Hardarson, B. S., Saunders, A. D., & Storey, M. (1996). Plateaux ancient and
 3961 modern: Geochemical and sedimentological perspectives on Archaean oceanic
 3962 magmatism. *Lithos*, 37(2), 129-142. [https://doi.org/10.1016/0024-4937\(95\)00033-X](https://doi.org/10.1016/0024-4937(95)00033-X)
- 3963 Keranen, K., & Klemperer, S. L. (2008). Discontinuous and diachronous evolution of the
 3964 Main Ethiopian Rift: Implications for development of continental rifts. *Earth and*
 3965 *Planetary Science Letters*, 265(1), 96-111.
 3966 <https://doi.org/10.1016/j.epsl.2007.09.038>
- 3967 Kerr, A. C. (2015). Oceanic Plateaus. In J. Harff, M. Meschede, S. Petersen & J. Thiede
 3968 (Eds.), *Encyclopedia of Marine Geosciences* (pp. 1-15). Dordrecht: Springer
 3969 Netherlands.
- 3970 Kerrich, R., & Polat, A. (2006). Archean greenstone-tonalite duality: Thermochemical
 3971 mantle convection models or plate tectonics in the early Earth global dynamics?
 3972 *Tectonophysics*, 415(1), 141-165. <https://doi.org/10.1016/j.tecto.2005.12.004>
- 3973 Klemperer, S. L. (2006). Crustal flow in Tibet: geophysical evidence for the physical state
 3974 of Tibetan lithosphere, and inferred patterns of active flow. *Geological Society*,

- 3975 *London, Special Publications, 268(1), 39-70.*
 3976 <https://doi.org/10.1144/gsl.sp.2006.268.01.03>
- 3977 Knapmeyer-Endrun, B., Krüger, F., & Geissler, W. H. (2017). Upper mantle structure across
 3978 the Trans-European Suture Zone imaged by S-receiver functions. *Earth and*
 3979 *Planetary Science Letters, 458*, 429-441. <https://doi.org/10.1016/j.epsl.2016.11.011>
- 3980 Kopf, C. F. (2002). Archean and Early Proterozoic events along the snowbird tectonic zone
 3981 in Northern Saskatchewan, Canada. *Gondwana Research, 5(1)*, 79-83.
 3982 [https://doi.org/10.1016/S1342-937X\(05\)70891-1](https://doi.org/10.1016/S1342-937X(05)70891-1)
- 3983 Korenaga, J. (2013). Initiation and evolution of plate tectonics on earth: Theories and
 3984 observations. *Annual Review of Earth and Planetary Sciences, 41(1)*, 117-151.
 3985 <https://doi.org/10.1146/annurev-earth-050212-124208>
- 3986 Korenaga, J. (2018). Estimating the formation age distribution of continental crust by
 3987 unmixing zircon ages. *Earth and Planetary Science Letters, 482*, 388-395.
 3988 <https://doi.org/10.1016/j.epsl.2017.11.039>
- 3989 Kramers, J. D., Kreissig, K., & Jones, M. Q. W. (2001). Crustal heat production and style of
 3990 metamorphism: a comparison between two Archean high grade provinces in the
 3991 Limpopo Belt, southern Africa. *Precambrian Research, 112(1)*, 149-163.
 3992 [https://doi.org/10.1016/S0301-9268\(01\)00173-5](https://doi.org/10.1016/S0301-9268(01)00173-5)
- 3993 Kronenke, L. W. (1974). Origin of continents through development and coalescence of
 3994 oceanic flood basalt plateau. *Eos, Transactions of the American Geophysical Union,*
 3995 *55*, 443-443.
- 3996 Kumar, P., Yuan, X., Kumar, M. R., Kind, R., Li, X., & Chadha, R. K. (2007). The rapid
 3997 drift of the Indian tectonic plate. *Nature, 449(7164)*, 894-897.
 3998 <https://doi.org/10.1038/nature06214>
- 3999 Kusky, T. M. (1989). Accretion of the Archean Slave province. *Geology, 17(1)*, 63-67.
 4000 [https://doi.org/10.1130/0091-7613\(1989\)017<0063:aotasp>2.3.co;2](https://doi.org/10.1130/0091-7613(1989)017<0063:aotasp>2.3.co;2)
- 4001 Kusky, T. M. (2011). Geophysical and geological tests of tectonic models of the North
 4002 China Craton. *Gondwana Research, 20(1)*, 26-35.
 4003 <https://doi.org/10.1016/j.gr.2011.01.004>
- 4004 Kusky, T. M., & Li, J. (2003). Paleoproterozoic tectonic evolution of the North China
 4005 Craton. *Journal of Asian Earth Sciences, 22(4)*, 383-397.
 4006 [https://doi.org/10.1016/S1367-9120\(03\)00071-3](https://doi.org/10.1016/S1367-9120(03)00071-3)
- 4007 Kusky, T. M., Li, X., Wang, Z., Fu, J., Ze, L., & Zhu, P. (2013). Are Wilson cycles preserved

4008 in Archean cratons? A comparison of the North China and Slave cratons. *Canadian*
4009 *Journal of Earth Sciences*, 51(3), 297-311. <https://doi.org/10.1139/cjes-2013-0163>

4010 Kusky, T. M., Polat, A., Windley, B. F., Burke, K. C., Dewey, J. F., Kidd, W. S. F., et al.
4011 (2016). Insights into the tectonic evolution of the North China Craton through
4012 comparative tectonic analysis: A record of outward growth of Precambrian
4013 continents. *Earth-Science Reviews*, 162, 387-432.
4014 <https://doi.org/10.1016/j.earscirev.2016.09.002>

4015 Langford, F. F., & Morin, J. A. (1976). The development of the Superior Province of
4016 northwestern Ontario by merging island arcs. *American Journal of Science*, 276(9),
4017 1023-1034. <https://doi.org/10.2475/ajs.276.9.1023>

4018 Larson, R. L. (1991). Geological consequences of superplumes. *Geology*, 19(10), 963-966.
4019 [https://doi.org/10.1130/0091-7613\(1991\)019<0963:gcoss>2.3.co;2](https://doi.org/10.1130/0091-7613(1991)019<0963:gcoss>2.3.co;2)

4020 Le Pourhiet, L., Gurnis, M., & Saleeby, J. (2006). Mantle instability beneath the Sierra
4021 Nevada Mountains in California and Death Valley extension. *Earth and Planetary*
4022 *Science Letters*, 251(1), 104-119. <https://doi.org/10.1016/j.epsl.2006.08.028>

4023 Leat, P. T., & Larter, R. D. (2003). Intra-oceanic subduction systems: introduction.
4024 *Geological Society of London, Special Publications*, 219, 1-17.
4025 <https://doi.org/10.1144/gsl.sp.2003.219.01.01>

4026 Lebedev, S., Meier, T., & van der Hilst, R. D. (2006). Asthenospheric flow and origin of
4027 volcanism in the Baikal Rift area. *Earth and Planetary Science Letters*, 249(3),
4028 415-424. <https://doi.org/10.1016/j.epsl.2006.07.007>

4029 Lee, C.-T. A., Luffi, P., & Chin, E. J. (2011). Building and destroying continental mantle.
4030 *Annual Review of Earth and Planetary Sciences*, 39(1), 59-90.
4031 <https://doi.org/10.1146/annurev-earth-040610-133505>

4032 Lee, C. T. A., Lenardic, A., Cooper, C. M., Niu, F. L., & Levander, A. (2005). The role of
4033 chemical boundary layers in regulating the thickness of continental and oceanic
4034 thermal boundary layers. *Earth and Planetary Science Letters*, 230(3-4), 379-395.
4035 <https://doi.org/10.1016/j.epsl.2004.11.019>

4036 Leech, M. L. (2001). Arrested orogenic development: eclogitization, delamination, and
4037 tectonic collapse. *Earth and Planetary Science Letters*, 185(1), 149-159.
4038 [https://doi.org/10.1016/S0012-821X\(00\)00374-5](https://doi.org/10.1016/S0012-821X(00)00374-5)

4039 Lehmann, B., Burgess, R., Frei, D., Belyatsky, B., Mainkar, D., Rao, N. V. C., et al. (2010).
4040 Diamondiferous kimberlites in central India synchronous with Deccan flood basalts.

4041 *Earth and Planetary Science Letters*, 290(1), 142-149.
 4042 <https://doi.org/10.1016/j.epsl.2009.12.014>

4043 Lenardic, A., & Moresi, L.-N. (1999). Some thoughts on the stability of cratonic lithosphere:
 4044 Effects of buoyancy and viscosity. *Journal of Geophysical Research: Solid Earth*,
 4045 104(B6), 12747-12758. <https://doi.org/10.1029/1999JB900035>

4046 Lenardic, A., Moresi, L.-N., & Mühlhaus, H. (2003). Longevity and stability of cratonic
 4047 lithosphere: Insights from numerical simulations of coupled mantle convection and
 4048 continental tectonics. *Journal of Geophysical Research: Solid Earth*, 108(B6).
 4049 <https://doi.org/10.1029/2002JB001859>

4050 Lewry, J. F., Hajnal, Z., Green, A., Lucas, S. B., White, D., Stauffer, M. R., et al. (1994).
 4051 Structure of a Paleoproterozoic continent-continent collision zone: a LITHOPROBE
 4052 seismic reflection profile across the Trans-Hudson Orogen, Canada. *Tectonophysics*,
 4053 232(1), 143-160. [https://doi.org/10.1016/0040-1951\(94\)90081-7](https://doi.org/10.1016/0040-1951(94)90081-7)

4054 Li, X., Huanglu, Y., Lifei, Z., Wei, C., & Thomas, B. (2017). 1.9 Ga eclogite from the
 4055 Archean-Paleoproterozoic Belomorian Province, Russia. *Science Bulletin*, 62,
 4056 239-241. <https://doi.org/10.1016/j.scib.2017.01.026>

4057 Li, Z.-X., & Zhong, S. (2009). Supercontinent–superplume coupling, true polar wander and
 4058 plume mobility: Plate dominance in whole-mantle tectonics. *Physics of the Earth*
 4059 *and Planetary Interiors*, 176(3), 143-156.
 4060 <https://doi.org/10.1016/j.pepi.2009.05.004>

4061 Li, Z. H., Xu, Z. Q., & Gerya, T. V. (2011). Flat versus steep subduction: Contrasting modes
 4062 for the formation and exhumation of high- to ultrahigh-pressure rocks in continental
 4063 collision zones. *Earth and Planetary Science Letters*, 301(1), 65-77.
 4064 <https://doi.org/10.1016/j.epsl.2010.10.014>

4065 Li, Z. X., Bogdanova, S. V., Collins, A. S., Davidson, A., De Waele, B., Ernst, R. E., et al.
 4066 (2008). Assembly, configuration, and break-up history of Rodinia: A synthesis.
 4067 *Precambrian Research*, 160(1), 179-210.
 4068 <https://doi.org/10.1016/j.precamres.2007.04.021>

4069 Li, Z. X., & Li, X.-H. (2007). Formation of the 1300-km-wide intracontinental orogen and
 4070 postorogenic magmatic province in Mesozoic South China: A flat-slab subduction
 4071 model. *Geology*, 35. <https://doi.org/10.1130/G23193A.1>

4072 Li, Z. X., Mitchell, R. N., Spencer, C. J., Ernst, R., Pisarevsky, S., Kirscher, U., et al. (2019).
 4073 Decoding Earth's rhythms: Modulation of supercontinent cycles by longer

4074 superocean episodes. *Precambrian Research*, 323, 1-5.
 4075 <https://doi.org/10.1016/j.precamres.2019.01.009>
 4076 Liao, J., & Gerya, T. (2014). Influence of lithospheric mantle stratification on craton
 4077 extension: Insight from two-dimensional thermo-mechanical modeling.
 4078 *Tectonophysics*, 631, 50-64. <https://doi.org/10.1016/j.tecto.2014.01.020>
 4079 Lin, A. B., Zheng, J. P., Xiong, Q., Aulbach, S., Lu, J. G., Pan, S. K., et al. (2019). A refined
 4080 model for lithosphere evolution beneath the decratonized northeastern North China
 4081 Craton. *Contributions to Mineralogy and Petrology*, 174(2).
 4082 <https://doi.org/10.1007/s00410-019-1551-0>
 4083 Lin, S. (2005). Synchronous vertical and horizontal tectonism in the Neoarchean: Kinematic
 4084 evidence from a synclinal keel in the northwestern Superior craton, Canada.
 4085 *Precambrian Research*, 139(3), 181-194.
 4086 <https://doi.org/10.1016/j.precamres.2005.07.001>
 4087 Lin, S., & Beakhouse, G. P. (2013). Synchronous vertical and horizontal tectonism at late
 4088 stages of Archean cratonization and genesis of Hemlo gold deposit, Superior craton,
 4089 Ontario, Canada. *Geology*, 41(3), 359-362. <https://doi.org/10.1130/g33887.1>
 4090 Lister, G. S., & Davis, G. A. (1989). The origin of metamorphic core complexes and
 4091 detachment faults formed during Tertiary continental extension in the northern
 4092 Colorado River region, U.S.A. *Journal of Structural Geology*, 11(1), 65-94.
 4093 [https://doi.org/10.1016/0191-8141\(89\)90036-9](https://doi.org/10.1016/0191-8141(89)90036-9)
 4094 Liu, D. Y., Nutman, A. P., Compston, W., Wu, J. S., & Shen, Q. H. (1992). Remnants of
 4095 ≥ 3800 Ma crust in the Chinese part of the Sino-Korean craton. *Geology*, 20(4),
 4096 339-342. [https://doi.org/10.1130/0091-7613\(1992\)020<0339:romcit>2.3.co;2](https://doi.org/10.1130/0091-7613(1992)020<0339:romcit>2.3.co;2)
 4097 Liu, J., Rudnick, R. L., Walker, R. J., Xu, W., Gao, S., & Wu, F. (2015). Big insights from
 4098 tiny peridotites: Evidence for persistence of Precambrian lithosphere beneath the
 4099 eastern North China Craton. *Tectonophysics*, 650, 104-112.
 4100 <http://dx.doi.org/10.1016/j.tecto.2014.05.009>
 4101 Liu, L. (2014). Rejuvenation of Appalachian topography caused by subsidence-induced
 4102 differential erosion. *Nature Geoscience*, 7(7), 518-523.
 4103 <https://doi.org/10.1038/ngeo2187>
 4104 Liu, L., Morgan, J. P., Xu, Y., & Menzies, M. (2018a). Craton destruction 1: Cratonic keel
 4105 delamination along a weak midlithospheric discontinuity layer. *Journal of*
 4106 *Geophysical Research: Solid Earth*, 123(11), 10,040-10,068.

- 4107 <https://doi.org/10.1029/2017JB015372>
- 4108 Liu, L., Morgan, J. P., Xu, Y., & Menzies, M. (2018b). Craton destruction 2: Evolution of
 4109 cratonic lithosphere after a rapid keel delamination event. *Journal of Geophysical*
 4110 *Research: Solid Earth*, 123(11), 10,069-010,090.
 4111 <https://doi.org/10.1029/2017JB015374>
- 4112 Liu, M. (2001). Cenozoic extension and magmatism in the North American Cordillera: the
 4113 role of gravitational collapse. *Tectonophysics*, 342(3), 407-433.
 4114 [https://doi.org/10.1016/S0040-1951\(01\)00173-1](https://doi.org/10.1016/S0040-1951(01)00173-1)
- 4115 Liu, Q. Y., van der Hilst, R. D., Li, Y., Yao, H. J., Chen, J. H., Guo, B., et al. (2014).
 4116 Eastward expansion of the Tibetan Plateau by crustal flow and strain partitioning
 4117 across faults. *Nature Geoscience*, 7(5), 361-365. <https://doi.org/10.1038/ngeo2130>
- 4118 Liu, S., Gurnis, M., Ma, P., & Zhang, B. (2017). Reconstruction of northeast Asian
 4119 deformation integrated with western Pacific plate subduction since 200Ma.
 4120 *Earth-Science Reviews*, 175, 114-142.
 4121 <https://doi.org/10.1016/j.earscirev.2017.10.012>
- 4122 Logatchev, N. A., & Florensov, N. A. (1978). The Baikal system of rift valleys.
 4123 *Tectonophysics*, 45(1), 1-13. [https://doi.org/10.1016/0040-1951\(78\)90218-4](https://doi.org/10.1016/0040-1951(78)90218-4)
- 4124 Long, L., Gao, J., Klemd, R., Beier, C., Qian, Q., Zhang, X., et al. (2011). Geochemical and
 4125 geochronological studies of granitoid rocks from the Western Tianshan Orogen:
 4126 Implications for continental growth in the southwestern Central Asian Orogenic
 4127 Belt. *Lithos*, 126(3), 321-340. <https://doi.org/10.1016/j.lithos.2011.07.015>
- 4128 Lu, S., Li, H., Zhang, C., & Niu, G. (2008). Geological and geochronological evidence for
 4129 the Precambrian evolution of the Tarim Craton and surrounding continental
 4130 fragments. *Precambrian Research*, 160(1), 94-107.
 4131 <https://doi.org/10.1016/j.precamres.2007.04.025>
- 4132 Lucas, S. B., Green, A., Hajnal, Z., White, D., Lewry, J., Ashton, K., et al. (1993). Deep
 4133 seismic profile across a Proterozoic collision zone: surprises at depth. *Nature*,
 4134 363(6427), 339-342. <https://doi.org/10.1038/363339a0>
- 4135 Müller, R. D., Seton, M., Zahirovic, S., Williams, S. E., Matthews, K. J., Wright, N. M., et al.
 4136 (2016). Ocean Basin Evolution and Global-Scale Plate Reorganization Events Since
 4137 Pangea Breakup. *Annual Review of Earth and Planetary Sciences*, 44(1), 107-138.
 4138 <https://doi.org/10.1146/annurev-earth-060115-012211>
- 4139 Müller, R. D., Zahirovic, S., Williams, S. E., Cannon, J., Seton, M., Bower, D. J., et al.

4140 (2019). A global plate model including lithospheric deformation along major rifts
 4141 and orogens since the Triassic. *Tectonics*, 38(6), 1884-1907.
 4142 <https://doi.org/10.1029/2018TC005462>
 4143 Maas, A. T., & Henry, D. J. (2002). Heterogeneous growth and dissolution of sillimanite in
 4144 migmatites: evidence from cathodoluminescence imaging. *GSA Abstracts with*
 4145 *Program*(189), 17.
 4146 Macambira, M. J. B., Vasquez, M. L., Silva, D. C. C. d., Galarza, M. A., Barros, C. E. d. M.,
 4147 & Camelo, J. d. F. (2009). Crustal growth of the central-eastern Paleoproterozoic
 4148 domain, SW Amazonian craton: Juvenile accretion vs. reworking. *Journal of South*
 4149 *American Earth Sciences*, 27(4), 235-246.
 4150 <https://doi.org/10.1016/j.jsames.2009.02.001>
 4151 Machado, N., Clark, T., David, J., & Goulet, N. (1997). U–Pb ages for magmatism and
 4152 deformation in the New Quebec Orogen. *Canadian Journal of Earth Sciences*, 34(5),
 4153 716-723. <https://doi.org/10.1139/e17-058>
 4154 Mainprice, D., & Silver, P. G. (1993). Interpretation of SKS-waves using samples from the
 4155 subcontinental lithosphere. *Physics of the Earth and Planetary Interiors*, 78(3),
 4156 257-280. [https://doi.org/10.1016/0031-9201\(93\)90160-B](https://doi.org/10.1016/0031-9201(93)90160-B)
 4157 Martin, H. (1987). Petrogenesis of Archaean trondhjemites, tonalites, and granodiorites from
 4158 eastern Finland: Major and trace element geochemistry. *Journal of Petrology*, 28(5),
 4159 921-953. <https://doi.org/10.1093/petrology/28.5.921>
 4160 Martin, H. (1999). Adakitic magmas: modern analogues of Archaean granitoids. *Lithos*,
 4161 46(3), 411-429. [https://doi.org/10.1016/S0024-4937\(98\)00076-0](https://doi.org/10.1016/S0024-4937(98)00076-0)
 4162 Martin, H., Moyen, J.-F., Guitreau, M., Blichert-Toft, J., & Le Pennec, J.-L. (2014). Why
 4163 Archaean TTG cannot be generated by MORB melting in subduction zones. *Lithos*,
 4164 198-199, 1-13. <https://doi.org/10.1016/j.lithos.2014.02.017>
 4165 Martin, H., Moyen, J.-F., & Rapp, R. (2009). The sanukitoid series: magmatism at the
 4166 Archaean–Proterozoic transition. *Earth and Environmental Science Transactions of*
 4167 *the Royal Society of Edinburgh*, 100(1-2), 15-33.
 4168 <https://doi.org/10.1017/S1755691009016120>
 4169 Martin, H., & Moyen, J.-F. o. (2002). Secular changes in tonalite-trondhjemite-granodiorite
 4170 composition as markers of the progressive cooling of Earth. *Geology*, 30(4),
 4171 319-322. [https://doi.org/10.1130/0091-7613\(2002\)030<0319:scittg>2.0.co;2](https://doi.org/10.1130/0091-7613(2002)030<0319:scittg>2.0.co;2)
 4172 McKenzie, D. (1984). The generation and compaction of partially molten rock. *Journal of*

4173 *Petrology*, 25(3), 713-765. <https://doi.org/10.1093/petrology/25.3.713>

4174 McKenzie, D., & Bickle, M. J. (1988). The volume and composition of melt generated by
 4175 extension of the lithosphere. *Journal of Petrology*, 29(3), 625-679.
 4176 <https://doi.org/10.1093/petrology/29.3.625>

4177 McLennan, S. M., & Taylor, S. R. (1982). Geochemical constraints on the growth of the
 4178 continental crust. *The Journal of Geology*, 90(4), 347-361.
 4179 <https://doi.org/10.1086/628690>

4180 Meng, Q.-R., & Zhang, G.-W. (1999). Timing of collision of the North and South China
 4181 blocks: Controversy and reconciliation. *Geology*, 27(2), 123-126.
 4182 [https://doi.org/10.1130/0091-7613\(1999\)027<0123:tocotn>2.3.co;2](https://doi.org/10.1130/0091-7613(1999)027<0123:tocotn>2.3.co;2)

4183 Merle, O., & Michon, L. (2001). The formation of the West European Rift; a new model as
 4184 exemplified by the Massif Central area. *Bulletin de la Société Géologique de*
 4185 *France*, 172(2), 213-221. <https://doi.org/10.2113/172.2.213>

4186 Mjelde, R., Faleide, J. I., Breivik, A. J., & Raum, T. (2009). Lower crustal composition and
 4187 crustal lineaments on the Vøring Margin, NE Atlantic: A review. *Tectonophysics*,
 4188 472(1), 183-193. <https://doi.org/10.1016/j.tecto.2008.04.018>

4189 Molnar, P., England, P., & Martinod, J. (1993). Mantle dynamics, uplift of the Tibetan
 4190 Plateau, and the Indian Monsoon. *Reviews of Geophysics*, 31(4), 357-396.
 4191 <https://doi.org/10.1029/93RG02030>

4192 Molnar, P., & Tapponnier, P. (1975). Cenozoic tectonics of Asia: Effects of a continental
 4193 collision. *Science*, 189(4201), 419-426.
 4194 <https://doi.org/10.1126/science.189.4201.419>

4195 Monger, J. W. H. (1997). Plate tectonics and northern Cordilleran geology: An unfinished
 4196 revolution. *Geoscience Canada*, 24(4), 189-198.
 4197 <https://journals.lib.unb.ca/index.php/GC/article/view/3953>

4198 Morgan, W. J. (1971). Convection plumes in the lower mantle. *Nature*, 230(5288), 42-43.
 4199 <https://doi.org/10.1038/230042a0>

4200 Mouthereau, F., Lacombe, O., & Vergés, J. (2012). Building the Zagros collisional orogen:
 4201 Timing, strain distribution and the dynamics of Arabia/Eurasia plate convergence.
 4202 *Tectonophysics*, 532-535, 27-60. <https://doi.org/10.1016/j.tecto.2012.01.022>

4203 Moyen, J.-F. (2011). The composite Archaean grey gneisses: Petrological significance, and
 4204 evidence for a non-unique tectonic setting for Archaean crustal growth. *Lithos*,
 4205 123(1), 21-36. <https://doi.org/10.1016/j.lithos.2010.09.015>

- 4206 Moyen, J.-F., & Laurent, O. (2018). Archaean tectonic systems: A view from igneous rocks.
 4207 *Lithos*, 302-303, 99-125. <https://doi.org/10.1016/j.lithos.2017.11.038>
- 4208 Moyen, J.-F., & Martin, H. (2012). Forty years of TTG research. *Lithos*, 148, 312-336.
 4209 <https://doi.org/10.1016/j.lithos.2012.06.010>
- 4210 Mueller, P. A., & Wooden, J. L. (1988). Evidence for Archean subduction and crustal
 4211 recycling, Wyoming province. *Geology*, 16(10), 871-874.
 4212 [https://doi.org/10.1130/0091-7613\(1988\)016<0871:efasac>2.3.co;2](https://doi.org/10.1130/0091-7613(1988)016<0871:efasac>2.3.co;2)
- 4213 Murphy, J. B., & Keppie, J. D. (2005). The Acadian orogeny in the northern Appalachians.
 4214 *International Geology Review*, 47(7), 663-687.
 4215 <https://doi.org/10.2747/0020-6814.47.7.663>
- 4216 Murray, C. G., & Kirkegaard, A. G. (1978). The Thomson orogen of the Tasman orogenic
 4217 zone. *Tectonophysics*, 48(3), 299-325.
 4218 [https://doi.org/10.1016/0040-1951\(78\)90122-1](https://doi.org/10.1016/0040-1951(78)90122-1)
- 4219 Mvondo, H., Lentz, D., & Bardoux, M. (2017). Metamorphism in Neoarchean
 4220 granite-greenstone belts: Insights from the link between Elu and Hope Bay belts
 4221 (~2.7 Ga), northeastern Slave craton. *The Journal of Geology*, 125(2), 203-221.
 4222 <https://doi.org/10.1086/690214>
- 4223 Myers, J. S. (1993). Precambrian history of the west Australian craton and adjacent orogens.
 4224 *Annual Review of Earth and Planetary Sciences*, 21(1), 453-485.
 4225 <https://doi.org/10.1146/annurev.earth.21.050193.002321>
- 4226 Myers, J. S., Shaw, R. D., & Tyler, I. M. (1996). Tectonic evolution of Proterozoic Australia.
 4227 *Tectonics*, 15(6), 1431-1446. <https://doi.org/10.1029/96TC02356>
- 4228 Nair, R., & Chacko, T. (2008). Role of oceanic plateaus in the initiation of subduction and
 4229 origin of continental crust. *Geology*, 36(7), 583-586.
 4230 <https://doi.org/10.1130/g24773a.1>
- 4231 Nelson, K. D., Zhao, W., Brown, L. D., Kuo, J., Che, J., Liu, X., et al. (1996). Partially
 4232 molten middle crust beneath southern Tibet: Synthesis of project INDEPTH results.
 4233 *Science*, 274(5293), 1684-1688. <https://doi.org/10.1126/science.274.5293.1684>
- 4234 Nguuri, T. K., Gore, J., James, D. E., Webb, S. J., Wright, C., Zengeni, T. G., et al. (2001).
 4235 Crustal structure beneath southern Africa and its implications for the formation and
 4236 evolution of the Kaapvaal and Zimbabwe cratons. *Geophysical Research Letters*,
 4237 28(13), 2501-2504. <https://doi.org/10.1029/2000GL012587>
- 4238 Nijman, W., Kloppeburg, A., & de Vries, S. T. (2017). Archaean basin margin geology and

4239 crustal evolution: an East Pilbara traverse. *Journal of the Geological Society*, 174(6),
4240 1090-1112. <https://doi.org/10.1144/jgs2016-127>

4241 Nisbet, E. G., Cheadle, M. J., Arndt, N. T., & Bickle, M. J. (1993). Constraining the
4242 potential temperature of the Archaean mantle: A review of the evidence from
4243 komatiites. *Lithos*, 30(3), 291-307. [https://doi.org/10.1016/0024-4937\(93\)90042-B](https://doi.org/10.1016/0024-4937(93)90042-B)

4244 Novella, D., Bolfan-Casanova, N., Nestola, F., & Harris, J. W. (2015). H₂O in olivine and
4245 garnet inclusions still trapped in diamonds from the Siberian craton: Implications
4246 for the water content of cratonic lithosphere peridotites. *Lithos*, 230, 180-183.
4247 <https://doi.org/10.1016/j.lithos.2015.05.013>

4248 Nutman, A. P., Bennett, V. C., & Friend, C. R. L. (2015). The emergence of the Eoarchaean
4249 proto-arc: evolution of a c. 3700 Ma convergent plate boundary at Isua, southern
4250 West Greenland. *Geological Society of London, Special Publications*, 389, 113-133.
4251 <https://doi.org/10.1144/sp389.5>

4252 O'Neill, C. J., Lenardic, A., Griffin, W. L., & O'Reilly, S. Y. (2008). Dynamics of cratons in
4253 an evolving mantle. *Lithos*, 102(1), 12-24.
4254 <https://doi.org/10.1016/j.lithos.2007.04.006>

4255 O'Reilly, S. Y., Griffin, W. L., Poudjom, Y. H., & Morgan, P. (2001). Are lithospheres
4256 forever? Tracking changes in subcontinental lithospheric mantle through time. *GSA*
4257 *Today*, 11, 4-10.
4258 [http://dx.doi.org/10.1130/1052-5173\(2001\)011<0004:ALFTCI>2.0.CO;2](http://dx.doi.org/10.1130/1052-5173(2001)011<0004:ALFTCI>2.0.CO;2)

4259 O'Neil, J., & Carlson, R. W. (2017). Building Archean cratons from Hadean mafic crust.
4260 *Science*, 355(6330), 1199-1202. <https://doi.org/10.1126/science.aah3823>

4261 Ohuchi, T., Karato, S.-i., & Fujino, K. (2011). Strength of single-crystal orthopyroxene
4262 under lithospheric conditions. *Contributions to Mineralogy and Petrology*, 161(6),
4263 961-975. <https://doi.org/10.1007/s00410-010-0574-3>

4264 Olugboji, T. M., Park, J., Karato, S.-i., & Shinohara, M. (2016). Nature of the seismic
4265 lithosphere-asthenosphere boundary within normal oceanic mantle from
4266 high-resolution receiver functions. *Geochemistry, Geophysics, Geosystems*, 17(4),
4267 1265-1282. <https://doi.org/10.1002/2015GC006214>

4268 Ortiz, K., Nyblade, A., van der Meijde, M., Paulssen, H., Kwadiba, M., Ntibinyane, O., et al.
4269 (2019). Upper mantle P and S wave velocity structure of the Kalahari craton and
4270 surrounding Proterozoic terranes, southern Africa. *Geophysical Research Letters*,
4271 46(16), 9509-9518. <https://doi.org/10.1029/2019GL084053>

- 4272 Oyhantçabal, P., Siegesmund, S., & Wemmer, K. (2011). The Río de la Plata Craton: a
4273 review of units, boundaries, ages and isotopic signature. *International Journal of*
4274 *Earth Sciences*, 100(2), 201-220. <https://doi.org/10.1007/s00531-010-0580-8>
- 4275 Parmenter, A. C., Lin, S., & Timothy Corkery, M. (2006). Structural evolution of the Cross
4276 Lake greenstone belt in the northwestern Superior province, Manitoba: implications
4277 for relationship between vertical and horizontal tectonism. *Canadian Journal of*
4278 *Earth Sciences*, 43(7), 767-787. <https://doi.org/10.1139/e06-006>
- 4279 Pawlak, A., Eaton, D. W., Darbyshire, F., Lebedev, S., & Bastow, I. D. (2012). Crustal
4280 anisotropy beneath Hudson Bay from ambient noise tomography: Evidence for
4281 post-orogenic lower-crustal flow? *Journal of Geophysical Research: Solid Earth*,
4282 117(B8), doi:10.1029/2011JB009066. <https://doi.org/10.1029/2011JB009066>
- 4283 Pearson, D. G. (1999). The age of continental roots. *Lithos*, 48(1-4), 171-194.
4284 [https://doi.org/10.1016/S0024-4937\(99\)00026-2](https://doi.org/10.1016/S0024-4937(99)00026-2)
- 4285 Pearson, D. G., Snyder, G. A., Shirey, S. B., Taylor, L. A., Carlson, R. W., & Sobolev, N. V.
4286 (1995). Archaean Re-Os age for Siberian eclogites and constraints on Archaean
4287 tectonics. *Nature*, 374(6524), 711-713. <https://doi.org/10.1038/374711a0>
- 4288 Pepper, M., Gehrels, G., Pullen, A., Ibanez-Mejia, M., Ward, K. M., & Kapp, P. (2016).
4289 Magmatic history and crustal genesis of western South America: Constraints from
4290 U-Pb ages and Hf isotopes of detrital zircons in modern rivers. *Geosphere*, 12(5),
4291 1532-1555. <https://doi.org/10.1130/ges01315.1>
- 4292 Perchuk, A. L., Gerya, T. V., Zakharov, V. S., & Griffin, W. L. (2020). Building cratonic
4293 keels in Precambrian plate tectonics. *Nature*, 586(7829), 395-401.
4294 <https://doi.org/10.1038/s41586-020-2806-7>
- 4295 Percival, J. A. (1994). Archean high-grade metamorphism. *Developments in Precambrian*
4296 *Geology*, 11, 357-410. [https://doi.org/10.1016/S0166-2635\(08\)70227-5](https://doi.org/10.1016/S0166-2635(08)70227-5)
- 4297 Percival, J. A., Sanborn-Barrie, M., Skulski, T., Stott, G. M., Helmstaedt, H., & White, D. J.
4298 (2006). Tectonic evolution of the western Superior Province from NATMAP and
4299 Lithoprobe studies. *Canadian Journal of Earth Sciences*, 43(7), 1085-1117.
4300 <https://doi.org/10.1139/e06-062>
- 4301 Peron-Pinvidic, G., Manatschal, G., & Osmundsen, P. T. (2013). Structural comparison of
4302 archetypal Atlantic rifted margins: A review of observations and concepts. *Marine*
4303 *and Petroleum Geology*, 43, 21-47. <https://doi.org/10.1016/j.marpetgeo.2013.02.002>
- 4304 Peslier, A. H., Schönbächler, M., Busemann, H., & Karato, S.-I. (2017). Water in the earth's

4305 interior: Distribution and origin. *Space Science Reviews*, 212(1), 743-810.
 4306 <https://doi.org/10.1007/s11214-017-0387-z>
 4307 Peslier, A. H., Woodland, A. B., Bell, D. R., & Lazarov, M. (2010). Olivine water contents
 4308 in the continental lithosphere and the longevity of cratons. *Nature*, 467(7311), 78-81.
 4309 <https://doi.org/10.1038/nature09317>
 4310 Peters, B. J., & Day, J. M. D. (2017). A geochemical link between plume head and tail
 4311 volcanism. *Geochemical Perspectives Letters*, 5, 29-34.
 4312 <http://dx.doi.org/10.7185/geochemlet.1742>
 4313 Petitjean, S., Rabinowicz, M., Grégoire, M., & Chevrot, S. (2006). Differences between
 4314 Archean and Proterozoic lithospheres: Assessment of the possible major role of
 4315 thermal conductivity. *Geochemistry, Geophysics, Geosystems*, 7(3).
 4316 <https://doi.org/10.1029/2005GC001053>
 4317 Petrescu, L., Bastow, I. D., Darbyshire, F. A., Gilligan, A., Bodin, T., Menke, W., et al.
 4318 (2016). Three billion years of crustal evolution in eastern Canada: Constraints from
 4319 receiver functions. *Journal of Geophysical Research: Solid Earth*, 121(2), 788-811.
 4320 <https://doi.org/10.1002/2015JB012348>
 4321 Peucat, J. J., Mascarenhas, J. F., Barbosa, J. S. F., de Souza, S. L., Marinho, M. M., Fanning,
 4322 C. M., et al. (2002). 3.3Ga SHRIMP U–Pb zircon age of a felsic metavolcanic rock
 4323 from the Mundo Novo greenstone belt in the São Francisco craton, Bahia (NE
 4324 Brazil). *Journal of South American Earth Sciences*, 15(3), 363-373.
 4325 [https://doi.org/10.1016/S0895-9811\(02\)00044-5](https://doi.org/10.1016/S0895-9811(02)00044-5)
 4326 Polat, A., Frei, R., Longstaffe, F. J., & Woods, R. (2017). Petrogenetic and geodynamic
 4327 origin of the Neoarchean Doré Lake Complex, Abitibi subprovince, Superior
 4328 Province, Canada. *International Journal of Earth Sciences*, 107(3), 811-843.
 4329 <https://doi.org/10.1007/s00531-017-1498-1>
 4330 Pollack, H. N. (1986). Cratonization and thermal evolution of the mantle. *Earth and*
 4331 *Planetary Science Letters*, 80(1), 175-182.
 4332 [https://doi.org/10.1016/0012-821X\(86\)90031-2](https://doi.org/10.1016/0012-821X(86)90031-2)
 4333 Ponthus, L., de Saint Blanquat, M., Guillaume, D., Le Romancer, M., Pearson, N., O'Reilly,
 4334 S., et al. (2020). Plutonic processes in transitional oceanic plateau crust: Structure,
 4335 age and emplacement of the South Rallier du Baty laccolith, Kerguelen Islands.
 4336 *Terra Nova*, 32(6), 408-414. <https://doi.org/10.1111/ter.12471>
 4337 Poudjom Djomani, Y. H., O'Reilly, S. Y., Griffin, W. L., & Morgan, P. (2001). The density

4338 structure of subcontinental lithosphere through time. *Earth and Planetary Science*
 4339 *Letters*, 184(3), 605-621. [https://doi.org/10.1016/S0012-821X\(00\)00362-9](https://doi.org/10.1016/S0012-821X(00)00362-9)

4340 Priestley, K., McKenzie, D., & Ho, T. (2019). A lithosphere–asthenosphere boundary—a
 4341 global model derived from multimode surface-wave tomography and petrology. In
 4342 H. Yuan & B. Romanowicz (Eds.), *Lithospheric Discontinuities* (pp. 111-123): AGU
 4343 Geophysical Monograph 239.

4344 Prieto, G. A., Froment, B., Yu, C., Poli, P., & Abercrombie, R. (2017). Earthquake rupture
 4345 below the brittle-ductile transition in continental lithospheric mantle. *Science*
 4346 *Advances*, 3(3), e1602642. <https://doi.org/10.1126/sciadv.1602642>

4347 Puchtel, I. S., Hofmann, A. W., Mezger, K., Jochum, K. P., Shchipansky, A. A., & Samsonov,
 4348 A. V. (1998). Oceanic plateau model for continental crustal growth in the Archaean:
 4349 A case study from the Kostomuksha greenstone belt, NW Baltic Shield. *Earth and*
 4350 *Planetary Science Letters*, 155(1), 57-74.
 4351 [https://doi.org/10.1016/S0012-821X\(97\)00202-1](https://doi.org/10.1016/S0012-821X(97)00202-1)

4352 Pujol, M., Marty, B., Burgess, R., Turner, G., & Philippot, P. (2013). Argon isotopic
 4353 composition of Archaean atmosphere probes early Earth geodynamics. *Nature*,
 4354 498(7452), 87-90. <https://doi.org/10.1038/nature12152>

4355 Qian, Q., & Hermann, J. (2013). Partial melting of lower crust at 10–15 kbar: constraints on
 4356 adakite and TTG formation. *Contributions to Mineralogy and Petrology*, 165(6),
 4357 1195-1224. <https://doi.org/10.1007/s00410-013-0854-9>

4358 Rader, E., Emry, E., Schmerr, N., Frost, D., Cheng, C., Menard, J., et al. (2015).
 4359 Characterization and petrological constraints of the midlithospheric discontinuity.
 4360 *Geochemistry, Geophysics, Geosystems*, 16(10), 3484-3504.
 4361 <https://doi.org/10.1002/2015GC005943>

4362 Raimondo, T., Collins, A. S., Hand, M., Walker-Hallam, A., Smithies, R. H., Evins, P. M., et
 4363 al. (2010). The anatomy of a deep intracontinental orogen. *Tectonics*, 29(4).
 4364 <https://doi.org/10.1029/2009TC002504>

4365 Raith, M., Srikantappa, C., Ashamanjari, K., & Spiering, B. (1990). The granulite terrane of
 4366 the Nilgiri Hills (Southern India): Characterization of high-grade metamorphism. In
 4367 D. Vielzeuf & P. Viadal (Eds.), *Granulites And Crustal Evolution* (Vol. 311, pp.
 4368 339-365). Springer, Dordrecht.

4369 Raith, M. M., Srikantappa, C., Buhl, D., & Koehler, H. (1999). The Nilgiri enderbites, South
 4370 India: nature and age constraints on protolith formation, high-grade metamorphism

4371 and cooling history. *Precambrian Research*, 98(1), 129-150.
 4372 [https://doi.org/10.1016/S0301-9268\(99\)00045-5](https://doi.org/10.1016/S0301-9268(99)00045-5)

4373 Ramos, V. A. (1999). Plate tectonic setting of the Andean Cordillera. *Episodes*, 22(3),
 4374 183-190. <https://doi.org/10.18814/epiugs/1999/v22i3/005>

4375 Rawlings-Hinchey, A. M., Sylvester, P. J., Myers, J. S., Dunning, G. R., & Kosler, J. (2003).
 4376 Paleoproterozoic crustal genesis: calc-alkaline magmatism of the Torngat Orogen,
 4377 Voisey's Bay area, Labrador. *Precambrian Research*, 125(1), 55-85.
 4378 [https://doi.org/10.1016/S0301-9268\(03\)00077-9](https://doi.org/10.1016/S0301-9268(03)00077-9)

4379 Reichow, M. K., Pringle, M. S., Al'Mukhamedov, A. I., Allen, M. B., Andreichev, V. L.,
 4380 Buslov, M. M., et al. (2009). The timing and extent of the eruption of the Siberian
 4381 Traps large igneous province: Implications for the end-Permian environmental crisis.
 4382 *Earth and Planetary Science Letters*, 277(1), 9-20.
 4383 <https://doi.org/10.1016/j.epsl.2008.09.030>

4384 Reimink, J. R., Chacko, T., Stern, R. A., & Heaman, L. M. (2014). Earth's earliest evolved
 4385 crust generated in an Iceland-like setting. *Nature Geoscience*, 7(7), 529-533.
 4386 <https://doi.org/10.1038/ngeo2170>

4387 Reuber, I., Michard, A., Chalouan, A., Juteau, T., & Jermoumi, B. (1982). Structure and
 4388 emplacement of the Alpine-type peridotites from Beni Bousera, Rif, Morocco: A
 4389 polyphase tectonic interpretation. *Tectonophysics*, 82(3), 231-251.
 4390 [https://doi.org/10.1016/0040-1951\(82\)90047-6](https://doi.org/10.1016/0040-1951(82)90047-6)

4391 Rey, P. F., Coltice, N., & Flament, N. (2014). Spreading continents kick-started plate
 4392 tectonics. *Nature*, 513(7518), 405-408. <https://doi.org/10.1038/nature13728>

4393 Rey, P. F., & Houseman, G. (2006). Lithospheric scale gravitational flow: the impact of body
 4394 forces on orogenic processes from Archaean to Phanerozoic. *Geological Society,*
 4395 *London, Special Publications*, 253, 153-167.
 4396 <https://doi.org/10.1144/gsl.sp.2006.253.01.08>

4397 Rey, P. F., Philippot, P., & Thébaud, N. (2003). Contribution of mantle plumes, crustal
 4398 thickening and greenstone blanketing to the 2.75–2.65Ga global crisis. *Precambrian*
 4399 *Research*, 127(1), 43-60. [https://doi.org/10.1016/S0301-9268\(03\)00179-7](https://doi.org/10.1016/S0301-9268(03)00179-7)

4400 Richardson, S. H., Gurney, J. J., Erlank, A. J., & Harris, J. W. (1984). Origin of diamonds in
 4401 old enriched mantle. *Nature*, 310(5974), 198-202. <https://doi.org/10.1038/310198a0>

4402 Riggs, N. R., Oberling, Z. A., Howell, E. R., Parker, W. G., Barth, A. P., Cecil, M. R., et al.
 4403 (2016). Sources of volcanic detritus in the basal Chinle Formation, southwestern

4404 Laurentia, and implications for the Early Mesozoic magmatic arc. *Geosphere*, 12(2),
4405 439-463. <https://doi.org/10.1130/ges01238.1>

4406 Rivers, T., Mengel, F., Scott, D. J., Campbell, L. M., & Goulet, N. (1996). Torngat Orogen
4407 — a Palaeoproterozoic example of a narrow doubly vergent collisional orogen.
4408 *Geological Society, London, Special Publications*, 112(1), 117-136.
4409 <https://doi.org/10.1144/gsl.sp.1996.112.01.07>

4410 Roberts, N. M. W., Kranendonk, M. V., Parman, S., Shirey, S., & Clift, P. D. (2015).
4411 Continent formation through time. *Geological Society of London, Special*
4412 *Publication*, 389, 1-16. <https://doi.org/10.1144/sp389>

4413 Rollinson, H. (1989). Garnet--orthopyroxene thermobarometry of granulites from the north
4414 marginal zone of the Limpopo belt, Zimbabwe. *Geological Society, London, Special*
4415 *Publications*, 43, 331-335. <https://doi.org/10.1144/GSL.SP.1989.043.01.27>

4416 Rosen, O. M., Levskii, L. K., Zhuravlev, D. Z., Rotman, A. Y., Spetsius, Z. V., Makeev, A. F.,
4417 et al. (2006). Paleoproterozoic accretion in the Northeast Siberian craton: Isotopic
4418 dating of the Anabar collision system. *Stratigraphy and Geological Correlation*,
4419 14(6), 581-601. <https://doi.org/10.1134/S0869593806060013>

4420 Rosenbaum, G. (2018). The Tasmanides: Phanerozoic tectonic evolution of eastern Australia.
4421 *Annual Review of Earth and Planetary Sciences*, 46(1), 291-325.
4422 <https://doi.org/10.1146/annurev-earth-082517-010146>

4423 Rosenbaum, G., Li, P., & Rubatto, D. (2012). The contorted New England Orogen (eastern
4424 Australia): New evidence from U-Pb geochronology of early Permian granitoids.
4425 *Tectonics*, 31(1). <https://doi.org/10.1029/2011TC002960>

4426 Royden, L. H., Burchfiel, B. C., King, R. W., Wang, E., Chen, Z., Shen, F., et al. (1997).
4427 Surface deformation and lower crustal flow in eastern Tibet. *Science*, 276(5313),
4428 788-790. <https://doi.org/10.1126/science.276.5313.788>

4429 Rozel, A. B., Golabek, G. J., Jain, C., Tackley, P. J., & Gerya, T. (2017). Continental crust
4430 formation on early Earth controlled by intrusive magmatism. *Nature*, 545(7654),
4431 332-335. <https://doi.org/10.1038/nature22042>

4432 Rudnick, R. L. (1995). Making continental crust. *Nature*, 378(6557), 571-578.
4433 <https://doi.org/10.1038/378571a0>

4434 Rychert, C. A., Shearer, P. M., & Fischer, K. M. (2010). Scattered wave imaging of the
4435 lithosphere–asthenosphere boundary. *Lithos*, 120(1), 173-185.
4436 <https://doi.org/10.1016/j.lithos.2009.12.006>

4437 Ryerson, F. J., & Watson, E. B. (1987). Rutile saturation in magmas: implications for
4438 Ti-Nb-Ta depletion in island-arc basalts. *Earth and Planetary Science Letters*, 86(2),
4439 225-239. [https://doi.org/10.1016/0012-821X\(87\)90223-8](https://doi.org/10.1016/0012-821X(87)90223-8)

4440 Saha, S., Dasgupta, R., & Tsuno, K. (2018). High pressure phase relations of a depleted
4441 peridotite fluxed by CO₂-H₂O-bearing siliceous melts and the origin of
4442 mid-lithospheric discontinuity. *Geochemistry, Geophysics, Geosystems*, 19(3),
4443 595-620. <https://doi.org/10.1002/2017GC007233>

4444 Saleeby, J. B. (1983). Accretionary tectonics of the north American Cordillera. *Annual*
4445 *Review of Earth and Planetary Sciences*, 11(1), 45-73.
4446 <https://doi.org/10.1146/annurev.ea.11.050183.000401>

4447 Sandiford, M. (1985). The metamorphic evolution of granulites at Fyfe Hills; implications
4448 for Archaean crustal thickness in Enderby Land, Antarctica. *Journal of*
4449 *Metamorphic Geology*, 3, 155-178.
4450 <https://doi.org/10.1111/j.1525-1314.1985.tb00312.x>

4451 Sandiford, M., & Hand, M. (1998). Controls on the locus of intraplate deformation in
4452 central Australia. *Earth and Planetary Science Letters*, 162(1), 97-110.
4453 [https://doi.org/10.1016/S0012-821X\(98\)00159-9](https://doi.org/10.1016/S0012-821X(98)00159-9)

4454 Sandiford, M., & Powell, R. (1986). Deep crustal metamorphism during continental
4455 extension: modern and ancient examples. *Earth and Planetary Science Letters*,
4456 79(1), 151-158. [https://doi.org/10.1016/0012-821X\(86\)90048-8](https://doi.org/10.1016/0012-821X(86)90048-8)

4457 Sanislav, I. V., Blenkinsop, T. G., & Dirks, P. H. G. M. (2018). Archaean crustal growth
4458 through successive partial melting events in an oceanic plateau-like setting in the
4459 Tanzania Craton. *Terra Nova*, 30(3), 169-178. <https://doi.org/10.1111/ter.12323>

4460 Santos, J. O. S., Hartmann, L. A., Gaudette, H. E., Groves, D. I., McNaughton, N. J., &
4461 Fletcher, I. R. (2000). A new understanding of the provinces of the Amazon craton
4462 based on integration of field mapping and U-Pb and Sm-Nd geochronology.
4463 *Gondwana Research*, 3(4), 453-488.
4464 [https://doi.org/10.1016/S1342-937X\(05\)70755-3](https://doi.org/10.1016/S1342-937X(05)70755-3)

4465 Schaeffer, A. J., & Lebedev, S. (2014). Imaging the North American continent using
4466 waveform inversion of global and USArray data. *Earth and Planetary Science*
4467 *Letters*, 402, 26-41. <https://doi.org/10.1016/j.epsl.2014.05.014>

4468 Schellart, W. P. (2017). Andean mountain building and magmatic arc migration driven by
4469 subduction-induced whole mantle flow. *Nature Communications*, 8(1), 2010.

4470 <https://doi.org/10.1038/s41467-017-01847-z>

4471 Schmandt, B., & Lin, F.-C. (2014). P and S wave tomography of the mantle beneath the
 4472 United States. *Geophysical Research Letters*, 41(18), 6342-6349.
 4473 <https://doi.org/10.1002/2014GL061231>

4474 Scholl, D. W., & von Huene, R. (2009). Implications of estimated magmatic additions and
 4475 recycling losses at the subduction zones of accretionary (non-collisional) and
 4476 collisional (suturing) orogens. *Geological Society, London, Special Publications*,
 4477 318(1), 105-125. <https://doi.org/10.1144/sp318.4>

4478 Schulte-Pelkum, V., Monsalve, G., Sheehan, A. F., Shearer, P., Wu, F., & Rajaure, S. (2019).
 4479 Mantle earthquakes in the Himalayan collision zone. *Geology*, 47(9), 815-819.
 4480 <https://doi.org/10.1130/g46378.1>

4481 Schulz, K. J., & Cannon, W. F. (2007). The Penokean orogeny in the Lake Superior region.
 4482 *Precambrian Research*, 157(1), 4-25.
 4483 <https://doi.org/10.1016/j.precamres.2007.02.022>

4484 Scott, D. J. (1998). An overview of the UPb geochronology of the Paleoproterozoic Torngat
 4485 Orogen, Northeastern Canada. *Precambrian Research*, 91(1), 91-107.
 4486 [https://doi.org/10.1016/S0301-9268\(98\)00040-0](https://doi.org/10.1016/S0301-9268(98)00040-0)

4487 Scrimgeour, I. (2006). An overview of the North Australian craton. In P. Lyons & D. L.
 4488 Huston (Eds.), *Evolution and Metallogenesis of the North Australian Craton* (Vol.
 4489 16, pp. 1-2). Canberra: Geoscience Australia Record.

4490 Searle, M. P., Elliott, J. R., Phillips, R. J., & Chung, S.-L. (2011). Crustal–lithospheric
 4491 structure and continental extrusion of Tibet. *Journal of the Geological Society*,
 4492 168(3), 633-672. <https://doi.org/10.1144/0016-76492010-139>

4493 Selway, K., Ford, H., & Kelemen, P. (2015). The seismic mid-lithosphere discontinuity.
 4494 *Earth and Planetary Science Letters*, 414, 45-57.
 4495 <https://doi.org/10.1016/j.epsl.2014.12.029>

4496 Şengör, A. M. C. (1987). Tectonics of the Tethysides: Orogenic collage development in a
 4497 collisional setting. *Annual Review of Earth and Planetary Sciences*, 15(1), 213-244.
 4498 <https://doi.org/10.1146/annurev.earth.15.050187.001241>

4499 Şengör, A. M. C., & Natal'in, B. A. (1996). Turkic-type orogeny and its role in the making
 4500 of the continental crust. *Annual Review of Earth and Planetary Sciences*, 24(1),
 4501 263-337. <https://doi.org/10.1146/annurev.earth.24.1.263>

4502 Şengör, A. M. C., Natal'in, B. A., & Burtman, V. S. (1993). Evolution of the Altaid tectonic

4503 collage and Palaeozoic crustal growth in Eurasia. *Nature*, 364(6435), 299-307.
 4504 <https://doi.org/10.1038/364299a0>

4505 Şengör, A. M. C., Natal'in, B. A., Sunal, G., & van der Voo, R. (2018). The tectonics of the
 4506 Altaids: Crustal growth during the construction of the continental lithosphere of
 4507 Central Asia Between ~750 and ~130 Ma Ago. *Annual Review of Earth and*
 4508 *Planetary Sciences*, 46(1), 439-494.
 4509 <https://doi.org/10.1146/annurev-earth-060313-054826>

4510 Shomali, Z. H., Roberts, R. G., Pedersen, L. B., & TOR Working Group. (2006).
 4511 Lithospheric structure of the Tornquist Zone resolved by nonlinear P and S
 4512 teleseismic tomography along the TOR array. *Tectonophysics*, 416(1), 133-149.
 4513 <https://doi.org/10.1016/j.tecto.2005.11.019>

4514 Shu, Q., Brey, G. P., Pearson, D. G., Liu, J., Gibson, S. A., & Becker, H. (2019). The
 4515 evolution of the Kaapvaal craton: A multi-isotopic perspective from lithospheric
 4516 peridotites from Finsch diamond mine. *Precambrian Research*, 331.
 4517 <https://doi.org/10.1016/j.precamres.2019.105380>

4518 Simon, N. S. C., Carlson, R. W., Pearson, D. G., & Davies, G. R. (2007). The origin and
 4519 evolution of the Kaapvaal cratonic lithospheric mantle. *Journal of Petrology*, 48(3),
 4520 589-625. <https://doi.org/10.1093/petrology/egl074>

4521 Sims, P. K., & Petermar, Z. E. (1986). Early Proterozoic Central Plains orogen: A major
 4522 buried structure in the north-central United States. *Geology*, 14(6), 488-491.
 4523 [https://doi.org/10.1130/0091-7613\(1986\)14<488:epcpoa>2.0.co;2](https://doi.org/10.1130/0091-7613(1986)14<488:epcpoa>2.0.co;2)

4524 Sizova, E., Gerya, T., Brown, M., & Perchuk, L. L. (2010). Subduction styles in the
 4525 Precambrian: Insight from numerical experiments. *Lithos*, 116(3), 209-229.
 4526 <https://doi.org/10.1016/j.lithos.2009.05.028>

4527 Sleep, N. H. (2000). Evolution of the mode of convection within terrestrial planets. *Journal*
 4528 *of Geophysical Research: Planets*, 105(E7), 17563-17578.
 4529 <https://doi.org/10.1029/2000JE001240>

4530 Sleep, N. H., & Windley, B. F. (1982). Archean plate tectonics: Constraints and inferences.
 4531 *The Journal of Geology*, 90(4), 363-379. <https://doi.org/10.1086/628691>

4532 Smith, D., & Boyd, F. R. (1987). Compositional heterogeneities in a high-temperature
 4533 lherzolite nodule and implications for mantle processes. In P. H. Nixon (Ed.),
 4534 *Mantle Xenoliths* (pp. 551-562). New York: John Wiley.

4535 Smith, J. B., Barley, M. E., Groves, D. I., Krapez, B., McNaughton, N. J., Bickle, M. J., et al.

4536 (1998). The Sholl shear zone, west Pilbara: evidence for a domain boundary
 4537 structure from integrated tectonostratigraphic analyses, SHRIMP U-Pb dating and
 4538 isotopic and geochemical data of granitoids. *Precambrian Research*, 88(1), 143-171.
 4539 [https://doi.org/10.1016/S0301-9268\(97\)00067-3](https://doi.org/10.1016/S0301-9268(97)00067-3)
 4540 Smithies, R. H., Champion, D. C., & Van Kranendonk, M. J. (2009). Formation of
 4541 Paleoproterozoic continental crust through infracrustal melting of enriched basalt. *Earth*
 4542 *and Planetary Science Letters*, 281(3), 298-306.
 4543 <https://doi.org/10.1016/j.epsl.2009.03.003>
 4544 Smithies, R. H., Lu, Y., Johnson, T. E., Kirkland, C. L., Cassidy, K. F., Champion, D. C., et
 4545 al. (2019). No evidence for high-pressure melting of Earth's crust in the Archean.
 4546 *Nature Communications*, 10(1), 55-59. <https://doi.org/10.1038/s41467-019-13547-x>
 4547 Snyder, D. B., Humphreys, E., & Pearson, D. G. (2017). Construction and destruction of
 4548 some North American cratons. *Tectonophysics*, 694, 464-485.
 4549 <https://doi.org/10.1016/j.tecto.2016.11.032>
 4550 Sodoudi, F., Yuan, X., Kind, R., Lebedev, S., Adam, J. M.-C., Kästle, E., et al. (2013).
 4551 Seismic evidence for stratification in composition and anisotropic fabric within the
 4552 thick lithosphere of Kalahari Craton. *Geochemistry, Geophysics, Geosystems*,
 4553 14(12), 5393-5412. <https://doi.org/10.1002/2013GC004955>
 4554 Song, D., Xiao, W., Windley, B. F., Han, C., & Tian, Z. (2015). A Paleozoic Japan-type
 4555 subduction-accretion system in the Beishan orogenic collage, southern Central
 4556 Asian Orogenic Belt. *Lithos*, 224-225, 195-213.
 4557 <https://doi.org/10.1016/j.lithos.2015.03.005>
 4558 Spampinato, G. P. T., Betts, P. G., Ailleres, L., & Armit, R. J. (2015). Early tectonic
 4559 evolution of the Thomson orogen in Queensland inferred from constrained magnetic
 4560 and gravity data. *Tectonophysics*, 651-652, 99-120.
 4561 <https://doi.org/10.1016/j.tecto.2015.03.016>
 4562 Spencer, C. J., Cawood, P. A., Hawkesworth, C. J., Raub, T. D., Prave, A. R., & Roberts, N.
 4563 M. W. (2014). Proterozoic onset of crustal reworking and collisional tectonics:
 4564 Reappraisal of the zircon oxygen isotope record. *Geology*, 42(5), 451-454.
 4565 <https://doi.org/10.1130/g35363.1>
 4566 Spetsius, Z. V., Belousova, E. A., Griffin, W. L., O'Reilly, S. Y., & Pearson, N. J. (2002).
 4567 Archean sulfide inclusions in Paleozoic zircon megacrysts from the Mir kimberlite,
 4568 Yakutia: implications for the dating of diamonds. *Earth and Planetary Science*

4569 *Letters*, 199(1), 111-126. [https://doi.org/10.1016/S0012-821X\(02\)00539-3](https://doi.org/10.1016/S0012-821X(02)00539-3)

4570 Stein, C. A., Kley, J., Stein, S., Hindle, D., & Keller, G. R. (2015). North America's
4571 midcontinent rift: When rift met LIP. *Geosphere*, 11(5), 1607-1616.
4572 <https://doi.org/10.1130/ges01183.1>

4573 Stein, C. A., & Stein, S. (1992). A model for the global variation in oceanic depth and heat
4574 flow with lithospheric age. *Nature*, 359(6391), 123-129.
4575 <https://doi.org/10.1038/359123a0>

4576 Stein, M., & Hofmann, A. W. (1994). Mantle plumes and episodic crustal growth. *Nature*,
4577 372(6501), 63-68. <https://doi.org/10.1038/372063a0>

4578 Stern, C. R. (2011). Subduction erosion: Rates, mechanisms, and its role in arc magmatism
4579 and the evolution of the continental crust and mantle. *Gondwana Research*, 20(2),
4580 284-308. <https://doi.org/10.1016/j.gr.2011.03.006>

4581 Stern, R. J. (1994). Arc assembly and continental collision in the Neoproterozoic East
4582 African Orogen: Implications for the consolidation of Gondwanaland. *Annual*
4583 *Review of Earth and Planetary Sciences*, 22(1), 319-351.
4584 <https://doi.org/10.1146/annurev.ea.22.050194.001535>

4585 Stern, R. J. (2007). When and how did plate tectonics begin? Theoretical and empirical
4586 considerations. *Chinese Science Bulletin*, 52(5), 578-591.
4587 <https://doi.org/10.1007/s11434-007-0073-8>

4588 Stern, R. J. (2008). Modern-style plate tectonics began in Neoproterozoic time: An
4589 alternative interpretation of Earth's tectonic history. In K. C. Condie & V. Pease
4590 (Eds.), *When Did Plate Tectonics Begin on Planet Earth?* (Vol. 440, pp. 265-280):
4591 Geological Society of America Special Paper.

4592 Stern, R. J., & Scholl, D. W. (2010). Yin and yang of continental crust creation and
4593 destruction by plate tectonic processes. *International Geology Review*, 52(1), 1-31.
4594 <https://doi.org/10.1080/00206810903332322>

4595 Stewart, M., Holdsworth, R. E., & Strachan, R. A. (2000). Deformation processes and
4596 weakening mechanisms within the frictional-viscous transition zone of major
4597 crustal-scale faults: insights from the Great Glen Fault Zone, Scotland. *Journal of*
4598 *Structural Geology*, 22(5), 543-560.
4599 [https://doi.org/10.1016/S0191-8141\(99\)00164-9](https://doi.org/10.1016/S0191-8141(99)00164-9)

4600 Storey, B. C. (1995). The role of mantle plumes in continental breakup: case histories from
4601 Gondwanaland. *Nature*, 377(6547), 301-308. <https://doi.org/10.1038/377301a0>

- 4602 Stovba, S., Stephenson, R. A., & Kivshik, M. (1996). Structural features and evolution of
4603 the Dniepr-Donets Basin, Ukraine, from regional seismic reflection profiles.
4604 *Tectonophysics*, 268(1), 127-147. [https://doi.org/10.1016/S0040-1951\(96\)00222-3](https://doi.org/10.1016/S0040-1951(96)00222-3)
- 4605 Sutra, E., & Manatschal, G. (2012). How does the continental crust thin in a hyperextended
4606 rifted margin? Insights from the Iberia margin. *Geology*, 40(2), 139-142.
4607 <https://doi.org/10.1130/g32786.1>
- 4608 Tang, M., Chen, K., & Rudnick, R. L. (2016). Archean upper crust transition from mafic to
4609 felsic marks the onset of plate tectonics. *Science*, 351(6271), 372-375.
4610 <https://doi.org/10.1126/science.aad5513>
- 4611 Tang, Y. J., Zhang, H. F., Santosh, M., & Ying, J. F. (2013). Differential destruction of the
4612 North China Craton: A tectonic perspective. *Journal of Asian Earth Sciences*, 78,
4613 71-82. <http://dx.doi.org/10.1016/j.jseaes.2012.11.047>
- 4614 Tang, Y. J., Zhang, H. F., Ying, J. F., & Su, B. X. (2013). Widespread refertilization of
4615 cratonic and circum-cratonic lithospheric mantle. *Earth-Science Reviews*, 118,
4616 45-68. <https://doi.org/10.1016/j.earscirev.2013.01.004>
- 4617 Tang, Y. J., Zhang, H. F., Ying, J. F., Su, B. X., Chu, Z. Y., Xiao, Y., et al. (2013). Highly
4618 heterogeneous lithospheric mantle beneath the Central Zone of the North China
4619 Craton evolved from Archean mantle through diverse melt refertilization.
4620 *Gondwana Research*, 23(1), 130-140. <https://doi.org/10.1016/j.gr.2012.01.006>
- 4621 Tao, K., Grand, S. P., & Niu, F. (2018). Seismic structure of the upper mantle beneath
4622 eastern Asia from full waveform seismic tomography. *Geochemistry, Geophysics,*
4623 *Geosystems*, 19(8), 2732-2763. <https://doi.org/10.1029/2018GC007460>
- 4624 Tapponnier, P., & Molnar, P. (1977). Active faulting and tectonics in China. *Journal of*
4625 *Geophysical Research*, 82(20), 2905-2930.
4626 <https://doi.org/10.1029/JB082i020p02905>
- 4627 Tapponnier, P., & Molnar, P. (1979). Active faulting and cenozoic tectonics of the Tien Shan,
4628 Mongolia, and Baykal Regions. *Journal of Geophysical Research: Solid Earth*,
4629 84(B7), 3425-3459. <https://doi.org/10.1029/JB084iB07p03425>
- 4630 Tassara, S., González-Jiménez, J. M., Reich, M., Schilling, M. E., Morata, D., Begg, G., et al.
4631 (2017). Plume-subduction interaction forms large auriferous provinces. *Nature*
4632 *Communications*, 8(1), 843. . <https://doi.org/10.1038/s41467-017-00821-z>
- 4633 Taylor, J., Stevens, G., Armstrong, R., & Kisters, A. F. M. (2010). Granulite facies anatexis
4634 in the Ancient Gneiss Complex, Swaziland, at 2.73Ga: Mid-crustal metamorphic

4635 evidence for mantle heating of the Kaapvaal craton during Ventersdorp magmatism.
 4636 *Precambrian Research*, 177(1), 88-102.
 4637 <https://doi.org/10.1016/j.precamres.2009.11.005>
 4638 Taylor, L. A., Logvinova, A. M., Howarth, G. H., Liu, Y., Peslier, A. H., Rossman, G. R., et
 4639 al. (2016). Low water contents in diamond mineral inclusions: Proto-genetic origin
 4640 in a dry cratonic lithosphere. *Earth and Planetary Science Letters*, 433, 125-132.
 4641 <https://doi.org/10.1016/j.epsl.2015.10.042>
 4642 Taylor, R. J. M., Johnson, T. E., Clark, C., & Harrison, R. J. (2020). Persistence of
 4643 melt-bearing Archean lower crust for >200 m.y.—An example from the Lewisian
 4644 Complex, northwest Scotland. *Geology*, 48(3), 221-225.
 4645 <https://doi.org/10.1130/g46834.1>
 4646 Taylor, S. R. (1989). Growth of planetary crusts. *Tectonophysics*, 161(3), 147-156.
 4647 [https://doi.org/10.1016/0040-1951\(89\)90151-0](https://doi.org/10.1016/0040-1951(89)90151-0)
 4648 Taylor, S. R., & McLennan, S. (2008). *Planetary crusts: Their composition, origin and*
 4649 *evolution*. Cambridge: Cambridge University Press.
 4650 Taylor, S. R., & McLennan, S. M. (1981). The rare earth element evidence in Precambrian
 4651 sedimentary rocks: Implications for crustal evolution. In A. Kröner (Ed.),
 4652 *Developments in Precambrian Geology* (Vol. 4, pp. 527-548). Amsterdam: Elsevier.
 4653 Teng, J., Zhang, Z., Zhang, X., Wang, C., Gao, R., Yang, B., et al. (2013). Investigation of
 4654 the Moho discontinuity beneath the Chinese mainland using deep seismic sounding
 4655 profiles. *Tectonophysics*, 609, 202-216. <https://doi.org/10.1016/j.tecto.2012.11.024>
 4656 Thiéblemont, D., Delor, C., Cocherie, A., Lafon, J. M., Goujou, J. C., Baldé, A., et al. (2001).
 4657 A 3.5 Ga granite–gneiss basement in Guinea: further evidence for early archean
 4658 accretion within the West African Craton. *Precambrian Research*, 108(3), 179-194.
 4659 [https://doi.org/10.1016/S0301-9268\(00\)00160-1](https://doi.org/10.1016/S0301-9268(00)00160-1)
 4660 Thomas, W. A. (2006). Tectonic inheritance at a continental margin. *Gsa Today*, 16(2), 4-11.
 4661 [https://doi.org/10.1130/1052-5173\(2006\)016\[4:TIAACM\]2.0.CO;2](https://doi.org/10.1130/1052-5173(2006)016[4:TIAACM]2.0.CO;2)
 4662 Thybo, H. (2006). The heterogeneous upper mantle low velocity zone. *Tectonophysics*,
 4663 416(1), 53-79. <https://doi.org/10.1016/j.tecto.2005.11.021>
 4664 Thybo, H., & Artemieva, I. M. (2013). Moho and magmatic underplating in continental
 4665 lithosphere. *Tectonophysics*, 609, 605-619.
 4666 <https://doi.org/10.1016/j.tecto.2013.05.032>
 4667 Thybo, H., & Nielsen, C. A. (2012). Seismic velocity structure of crustal intrusions in the

- 4668 Danish Basin. *Tectonophysics*, 572-573, 64-75.
 4669 <https://doi.org/10.1016/j.tecto.2011.11.019>
- 4670 Tollo, R. P., Corriveau, L., McLelland, J., & Bartholomew, M. J. (2004). Proterozoic
 4671 tectonic evolution of the Grenville orogen in North America: An introduction. In R.
 4672 P. Tollo, J. McLelland, L. Corriveau & M. J. Bartholomew (Eds.), *Proterozoic*
 4673 *Tectonic Evolution of the Grenville Orogen in North America* (Vol. 197, pp. 1-18):
 4674 Geological Society of America.
- 4675 Tomlinson, K. Y., & Condie, K. C. (2001). Archean mantle plumes: Evidence from
 4676 greenstone belt geochemistry. In R. E. Ernst & K. L. Buchan (Eds.), *Mantle plumes:*
 4677 *their identification through time* (Vol. 352, pp. 341-357). Boulder, Colorado:
 4678 Geological Society of America.
- 4679 Tommasi, A., Gibert, B., Seipold, U., & Mainprice, D. (2001). Anisotropy of thermal
 4680 diffusivity in the upper mantle. *Nature*, 411(6839), 783-786.
 4681 <https://doi.org/10.1038/35081046>
- 4682 Tsunogae, T., Miyano, T., & Ridley, J. (1992). Metamorphic P-T profiles from the
 4683 Zimbabwe craton to the Limpopo belt, Zimbabwe. *Precambrian Research*, 55(1),
 4684 259-277. [https://doi.org/10.1016/0301-9268\(92\)90027-L](https://doi.org/10.1016/0301-9268(92)90027-L)
- 4685 Tsunogae, T., Osanai, Y., Toyoshima, T., Owada, M., Hokada, T., & Crowe, W. A. (1999).
 4686 Metamorphic reactions and preliminary P-T estimates of ultrahigh-temperature
 4687 mafic granulite from Tonagh Island in the Napier Complex, East Antarctica. *Polar*
 4688 *Geosci.*, 12, 71-86. <http://doi.org/10.15094/00003043>
- 4689 Turner, S., Haines, P., Foster, D., Powell, R., Sandiford, M., & Offler, R. (2009). Did the
 4690 delamerian orogeny start in the Neoproterozoic? *The Journal of Geology*, 117(5),
 4691 575-583. <https://doi.org/10.1086/600866>
- 4692 Turner, S., Rushmer, T., Reagan, M., & Moyen, J.-F. (2014). Heading down early on? Start
 4693 of subduction on Earth. *Geology*, 42(2), 139-142. <https://doi.org/10.1130/g34886.1>
- 4694 Valli, F., Guillot, S., & Hattori, K. H. (2004). Source and tectono-metamorphic evolution of
 4695 mafic and pelitic metasedimentary rocks from the central Quetico metasedimentary
 4696 belt, Archean Superior Province of Canada. *Precambrian Research*, 132(1),
 4697 155-177. <https://doi.org/10.1016/j.precamres.2004.03.002>
- 4698 Van Hinsbergen, D. J. J., Buiter, S. J. H., Torsvik, T. H., Gaina, C., & Webb, S. J. (2011).
 4699 The formation and evolution of Africa from the Archaean to Present: introduction.
 4700 *Geological Society, London, Special Publications*, 357, 1-8.

4701 <https://doi.org/10.1144/sp357.1>

4702 Van Kranendonk, M. J. (2010). Two types of Archean continental crust: Plume and plate
 4703 tectonics on early Earth. *American Journal of Science*, 310(10), 1187-1209.
 4704 <https://doi.org/10.2475/10.2010.01>

4705 Van Kranendonk, M. J. (2011). Cool greenstone drips and the role of partial convective
 4706 overturn in Barberton greenstone belt evolution. *Journal of African Earth Sciences*,
 4707 60(5), 346-352. <https://doi.org/10.1016/j.jafrearsci.2011.03.012>

4708 Van Kranendonk, M. J., Collins, W. J., Hickman, A., & Pawley, M. J. (2004). Critical tests
 4709 of vertical vs. horizontal tectonic models for the Archaean East Pilbara
 4710 Granite–Greenstone Terrane, Pilbara Craton, Western Australia. *Precambrian
 4711 Research*, 131(3), 173-211. <https://doi.org/10.1016/j.precamres.2003.12.015>

4712 Van Kranendonk, M. J., Kröner, A., Hoffmann, J. E., Nagel, T., & Anhaeusser, C. R. (2014).
 4713 Just another drip: Re-analysis of a proposed Mesoarchean suture from the Barberton
 4714 Mountain Land, South Africa. *Precambrian Research*, 254, 19-35.
 4715 <https://doi.org/10.1016/j.precamres.2014.07.022>

4716 Van Kranendonk, M. J., Smithies, R. H., Hickman, A. H., & Champion, D. C. (2007a).
 4717 Paleoproterozoic Development of a Continental Nucleus: the East Pilbara Terrane of the
 4718 Pilbara Craton, Western Australia. In M. J. van Kranendonk, R. H. Smithies & V. C.
 4719 Bennett (Eds.), *Developments in Precambrian Geology* (Vol. 15, pp. 307-337).
 4720 Amsterdam: Elsevier.

4721 Van Kranendonk, M. J., Smithies, R. H., Hickman, A. H., & Champion, D. C. (2007b).
 4722 Review: secular tectonic evolution of Archean continental crust: interplay between
 4723 horizontal and vertical processes in the formation of the Pilbara Craton, Australia.
 4724 *Terra Nova*, 19(1), 1-38. <https://doi.org/10.1111/j.1365-3121.2006.00723.x>

4725 Vauchez, A., Barruol, G., & Tommasi, A. (1997). Why do continents break-up parallel to
 4726 ancient orogenic belts? *Terra Nova*, 9(2), 62-66.
 4727 <https://doi.org/10.1111/j.1365-3121.1997.tb00003.x>

4728 Vauchez, A., Tommasi, A., & Barruol, G. (1998). Rheological heterogeneity, mechanical
 4729 anisotropy and deformation of the continental lithosphere. *Tectonophysics*, 296(1),
 4730 61-86. [https://doi.org/10.1016/S0040-1951\(98\)00137-1](https://doi.org/10.1016/S0040-1951(98)00137-1)

4731 Voice, P. J., Kowalewski, M., & Eriksson, K. A. (2011). Quantifying the timing and rate of
 4732 crustal evolution: Global compilation of radiometrically dated detrital zircon grains.
 4733 *The Journal of Geology*, 119(2), 109-126. <https://doi.org/10.1086/658295>

- 4734 Walker, R. J., Carlson, R. W., Shirey, S. B., & Boyd, F. R. (1989). Os, Sr, Nd, and Pb isotope
4735 systematics of southern African peridotite xenoliths: Implications for the chemical
4736 evolution of subcontinental mantle. *Geochimica et Cosmochimica Acta*, 53,
4737 1583-1595. [https://doi.org/10.1016/0016-7037\(89\)90240-8](https://doi.org/10.1016/0016-7037(89)90240-8)
- 4738 Walsh, A. K., Kelsey, D. E., Kirkland, C. L., Hand, M., Smithies, R. H., Clark, C., et al.
4739 (2015). P–T–t evolution of a large, long-lived, ultrahigh-temperature Grenvillian
4740 belt in central Australia. *Gondwana Research*, 28(2), 531-564.
4741 <https://doi.org/10.1016/j.gr.2014.05.012>
- 4742 Wan, B., Wu, F., Chen, L., Zhao, L., Liang, X., Xiao, W., et al. (2019). Cyclical one-way
4743 continental rupture-drift in the Tethyan evolution: Subduction-driven plate tectonics.
4744 *Science China Earth Sciences*, 62(12), 2005-2016.
4745 <https://doi.org/10.1007/s11430-019-9393-4>
- 4746 Wang, H., van Hunen, J., & Pearson, D. G. (2015). The thinning of subcontinental
4747 lithosphere: The roles of plume impact and metasomatic weakening. *Geochemistry,*
4748 *Geophysics, Geosystems*, 16(4), 1156-1171. <https://doi.org/10.1002/2015GC005784>
- 4749 Wang, H., van Hunen, J., Pearson, D. G., & Allen, M. B. (2014). Craton stability and
4750 longevity: The roles of composition-dependent rheology and buoyancy. *Earth and*
4751 *Planetary Science Letters*, 391(0), 224-233.
4752 <http://dx.doi.org/10.1016/j.epsl.2014.01.038>
- 4753 Wang, X., Liou, J. G., & Mao, H. K. (1989). Coesite-bearing eclogite from the Dabie
4754 Mountains in central China. *Geology*, 17(12), 1085-1088.
4755 [https://doi.org/10.1130/0091-7613\(1989\)017<1085:cbeftd>2.3.co;2](https://doi.org/10.1130/0091-7613(1989)017<1085:cbeftd>2.3.co;2)
- 4756 Wang, Z., Kusky, T. M., & Capitanio, F. A. (2018). On the role of lower crust and
4757 midlithosphere discontinuity for cratonic lithosphere delamination and recycling.
4758 *Geophysical Research Letters*, 45(15), 7425-7433.
4759 <https://doi.org/10.1029/2017GL076948>
- 4760 Warren, J. M. (2016). Global variations in abyssal peridotite compositions. *Lithos*, 248-251,
4761 193-219. <https://doi.org/10.1016/j.lithos.2015.12.023>
- 4762 Wei, Z., Chen, L., Li, Z., Ling, Y., & Li, J. (2016). Regional variation in Moho depth and
4763 Poisson's ratio beneath eastern China and its tectonic implications. *Journal of Asian*
4764 *Earth Sciences*, 115, 308-320. <https://doi.org/10.1016/j.jseaes.2015.10.010>
- 4765 Wei, Z., Chu, R., & Chen, L. (2015). Regional differences in crustal structure of the North
4766 China Craton from receiver functions. *Science China Earth Sciences*, 58(12),

4767 2200-2210. <https://doi.org/10.1007/s11430-015-5162-y>

4768 Weller, O. M., & St-Onge, M. R. (2017). Record of modern-style plate tectonics in the
 4769 Palaeoproterozoic Trans-Hudson orogen. *Nature Geoscience*, 10(4), 305-311.
 4770 <https://doi.org/10.1038/ngeo2904>

4771 Whalen, J. B., Percival, J. A., McNicoll, V. J., & Longstaffe, F. J. (2002). A mainly crustal
 4772 origin for tonalitic gneissoid rocks, Superior province, Canada: implications for Late
 4773 Archean tectonomagmatic processes. *Journal of Petrology*, 43(8), 1551-1570.
 4774 <https://doi.org/10.1093/petrology/43.8.1551>

4775 White, R. V., Tarney, J., Kerr, A. C., Saunders, A. D., Kempton, P. D., Pringle, M. S., et al.
 4776 (1999). Modification of an oceanic plateau, Aruba, Dutch Caribbean: Implications
 4777 for the generation of continental crust. *Lithos*, 46(1), 43-68.
 4778 [https://doi.org/10.1016/S0024-4937\(98\)00061-9](https://doi.org/10.1016/S0024-4937(98)00061-9)

4779 Whitmeyer, S. J., & Karlstrom, K. E. (2007). Tectonic model for the Proterozoic growth of
 4780 North America. *Geosphere*, 3(4), 220-259. <https://doi.org/10.1130/ges00055.1>

4781 Wicander, R., & Monroe, J. S. (2016). *Historical geology : Evolution of earth and life*
 4782 *through time* (8th ed.). Boston: Cengage Learning.

4783 Wilde-Piórko, M., Świeczak, M., Grad, M., & Majdański, M. (2010). Integrated seismic
 4784 model of the crust and upper mantle of the Trans-European Suture zone between the
 4785 Precambrian craton and Phanerozoic terranes in Central Europe. *Tectonophysics*,
 4786 481(1), 108-115. <https://doi.org/10.1016/j.tecto.2009.05.002>

4787 Wilde, S. A., Valley, J. W., Peck, W. H., & Graham, C. M. (2001). Evidence from detrital
 4788 zircons for the existence of continental crust and oceans on the earth 4.4 Gyr ago.
 4789 *Nature*, 409, 175-178. <https://doi.org/10.1038/35051550>

4790 Willbold, M., Hegner, E., Stracke, A., & Rocholl, A. (2009). Continental geochemical
 4791 signatures in dacites from Iceland and implications for models of early Archaean
 4792 crust formation. *Earth and Planetary Science Letters*, 279(1), 44-52.
 4793 <https://doi.org/10.1016/j.epsl.2008.12.029>

4794 Wilson, J. T. (1963). Hypothesis of Earth's Behaviour. *Nature*, 198, 925-929.
 4795 <https://doi.org/10.1038/198925a0>

4796 Windley, B. F., Alexeiev, D., Xiao, W., Kröner, A., & Badarch, G. (2007). Tectonic models
 4797 for accretion of the Central Asian Orogenic Belt. *Journal of the Geological Society*,
 4798 164(1), 31-47. <https://doi.org/10.1144/0016-76492006-022>

4799 Windley, B. F., & Xiao, W. (2018). Ridge subduction and slab windows in the Central Asian

4800 Orogenic Belt: Tectonic implications for the evolution of an accretionary orogen.
4801 *Gondwana Research*, 61, 73-87. <https://doi.org/10.1016/j.gr.2018.05.003>

4802 Wirth, E. A., & Long, M. D. (2014). A contrast in anisotropy across mid-lithospheric
4803 discontinuities beneath the central United States—A relic of craton formation.
4804 *Geology*, 42(10), 851-854. <https://doi.org/10.1130/g35804.1>

4805 Withnall, I., Hutton, L., Armit, R., Betts, P., Blewett, R., & Champion, D. J., P A. (2013).
4806 North Australian Craton. In P. A. Jell (Ed.), *Geology of Queensland* (pp. 23-112).
4807 Brisbane Qld Australia: Geological Survey of Queensland.

4808 Wu, C., Tian, X., Xu, T., Liang, X., Chen, Y., Taylor, M., et al. (2019). Deformation of crust
4809 and upper mantle in central Tibet caused by the northward subduction and slab
4810 tearing of the Indian lithosphere: New evidence based on shear wave splitting
4811 measurements. *Earth and Planetary Science Letters*, 514, 75-83.
4812 <https://doi.org/10.1016/j.epsl.2019.02.037>

4813 Wu, F., Xu, Y., Zhu, R., & Zhang, G. (2014). Thinning and destruction of the cratonic
4814 lithosphere: A global perspective. *Science China Earth sciences*, 57(12), 2878-2890.
4815 <https://doi.org/10.1007/s11430-014-4995-0>

4816 Wu, F. Y., Arzamastsev, A. A., Mitchell, R. H., Li, Q. L., Sun, J., Yang, Y. H., et al. (2013).
4817 Emplacement age and Sr–Nd isotopic compositions of the Afrikanda alkaline
4818 ultramafic complex, Kola Peninsula, Russia. *Chemical Geology*, 353, 210-229.
4819 <https://doi.org/10.1016/j.chemgeo.2012.09.027>

4820 Wu, F. Y., Li, X. H., Yang, J. H., & Zheng, Y. F. (2007). Discussions on the petrogenesis of
4821 granites. *Acta Petrologica Sinica*, 23(6), 1217-1238. In Chinese with English
4822 abstract

4823 Wu, F. Y., Xu, Y. G., Gao, S., & Zheng, J. P. (2008). Lithospheric thinning and destruction of
4824 the North China Craton. *Acta Petrologica Sinica*, 24, 1145-1174. In Chinese with
4825 English abstract

4826 Wu, F. Y., Yang, J. H., Lo, C. H., Wilde, S. A., Sun, D. Y., & Jahn, B. M. (2007). The
4827 Heilongjiang group: A Jurassic accretionary complex in the Jiamusi massif at the
4828 western Pacific margin of northeastern China. *Island Arc*, 16(1), 156-172.
4829 <https://doi.org/10.1111/j.1440-1738.2007.00564.x>

4830 Wu, F. Y., Yang, J. H., Xu, Y. G., Wilde, S. A., & Walker, R. J. (2019). Destruction of the
4831 North China Craton in the Mesozoic. *Annual Review of Earth and Planetary
4832 Sciences*, 47(1), 173-195. <https://doi.org/10.1146/annurev-earth-053018-060342>

- 4833 Wu, Z., Chen, L., Talebian, M., Wang, X., Jiang, M., Ai, Y., et al. (2020). Lateral structural
4834 variation of the lithosphere-asthenosphere system in the northeastern to eastern
4835 Iranian plateau and its tectonic implications. *Journal of Geophysical Research:*
4836 *Solid Earth*, <https://doi.org/10.1029/2020JB020256>
- 4837 Wyman, D. A. (2013). A critical assessment of Neoarchean “plume only” geodynamics:
4838 Evidence from the Superior Province. *Precambrian Research*, 229, 3-19.
4839 <https://doi.org/10.1016/j.precamres.2012.01.010>
- 4840 Xia, Q., & Hao, Y. (2013). The distribution of water in the continental lithospheric mantle
4841 and its implications for the stability of continents. *Chinese Science Bulletin*, 58(32),
4842 3879-3889. <https://doi.org/10.1007/s11434-013-5949-1>
- 4843 Xia, Q. K., Liu, J., Liu, S. C., Kovács, I., Feng, M., & Dang, L. (2013). High water content
4844 in Mesozoic primitive basalts of the North China Craton and implications on the
4845 destruction of cratonic mantle lithosphere. *Earth and Planetary Science Letters*,
4846 361(0), 85-97. <http://dx.doi.org/10.1016/j.epsl.2012.11.024>
- 4847 Xiao, W., Song, D., Windley, B. F., Li, J., Han, C., Wan, B., et al. (2020). Accretionary
4848 processes and metallogenes of the Central Asian Orogenic Belt: Advances and
4849 perspectives. *Science China(Earth Sciences)*, 63(03), 329-361.
4850 <https://doi.org/10.1007/s11430-019-9524-6>
- 4851 Xiao, W., Windley, B. F., Sun, S., Li, J., Huang, B., Han, C., et al. (2015). A Tale of
4852 Amalgamation of Three Permo-Triassic Collage Systems in Central Asia: Oroclines,
4853 Sutures, and Terminal Accretion. *Annual Review of Earth and Planetary Sciences*,
4854 43(1), 477-507. <https://doi.org/10.1146/annurev-earth-060614-105254>
- 4855 Xiao, W. J., Windley, B. F., Huang, B. C., Han, C. M., Yuan, C., Chen, H. L., et al. (2009).
4856 End-Permian to mid-Triassic termination of the accretionary processes of the
4857 southern Altaids: implications for the geodynamic evolution, Phanerozoic
4858 continental growth, and metallogeny of Central Asia. *International Journal of Earth*
4859 *Sciences*, 98(6), 1189-1217. <https://doi.org/10.1007/s00531-008-0407-z>
- 4860 Xiao, Y., Teng, F. Z., Zhang, H. F., & Yang, W. (2013). Large magnesium isotope
4861 fractionation in peridotite xenoliths from eastern North China craton: Product of
4862 melt-rock interaction. *Geochimica et Cosmochimica Acta*, 115(0), 241-261.
4863 <http://dx.doi.org/10.1016/j.gca.2013.04.011>
- 4864 Xiao, Y., & Zhang, H. F. (2011). Effects of melt percolation on platinum group elements and
4865 Re-Os systematics of peridotites from the Tan-Lu fault zone, eastern North China

- 4866 Craton. *Journal of the Geological Society, London*, 168, 1201-1214.
 4867 <https://doi.org/10.1144/0016-76492010-113>
- 4868 Xu, S., Su, W., Liu, Y., Jiang, L., Ji, S., Okay, A. I., et al. (1992). Diamond from the Dabie
 4869 Shan Metamorphic Rocks and Its Implication for Tectonic Setting. *Science*,
 4870 256(5053), 80-82. <https://doi.org/10.1126/science.256.5053.80>
- 4871 Xu, W. L., Pei, F. P., Wang, F., Meng, E., Ji, W. Q., Yang, D. B., et al. (2013).
 4872 Spatial-temporal relationships of Mesozoic volcanic rocks in NE China: Constraints
 4873 on tectonic overprinting and transformations between multiple tectonic regimes.
 4874 *Journal of Asian Earth Sciences*, 74, 167-193.
 4875 <https://doi.org/10.1016/j.jseaes.2013.04.003>
- 4876 Xu, X., Zhao, L., Wang, K., & Yang, J. (2018). Indication from finite-frequency tomography
 4877 beneath the North China Craton: The heterogeneity of craton destruction. *Science*
 4878 *China Earth Sciences*, 61(9), 1238-1260.
 4879 <https://doi.org/10.1007/s11430-017-9201-y>
- 4880 Xu, X. S., Griffin, W. L., O'Reilly, S. Y., Pearson, N. J., Geng, H. Y., & Zheng, J. P. (2008).
 4881 Re-Os isotopes of sulfides in mantle xenoliths from eastern China: Progressive
 4882 modification of lithospheric mantle. *Lithos*, 102(1-2), 43-64.
 4883 <https://doi.org/10.1016/j.lithos.2007.06.010>
- 4884 Xu, Y. G. (2001). Thermo-tectonic destruction of the Archean lithospheric keel beneath the
 4885 Sino-Korean Craton in China: Evidence, timing and mechanism. *Physics and*
 4886 *Chemistry of the Earth (A)*, 26, 747-757.
 4887 [https://doi.org/10.1016/S1464-1895\(01\)00124-7](https://doi.org/10.1016/S1464-1895(01)00124-7)
- 4888 Xu, Y. G., He, B., Chung, S. L., Menzies, M. A., & Frey, F. A. (2004). Geologic,
 4889 geochemical, and geophysical consequences of plume involvement in the Emeishan
 4890 flood-basalt province. *Geology*, 32(10), 917-920. <https://doi.org/10.1130/g20602.1>
- 4891 Xu, Y. G., Wei, X., Luo, Z. Y., Liu, H. Q., & Cao, J. (2014). The Early Permian Tarim large
 4892 igneous province: Main characteristics and a plume incubation model. *Lithos*, 204,
 4893 20-35. <https://doi.org/10.1016/j.lithos.2014.02.015>
- 4894 Yang, J. H., Zhang, M., & Wu, F. Y. (2018). Mesozoic decratonization of the North China
 4895 Craton by lithospheric delamination: Evidence from Sr-Nd-Hf-Os isotopes of
 4896 mantle xenoliths of Cenozoic alkaline basalts in Yangyuan, Hebei Province, China.
 4897 *Journal of Asian Earth Sciences*, 160, 396-407.
 4898 <https://doi.org/10.1016/j.jseaes.2017.09.002>

- 4899 Yang, X. M., Drayson, D., & Polat, A. (2019). S-type granites in the western Superior
4900 Province: a marker of Archean collision zones. *Canadian Journal of Earth Sciences*,
4901 56(12), 1409-1436. <https://doi.org/10.1139/cjes-2018-0056>
- 4902 Yin, A. (2010). Cenozoic tectonic evolution of Asia: A preliminary synthesis.
4903 *Tectonophysics*, 488(1), 293-325. <https://doi.org/10.1016/j.tecto.2009.06.002>
- 4904 Yonkee, W. A., & Weil, A. B. (2015). Tectonic evolution of the Sevier and Laramide belts
4905 within the North American Cordillera orogenic system. *Earth-Science Reviews*, 150,
4906 531-593. <https://doi.org/10.1016/j.earscirev.2015.08.001>
- 4907 Yoshida, M. (2012). Dynamic role of the rheological contrast between cratonic and oceanic
4908 lithospheres in the longevity of cratonic lithosphere: A three-dimensional numerical
4909 study. *Tectonophysics*, 532-535, 156-166.
4910 <https://doi.org/10.1016/j.tecto.2012.01.029>
- 4911 Yuan, H., & Bodin, T. (2018). A probabilistic shear wave velocity model of the crust in the
4912 central west Australian craton constrained by transdimensional inversion of ambient
4913 noise dispersion. *Tectonics*, 37(7), 1994-2012.
4914 <https://doi.org/10.1029/2017TC004834>
- 4915 Yuan, H., & Romanowicz, B. (2019). Introduction—Lithospheric discontinuities. In H. Yuan
4916 & B. Romanowicz (Eds.), *Lithospheric Discontinuities* (pp. 1-3): American
4917 Geophysical Union.
- 4918 Yuan, X., Heit, B., Brune, S., Steinberger, B., Geissler, W. H., Jokat, W., et al. (2017).
4919 Seismic structure of the lithosphere beneath NW Namibia: Impact of the Tristan da
4920 Cunha mantle plume. *Geochemistry, Geophysics, Geosystems*, 18(1), 125-141.
4921 <https://doi.org/10.1002/2016GC006645>
- 4922 Yuan, X., Sobolev, S. V., Kind, R., Oncken, O., Bock, G., Asch, G., et al. (2000). Subduction
4923 and collision processes in the Central Andes constrained by converted seismic
4924 phases. *Nature*, 408(6815), 958-961. <https://doi.org/10.1038/35050073>
- 4925 Zahnle, K., Schaefer, L., & Fegley, B. (2010). Earth's earliest atmospheres. *Cold Spring*
4926 *Harbor Perspectives in Biology*, 2(10), 1-17.
4927 <https://doi.org/10.1101/cshperspect.a004895>
- 4928 Zeh, A., Gerdes, A., & Barton, J. M. (2009). Archean accretion and crustal evolution of the
4929 Kalahari craton—the zircon age and Hf isotope record of granitic rocks from
4930 Barberton/Swaziland to the Francistown arc. *Journal of Petrology*, 50(5), 933-966.
4931 <https://doi.org/10.1093/petrology/egp027>

- 4932 Zellmer, G. F., Iizuka, Y., Miyoshi, M., Tamura, Y., & Tatsumi, Y. (2012). Lower crustal H₂O
4933 controls on the formation of adakitic melts. *Geology*, 40(6), 487-490.
4934 <https://doi.org/10.1130/g32912.1>
- 4935 Zhai, M., & Liu, W. (2003). Palaeoproterozoic tectonic history of the North China craton: a
4936 review. *Precambrian Research*, 122(1), 183-199.
4937 [https://doi.org/10.1016/S0301-9268\(02\)00211-5](https://doi.org/10.1016/S0301-9268(02)00211-5)
- 4938 Zhang, H. F. (2005). Transformation of lithospheric mantle through peridotite-melt reaction:
4939 A case of Sino-Korean craton. *Earth and Planetary Science Letters*, 237, 768-780.
4940 <https://doi.org/10.1016/j.epsl.2005.06.041>
- 4941 Zhang, H. F. (2009). Peridotite-melt interaction: A key point for the destruction of cratonic
4942 lithospheric mantle. *Chinese Science Bulletin*, 54, 3417-3437.
4943 <https://doi.org/10.1007/s11434-009-0307-z>
- 4944 Zhang, H. F., Sun, Y. L., Tang, Y. J., Xiao, Y., Zhang, W. H., Zhao, X. M., et al. (2012).
4945 Melt-peridotite interaction in the Pre-Cambrian mantle beneath the western North
4946 China Craton: Petrology, geochemistry and Sr, Nd and Re isotopes. *Lithos*, 149,
4947 100-114. <https://doi.org/10.1016/j.lithos.2012.01.027>
- 4948 Zhang, J., Lin, S., Linnen, R., & Martin, R. (2014). Structural setting of the
4949 Young-Davidson syenite-hosted gold deposit in the Western Cadillac-Larder Lake
4950 Deformation Zone, Abitibi Greenstone Belt, Superior Province, Ontario.
4951 *Precambrian Research*, 248, 39-59. <https://doi.org/10.1016/j.precamres.2014.04.007>
- 4952 Zhang, Q., Buckman, S., Bennett, V. C., Nutman, A., & Song, Y. (2019). Lachlan orogen,
4953 eastern Australia: Triangle formation records the Late Ordovician arrival of the
4954 Macquarie arc atterrane at the margin of eastern Gondwana. *Tectonics*, 38(9),
4955 3373-3393. <https://doi.org/10.1029/2019TC005480>
- 4956 Zhang, Q., & Zhai, M. (2012). What is the Archean TTG? *Acta Petrologica Sinica*, 28(11),
4957 3446-3456. In Chinese with English abstract
- 4958 Zhang, Y., Chen, L., Ai, Y., & Jiang, M. (2019). Lithospheric structure beneath the central
4959 and western North China Craton and adjacent regions from S-receiver function
4960 imaging. *Geophysical Journal International*, 219(1), 619-632.
4961 <https://doi.org/10.1093/gji/ggz322>
- 4962 Zhang, Y. Q., Mercier, J. L., & Vergély, P. (1998). Extension in the graben systems around
4963 the Ordos (China), and its contribution to the extrusion tectonics of south China
4964 with respect to Gobi-Mongolia. *Tectonophysics*, 285, 41-75.

- 4965 [https://doi.org/10.1016/S0040-1951\(97\)00170-4](https://doi.org/10.1016/S0040-1951(97)00170-4)
- 4966 Zhang, Z., Wang, Y., Houseman, G. A., Xu, T., Wu, Z., Yuan, X., et al. (2014). The Moho
4967 beneath western Tibet: Shear zones and eclogitization in the lower crust. *Earth and*
4968 *Planetary Science Letters*, 408, 370-377. <https://doi.org/10.1016/j.epsl.2014.10.022>
- 4969 Zhao, G., Cawood, P. A., Li, S., Wilde, S. A., Sun, M., Zhang, J., et al. (2012).
4970 Amalgamation of the North China Craton: Key issues and discussion. *Precambrian*
4971 *Research*, 222–223(0), 55-76. <http://dx.doi.org/10.1016/j.precamres.2012.09.016>
- 4972 Zhao, G., Cawood, P. A., Wilde, S. A., & Sun, M. (2002). Review of global 2.1–1.8 Ga
4973 orogens: implications for a pre-Rodinia supercontinent. *Earth-Science Reviews*,
4974 59(1), 125-162. [https://doi.org/10.1016/S0012-8252\(02\)00073-9](https://doi.org/10.1016/S0012-8252(02)00073-9)
- 4975 Zhao, G., Wang, Y., Huang, B., Dong, Y., Li, S., Zhang, G., et al. (2018). Geological
4976 reconstructions of the East Asian blocks: From the breakup of Rodinia to the
4977 assembly of Pangea. *Earth-Science Reviews*, 186, 262-286.
4978 <https://doi.org/10.1016/j.earscirev.2018.10.003>
- 4979 Zhao, G. C. (2014). *Precambrian evolution of the North China Craton*. Amsterdam:
4980 Elsevier.
- 4981 Zhao, G. C., Cawood, P. A., Wilde, S. A., & Sun, M. (2000). Metamorphism of basement
4982 rocks in the Central Zone of the North China craton: implications for
4983 Paleoproterozoic tectonic evolution. *Precambrian Research*, 103, 55-88.
4984 [https://doi.org/10.1016/S0301-9268\(00\)00076-0](https://doi.org/10.1016/S0301-9268(00)00076-0)
- 4985 Zhao, G. C., Sun, M., Wilde, S. A., & Li, S. (2005). Late Archean to Paleoproterozoic
4986 evolution of the North China Craton: key issues revisited. *Precambrian Research*,
4987 136, 177-202. <https://doi.org/10.1016/j.precamres.2004.10.002>
- 4988 Zhao, G. C., Wilde, S. A., Cawood, P. A., & Lu, L. Z. (1998). Thermal evolution of Archean
4989 basement rocks from the eastern part of the north China craton and its bearing on
4990 tectonic setting. *Int. Geol. Rev.*, 40, 706-721.
4991 <https://doi.org/10.1080/00206819809465233>
- 4992 Zhao, G. C., Wilde, S. A., Cawood, P. A., & Sun, M. (2001). Archean blocks and their
4993 boundaries in the North China Craton: lithological, geochemical, structural and P-T
4994 path constraints and tectonic evolution. *Precambrian Research*, 107, 45-73.
4995 [https://doi.org/10.1016/S0301-9268\(00\)00154-6](https://doi.org/10.1016/S0301-9268(00)00154-6)
- 4996 Zhao, G. C., & Zhang, G. W. (2021). Origin of continents. *Acta Geologica Sinica*, 95(1), in
4997 press.

- 4998 Zheng, T., Chen, L., Zhao, L., Xu, W., & Zhu, R. (2006). Crust-mantle structure difference
4999 across the gravity gradient zone in North China Craton: Seismic image of the
5000 thinned continental crust. *Physics of The Earth and Planetary Interiors*, 159(1-2),
5001 43-58. <https://doi.org/10.1016/j.pepi.2006.05.004>
- 5002 Zheng, T., Duan, Y., Xu, W., & Ai, Y. (2017). A seismic model for crustal structure in North
5003 China Craton. *Earth and Planetary Physics*, 1(1), 26-34.
5004 <https://doi.org/10.26464/epp2017004>
- 5005 Zheng, Y., Xu, Z., Zhao, Z., & Dai, L. (2018). Mesozoic mafic magmatism in North China:
5006 Implications for thinning and destruction of cratonic lithosphere. *Science China*
5007 *Earth Sciences*, 61(4), 353-385. <https://doi.org/10.1007/s11430-017-9160-3>
- 5008 Zheng, Y. F., & Zhao, G. C. (2020). Two styles of plate tectonics in Earth's history. *Science*
5009 *Bulletin*, 65(4), 329-334. <https://doi.org/10.1016/j.scib.2018.12.029>
- 5010 Zhu, R., & Xu, Y. (2019). The subduction of the west Pacific plate and the destruction of the
5011 North China Craton. *Science China Earth Sciences*, 62(9), 1340-1350.
5012 <https://doi.org/10.1007/s11430-018-9356-y>
- 5013 Zhu, R., Zhang, H., Zhu, G., Meng, Q., Fan, H., Yang, J., et al. (2017). Craton destruction
5014 and related resources. *International Journal of Earth Sciences*, 106(7), 2233-2257.
5015 <https://doi.org/10.1007/s00531-016-1441-x>
- 5016 Zhu, R. X., Chen, L., Wu, F. Y., & Liu, J. L. (2011). Timing, scale and mechanism of the
5017 destruction of the North China Craton. *Science China Earth Sciences*, 54(6),
5018 789-797. <https://doi.org/10.1007/s11430-011-4203-4>
- 5019 Zhu, R. X., Xu, Y. G., Zhu, G., Zhang, H. F., Xia, Q. K., & Zheng, T. Y. (2012a). Destruction
5020 of the North China Craton. *Science China Earth Sciences*, 55(10), 1565-1587.
5021 <https://doi.org/10.1007/s11430-012-4516-y>
- 5022 Zhu, R. X., Yang, J. H., & Wu, F. Y. (2012b). Timing of destruction of the North China
5023 Craton. *Lithos*, 149(0), 51-60. <https://doi.org/10.1016/j.lithos.2012.05.013>
- 5024 Zhu, R. X., Zhou, Z. H., & Meng, Q. R. (2020). Destruction of the North China Craton and
5025 its influence on surface geology and terrestrial biotas. *Chinese science Bulletin*,
5026 65(27), 2954-2965. <https://doi.org/10.1360/TB-2020-0219>
- 5027 Ziegler, P. A., & Dèzes, P. (2007). Cenozoic uplift of Variscan Massifs in the Alpine
5028 foreland: Timing and controlling mechanisms. *Global and Planetary Change*, 58(1),
5029 237-269. <https://doi.org/10.1016/j.gloplacha.2006.12.004>
- 5030 Ziegler, P. A., van Wees, J.-D., & Cloetingh, S. (1998). Mechanical controls on

5031 collision-related compressional intraplate deformation. *Tectonophysics*, 300(1),
 5032 103-129. [https://doi.org/10.1016/S0040-1951\(98\)00236-4](https://doi.org/10.1016/S0040-1951(98)00236-4)

5033 Zou, D., Zhang, H., Hu, Z., & Santosh, M. (2016). Complex metasomatism of lithospheric
 5034 mantle by asthenosphere-derived melts: Evidence from peridotite xenoliths in
 5035 Weichang at the northern margin of the North China Craton. *Lithos*, 264, 210-223.
 5036 <http://dx.doi.org/10.1016/j.lithos.2016.08.036>

5037 Zulbati, F., & Harley, S. L. (2007). Late Archaean granulite facies metamorphism in the
 5038 Vestfold Hills, East Antarctica. *Lithos*, 93(1), 39-67.
 5039 <https://doi.org/10.1016/j.lithos.2006.04.004>